Synthesis and characterization of catalysts for photo-oxidation of water

Sujitraj Sheth

UNIVERSITE PARIS-SUD

ÉCOLE DOCTORALE DE CHIMIE (ED470)
LMB, iBiTec-S, CEA Saclay

Chimie

THÈSE DE DOCTORAT

soutenue le 11/12/2013

par

Sujitraj SHETH

Synthesis and Characterization of Catalysts for Photo-oxidation of Water

Directeur de thèse :	Winfried LEIBL	Directeur de Recherche CEA, CEA Saclay
Composition du jury :		
Président du jury:	Ally AUKAULOO	Professeur, Université Paris Sud, Orsay
Rapporteurs:	Yann PELLEGRIN	Chargé de Recherches, Université de Nantes, Nantes
	Frédérique LOISEAU	Professeur, Université Joseph Fourier, Grenoble
Examinateurs:	A. William RUTHERFORD	Professeur, Imperial College, London
	Athanassios COUTSOLELOS	Professeur, University of Crete, Heraklion

Acknowledgement

First and foremost, I would like to take an opportunity to thank my PhD supervisor Dr. Winfried LEIBL for giving me an opportunity to work under his supervision. I extend my warm thanks for his continuous and immense support, encouragement, patience and guidance. He was always there to find the solution whenever I had come across with a difficulty. His kindness and humanity have always been the positive assets.

I would like to thank Professor Dr. Ally AUKAULOO for his support and guidance on the chemistry part during the thesis. His sentence "Go and work hard" always encouraged me. His motivation and the sound knowledge in the field of chemistry are profoundly acknowledged.

I am thankful to Sandra ANDRIANAMBININTSOA for her assistance in several experiments and improving my French from time to time.

Thank you Aurélie BARON and Christian HERRERO for introducing me synthetic methodology at the beginning of the PhD and getting acquainted with the working environment in our chemistry laboratory. I extend my thanks to Annamaria, Sanae, all our group members and short term visiting scholars who had made my stay in the lab amicable.

I would like to thank Dr. Yann PELLEGRIN and Professor Dr. Frédérique LOISEAU for having accepted the task of being reporters and evaluating my thesis. Furthermore, I also thank Professor Dr. A. William RUTHERFORD and Professor Dr. Athanassios COUTSOLELOS for examining my thesis.

The programme SERP Chem gave me a platform to study at international level. I am thankful to the director of the SERP Chem programme, Dr. Sandrine LACOMBE for giving me such an opportunity to study and her encouragement all time. This programme gave me the chance to find many friends and to interact with people from different parts of the world, I thank all of them.

Working in the CEA was a great experience thanks to IRTELIS programme for fellowship for PhD. During my stay at our institute (iBiTec-S) I had encountered with many PhD students, post docs and researchers. It was always nice to have a chat with them, without mentioning their names individually, I thank you all.

Many people I met in acquaintances, it can be anywhere thanks to all of them who had given me a smile and gentle breeze of happiness.

Paris is one of the most beautiful cities in the world, its glory can be seen in museums and monuments located in the city. I had explored some of them during my PhD with nice friends and this will be in my memory forever.

I must be fortunate to have such wonderful parents and sister without their love and moral support this work would have never led to its completion. Many many thanks to Papa, Mummy and Rani.

This thank to all of you guys if by chance I had ever forgotten to say thanks for your help and support during my stay in Paris.

Paris, 3rd January 2014

Table of Contents

Thesis overview

This thesis work describes a study related to the area of Artificial photosynthesis.

Chapter 1: Introduction gives a glimpse of photosystem II and our approach to mimic its donor side electron transfer chain. This chapter ends with description of our strategy and the objectives of this thesis work. We have synthesized several organometallic complexes based on ruthenium bipyridyl derivatives. Characterization of the complexes was performed using electrochemical and spectroscopic techniques, the description of which can be found in the **Chapter 2: Experimental techniques**. The next four chapters present the main results obtained during the thesis period. **Chapter 3: Artificial mimics of TyrZ/His190 electron relay of photosystem II** gives the details of characterization of ruthenium/imidazole-phenol (chromophore-electron relay) complexes mainly focused on the intramolecular electron transfer processes and their kinetics and energetics, with particular attention to the effect of coupling between electron transfer and deprotonation processes. Later on in **Chapter 4: Light induced Tryptophan oxidation** we have put forward a potentially more efficient synthetic methodology, based on "click chemistry", to synthesize larger, modular photocatalytic assemblies. Using this approach we have connected a tryptophan residue to a chromophore and investigated the mechanism of Tryptophan radical formation. As a continuation of the work described in Chapter 3 we have tried to covalently link our chromophore-electron relay system to an oxidation catalyst as described in **Chapter 5: Water oxidation catalysts**. This approach was not successful and therefore we have investigated on the possibility of catalyst activation in a bimolecular reaction. For use in a functional device the photocatalyst should be grafted on the surface of an electrode. As the target complete photocatalysts were not available we have performed functionalization of a chromophore with phosphonate anchoring groups. Details can be found in the **Chapter 6: Grafting of photosensitizer onto a TiO_2 surface and photoelectrochemical measurements**. At the end of this thesis conclusions and perspectives of this work are given in **Chapter 7: Conclusions and perspectives**.

1.0 Introduction

1.1 General concept

In this growing world there is increasing demand of energy and this demand will go as high as 28-35 TW in 2050[1]compared to current 16 TW in 2012.[2] Population of the world is projected to grow to 10-11 billion in 2050, the factor which mainly brings this difference in energy consumption.[3] In order to fulfill this demand we mostly depend on fossil fuels (Figure 1.1).Recent statistics shows that 87% of the world energy is produced from fossil fuels in 2012.[2]The sources of these fossil fuels are limited and overconsumption will lead to their shortage in the near future. Additionally, their combustion produces carbon dioxide, carbon monoxide, smoke and suspended particulate matter which causes environmental problems. Gases such as carbon dioxide are greenhouse gases and minimization of their emission is of great concern.[4-6] Thus in order to meet the additional 15-20 TW of energy demand in sustainable way energy must come from carbon free sources. Therefore alternative, renewable energy sources have to be developed.[7,8]

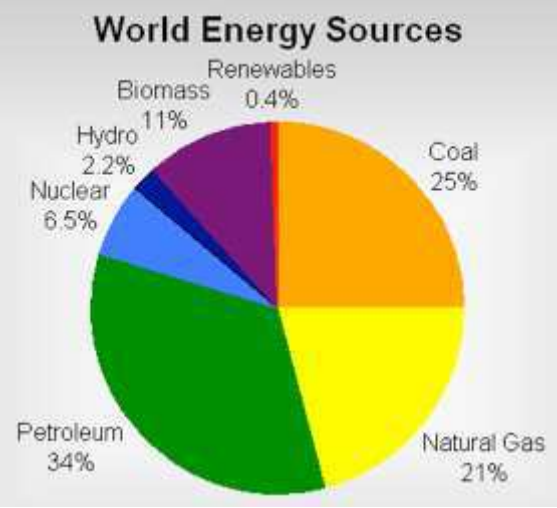

Figure 1.1: *World energy scenario*

As seen in Figure 1.1 we use only 0.4% of renewable energy from all available sources (Figure 1.2). There are many options available for renewable energy sources like wind energy, hydroelectric, biomass and solar energy. Among these solar energy is the most important resource, available in far excess of our requirement. The amount of energy from the sun arriving at the earth per hour about equals the energy utilized by humankind for all its activities in one year.[9] Thus utilizing solar energy in a proper way will help us to tackle the energy problem.

Figure 1.2: *Available renewable energy resources*

The available energy from the sun is not equally distributed on the earth therefore some parts have more or less energy than other parts. Also uneven distribution of sun energy due to seasonal variation and diurnal cycle causes difficulties in its proper utilization. These things make handling, storage and supply of solar energy a big problem.[10] There are some ways out to utilize available solar energy either by direct use or by suitable conversion into a form which can be further used as a source of energy (Figure 1.3).[11]

i) Direct use of sunlight to generate electricity using semiconductor material as in photovoltaic devices (Figure 1.3, right)

ii) Plants use sunlight via photosynthesis to produce carbohydrates and oxygen (Figure 1.3, left)

iii) A third way which mainly interests us is, use of sunlight to split water (Eq. 1.1) by using suitable photo-catalysts and produce protons which can be reduced further to generate hydrogen by employing another catalyst (Eq. 1.2).

$$2H_2O \rightarrow 4H^+ + 4e^- + O_2 \qquad \text{(Eq. 1.1)}$$

$$4H^+ + 4e^- \rightarrow 2H_2 \qquad \text{(Eq. 1.2)}$$

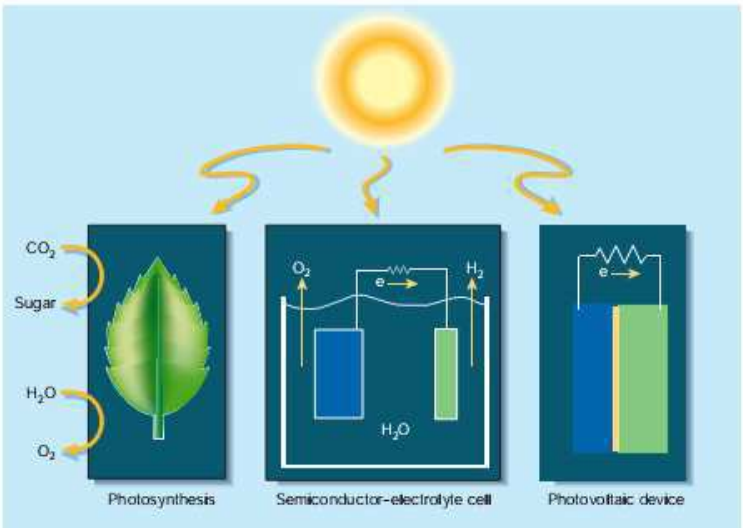

Figure 1.3*: Solar energy can be used by three means to generate energy:* ***Left:*** *in photosynthesis plants use solar radiation in conjunction with CO_2 and water to produce sugars and oxygen.* ***Right:*** *photovoltaic devices can directly convert solar energy into electricity* ***Center:*** *water splitting cell with electrodes.*[11]

Water is a most abundant (79%) on the earth and sunlight is freely available on our planet. By using water and sunlight to generate hydrogen which is considered as a green fuel (since its combustion results into water, Eq. 1.3) can be a solution for future energy crisis.

$$2H_2 + O_2 \rightarrow 2H_2O \qquad \text{(Eq. 1.3)}$$

The water splitting reaction, Eq. 1.1 is an integral part of natural photosynthesis. Therefore, by mimicking the process of natural photosynthesis it should be possible to split water. For this purpose there is a need of robust photo-catalysts.

Our research work concerns water splitting using bio-inspired molecular photo-catalyst and in the following we will present basic concepts of natural process to clearly understand mechanistic aspects required to move a step forward in this area of research.

1.2 Natural Photosynthesis

The origin of Photosynthesis goes back to billions years ago.[4,12] It is a process in which organelles like photosynthetic bacteria[2] (e.g. Cyanobacteria, purple sulfur bacteria), algae and plants utilize light energy to make energy rich organic compounds (Eq. 1.4).[1]This transformation of light energy into chemical energy is carried out by multiple protein subunits called reaction centers (RCs).

Photosynthetic products like carbohydrates or ATP are used as a source of energy in photosynthetic organisms. These autotrophs are basic element of the food chain on the earth. Thus basically all life on our planet directly or indirectly depends on photosynthesis. The photosynthetic process can be termed as oxygenic or anoxygenic photosynthesis depending on whether oxygen evolves in the process or not. Here we mostly consider oxygenic photosynthesis (Eq. 1.4)

$$6CO_2 + 12H_2O + \text{Light Energy} \rightarrow C_6H_{12}O_6 + 6O_2 + 6H_2O \qquad \text{(Eq. 1.4)}$$

The photosynthetic process gets initiated by light harvesting antennas after receiving light energy from the sun. Antennas can be pigments like chlorophyll, carotenoid, bilin depending on the organism.

In plants, photosynthesis occurs in a thylakoid membrane located inside chloroplasts (Figure 1.4). Thylakoid membranes are disk-like structures stacked over one another, resembling stacks of coins. Chlorophyll and carotenoid pigments are located inside the thylakoid membrane.

In a broad sense photosynthetic processes can be divided into two kinds of reactions depending on their requirement of light:

1) Light dependent reactions: useful to increase free energy of the system
2) Light independent reactions (Calvin cycle): useful to convert free energy into chemical bonds by forming carbohydrates

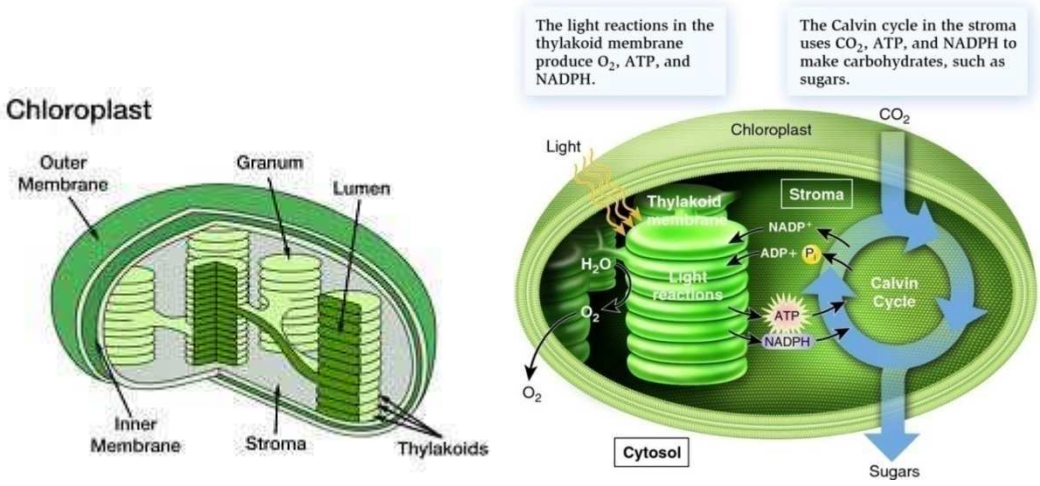

Figure 1.4: *Open structure of chloroplast showing thylakoid membrane and light and dark reactions*

The light dependent reactions occur in the thylakoid membrane while dark reactions occur in the stroma of the chloroplast (Figure 1.4). Light reactions are responsible for oxidation of water (Eq. 1.1) and production of ATP and NADPH. These NADPH and ATP are further used in dark reactions to reduce CO_2 to form carbohydrates. Energy is conserved in all of these processes.

1.2.1 Light dependent reactions

Light dependent reactions do proceed by using light energy from the sun. These reactions are mainly carried out by two reaction centers functioning in series, called photosystem I and photosystem II.

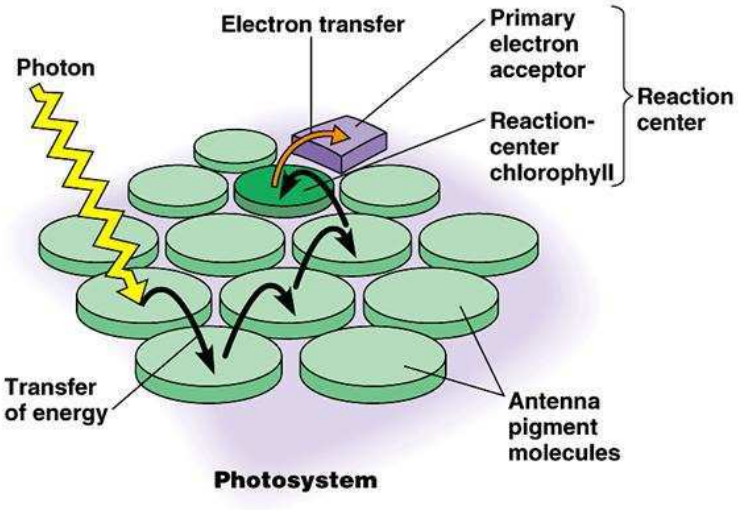

Figure 1.5*: Photochemical reaction center and light harvesting antenna*

1.2.2 Photosystems

When a photon strikes the chlorophyll molecule in the thylakoid membrane, the energy level of an electron is excited equivalent to the amount of energy absorbed. The absorbed energy migrates rapidly as excited state through light harvesting pigment molecules to the reaction centre of the photosystem by resonant energy transfer (Figure 1.5).

Light absorbing pigments and their associated electron carriers are arranged in a thylakoid membrane to form clusters. These clusters are photosystems. Photosystems absorb light in the visible region of the spectrum especially in the range from 400 to 500 nm and 600 to 700 nm.

Two main photosystems are,

Photosystem I: responsible for the reduction of NADP to NADPH (Figure 1.6)

Photosystem II: responsible for the oxidation of water. (Figure 1.6)

The detailed view of photosystems inside thylakoid membrane is as in Figure 1.6. As seen two photosystems function in series; several energy, electron and proton transfer reactions taking place to oxidize two molecules of water (in photosystem II) and to reduce $NADP^+$ to create reducing equivalents of NADPH (by electrons from photosystem I) and to convert ADP to ATP (via a transmembrane proton gradient). The latter being the primary source of energy for the organisms. NADPH is further used to reduce CO_2 to carbohydrates by dark reactions (Figure 1.4).

Each photosystem has a special ensemble of pigments which receive the excitation energy and induce the electron transfer processes, either P700 or P680 for photosystem I and photosystem II, respectively. The numbers 700 and 680 indicate the wavelength at which these photochemically active pigments absorb. At structural and functional level both photosystems have been well studied using advanced techniques and reported in literature.[13-16]

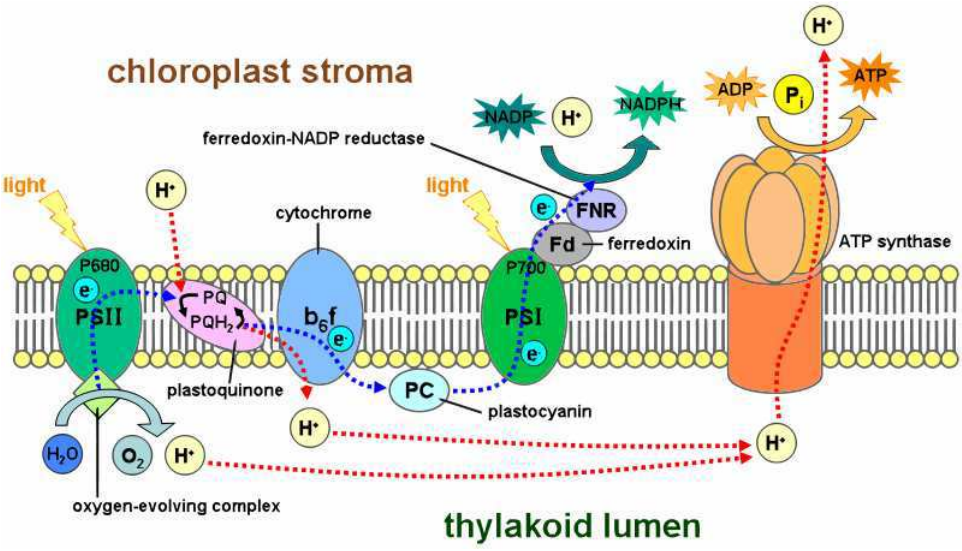

Figure 1.6: *Detailed view of the photosynthetic electron transfer chain with two photosystems*

1.2.3 The Photosystem I (PS I)

Photosystem I is responsible for the production of reducing equivalents of NADPH with the aid of the electron carrier ferredoxin which is also used for the dark reaction to reduce CO_2. Photosystem I (PS I) is an integral membrane protein complex and in presence of light it catalyses an electron transfer process from plastocyanin to ferredoxin. The PS I includes about110 co-factors. The primary electron donor of PS I is P700 which is a chlorophyll dimer.

1.2.4The photosystem II (PS II)

PSII is a unique enzyme which is responsible for oxidation of water to molecular oxygen in natural systems.[17,18] It consists of about 20 protein subunits in cyanobacterium *Thermosynechococcus (T.) elongates* with a total molecular mass of 350 kDa. These 20 protein subunits include 77 cofactors.[19,20] These 77 cofactors are: 35 Chl*a*, 14 lipids (+3 detergent molecules), 11 beta-carotenes, 2 plastoquinones (PQ), 2 pheophytines (Pheo), 1 Mn_4O_xCa complex, 2 heme Fe, 1non-heme Fe, 1 hydogencarbonate.

One important thing about PSII is that it uses visible light between 400 nm to 700 nm to drive the water oxidation reaction. The electron transfer process is initiated by excitation of the primary electron donor, P680. From its singlet excited state, P680 transfers an electron to Quinone (Q_A) resulting into the charge separated state $P680^+$ Q_A^-. The $P680^+$ is reduced by one of the tyrosine residues (TyrZ) resulting into neutral $TyrZ^\bullet$ radical. The generated $TyrZ^\bullet$ radical has been characterized by high field Electron paramagnetic resonance techniques. The

photogenerated TyrZ$^{\bullet}$ radical is subsequently reduced by deriving an electron from the oxygen evolving complex (OEC).

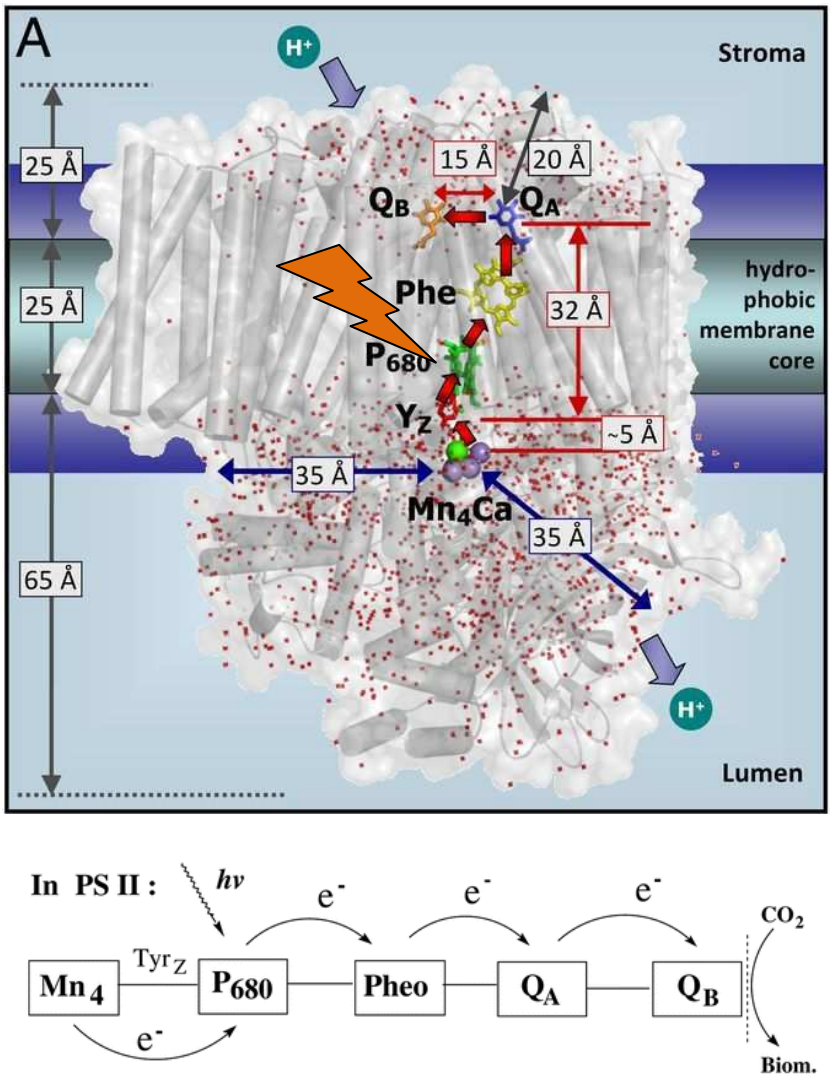

Figure 1.7: *Electron transport chain in photosystem II.*[46, 26]

1.2.5 Hydrogen bonding between TyrZ and His190

The recent crystal structure of 1.9 Å resolution brought new insight into water splitting site of photosystem II.[21] The hydrogen bonding between TyrZ and His190 plays an important role in the water oxidation (Figure 1.8).

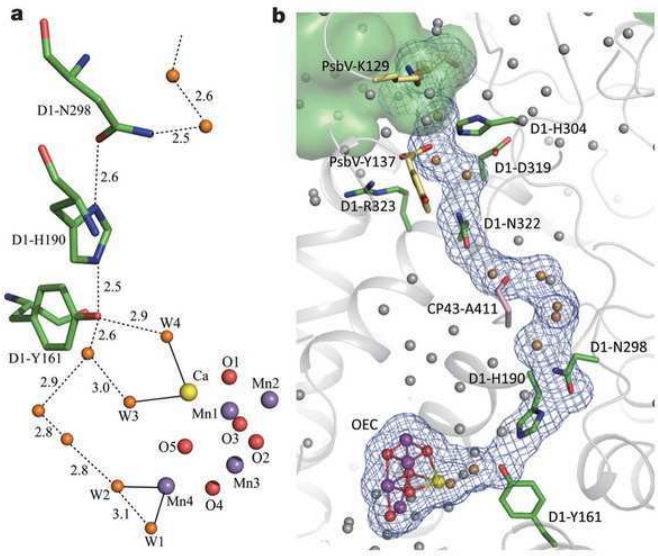

Figure 1.8: *Hydrogen bonds around* ***TyrZ*** *(labeled as D1-Y161): a) Bonds between metal atoms and water ligands are depicted as solid lines, and the hydrogen bonds are depicted as dashed lines. Distances are expressed in Ångströms. b) Hydrogen-bond network from the Mn4CaO5 cluster through TyrZ to the lumenal bulk phase. Water molecules participating in the hydrogen-bond network are depicted in orange, whereas those not participating are depicted in grey.*[21]

There are two redox active tyrosines in PS II, TyrZ and TyrD, out of these TyrZ is in close distance to Mn_4CaO_5 (OEC). TyrZ acts as a redox active link between the photosensitizer P680 and the OEC. Extensive hydrogen bonding network has been found between TyrZ and Mn_4CaO_5. The existence of H-bond between TyrZ and His 190 is important to for efficient electron transfer by coupling electron and proton transfer (Figure 1.9).

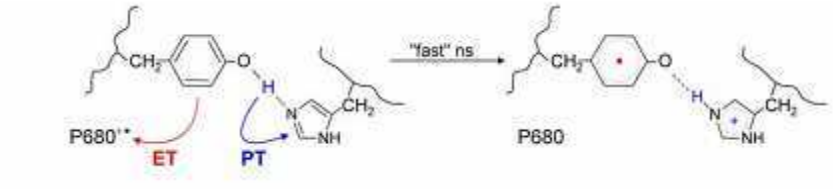

Figure 1.9: *A scheme for proton coupled electron transfer coupled to* $P680^{+\cdot}$ *reduction by TyrZ with His190 as hydrogen bonding partner*[22]

1.2.6 Oxygen evolving complex (OEC)

The oxygen evolving complex (OEC) or water oxidizing complex (WOC) is the site of water oxidation in photosystem II. The OEC has four Manganese ions, one Calcium ion and one chloride ion. Four Mn atoms and one Ca atom form a Mn_4Ca cluster.[20] Its precise structure and the oxidation state of each Mn is still an open question and many studies have been carried out using in particular spectroscopic techniques like high field EPR[22] or EXAFS[23,24].

The recently reported crystal structure of PS II at 1.9 Å resolution shows involvement of five oxygen atoms to form oxo bridges with five metal atoms (Figure 1.10) [21] thereby forming a Mn_4CaO_5 cluster. Out of these, three Mn, one Ca and four O atoms form a cubane like structure. Additionally, four water molecules and two chloride ions are found to be associated with the Mn_4CaO_5 cluster.[25] Two water molecules each are coordinated to one Mn and one Ca atom. Direct attachment of these water molecules indicates their involvement as a substrate in the water oxidation reaction.

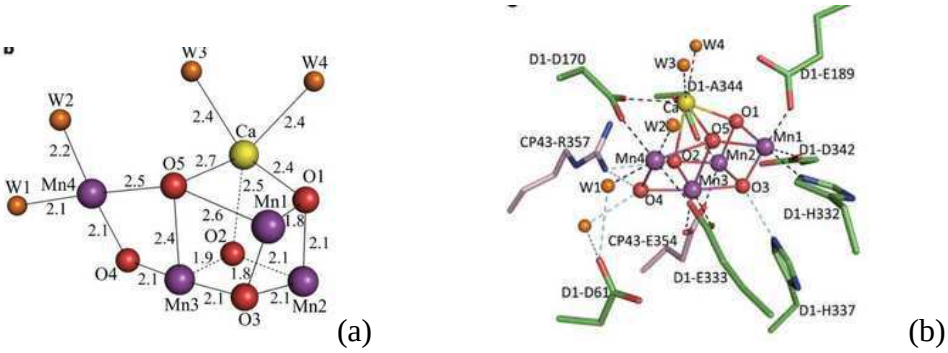

Figure 1.10: *a) Distances (in Å) between metal atoms and oxo bridges or water molecules b) View of the Mn_4CaO_5 cluster and its ligand environment.*[21]

1.2.7 S-states

Four photons are necessary to oxidize two water molecules to generate molecular oxygen, O_2 at the OEC. Each of these four photons advances the cluster through different oxidation states called S-states (Figure 1.9). Kok and Joliot independently found the four-step photocatalytic cycles where the OEC changes between five oxidation states hence named as Kok's cycle. In the Kok's cycle firstly the OEC is oxidized from the S_0 state to a highly oxidizing S_4 state via successive one-electron steps by photo-oxidized $P680^+$. Thus at the end of a cycle (S_4 state), the OEC accumulates four oxidizing equivalents which it uses to split two molecules of water to generate molecular oxygen and the OEC itself is reset back to its original S_0 state[26] (Figure 1.11).

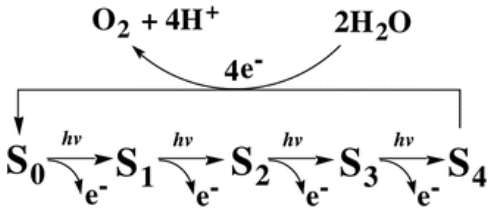

Figure 1.11*: Kok's cycle*

1.3 Artificial photosynthesis

Humans are often trying to mimic nature. We are trying to mimic the natural photosynthesis to solve the energy quest in front of entire human race. Mimicking of natural processes of photosynthesis is termed as "artificial photosynthesis".[27] Water oxidation to dioxygen is an important half reaction either in water splitting into molecular hydrogen and oxygen[28] or in reduction of $CO_2$to methanol.[29] Thus the main goal of artificial photosynthesis is to mimic photosynthetic organisms to make energy rich chemicals.[28,30-32] Therefore this is of considerable interest from a future energy prospects point of view.

Hundred years ago, Giacomo Ciamician, an Italian photochemist already talked about artificial photosynthesis in his speech and an article in Science.[33] In his own words: "With nature as a source of inspiration, many different approaches to achieve conversion and storage of solar energy can be applied."

Inspired from the natural photosynthesis artificial photosynthetic systems are based on the same designing principles. As the natural system, an artificial photosynthetic system requires three basic components (Figure 1.12)[30] i) A light-activated complex which generates redox equivalents ii) A water oxidation catalyst which splits water into protons, electrons and molecular oxygen and where the generated electrons get stored as reducing equivalents iii) A proton reduction catalyst which uses the reducing equivalents generated by the water oxidation catalyst to produce hydrogen as fuel.

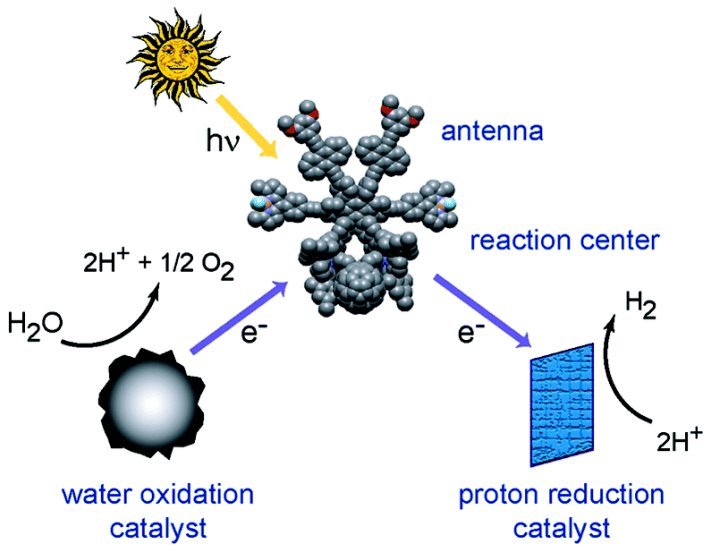

Figure 1.12: *Artificial photosynthetic system showing water oxidation and proton reduction*[30]

In the last few decades much effort has been made to construct such artificial systems which can convert solar energy to chemical energy. The main strategy behind this artificial constructs is to make supramolecular assemblies having photosensitizers (P), electron acceptors (A) and electron donors (D) and which can create a long lived charge separated state after light absorption similar to natural photosynthetic systems. (Figure 1.13)[30] The reducing state A^- activates a reduction catalyst (Cat_{Red}) and D^+ activates an oxidation catalyst (Cat_{Ox}) after repetitive light absorption-electron transfer sequence. This process accumulates required units of reductive and oxidative equivalents at Cat_{Red} and Cat_{Ox} for overall water photolysis.

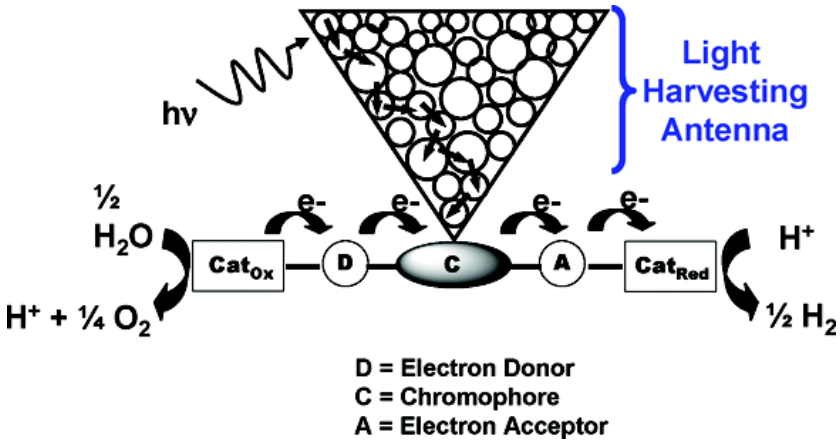

Figure 1.13: *Diagram illustrating the essential elements in an assembly for artificial photosynthesis and the sequence of events that occurs after light is absorbed. (Cat_{Red} = catalyst for chemical reduction, Cat_{Ox} = catalyst for chemical oxidation)*[30]

This forms a basis for the modular approach to artificial photosynthesis.[30] The modular approach has to fulfill various requirements like energy transfer, electron transfer, and catalysis. This represents a great complexity and difficulty for synthesis of such a structure with several functional units. In the modular approach, beside others, two types of chromophores are mainly employed and those are porphyrins and polypyridyl based complexes. These complexes are efficient in electron transfer and in creating charge separation states and their potentials can be tuned by varying functional groups.

1.3.1 Artificial mimics of photosystem II

The above explained principles of photosynthesis have inspired chemists to mimic the reactions of photosynthesis by using supramolecular synthetic assemblies. These supramolecular construct have been synthesized to mimic the donor side of photosystem II i.e. to oxidize water to molecular oxygen. Proton coupled electron transfer (PCET) plays a crucial

role in these artificial mimics as in natural systems and is severely discussed. Therefore we present in the following a few examples of artificial mimics of photosystem II extensively discussed in the literature.

Prior to this we would like to discuss the properties of **$[Ru(bpy)_3]^{2+}$** photosensitizers since our artificial mimics of photosystem II are based on **$[Ru(bpy)_3]^{2+}$** photosensitizer. Therefore it is indispensible to discuss its properties in detail.

1.3.2 $[Ru(bpy)_3]^{2+}$ as Photosensitizer / Chromophore

A chromophore is a colored substance which absorbs light of certain wavelengths in the visible spectrum.[34] The absorbed light thus causes an excitation of an electron from ground state to the excited state. This phenomenon can be studied by using various spectroscopic techniques like fluorescence spectroscopy, laser flash photolysis etc.

Many transition metals complexes of d^6 family have characteristic long lived excited states. This unique characteristic attracts photochemists to perform photo and redox chemistry of such complexes and ruthenium complexes also fall into this category. The most extensively studied and characterized[34-36] chromophore based on ruthenium metal is **$[Ru(bpy)_3]^{2+}$**(Figure 1.14) It has been studied for its photophysical properties over last three decades.[12,37] In artificial photosynthesis the main feature of **$[Ru(bpy)_3]^{2+}$** lies in its redox potential which is 1.26 *vs.*NHE[36] which is close to the redox potential of natural chromophore, P680 (1.25 *vs.* NHE)[38,39]. In addition it satisfies most of the requirements for a photosensitizer like kinetic, spectroscopic and excited state properties.[34,36]

In the literature hundreds of Ru polypyridine complexes are reported which are synthesized by changing ligands or its substituents, thus tuning of its potentials and excited state properties.[34,36] It is easy to play with its solvation properties by changing the counter ion of the complex.

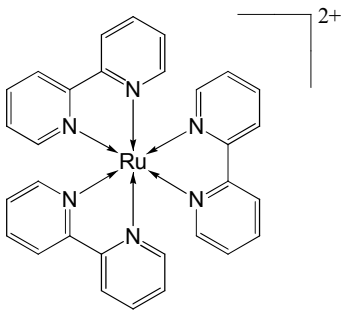

Figure 1.14:$[Ru(bpy)_3]^{2+}$complex

1.3.3 Properties of $[Ru(bpy)_3]^{2+}$

Before discussing the photochemistry of **$[Ru(bpy)_3]^{2+}$**, it is useful to consider the electronic structure of its excited state.

The Figure 1.15 is an absorption spectrum of **$[Ru(bpy)_3]^{2+}$** in acetonitrile. It shows distinct features of metal to ligand and ligand to ligand charge transfer transitions. The absorption maxima at 453 nm (ε = 13000 M^{-1} cm^{-1}) is due to the allowed metal to ligand charge transfer transitions (MLCT) between t_{2g} orbitals localized on ruthenium and π^* orbitals of the bipyridine. The sharp band in the UV region at 290 nm is attributed to intraligand π-π^* transition of the bipyridine orbitals.

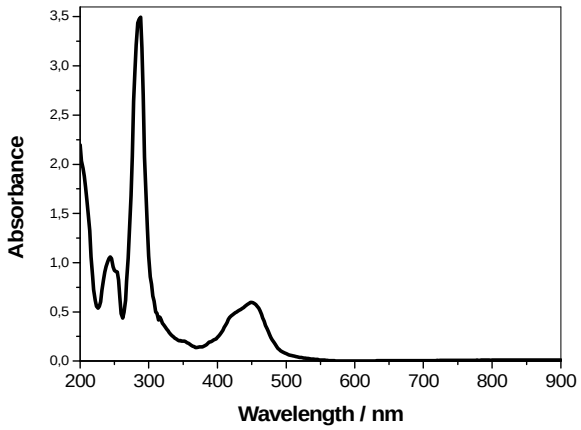

Figure 1.15: *Absorption spectrum of* ***$[Ru(bpy)_3]^{2+}$*** *in acetonitrile*

The unique combination of chemical, photophysical, photochemical, and electrochemical properties is summarized in Figure 1.16. The **$[Ru(bpy)_3]^{2+}$** in the ground state upon excitation forms a spin allowed excited state ****$[Ru(bpy)_3]^{2+}$** which relaxes via radiationless deactivation to the spin forbidden, long lived (0.6 µs and 0.8 µs in water and acetonitrile respectively) ***$[Ru(bpy)_3]^{2+}$** excited state with quantum yield of unity. Another interesting feature is that **$[Ru(bpy)_3]^{2+}$**as well as ***$[Ru(bpy)_3]^{2+}$** can undergo one electron redox (oxidation and reduction) processes. Due to the energy input by excitation ***$[Ru(bpy)_3]^{2+}$**is both, a good reductant and a good oxidant which can drive photoinduced electron transfer. The latter feature of **$[Ru(bpy)_3]^{2+}$** is most interesting concerning our present study.

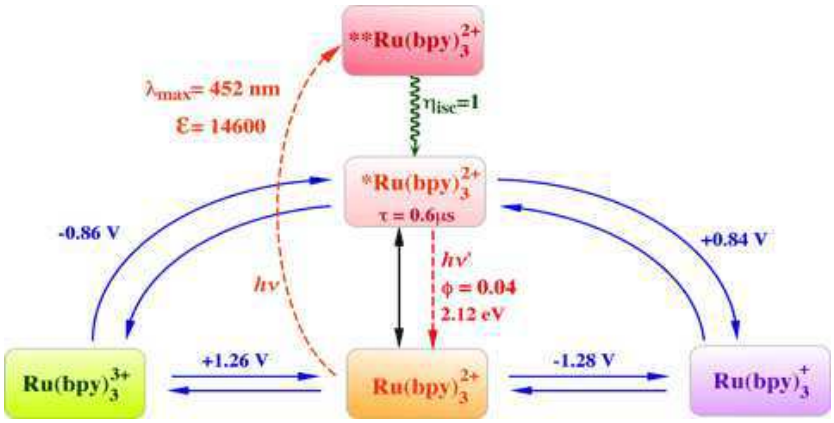

Figure 1.16: *Important properties of* ***[Ru(bpy)$_3$]$^{2+}$****; shows one electron excitation and redox behavior; all potentials mentioned are against SCE.*[35]

1.3.4 Artificial mimics based on [Ru(bpy)$_3$]$^{2+}$

In literature several supramolecular complexes have been reported based on the **[Ru(bpy)$_3$]$^{2+}$** photosensitizer which mimic photosystem II.[27,40-42] Among these supramolecular systems covalently linked photosensitizer and electron relay constructs play an important role in studying intramolecular electron transfer processes alike in natural system. In all we would like to mention one example, **Ru-Tyrosine,** a Ruthenium photosensitizer covalently linked to a tyrosine residue, (Figure 1.17), which is reported by Hammarström and co-workers.[41,43]

Upon light activation the **Ru-Tyrosine** complex shows fast recovery of Ru(III) to the Ru(II) state due to intramolecular electron transfer from the tyrosine residue (Figure 1.18) and generation of tyrosine radical was confirmed by electron paramagnetic spectroscopy (EPR). The electron transfer scheme was depicted as in Figure 1.19.

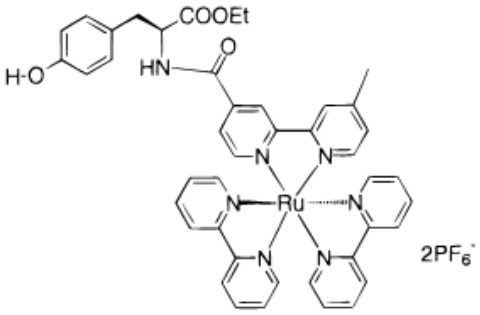

Figure 1.17: Ru-Tyrosine *complex*

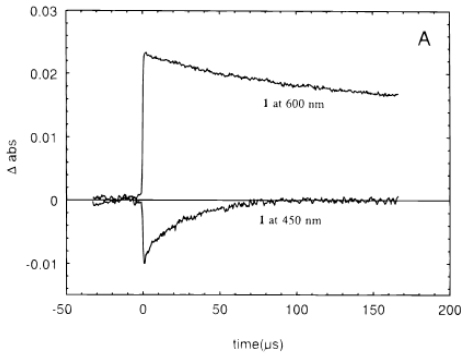

Figure 1.18*: Transient kinetic traces at 450 nm showing fast recovery for Ru(III) to Ru(II) (lower trace) than decay of electron acceptor monitored at 600 nm (upper trace).*[43]

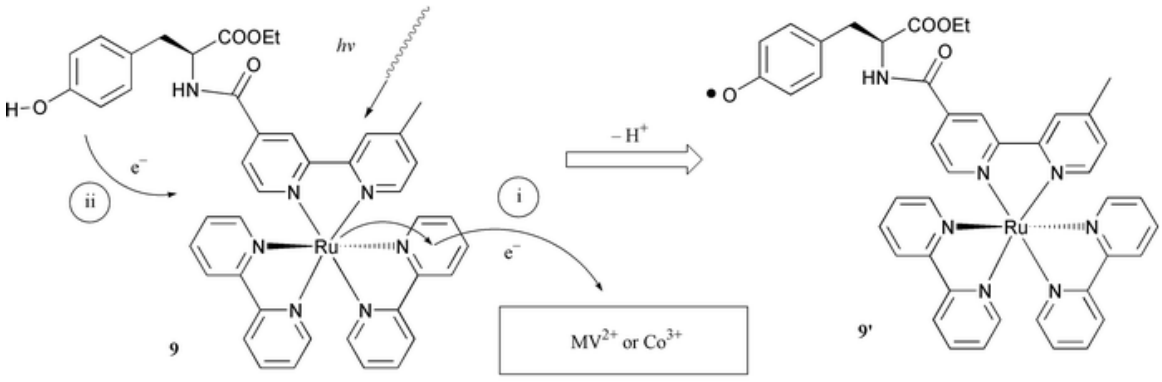

Figure 1.19: *Electron transfer scheme for* ***Ru-Tyrosine*** *in presence of external electron acceptor*[43]

Later on Licheng Sun, Hammarström and co workers have covalently linked a binuclear Mn complex to **Ru-Tyrosine** (Figure 1.20). This complete photocatalytic assembly was supposed to be one of the first examples to mimic the chromophore-electron relay-catalyst ensemble as in photosystem II. The photocatalytic complex was shown to undergo sequential electron transfer processes (Figure 1.20). At the end generation of Mn(II/III) oxidation states was confirmed by monitoring EPR spectra.

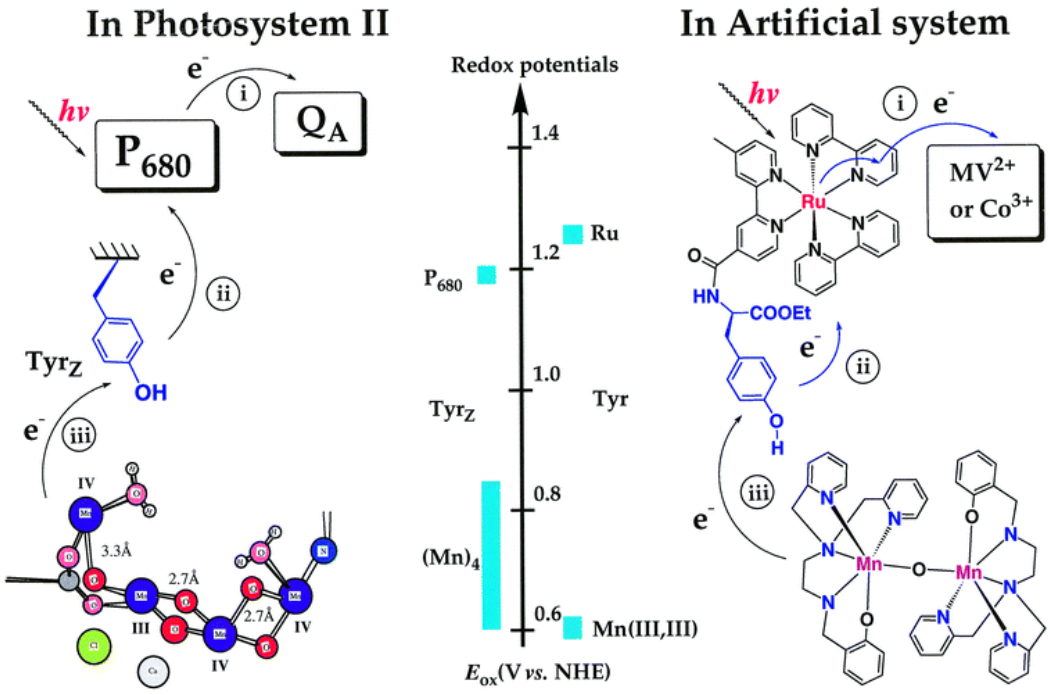

Figure 1.20: *Comparison of electron transfer sequence between photosystem II (left) and artificial system (right); illustrating chromophore, electron relay and Mn complex with respective potentials for each unit.*[40]

But one thing to be mentioned here is that their system had only a tyrosine unit. As already mentioned in the previous sections, photosystem II has tyrosine (TyrZ) alongside histidine

(His190) which is engaged in a hydrogen bond with TyrZ. Therefore the effect of H-bonding and its role for the function of the complete electron relay cannot be concluded.

1.4Objectives of the thesis work

In our group we have tried to overcome the drawback of the **Ru-Tyrosine** complex and we had already reported a family of complexes with a chromophore imidazole phenol motif (Figure 1.21)[44] which mimics more closely photosystem II. These systems had some drawbacks as discussed in the following chapter and therefore we have decided to synthesize new complexes within the same family with some modifications, to mimic PS II more closely than all existing models. The first goal of this work is to try to investigate with these new complexes the electron transfer and proton transfer mechanism, including the importance of H- bonding as observed in natural system.

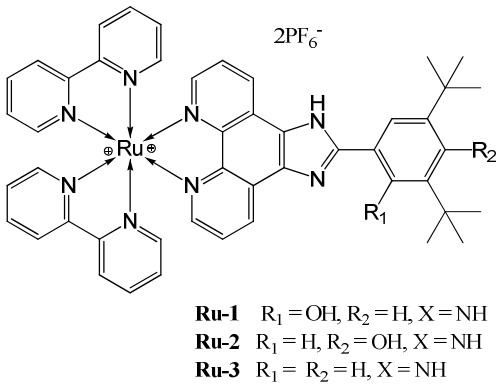

Figure 1.21: *Previously reported complexes from our group.*[44]

A second goal was to covalently link a catalytic unit to our chromophore electron relay system to investigate its function in a complete photocatalyst. This complete photocatalyst, with proper functionalization of the $\mathbf{[Ru(bpy)_3]^{2+}}$ unit, can be grafted on the surface of an electrode to obtain the photoanode of a photoelectrochemical cell (Figure 1.22).

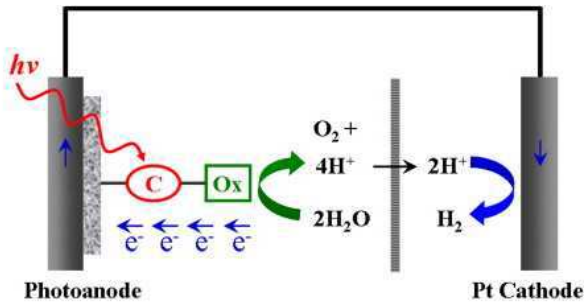

Figure 1.22:*Photoelectrochemical cell showing a photocatalytic system grafted on the anodic surface; c = chromophore, Ox = oxidation catalyst.*[45]

1.5 References

(1) Esswein, A. J.; Nocera, D. G., Hydrogen production by molecular photocatalysis. *Chem. Rev.*,**2007**, *107*, 4022-4047.

(2) Vesborg, P. C.; Jaramillo, T. F., Addressing the terawatt challenge: scalability in the supply of chemical elements for renewable energy. *RSC Adv.*,**2012**, *2*, 7933-7947.

(3) Lewis, N. S., *Workshop on Energy and Transportation***2003**.

(4) Keepin, B., Review of global energy and carbon dioxide projections. *Annu. Rev. Energy*,**1986**, *11*, 357-392.

(5) Jacobson, M. Z., Review of solutions to global warming, air pollution, and energy security. *Energy Environ. Sci.*,**2009**, *2*, 148-173.

(6) Solomon, S.; Plattner, G.-K.; Knutti, R.; Friedlingstein, P., Irreversible climate change due to carbon dioxide emissions. *Proc. Natl. Acad. Sci. U.S.A.*, **2009**, *106*, 1704-1709.

(7) Dincer, I., Renewable energy and sustainable development: a crucial review.*Renew. Sustain. Energy Rev.*,**2000**, *4*, 157 -175.

(8) Eisenberg, R.; Nocera, D. G., Preface: Overview of the forum on solar and renewable energy.*Inorg. Chem.*,**2005**, *44*, 6799 -6801.

(9) Lewis, N. S.; Nocera, D. G., Powering the planet: Chemical challenges in solar energy utilization. *Proc. Natl. Acad. Sci. U.S.A.*, **2006**, *103*, 15729 -15735.

(10) Cook, T. R.; Dogutan, D. K.; Reece, S. Y.; Surendranath, Y.; Teets, T. S.; Nocera, D. G., Solar energy supply and storage for the legacy and nonlegacy worlds.*Chem. Rev.*,**2010**, *110*, 6474 -6502.

(11) Lewis, N. S., Light work with water. *Nature*,**2001**, *414*, 589 -590.

(12) Campagna, S.; Puntoriero, F.; Nastasi, F.; Bergamini, G.; Balzani, V.,*Photochemistry and Photophysics of Coordination Compounds I*; Springer,**2007**, 117-214.

(13) Nelson, N.; Yocum, C. F., Structure and function of photosystems I and II.*Annu. Rev. Plant Biol.*, **2006**, *57*, 521-565.

(14) Andreasson, L.; Vanngard, T., Electron transport in photosystems I and II. *Annu. Rev. Plant Physiol. Plant Mole. Biol.*,**1988**, *39*, 379-411.

(15) Krauß, N., Mechanisms for photosystems I and II. *Curr. Opin. Chem. Biol.*, **2003**, *7*, 540-550.

(16) Mathis, P.; Rutherford, A., The primary reactions of photosystems I and II of algae and higher plants.*Photosynth.*,**1987**, 63-96.

(17) Babcock, G. T.; Barry, B.; Debus, R.; Hoganson, C.; Atamian, M.; McIntosh, L.; Sithole, I.; Yocum, C., Water oxidation in photosystem II: from radical chemistry to multielectron chemistry. *Biochemistry*,**1989**, *28*, 9557-9565.

(18) Rutherford, A., Photosystem II, the water-splitting enzyme*Trends Biochem. Sci.*,**1989**, *14*, 227-232.

(19) Ferreira, K. N.; Iverson, T. M.; Maghlaoui, K.; Barber, J.; Iwata, S., Architecture of the photosynthetic oxygen-evolving center. *Science*,**2004**, *303*, 1831- 1838.

(20) Loll, B.;Kern; Saenger, W.; Zouni, A.; Biesiadka, J.,Towards complete cofactor arrangement in the 3.0 Åresolution structure of photosystem II.*Nature*, **2005**, *438*, 1040 -1044.

(21) Umena, Y.; Kawakami, K.; Shen, J.-R.; Kamiya, N., Crystal structure of oxygen-evolving photosystem II at a resolution of 1.9 Å. *Nature*,**2011**, *473*, 55 -60.

(22) Renger, G.; Renger, T., Photosystem II: the machinery of photosynthetic water splitting. *Photosynth.Res.*, **2008**, *98*, 53-80.

(23) Hocking, R. K.; Brimblecombe, R.; Chang, L.-Y.; Singh, A.; Cheah, M. H.; Glover, C.; Casey, W. H.; Spiccia, L., Water-oxidation catalysis by manganese in a geochemical-like cycle. *Nature Chem.*,**2011**, *3*, 461 -466.

(24) Yano, J.; Kern, J.; Sauer, K.; Latimer, M. J.; Pushkar, Y.; Biesiadka, J.; Loll, B.; Saenger, W.; Messinger, J.; Zouni, A., Where water is oxidized to dioxygen: structure of the photosynthetic Mn_4Ca cluster. *Science*,**2006**, *314*, 821-825.

(25) Murray, J. W.; Maghlaoui, K.; Kargul, J.; Ishida, N.; Lai, T.-L.; Rutherford, A. W.; Sugiura, M.; Boussac, A.; Barber, X-ray crystallography identifies two chloride binding sites in the oxygen evolving centre of Photosystem II. *Energy Environ. Sci.*,**2008**, *1*, 161-166.

(26) Lubitz, W.; Reijerse, E. J.; Messinger, J., Solar water-splitting into H_2 and O_2: design principles of photosystem II and hydrogenases. *Energy Environ. Sci.*, **2008,** 1, 15-31.

(27) Alstrum-Acevedo, J. H.; Brennaman, M. K.; Meyer, T. J., Chemical approaches to artificial photosynthesis 2. *Inorg. Chem.*,**2005**, *44*, 6802-6827.

(28) Graetzel, M., Artificial photosynthesis: water cleavage into hydrogen and oxygen by visible light. *Acc. Chem. Res.*,**1981**, *14*, 376-384.

(29) Morris, A. J.; Meyer, G. J.; Fujita, E., Molecular approaches to the photocatalytic reduction of carbon dioxide for solar fuels. *Acc. Chem.Res.*,**2009**, *42*, 1983-1994.

(30) Gust, D.; Moore, T. A.; Moore, A. L., Solar fuels via artificial photosynthesis. *Acc. Chem.Res.*, **2009**, *42*, 1890-1898.

(31) Bard, A. J.; Fox, M. A., Artificial photosynthesis: solar splitting of water to hydrogen and oxygen.*Acc. Chem.Res.,* **1995**, *28*, 141-145.

(32) Meyer, T. J., Chemical approaches to artificial photosynthesis. *Acc. Chem.Res.,* **1989**, *22*, 163-170.

(33) Ciamician, G., The photochemistry of the future. *Science,***1912**, *36*, 385-394.

(34) Balzani, V.; Carassiti, V., *Photochemistry of Coordination Compounds;*Academic Press,**1970**.

(35) Balzani, V.; Campagna, S.; Accorsi, G. *Photochemistry and photophysics of coordination compounds*; Springer, **2007**.

(36) Kalyanasundaram, K., Photophysics, photochemistry and solar energy conversion with tris (bipyridyl) ruthenium (II) and its analogues. *Coord. Chem. Rev.,***1982**, *46*, 159-244.

(37) Juris, A.; Balzani, V.; Barigelletti, F.; Campagna, S.; Belser, P. l.; Von Zelewsky, A., Ru (II) polypyridine complexes: photophysics, photochemistry, electrochemistry, and chemiluminescence.*Coord. Chem. Rev.,***1988**, *84*, 85 -277.

(38) Ishikita, H.; Loll, B.; Biesiadka, J.; Saenger, W.; Knapp, E.-W., Redox potentials of chlorophylls in the photosystem II reaction center. *Biochemistry,***2005**, *44*, 4118-4124.

(39) Rappaport, F.; Guergova-Kuras, M.; Nixon, P. J.; Diner, B. A.; Lavergne, J., Kinetics and pathways of charge recombination in photosystem II. *Biochemistry,* **2002**, *41*, 8518-8527.

(40) Sun, L.; Hammarström, L.; Åkermark, B.; Styring, S., Towards artificial photosynthesis: ruthenium–manganese chemistry for energy production.*Chem. Soc. Rev.,***2001**, *30*, 36-49.

(41) Sjödin, M.; Styring, S.; Åkermark, B.; Sun, L.; Hammarström, L., Proton-coupled electron transfer from tyrosine in a tyrosine-ruthenium-tris-bipyridine complex: Comparison with tyrosineZ oxidation in photosystem II.,*J.Am. Chem. Soc.,***2000**, *122*, 3932-3936.

(42) Duan, L.; Bozoglian, F.; Mandal, S.; Stewart, B.; Privalov, T.; Llobet, A.; Sun, L., A molecular ruthenium catalyst with water-oxidation activity comparable to that of photosystem II.*Nature Chem.***2012**, *4*, 418-423.

(43) Magnuson, A.; Berglund, H.; Korall, P.; Hammarström, L.; Åkermark, B.; Styring, S.; Sun, L., Mimicking electron transfer reactions in photosystem II: Synthesis and

photochemical characterization of a ruthenium (II) tris (bipyridyl) complex with a covalently linked tyrosine.*J. Am. Chem. Soc.*,**1997**, *119*, 10720 -10725.

(44) Lachaud, F.; Quaranta, A.; Pellegrin, Y.; Dorlet, P.; Charlot, M. F.; Un, S.; Leibl, W.; Aukauloo, A., A Biomimetic Model of the Electron Transfer between P680 and the TyrZ–His190 Pair of PSII.*Angew. Chem. Int. Ed.*,**2005**, *44*, 1536-1540.

(45) McConnell, I.; Li, G.; Brudvig, G. W., Energy conversion in natural and artificial photosynthesis.*Chem. Biol.* **2010**, *17*, 434-447.

(46) Klauss, A.; Haumann, M.; Dau, H., Alternating electron and proton transfer steps in photosynthetic water oxidation. *Proc. Natl. Acad. Sci. U.S.A.*, **2012,***109*, 16035-16040.

2.0 Experimental techniques

This chapter gives the description of experimental techniques that have been used to characterize our complexes. These techniques are:

2.1) Electrochemistry (EC)
2.2) UV-Visible spectroscopy (UV-Vis)
2.3) Fluorescence spectroscopy
2.4) Laser Flash Photolysis (LFP)
2.5) Electron Paramagnetic Resonance (EPR)
2.6) Infrared spectroscopy (IR)

All the chemicals for experiments were used as received from Sigma Aldrich.

2.1 Electrochemistry

Techniques used: Cyclic voltammetry and differential pulse voltammetry

2.1.1 Cyclic voltammetry

Cyclic voltammetry (CV) is a versatile technique most frequently used in all disciplines of chemistry. It is a comparatively easy electroanalytical technique to study electroactive species. Cyclic voltammetry is based on the principle of linear sweep voltammetry. In linear sweep voltammetry the working electrode's potential is swept at a fixed scan rate between initial and final potential values while in CV the working electrode's potential is swept back to perform a reverse scan after reaching a certain potential value (forward and reverse scan, Figure 2.1). Figure 2.1 shows a voltage sweep between V1 and V2, once the voltage reaches V2 the scan is reversed back to V1.

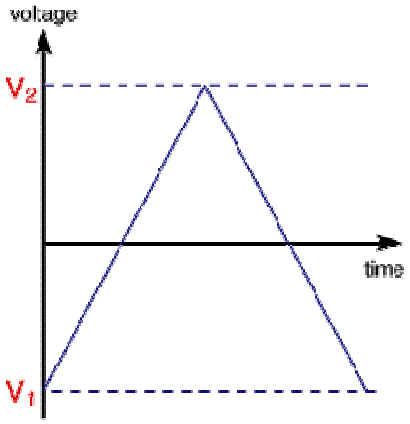

Figure 2.1*: reversible voltage scan between V1 and V2 values at fixed rate.*

Cyclic voltammetry uses a three electrode system consisting of a working electrode, a reference electrode and a counter electrode (Figure 2.2). In order to avoid oxygen interference the sample solution is usually purged with inert gas.

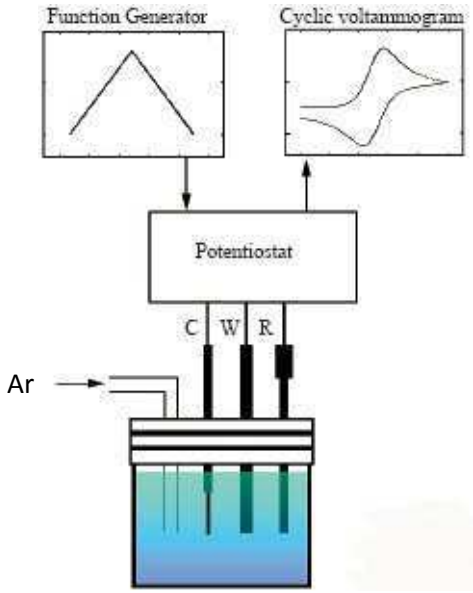

***Figure 2.2**: Typical experimental set up for measurement: R = Reference electrode: Ag/AgCl, W = working electrode: Glassy carbon, C= Counter electrode: Pt wire, Ar = Argon gas*

During operation the potential of the working electrode *vs*. the reference electrode potential is changed linearly versus time (with a scan rate expressed as V/s) and the current is measured between the working electrode and the counter electrode. The obtained result in the form of a plot of current (i) vs. potential (E) is called cyclic voltammogram; a typical cyclic voltammogram is shown in Figure 2.3.

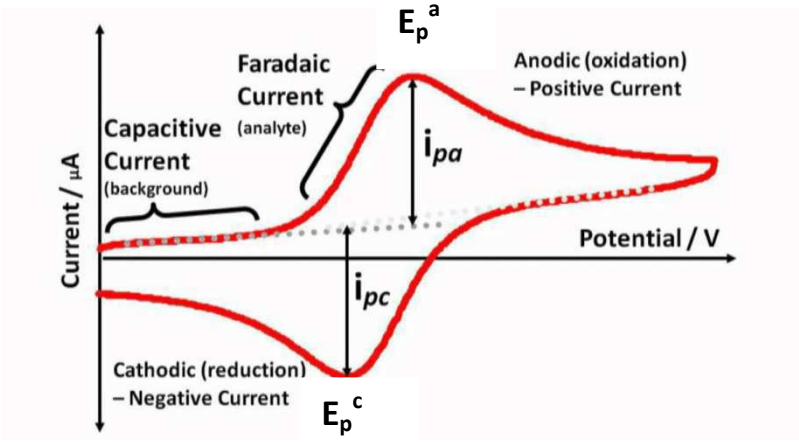

***Figure 2.3:** Typical cyclic voltammogram showing anodic and cathodic peak potentials E_p^a and E_p^c respectively.*

The reversible nature of the cyclic voltammogram in Figure 2.3 is not always the case in many electrochemical reactions. In the reversible case the midpoint potential, termed as "redox potential", can be measured by using the equation,

$$E_{1/2} = {}^{1}/_{2} * (E_p^a + E_p^c)$$

2.1.2 Differential pulse voltammetry (DPV)

Differential pulse voltammetry is similar to normal pulse voltammetry; the only difference lies in the application of pulse potential. In normal pulse voltammetry potential pulses of increasing amplitude are applied while in differential pulse voltammetry pulses with fixed potential steps of small amplitude (generally 10 to 100 mV) are applied superimposed on a slowly varying base potential (Figure 2.4) . The current is measured at two points for each of the pulse *i.e.* before application of the pulse and at the end of the pulse. The difference in respective current values between these two points is determined for each pulse and plotted as a function of potential. A typical differential pulse voltammogram is shown in Figure 2.4.

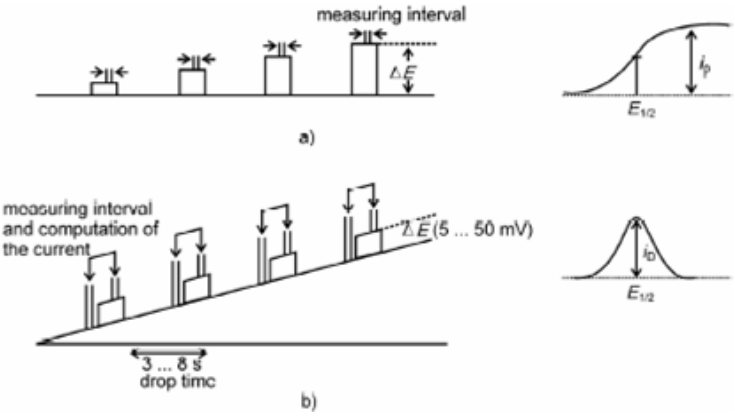

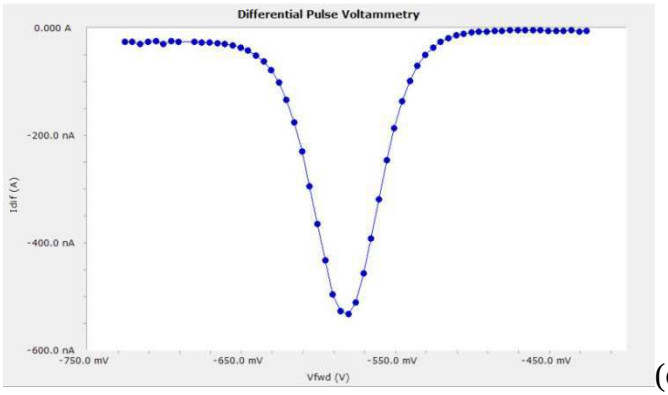

(c)

Figure 2.4: *Pulse application procedure and current potential curves for (a) Normal pulse voltammetry; and (b) Differential pulse voltammetry (c) Typical differential pulse voltammogram*

2.1.3 Experimental

We measured cyclic voltammograms and differential pulse voltammograms using a model 600E CHInstruments potentiostat. All measurements have been performed under an inert (argon) atmosphere. We have used a glassy carbon working electrode, a platinum wire as counter electrode, and a Ag/AgCl reference electrode. Ferrocene was used as a reference in most experiments. The working electrode was polished before each measurement by using 1 µm and 3 µm diamond paste and sonicated in ethanol for a few minutes. Prior to its utilization, the working electrode has been washed again with ethanol and dried with tissue paper. Tetra butyl ammonium hexafluorophosphate (TBAP) was used as a supporting electrolyte and its concentration was maintained at a hundred fold excess compared to the sample. For most experiments the sample concentration was 1.0 mM in acetonitrile. Typically a scan rate of 100 mV/ s was used to measure cyclic voltammograms.

Typical parameters for differential pulse voltammetry were:

Increment in potential = 0.004 V, Amplitude = 0.05 V, Pulse width = 0.05 sec

2.2 Ultraviolet and Visible Absorption Spectroscopy (UV-Vis spectroscopy)

Ultraviolet and Visible absorption spectroscopy is based on the principle of measurement of the amount of light absorbed after passing through the sample. The absorption measurement can be of two types, at particular wavelength or extended over the UV- Visible spectral range (200-800 nm). Some spectrophotometers are equipped to carry out measurement until 1000 nm. The UV-Visible light is quite energetic which is sufficient to enable electronic transitions from lower to higher energy levels within molecules or inorganic complexes in solution. For example, metal to ligand charge transfer transition (MLCT) and ligand to ligand charge transfer transition (LC) can give rise to distinguished absorption bands depending on the concentration and according to spin rule.

A spectrophotometer is used to measure absorption spectra. There are single beam and double beam spectrophotometers. Nowadays double beam spectrophotometers are most frequently used. The double beam UV-Visible spectrophotometer instrumentation scheme is shown in Figure 2.5. It consists of a light source, a monochromator (diffraction grating), sample and reference cells, detector (photomultiplier tube) and recorder (usually a computer, not shown). We have used a Jena Optics Specord 210 spectrophotometer, which is a double beam spectrophotometer.

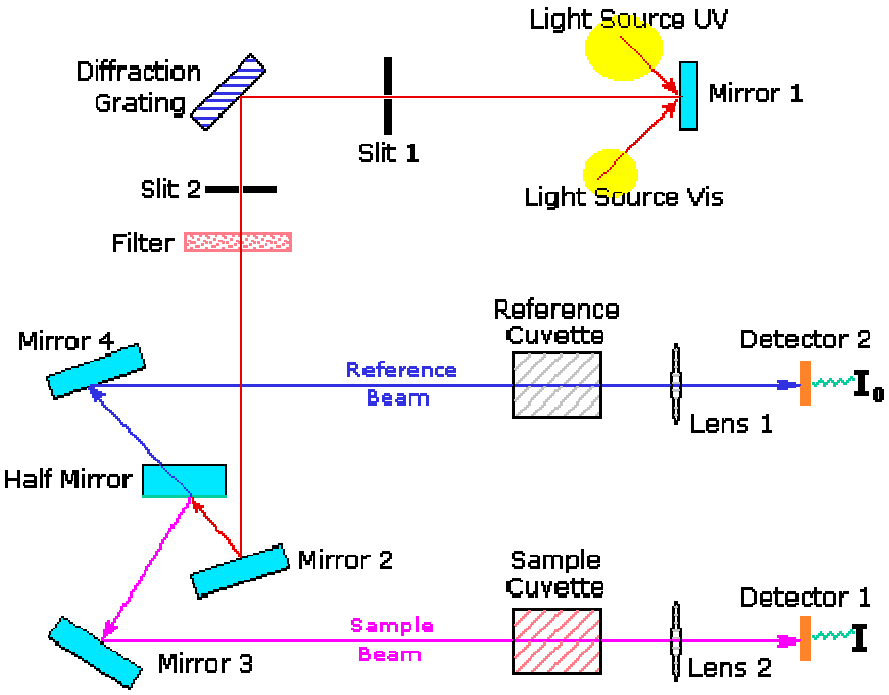

Figure 2.5: *Scheme showing double beam absorbance spectrophotometer*

Quantitative measurement of absorption of light is possible by using Beer Lamberts law.

2.2.1 Beer Lambert's law

Beer-Lambert's law is the combination of Lambert's and Beer's law and considers the relation between absorption of light and the thickness and concentration of solution.

The law states that "there is a logarithmic dependence between the transmission "T", of light through a substance and the product of the absorption coefficient of the substance, "α", and the distance the light travels through the material (i.e. the path length), "ℓ". The absorption coefficient can be written as a the product of the molar absorptivity (extinction coefficient) of the absorber, "ε", and the concentration "c" of absorbing species in the material

In equation form it is can be written as,

$$\log (I_0/ I) = \varepsilon\, c\, \ell \qquad (2.1)$$

This is a fundamental equation of Beer-Lambert's law, since absorbance (A) = log (1_0/I) this equation can be conveniently expressed as,

$$A = \varepsilon c \ell \qquad (2.2)$$

Where,

ε = molar absorptivity of the analyte in L mol^{-1} cm^{-1}

c = concentration of analyte in mol L^{-1}

ℓ = path length of the cell in cm

By using equation 2.2 it is easy to determine the concentration of the sample.

2.2.2 Experimental

Sample concentrations for our measurements of UV-visible spectra are about 50 µM for a 1 cm cell pathlength. The solvent used for the measurement is depending on the counter ion of the complex. The software WinASPECT® is used to visualize obtained absorption spectra.

2.3 Fluorescence spectroscopy

Fluorescence spectroscopy is a kind of electromagnetic spectroscopy which is used to measure fluorescence from a sample. The instrument which measures fluorescence is called fluorometer or fluorimeter.

2.3.1 Fluorescence –the phenomenon

When incident light falls on a substance, it gets absorbed depending on the concentration of analyte and wavelength of incident light in about a femto second (10^{-15} sec) and the atom or molecule is excited *i.e.* an electron moves from the ground singlet state to an excited singlet state. Several phenomena may occur after excitation of an electron from ground state to excited singlet states (Figure 2.6). The excited electron either can relax back to the ground state by following non radiative pathways or it can emit light (radiative pathways). The emissive pathway for decay from a singlet excited state is termed fluorescence. Sometimes electron in the excited singlet state undergo relaxation via intersystem crossing before emitting light to ground state and this process is called phosphorescence.

Fluorescence is fast, usually occurring in few nanoseconds time scale while phosphorescence is relatively slow and generally has lifetimes ranging from microseconds to seconds.

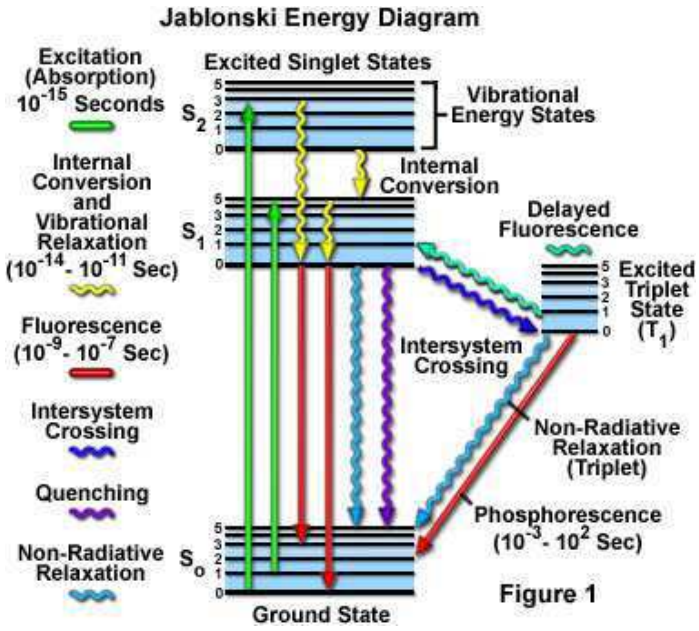

Figure 2.6: *Jablonski energy diagram*

We have used a Varian Eclipse fluorimeter to measure steady-state emission spectra. The general instrumental scheme is described in Figure 2.7. Fluorescence light has lower energy than incident light.

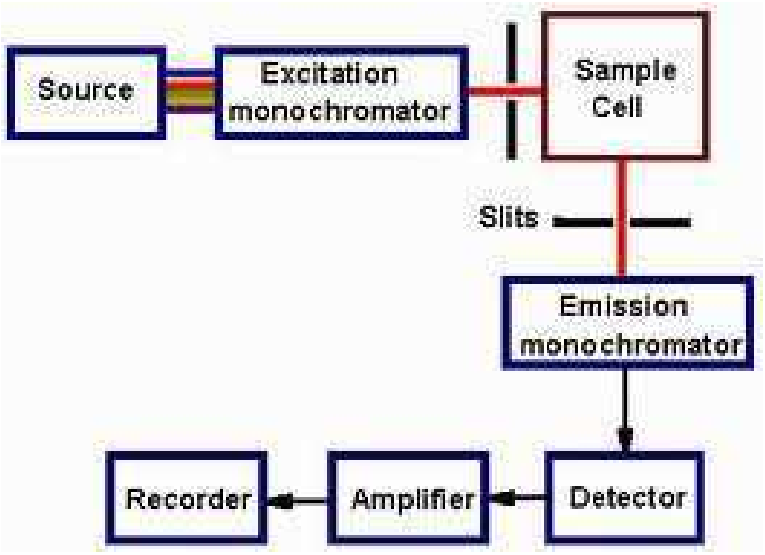

Figure 2.7: *Scheme showing different elements of fluorimeter*

This fluorimeter can be used to measure emission spectra by exciting at a particular wavelength or to measure excitation spectra by performing a scan of excitation wavelengths for a particular emission wavelength.

2.3.2 Experimental

We used this fluorometer to perform pH titrations by measuring emission spectra at different pH. We also employed it to determine quantum yields of emission for complexes by comparing their emission with that of a standard.

2.4Electron paramagnetic resonance (EPR)

Chemical species that have one or more unpaired electrons, such as organic and inorganic free radicals or inorganic complexes possessing a transition metal ion are studied by using Electron paramagnetic resonance (EPR) or electron spin resonance (ESR) spectroscopy. This technique was invented by Zavoisky in 1944.

Electron spin resonance is a branch of absorption spectroscopy in which paramagnetic substances cause absorption of microwaves which induce transitions between magnetic energy levels of electrons with unpaired spins. A magnetic field is applied in order to introduce magnetic energy splitting.

When a strong constant magnetic field H is applied to the unpaired spins of electrons a torque acts to make the electron dipoles line up either parallel or antiparallel to the direction of the magnetic field. For electron spins which are parallel in the field, E = μH, whereas, for those which are aligned antiparallel, E = - μH as shown in Figure 2.8.

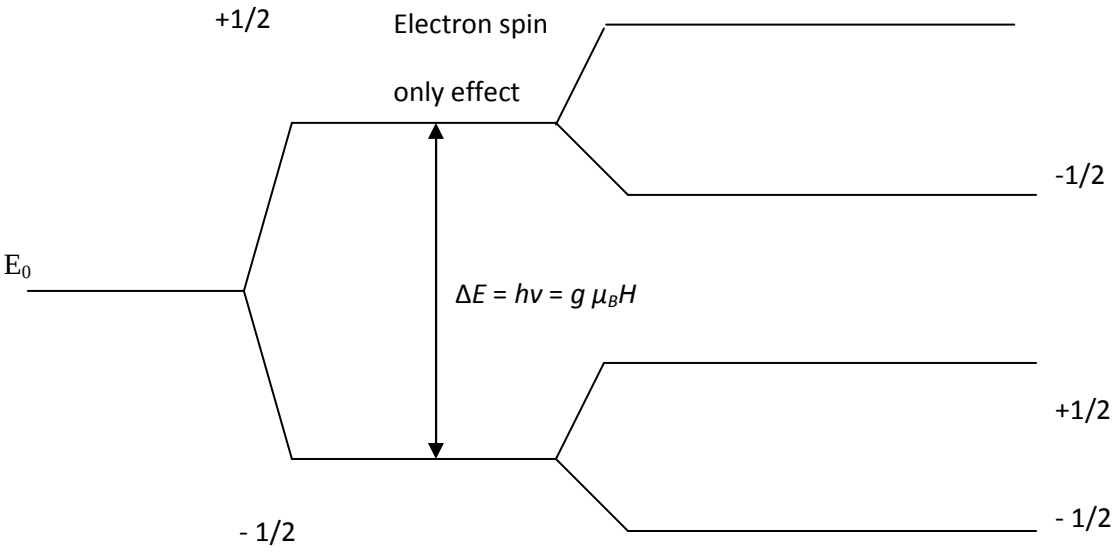

Figure 2.8: *Energy level splitting in EPR*

Electron spin resonance spectra are a result of transition from one spin state to the other state of an electron. The splitting pattern of the ESR spectra is governed by hyperfine splitting. Hyperfine fine splitting arises by the interaction between the spinning electrons and neighbouring spinning magnetic nuclei.

2.4.1 Zeeman effect

The Zeeman effect is named after the Dutch physicist Pieter Zeeman. In presence of static magnetic field atomic energy levels split into number of levels and the spectral lines are also split. This splitting is called the Zeeman effect. Transitions between different sub levels are governed by selection rules. This effect can be used as a measure of the magnetic field since the distance between sub levels is a function of magnetic field. Therefore Zeeman effect has important application in the spectroscopic techniques where magnetic field is applied like Electron Paramagnetic Resonance (EPR), Nuclear Magnetic Resonance (NMR), Magnetic Resonance Imaging (MRI).

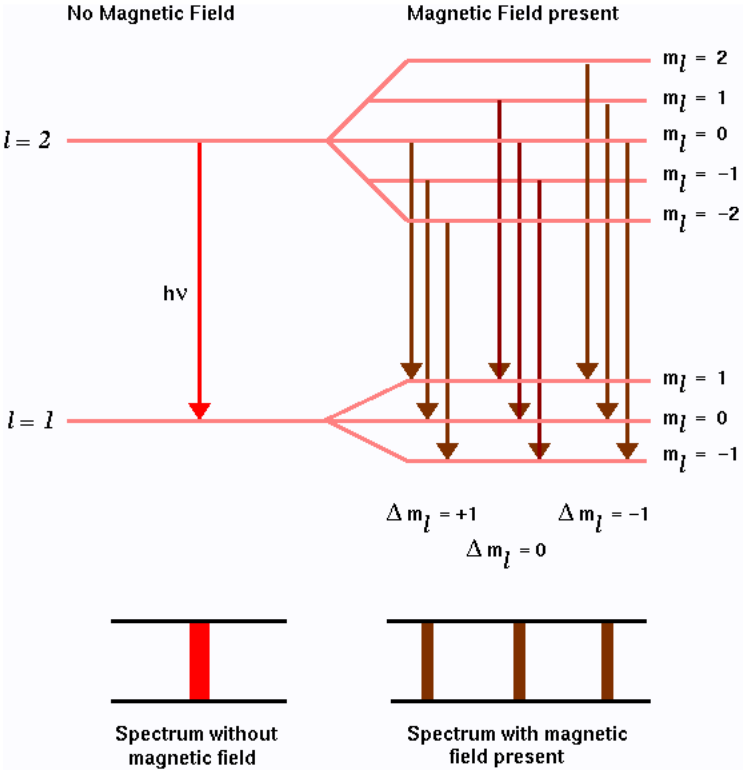

Figure 2.9: *Spectral splitting in the applied magnetic field, Zeeman effect*

During transitions between sub-atomic levels the electron follows selection rules (Δl = +/- 1). The allowed atomic transitions from l=2 to l=1 level are shown in the Figure 2.9 (l= angular quantum number).

In normal Zeeman effect the emission line splits into a triplet of equally spaced lines as predicted. But in experiments one observes more than three spectral lines. This is called anomalous Zeeman effect which is due to the existence of the electron spin.

2.4.2 Experimental

We used ESR spectra to detect transient species which are formed after an electron transfer reaction. These transient species can be either organic radicals or certain oxidation states of transition metal ions. These species were generated by using irreversible sacrificial electron acceptors like 4-Nitrobenzenediazonium tetrafluoro borate (diazonium salt). As the lifetime of the generated species is very short we freeze the samples in the EPR tube in dry ice before measuring the spectrum. The obtained splitting pattern tells us the nature of the generated transient species.

2.5Laser flash photolysis (LFP)

2.5.1 Principle

Flash photolysis technique was developed by George Porter and Norris in 1949. Laser flash photolysis is an important technique to study transient species in chemical and biological systems generated by laser pulses.

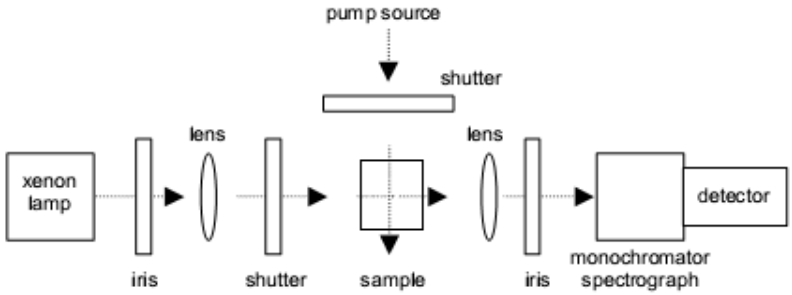

Figure 2.10:*Principle layout of a Laser flash spectrophotometer*

The experimental principle is depicted in Figure 2.10. When the laser light is absorbed by the sample a high concentration of electronically excited molecules is produced. These excited molecules are generally unstable and decay to the stable ground state. Transients and products that are formed during the lifetime of the excited state have characteristic absorption spectra. Formation and decay of transient species can be measured by kinetic traces. For that purpose

a monochromator and a photomultiplier tube (PMT) as a detector are used (Figure 2.11). The detector can be a PMT or a gated CCD camera depending on the kind of measurement performed either, kinetic or spectral, respectively.

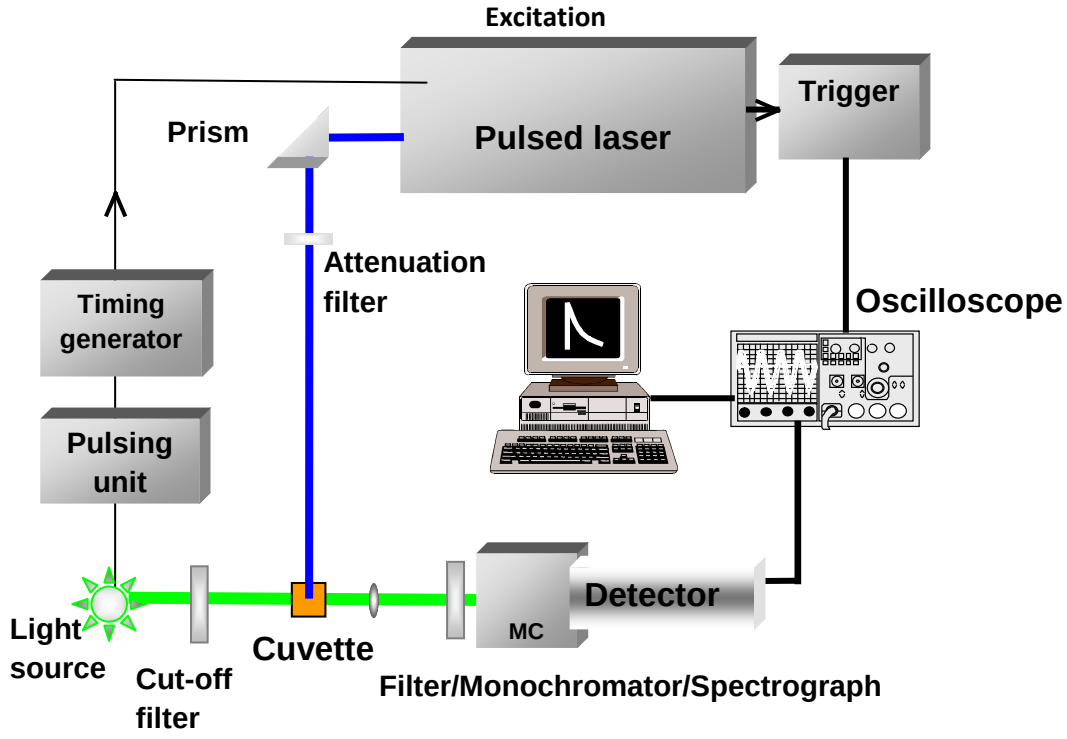

Figure 2.11: *Set up of laser flash photolysis with nanosecond pulsed laser (430 -650 nm) as excitation source, a pulsed Xenon lamp as measuring light source and a photomultiplier tube (PMT) or CCD camera as detector*

2.5.2 Experimental

We have used an Edinburgh Instruments LP 920 flash photolysis spectrometer system (Figure 2.12) for transient absorption kinetics and time-resolved spectral measurements. These measurements allow to characterize the excited state properties of the complexes and an intramolecular electron transfer process from the ligand to Ru(III). Our instrumental setup incorporated a Continuum Surelite optical parametric oscillator (OPO) for sample excitation (~5 ns pulse duration). The OPO was pumped by a Continuum Q-switched Nd:YAG laser operating at 355 nm. The laser energy was typically 4 mJ per flash. For $[Ru(bpy)_3]^{2+}$ based complexes we have used 460 nm as wavelength for excitation. The LP 920 was equipped with a 450 W pulsed Xenon arc lamp for the probe light. Detection of the signal was performed either by a PMT (Hamamatsu) or a water-cooled ICCD camera (Andor). The changes in absorbance (ΔA) are measured with correction for emission and probe background whenever

necessary. The software L900 provided with the LP920 was used to record and view spectra and kinetic traces.

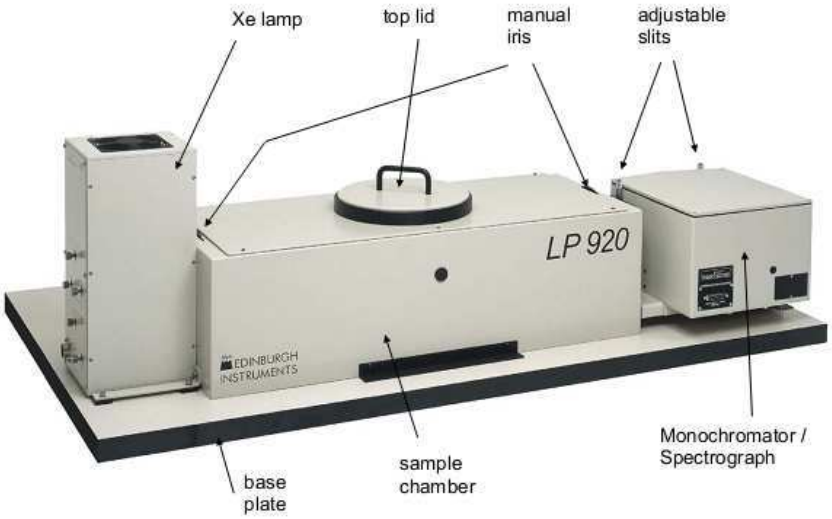

Figure 2.12: *Edinburgh Instruments LP 920 flash photolysis spectrometer system*

2.5.3 Sample preparation

For all UV-Vis measurements a 1 cm quartz cuvette were used. The cuvette were sealed with a rubber septum to allow to purge the samples with Argon (Figure 2.13 a). Purging with the inert gas Argon allows to avoid interference from molecular oxygen since oxygen is a good triplet quencher and electron acceptor. Most of the absorption experiments were carried out at 30 µM complex concentration in acetonitrile.

2.5.4 Electron acceptors

We have used reversible electron acceptors like methyl viologen (MV^{2+}, Figure 2.13 b), ruthenium (III) hexamine trichloride as well as irreversible electron acceptors like sodium persulfate, 4-Nitrobenzenediazonium tetrafluoro borate (diazonium salt) and cobalt-pentamine. When working with sodium persulfate and ruthenium (III) hexamine trichloride a sufficient amount of water was present (1:1 acetonitrile: water) to avoid solubility problems.

(a)  (b)

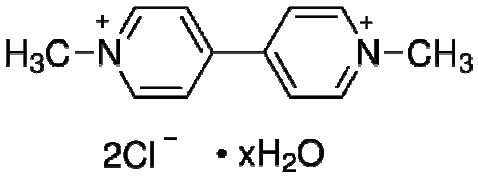

Figure 2.13: *a) cuvette 1 cm with rubber septum b) methyl viologen*

2.5.5 Data analysis

Data analysis is an important and crucial part in the treatment of obtained data. The software L900 was used to fit simple kinetic traces otherwise data were exported into Origin and plotted to fit kinetic traces using appropriate equations.

2.6 Infrared spectroscopy

Infrared spectroscopy (IR spectroscopy) is an analytical technique useful for characterization of functional groups and bonding interactions in chemical substances. IR spectroscopy is a vibrational spectroscopy. Absorption of IR radiation leads to excitation of vibrational modes of chemical bonds which give rise to characteristic absorption bands yielding an IR absorption spectrum. Absorption bands in the IR spectra correspond to characteristic functional groups and bonds present in the chemical substance. Therefore an IR spectrum is a fingerprint for identification of a particular chemical compound. The wavelength of IR spectra is ranging from 2.5 to 25 µm (*i.e.* 4000 to 400 cm^{-1}).

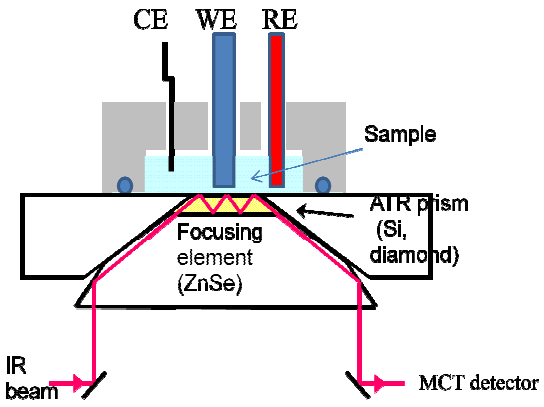

Figure 2.14*: Setup using an ATR prism for IR spectroelectrochemistry*

2.6.1 Experimental

We have used a Nicolet Infrared spectrometer to measure IR absolute spectra. We also performed experiments using differential infrared spectroscopy recoding the spectral difference induced by either photochemistry or electrochemistry. For Infrared spectroelectrochemistry we have mounted a three electrode systems (similar to cyclic voltammetry measurement) on the attenuated total reflection (ATR) prism (Figure 2.14)

2.7 References

1. Compton, R. G.; Banks, C. E., *Understanding voltammetry*; World Scientific, **2007**.
2. Vielstich, W., *Cyclic voltammetry*; Wiley Online Library,**2010.**
3. Skoog, D. A.; Holler, F. J.; Nieman, T. A., *Principles of instrumental analysis.***1998**.
4. Lakowicz, J. R., *Principles of fluorescence spectroscopy*; Springer, **2009**.
5. Willard, H. H.; Merritt Jr, L. L.; Dean, J. A.; Settle Jr, F. A., *Instrumental methods of analysis.***1988**.

3.0 Artificial mimics of TyrZ / His190 electron relay of photosystem II

3.1 Introduction

The amino acids tyrosine and histidine (Figure 3.1) play vital roles in several enzymatic reactions due to their redox activity.[1] A "tyrosine-histidine" couple (Figure 3.2) acts as an electron relay in Photosystem II (PS II).[2,3] The functioning of this electron relay in PS II is subject of numerous studies[4-7] using various biophysical techniques as well as site-directed mutagenesis and theoretical calculations.[8-11] One difficulty is related to the proximity of this amino acid couple to the oxygen evolving complex (OEC), the presence or absence of which modifies its function.[12,13]

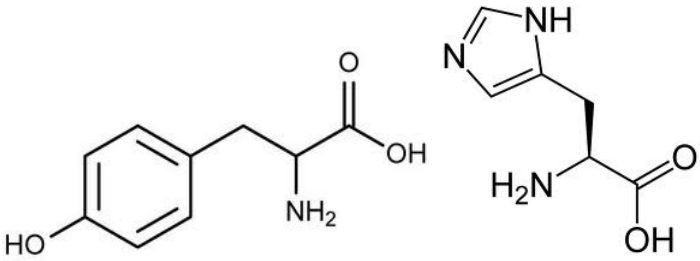

Figure 3.1: *Structures of tyrosine and histidine*

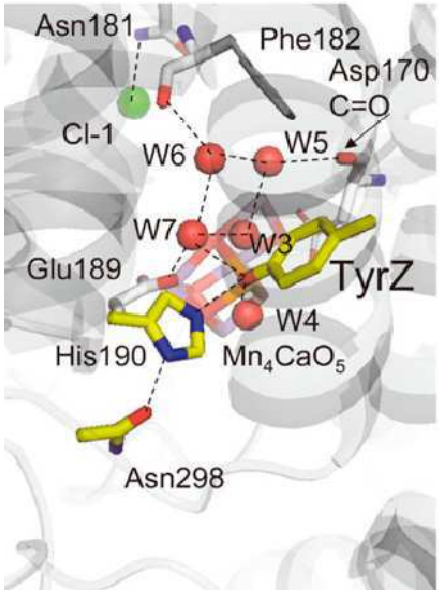

Figure 3.2: *H-bond network around TyrZ. Red and green spheres indicate water O and Cl atoms, respectively.*[3]

Mimicking the chromophore-electron relay in simpler, synthetic complexes permits to study the essential functional properties.[14,15] In the natural system the electron transfer reaction is governed by a difference in redox potentials between P680and TyrZ to make the reaction thermodynamically feasible. The respective redox potentials in the natural system are difficult to determine and not well known. In the synthetic approach these features can be more easily measured and also modified in a controlled manner.

In chemical mimics activation of the two units, imidazole and phenol, is mainly studied separately and less as a functional couple. Most studies on biomimetic complexes concentrate on the phenol unit and neglect the intimate connection with the imidazole unit. Indeed, phenol oxidation is nowadays intensively investigated as model reaction for the phenomenon of the proton coupled electron transfer (PCET). Before going to see some more information concerning PCET we would like to mention one example which concerns the connection between imidazole and phenol.

Moore and coworkers reported on a bioinspired construct based on a porphyrine macrocycle attached to an imidazole-phenol couple.[14] The low temperature D band EPR spectra demonstrated occurrence of a charge separated state and formation of a phenoxyl radical. With a similar complex they have performed another study to observe the effect of protonation state on the imidazole unit and the importance of the hydrogen bond between imidazole and phenol.[16] These authors concluded that in presence of base, when phenol is deprotonated, though H-bonding exists, its potential was too low to be thermodynamically able to drive water oxidation.

The phenol is the active functional group of tyrosine (Figure 3.1). The proton dependent equilibria can be studied by altering the pH of the solution. Thus proton dependent equilibria in phenols lead to the variation in the electrochemical properties (Figure 3.3).[17] This allows to predict mechanistic details concerning proton coupled electron transfer reaction of phenols. An important parameter in this context is the pK_a of tyrosine which is 10.3 for neutral and -2 for oxidized tyrosine[18]. For a pH in between these values the apparent standard potential of phenol is pH dependent with a slope of -60 mV per pH unit.

One point that can be noted here is that the study of isolated phenols can give only an idea about its individual redox chemistry which might not be identical to the redox chemistry at work in more complex ensembles (either biological or synthetic).

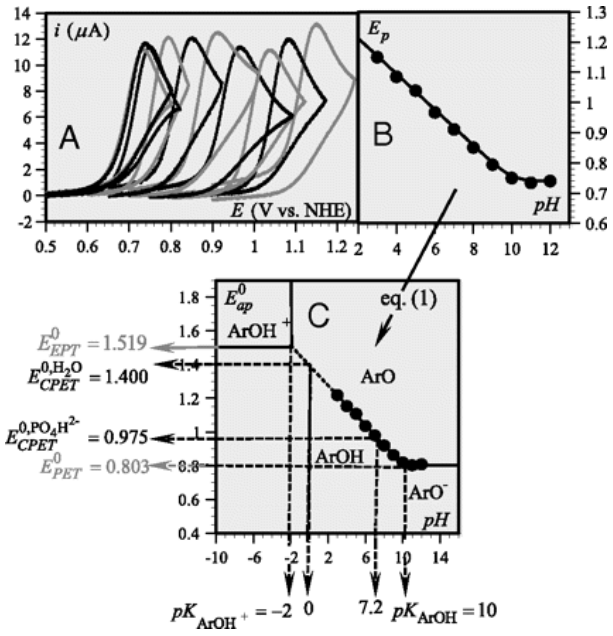

Figure 3.3: *Determination of thermodynamics of phenol oxidation: (A) cyclic voltammetry of 0.2 mM phenol as a function of pH (B) peak potential (in V vs NHE) as a function of pH (C) variation of apparent standard potential with pH, showing zones of thermodynamic stability of various species and* pK_a [17]

When tyrosine had been attached covalently to a **[Ru(bpy)$_3$]$^{2+}$** chromophore by Hammarström and his co-workers they were able to show intramolecular oxidation of the tyrosine by oxidized Ru(III) created by excitation with a laser flash in presence of a sacrificial electron acceptor.[19,20] On the same supramolecular complex (Figure 3.4) they have investigated pH dependent oxidation rates.[21,22] For pH below pK_a of tyrosine (pH < 10) the rate of electron transfer increased with pH and became independent of pH above pH 10. However, the slope of the increase of ET rate with pH was only about half that expected. They have concluded that electron transfer from tyrosine to chromophore occurs via concerted electron transfer proton transfer (CEP) mechanism (Scheme 3.1). Furthermore in 2012 a new study concerning similar complexes but with varying strength of Ru(III)/Ru(II) oxidant was published.[15] In this study four mechanistic regimes could be identified: Electron transfer followed by proton transfer (ETPT), concerted electron-proton transfer (CEP), proton transfer followed by electron transfer (PTET) and electron transfer (ET), all with different slope of rate *vs.* pH. From these and a series of related studies it must be concluded that the mechanism of PCET in such systems is not yet clearly understood.

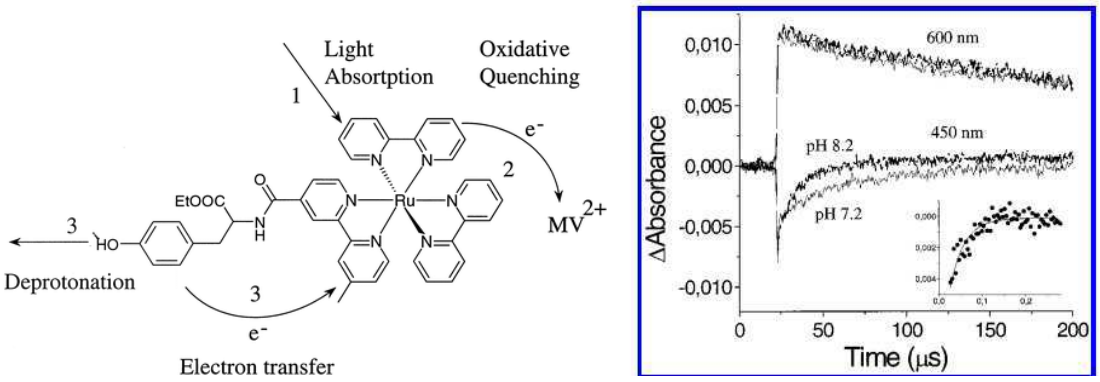

Figure 3.4:Ru-Tyrosine *complex (Left); Transients at 450 nm monitoring the recovery of ruthenium ground state absorption after excitation and oxidative quenching and at 600 nm, monitoring the formation and decay of* $MV^{\bullet+}$ *radical absorption. Kinetic traces at pH 7.2 and pH 8.2 reflects increase in electron transfer rate at higher pH (right).*[19, 22]

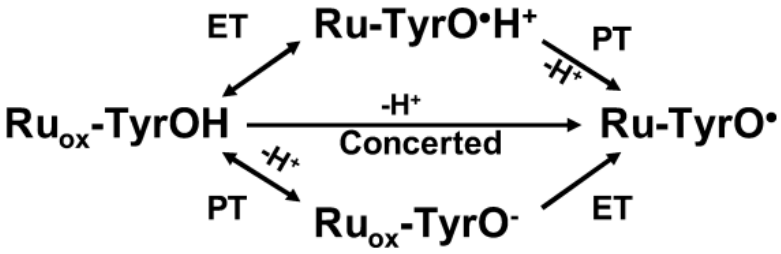

Scheme 3.1: *PCET mechanism for* ***Ru-Tyrosine***

We have already introduced the concept of synthetic artificial mimics using tyrosine-histidine as an electron relay and a series of complexes with a hydrogen-bonded imidazole-phenol couple has been synthesized and published in the lab before (Figure 3.5).[23] This has been the first approach to mimic this feature of natural PS II.

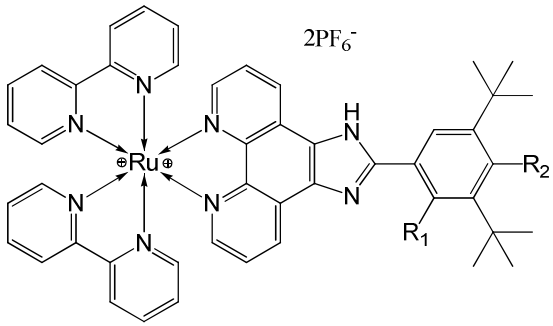

Ru-1 $R_1 = OH, R_2 = H, X = NH$
Ru-2 $R_1 = H, R_2 = OH, X = NH$
Ru-3 $R_1 = R_2 = H, X = NH$

Figure 3.5: *Previously studied complexes*

In aqueous solution all three complexes of this series were able to perform fast electron transfer from the ligand to the chromophore after photoactivation.[23] From a kinetic point of view all complexes seemed to work equally well, whether the phenol group was in *ortho* or *para* position and even in absence of a phenol function. In addition, the importance of an internal hydrogen bond, postulated as an essential feature for function of the electron relay in PS II was not put in evidence. But the main drawback of these complexes lies in the redox potential of the ligand. Due to the presence of strongly electron donating *tert*-butyl groups on the phenol the oxidation potentials of the ligands were quite low, with 0.58 and 0.38 V vs SCE for *ortho* and *para*-phenol, respectively. Together with a Ru(II)/Ru(III) potential of 1.3-1.4 V this yielded a large driving force for the internal electron transfer reaction. This is problematic for two reasons. First, as shown by Hammarström *et al*. the mechanism of PCET changes with the driving force of the reaction.[15] Second, a large driving force is not a good model for the situation in PS II, which is specifically optimized to drive water oxidation with very low overpotential and where the redox potential difference between P680 and TyrZ is only 150 mV.[24] Figure 3.6 shows proton coupled electron transfer in PS II.

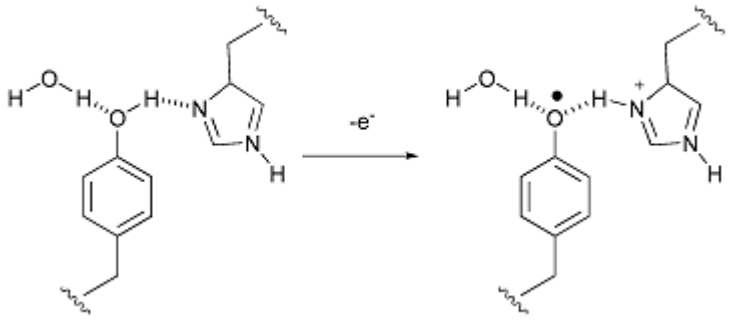

Figure 3.6: *Proton coupled electron transfer in photosystem II* [2]

In the previously reported complexes no detailed study of PCET had been performed and probably it was futile to study because of the high driving force for ET due to the low redox potential of the ligand. The main objective of this work was to increase the redox potential of the ligand to make it compatible with driving the water oxidation reaction thereby approaching the situation in the natural system. This implies using phenol groups without the strongly electron donating *tert*-butyl groups. We thought of synthetic modification of the phenol ring by less electron donating methyl substitutions which might be expected to result in higher redox potentials of the ligand compared to the previous *tert*-butyl substituted versions. In fact, we would not expect to see the potential of the Me-substituted phenol groups

very different from unsubstituted phenols since methyl substituents hardly affect the redox properties of the ligand. Once we have suitable complexes in our possession we will try to characterize ligand oxidation in these systems focusing on the issue of hydrogen bonding and giving emphasis on the proton coupled electron transfer and the role of the imidazole group as internal base. Additional control complexes are also synthesized.

Together with collection of control samples these studies should give us sufficient information concerning

1) The effect of H-bonding on the electrochemical and electron transfer properties
2) The effect of individual functional group either imidazole or phenol
3) The effect of distance and conjugation between chromophore and oxidizable ligand

3.2 Synthesis of complexes and their characterzation

We have synthesized a series of complexes by using a similar synthetic methodology as that for the previous complexes **Ru-*tert*-imi-phOH**[23] and our complexes with H-bonding on the ligand part were obtained with higher yields. This H-bonding on the ligand part (between nitrogen of imidazole and phenolic hydrogen) resembles that observed in photosystem II.[25] The reaction Scheme 3.2 shows our synthetic strategy to synthesize our complexes. The starting material is 1, 10- phenanthroline which upon oxidation in highly acidic media forms phendione.[26] This is the major intermediate to undergo a Steak and Day reaction[27] with respective aldehydes functionalized with methyl substituents at different positions with respect to the phenolic –OH group. The condensation reaction leads to the formation of our ligand[28] which then has to undergo metallation with ruthenium. For that purpose we used ruthenium bisbipyridyl chloride which is synthesized according to literature procedure.[29] The chloride units in ruthenium bisbipyridyl chloride are harder to undergo reaction and would need higher temperatures. Therefore, we replaced these chlorides with $-NO_3$ by stirring the solution of silver nitrate in methanol. Eventually the reaction with the ligand formed the desired coordination complex and further precipitated as PF_6 salt using ammonium hexaflurophosphate. Each complex has undergone a purification procedure whenever necessary by column chromatography and was characterized by Nuclear magnetic resonance (NMR) spectroscopy and mass spectrometry (MS) (see Experimental part for details).

Three complexes have been synthesized which differ with respect to the position of the methyl (Me) substitution on the phenol: **Ru-3Me**, **Ru-4Me** and **Ru-6Me** (Figure 3.7). The rational for this was to observe eventual differences in the electronic properties. In particular Me substitution on position 6 could lead to steric hindrance with twisting of the phenol ring and result in weakening of the H-bonding between the imidazole "N" and phenolic "H".

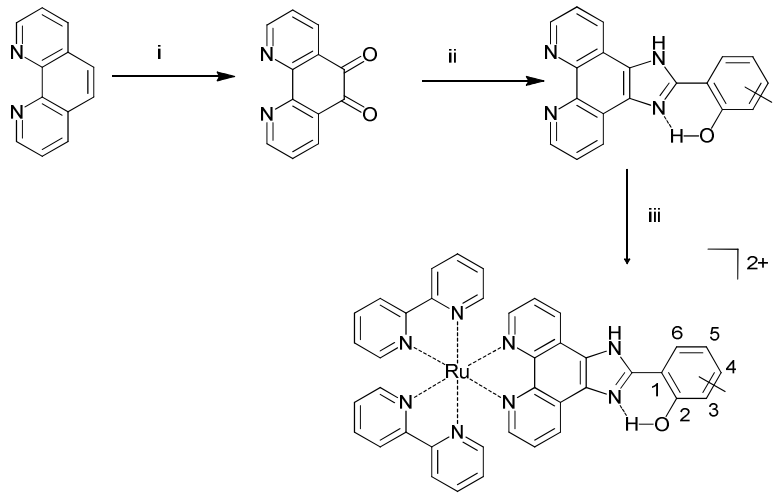

Scheme 3.2: *Synthetic pathway for* ***Ru-xMe*** *complex: Conditions: (i) Conc. H_2SO_4, Conc. HNO3, NaBr, 5h, 160 °C (ii) CH_3COOH, methyl salicylaldehyde, NH_4OAc, 3 h, 100 °C; (iii) MeOH, $Ru(bpy)_2Cl_2$*

To answer the question whether a methyl group substituent on the phenol ring modifies its electron transfer properties another complex without methyl group, **Ru-imi-phOH** has been synthesized using salicyaldehyde as a precursor in the Steak and Day reaction[27] (Figure 3.7).

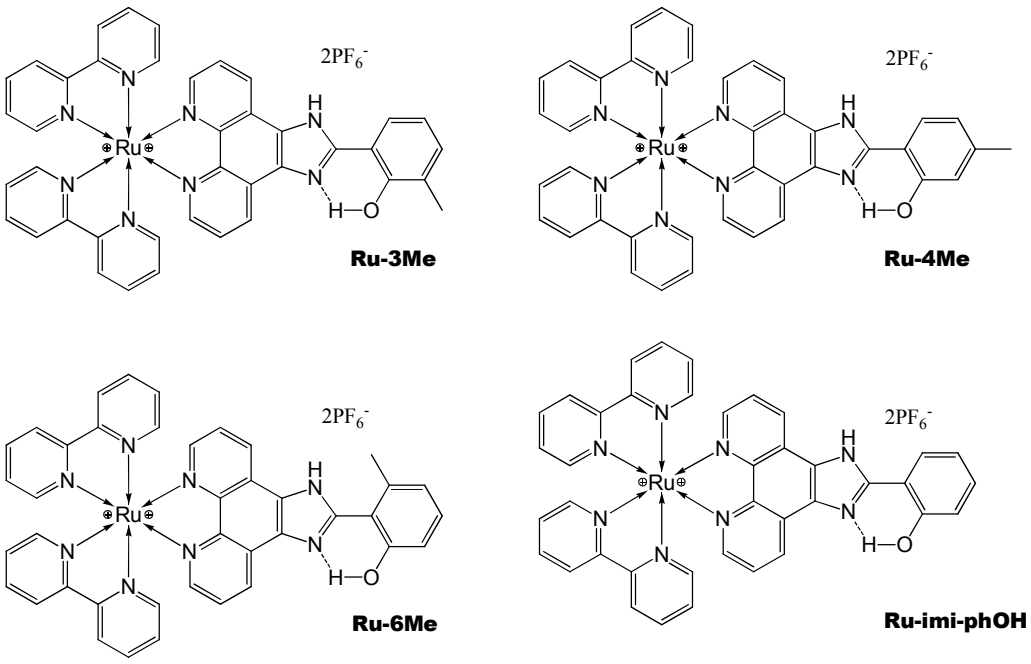

Figure: 3.7*: Complexes* ***Ru-3Me****,* ***Ru-4Me****,* ***Ru-6Me*** *and* ***Ru-imi-phOH*** *showing chromophore- electron relay system with H-bonding.*

As further reference samples for **Ru-3Me**, **Ru-4Me**, **Ru-6Me** and **Ru-imi-phOH,** we have used two other complexes, **Ru-imi** and **Ru-cT-phOH**[30], both with only one reactive functional group, either imidazole or phenol, respectively (Figure 3.8).

The **Ru-cT-phOH** was available from a previous study in our group.[30] **Ru-imi** was synthesized by replacing methyl salicyladehyde with benzaldehyde in the second step of the reaction Scheme 3.2 while other reactants and conditions were the same.

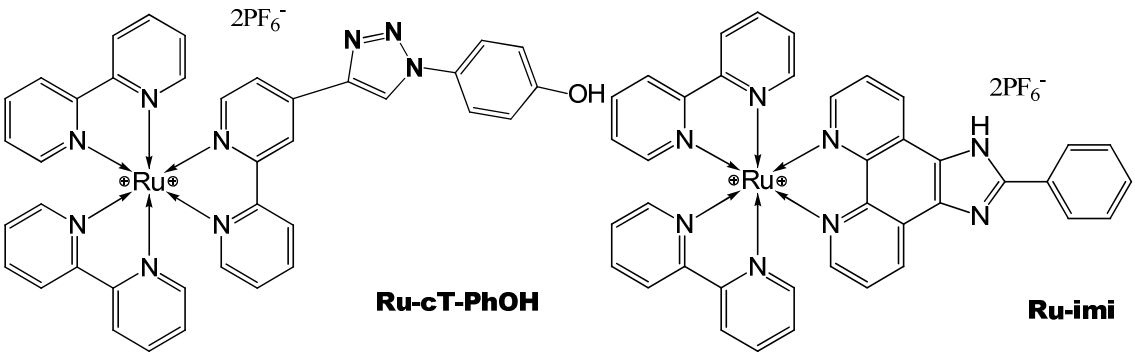

Figure 3.8: *Complexes as a control with individual functional group i.e. either imidazole or phenol*

Furthermore, we thought useful to use for comparison a system without protonatable group on the ligand. Therefore we have synthesized complex **Ru-Et-imi** by replacing the hydrogen present on the imidazole by an ethyl ($-C_2H_5$) group (Figure 3.9).

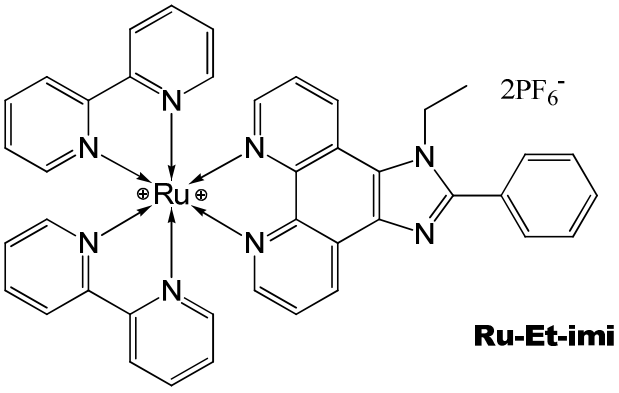

Figure 3.9: *Complex **Ru-Et-imi** synthesized to observe the importance of proton on the imidazole*

The entire chapter is based on the above mentioned complexes which are summarized in Chart 3.1.

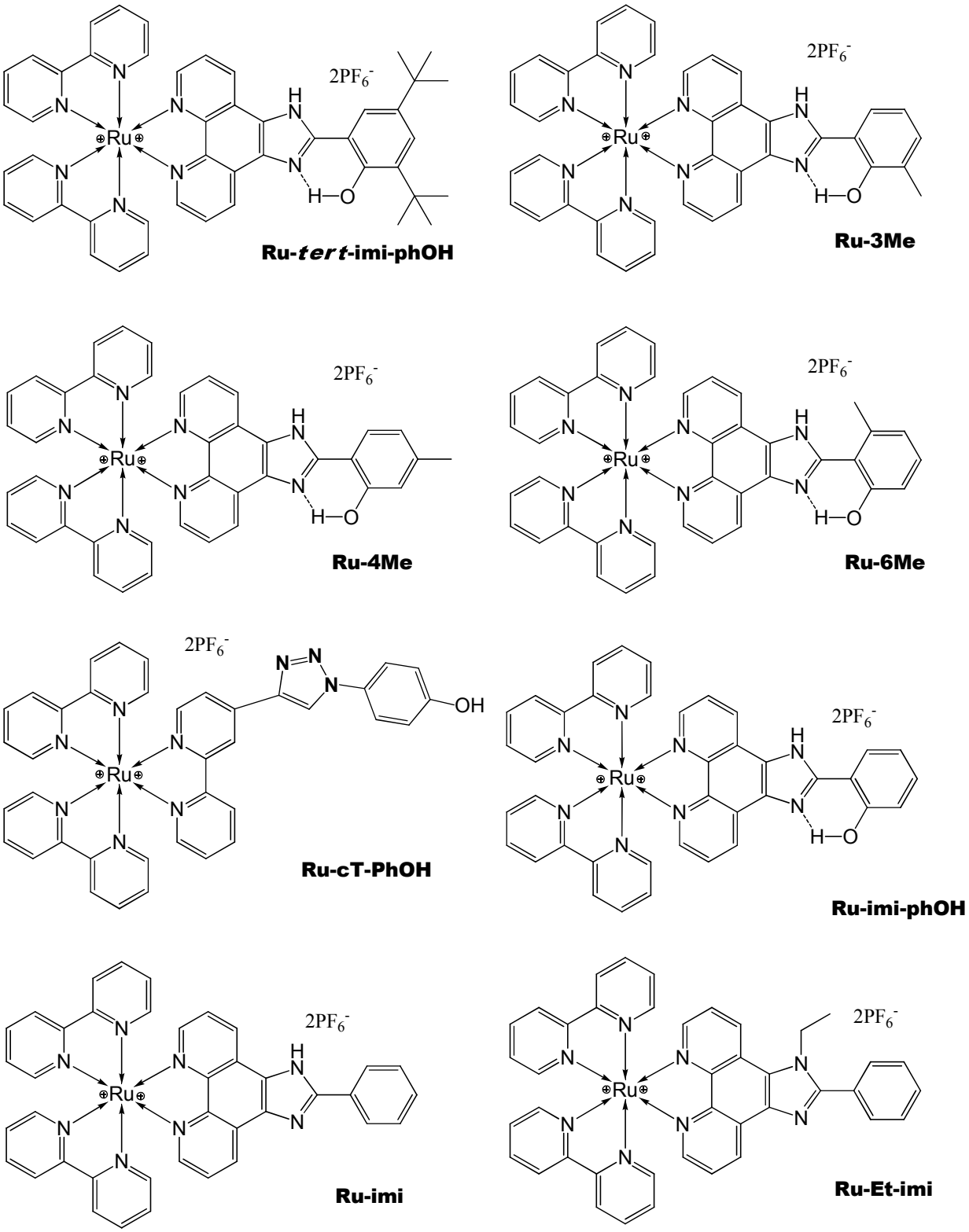

Chart 3.1: *Complexes studied in this chapter*

3.3 Electrochemistry

Replacement of strongly electron donating *tert*-butyl groups with moderately electron donating methyl groups is expected to impart drastic changes in the redox potential for the ligand for **Ru-xMe** compared to **Ru-*tert*-imi-phOH**. Thus in order to verify the redox potential of the ligands of our newly synthesized complexes, **Ru-xMe,** we have measured their electrochemical properties using cyclic voltammetry (CV) and differential pulse voltammetry (DPV).

Cyclic voltammetry and differential pulse voltammetry were performed with a CHI 600E potentiostat (CH Instruments) using a glassy carbon working electrode, a Ag/ AgCl reference electrode and a platinum wire counter electrode in a conventional three-electrode cell. Most of the time ferrocene was used a reference and potentials given in the following are *vs* Fc. Anhydrous acetonitrile was used as a solvent for electrochemical measurements. The supporting electrolyte was 100 mM tetrabutylammoniumhexafluorophosphate (TBAP), and the solution was deoxygenated by bubbling with argon. The working electrode was cleaned between experiments by polishing with a diamond paste and sonication in ethanol. A sample concentration of 1 mM was used. The voltammograms were measured at a scan rate of 100 mV/s.

The cyclic voltammograms of the **Ru-xMe** samples (Figure 3.10) resemble typical voltammogram of $\mathbf{[Ru(bpy)_3]^{2+}}$complexes which are characterized by one reversible oxidation wave for the ruthenium [Ru(III)/Ru(II)] couple at about 1.0 V *vs* ferrocene (Fc) and three reversible reduction waves for bipyridines between -1.7 and -2.3 V *vs* Fc. But differences to $\mathbf{[Ru(bpy)_3]^{2+}}$are noticed in the reversibility of the ruthenium oxidation wave as well as in the presence of one additional irreversible oxidation wave in the 0.9-1.0 V *vs* Fc range. The latter is attributed to oxidation of the ligand.[23] In previously studied complex, **Ru-*tert*-imi-phOH** due to the presence of strongly electron donating *tert*-butyl groups on the phenol the oxidation potential of the ligands were quite low, 0.58 and 0.38 V *vs.* SCE for *ortho* and *para* phenol, respectively.[23]

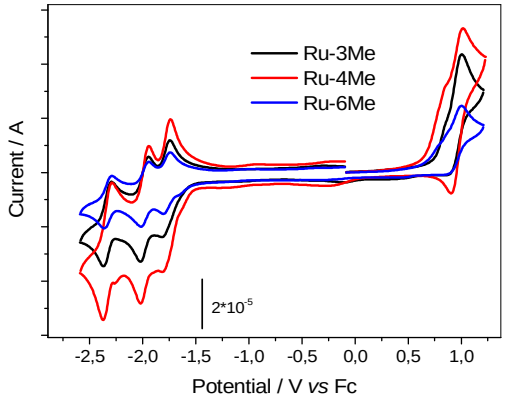

***Figure 3.10**: Cyclic voltammograms of **Ru-xMe** complexes in acetonitrile vs. ferrocene; scan rate 100 mV/s*

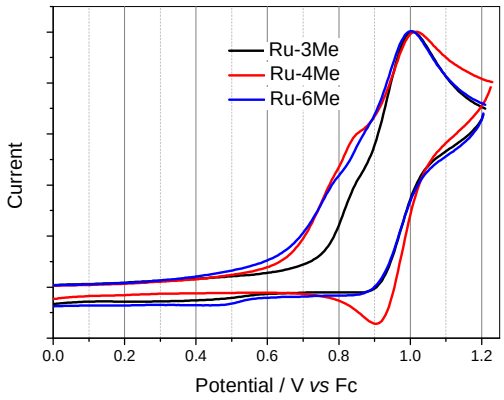

***Figure 3.11:** Normalized Cyclic voltammograms showing oxidation part for **Ru-xMe** complexes in acetonitrile vs. ferrocene; scan rate 100 mV/s*

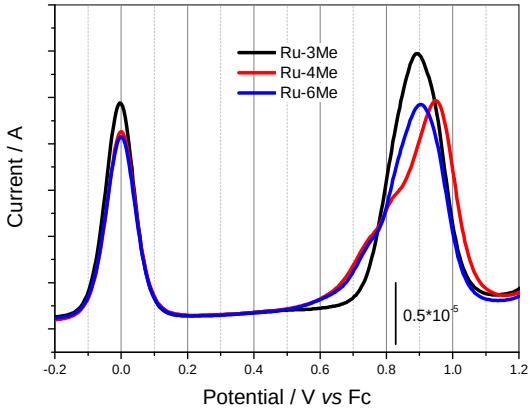

***Figure 3.12**: Differential pulse voltammograms of **Ru-xMe** in acetonitrile with ferrocene as a reference, wave at 0.0 V corresponds to ferrocene oxidation Fc^{+}/Fc.*

When the three **Ru-xMe** cyclic voltammograms are compared it is clear that **Ru-4Me** differs in the reversibility of the Ru(III)/Ru(II) oxidation wave. This is most obvious when looking only at oxidation part (Figure 3.11).The Ru(III)/Ru(II) wave is reversible in case of **Ru-4Me** while for the other two **Ru-xMe** it is quasi-reversible.

From the cyclic voltammograms it appears that oxidation of ligand and chromophore occur at similar potentials and they are therefore not well separated. Differential pulse voltammograms were recorded with the aim to better visualize these redox transitions (Figure 3.12). These data reveal only a single oxidation band in the case of **Ru-3Me,** for **Ru-6Me** a shoulder at 0.75 V, and for **Ru-4Me** shoulders at 0.75 and 0.82 V can be distinguished. In addition for

Ru-4Me the main oxidation peak is shifted by about 60 mV to higher potentials compared to the other two complexes. All obtained potentials are summarized in Table 3.1, together with **Ru-*tert*-imi-phOH** potentials from the published data for comparison.[23].

Comparison of potentials of **Ru-xMe** and **Ru-tert-imi-phOH** (Table 3.1) shows that the potential of the ligand oxidation is increased from 0.19 V to 0.75 V. This is attributed to the replacement of the electron donating *tert*-butyl groups. Thus our first aim in synthesizing **Ru-xMe** complexes with increased redox potential was successful. From a thermodynamic point of view these complexes are suited as electron relay in a water oxidation catalytic system (discussed more in detail in Chapter 5)

Table 3.1: *Summary of potentials vs ferrocene in acetonitrile [a] potentials are converted from SCE to Fc[E(Fc^+/Fc)] = 0.395 V vs. SCE. Note that attribution of the high potential values in the range 0.8 to 1 V to Ru or the ligand is preliminary.*

	$E_{1/2}$ Ru(III)/Ru(II)	$E_{1/2}$ Lig_{ox}/Lig (ligand)	$E_{1/2}$ (bipyridines)		
Ru-3Me	0.89	0.75	-1.78	-1.98	-2.33
Ru-4Me	0.95	0.75, 0.82	-1.78	-1.98	-2.33
Ru-6Me	0.89	0.75	-1.77	-1.98	-2.33
Ru-tert-imi-phOH[a]	0.90	0.19	-	-2.00	-2.40
Ru-imi	0.96	0.55, 0.80	n/d	n/d	n/d
Ru-Et-imi	0.96	0.52	n/d	n/d	n/d

Electrochemical characterization of **Ru-imi** and **Ru-Et-imi** was also performed and the obtained results are shown in Figure 3.13 and Figure 3.14 respectively. **Ru-imi** shows three oxidation waves, we can assume that one is for Ru(III)/Ru(II) and the other two for oxidation of the ligand.[23] In case of **Ru-Et-imi** we have observed two oxidation waves, both are reversible. Thus electrochemical properties are modified by elthylation of an imidazole (Figure 3.14). Summary of all potentials can be found in Table 3.1.

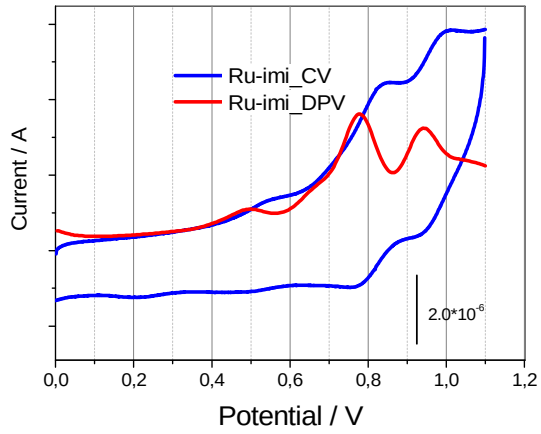

***Figure 3.13**: Cyclic voltammogram (blue) and differential pulse voltammogram (red) of **Ru-imi** in acetonitrile; scan rate 100 mV/s*

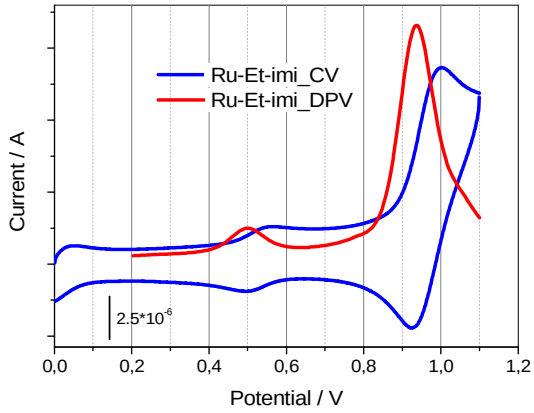

***Figure 3.14**: Cyclic voltammogram (blue) and differential pulse voltammogram (red) of **Ru-Et-imi** in acetonitrile; scan rate 100 mV/s*

3.4 Absorption and emission properties

Figure 3.15 shows absorption spectra of **Ru-3Me**, **Ru-4Me** and **Ru-6Me** along with $[\mathbf{Ru(bpy)_3}]^{2+}$ as a reference. These absorption spectra show an intense band in the visible region with maxima at 460 nm corresponding to the transition from metal, Ru(dπ) to ligand centered (π*) orbitals generally called metal to ligand charge transfer transition (MLCT). Another intense band in the UV region at 290 nm corresponds to intra-ligand (π→π*) transition of the bipyridines.

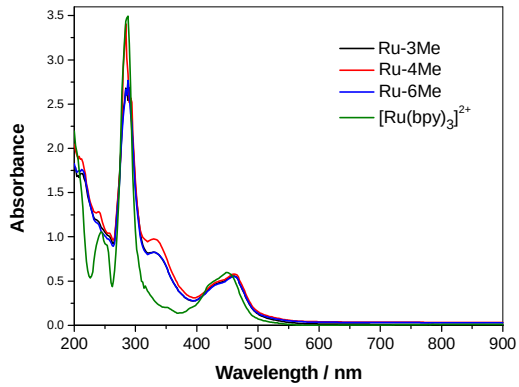

***Figure 3.15**: Absorption spectra of **Ru-3Me**, **Ru-4Me**, **Ru-6Me** and $[\mathbf{Ru(bpy)_3}]^{2+}$ in acetonitrile*

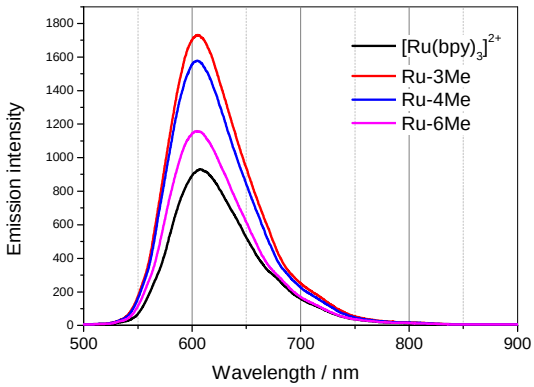

***Figure 3.16**: Steady state emission spectra of **Ru-3Me**, **Ru-4Me**, **Ru-6Me** and $[\mathbf{Ru(bpy)_3}]^{2+}$ in acetonitrile*

These features are similar to [**Ru(bpy)$_3$**]$^{2+}$, the reference compound.[31,32] In addition to these two bands there is an additional band observed around 330 nm and a shoulder on the MLCT transition tailing up to 550 nm. These features have already been observed in the case of **Ru-imi-*tert*-phOH** and are attributed to intraligand transitions involving the phenanthroline and imidazole groups.[33-35]

Emission spectra in acetonitrile are similar for **Ru-xMe** complexes. They closely resemble [**Ru(bpy)$_3$**]$^{2+}$ emission spectra with emission maxima at 605 nm (Figure 3.16).

3.5 Photophysical studies

In order to study excited state properties and photoinduced electron transfer we used laser flash photolysis. We normally used an excitation wavelength of 460 nm from a pulsed nanosecond laser unless otherwise specified (see Chapter 2 for details).

3.5.1 Emission Kinetics

All **Ru-xMe** complexes show typical emission decay with a lifetime of ~1.2 µs in acetonitrile (Figure 3.17). The lifetime is bit higher compared to [**Ru(bpy)$_3$**]$^{2+}$ (~800 ns) and previous phenol complexes, **Ru-imi-tert-phOH** (~1 µs).

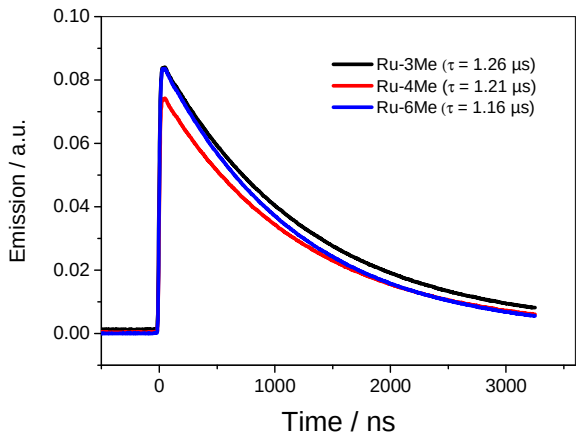

Figure 3.17: *Emission kinetics at 610 nm of* ***Ru-xMe*** *in acetonitrile; Ar-purged, excitation wavelength 460 nm.*

3.5.2 Electron transfer studies

As we have seen according to electrochemical measurements (and independent of exact attribution of the observed waves) the difference in redox potentials between ruthenium and ligand are small for all **Ru-xMe** complexes (ΔE ~80 to 100 mV). This indicates that the driving force for internal electron transfer must be relatively small[1]. To investigate whether the oxidized state of the chromophore is able to oxidize the ligand, electron-transfer experiments in the presence of MV^{2+} as an external electron acceptor were performed (MV=methyl viologen).

Figure 3.19 shows laser flash induced absorbance transients for **Ru-3Me**, **Ru-4Me** and **Ru-6Me,** along with **$[Ru(bpy)_3]^{2+}$**as a reference, in presence of 20 mM MV^{2+} as an external electron acceptor. The flash-induced absorbance changes in the MLCT band of the Ru-chromophore are due to formation of the excited state (instantaneous bleaching), followed by quenching of the latter due to the reduction of the external electron acceptor (MV) leading to formation of the oxidized state Ru(III) of the chromophore, and eventually reduction of the Ru(III) state by internal electron transfer (ET) from the ligand. The Scheme 3.3 describes the corresponding reaction sequence.

$$\mathrm{Ru(II)L + MV^{2+} \xrightarrow{h\nu} Ru(II)^{*}L + MV^{2+} \xrightarrow{k_q} Ru(III)L + MV^{\bullet+} \xrightarrow{k_{et}} Ru(II)L_{ox} + MV^{\bullet+} \xrightarrow{k_{rec}} Ru(II)L + MV^{2+}}$$

Scheme 3.3: *Simplified reaction scheme*[2]

The quenching of the Ru* state by the external electron acceptor is a pseudo first-order reaction due to the large excess of electron acceptor. Typical rates for the quenching rate constant k_q are $(80\ ns)^{-1}$ for $[MV^{2+}]$ =20 mM. Increased concentrations of MV therefore increase significantly the rates of emission quenching (Figure 3.18 a), *i.e.* excited state decay and formation of Ru(III), (Figure 3.18 b). The observed quenching is more for 10 mM and 20 mM MV concentration therefore we have used one of these concentrations for our experiments.

[1] In fact, the difference in potentials from electrochemistry should be considered as an upper limit as they refer to fully equilibrated final states, which are not necessarily the potentials relevant for a given (PCET) transfer step.

[2] Back reaction of MV^{+} with Ru(III) is neglected here as $k_{et} >> k_{rec} * [MV^{\bullet+}]_0$

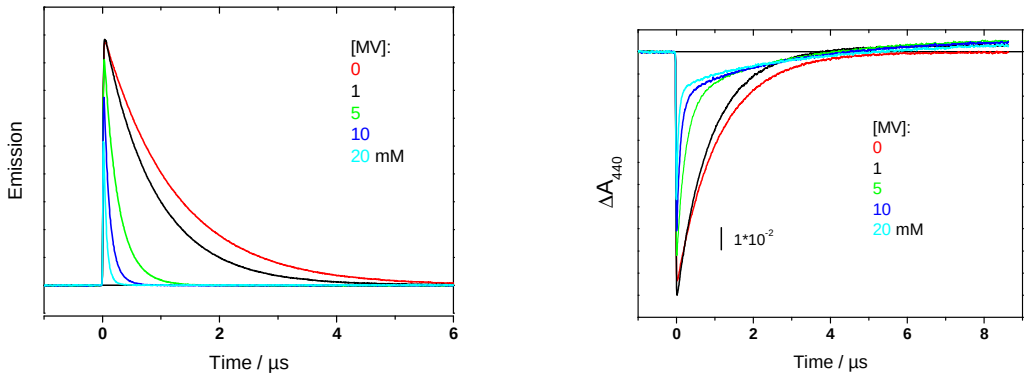

***Figure 3.18**: Effect of increasing methyl viologen concentration from 0 mM to 20 mM on the **Ru-4Me** on emission kinetics at 610 nm (left) and b) on absorption kinetics at 440 nm (right)*

In the reference compound **$[Ru(bpy)_3]^{2+}$**internal ET is absent and the Ru(III) state is reduced by $MV^{\bullet+}$ in a second order reaction with $k_{rec} \approx 5*10^9$ $M^{-1}s^{-1}$. As the flash-induced concentration of MV $[MV^{\bullet+}]_0$ is $1\text{-}2*10^{-6}$ M the back reaction occurs on a hundred µs time scale (black and grey traces in Figure 3.19). The absorbance transients for the complexes under study show a very different behavior.

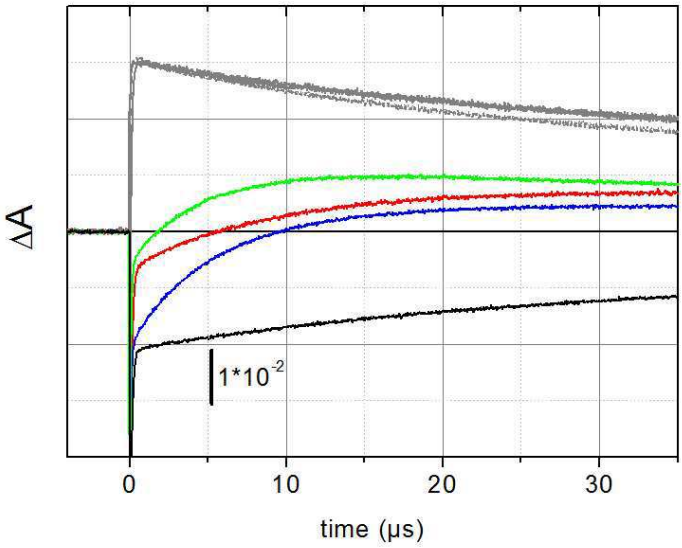

***Figure 3.19:** Transient absorbance traces at 440 nm for **Ru-3-Me (red), Ru-4-Me (blue), Ru-6-Me (green)** and **$[Ru(bpy)_3]^{2+}$** (black) upon excitation with nanosecond laser flashes at 460 nm in MeCN, Ar-saturated solution. 20 mM methyl viologen (MV^{2+}) was present as external electron acceptor. Traces were normalized to equal concentrations of reduced $MV^{\bullet+}$ as measured by absorption at 605 nm (grey lines).*

The transients in Figure 3.19 show biphasic kinetic behavior at 440 nm for all three complexes, as well as for **[Ru(bpy)$_3$]$^{2+}$**. One fast phase with an apparent time constant of 80-100 ns and a second, slower phase. In case of **[Ru(bpy)$_3$]$^{2+}$**, interpretation of these two phases is clear. We observed a strong bleaching at 440 nm due to disappearance of ground state Ru MLCT absorption. The bleaching indicates the formation of excited state Ru(II)* and subsequently of Ru(III) in a quenching process with MV^{2+} as electron acceptor. This excited state decay Ru(II)* →Ru(III) is fast and determined by the concentration of electron acceptor (see Figure 3.18). After decay of the Ru excited state some bleaching remains due to absorption of the Ru(III) state which decays by charge recombination with reduced MV at longer time scales (~200 µs). All three **Ru-xMe** complexes show a very different kinetic behavior, with a decay of the absorption changes at 440 nm much faster than the decay of the MV_{red} signal at 605 nm. This clearly demonstrates occurrence of internal electron transfer further confirmed by positive absorption at 440 nm at later times in all complexes. The latter feature had also been observed in earlier complexes and is attributed to absorption of the radical on the ligand formed by the electron transfer reaction.

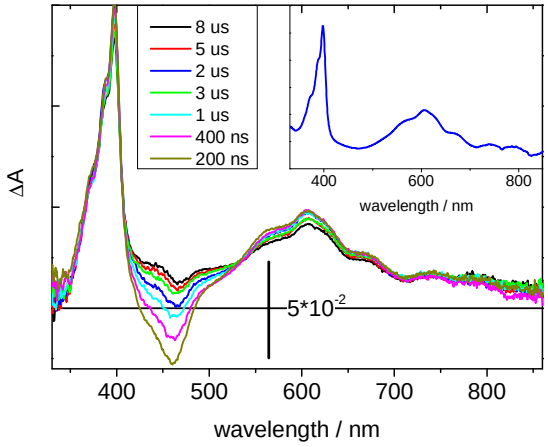

Figure 3.20: *Transient absorption spectra of* ***Ru-6Me*** *in MeCN, recorded from 0.2 to 8 µs after excitation.* ***Inset:*** *$MV^{\bullet+}$ absorption spectrum.*

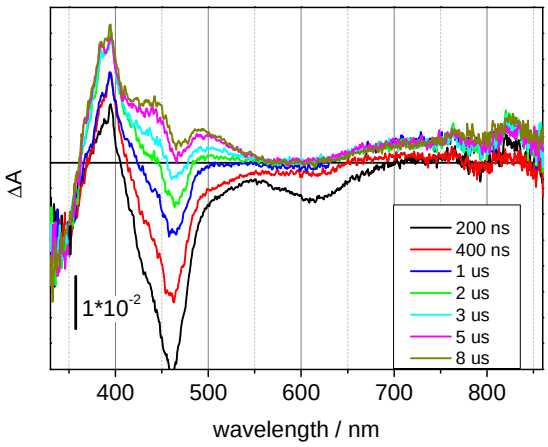

Figure 3.21: *Transient absorption spectra of* ***Ru-6Me*** *in MeCN after subtraction of $MV^{+\bullet}$ contribution.*

Transient absorption spectra (Figure 3.20) confirm the observations from kinetic traces at 440 nm and clearly show evolution, on a µs time scale, from a bleaching in the 420-500 nm regions to a positive absorption. These spectra are dominated by strong absorptions of MV (sharp peak at 390 nm and broad band around 605 nm, see inset in Figure 3.20). Therefore we performed an interactive subtraction of a $MV^{+\bullet}$ radical spectrum[3] and the results are shown in Figure 3.21.

Besides the absorption band around 440 nm these spectra reveal features of the absorption spectrum of the radical which were not clearly visible before subtraction of the $MV^{+\bullet}$ radical spectrum. The radical formed is characterized by absorption maxima at 390, 440 and 490 nm and a band in the near infrared around 850 nm. A bleaching is observed below 350 nm, attributed to disappearance of ground state absorption.

We have also used ruthenium hexamine *i.e.* $[(Ru(NH)_6]Cl_3$ as an electron acceptor. The advantage of $[(Ru(NH)_6]Cl_3$ lies in its absorption characteristics as it has no significant absorption in the visible region, neither in the oxidized nor in the reduced form. However, $[(Ru(NH)_6]Cl_3$ is not soluble in MeCN and experiments have to be performed in a $MeCN/H_2O$ mixture. The resulting spectra for the three complexes are shown in Figure 3.22. They confirm the features of the radical absorption identified above in presence of MV and in absence of water. They show very clearly the absorption band in the near infrared region. Closer inspection reveals that these spectra are similar for the three complexes, but not identical. In particular the relative amplitude of the 500 nm absorption band varies, being largest for **Ru-6Me** and smallest for **Ru-3Me**. We note that the fact that the radical shows close to zero absorption at 605 nm justifies the normalization employed in the presentation in Figure 3.19.

[3] The $MV^{+\bullet}$ spectrum was obtained in the LFP spectrometer by UV illumination of a solution of MV in ACN in presence of a small quantity of MeOH as electron donor.

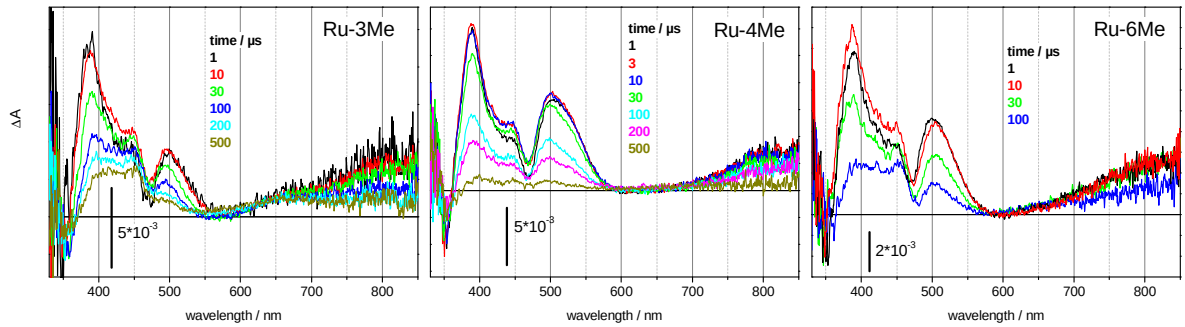

Figure 3.22: *Transient absorption spectra of* ***Ru-xMe*** *in MeCN/H_2O (1:1), with 20 mM [(Ru(NH)$_6$]Cl_3 as electron acceptor.*

Whereas the radical formed in the experiments with either MV^{2+}/MeCN or with [(Ru(NH)$_6$]Cl_3 / MeCN/H_2O appears to be the same, the kinetics of radical generation on the ligand was much faster in the latter case being complete in less than 1 µs. To find an explanation for this drastic effect we have closely looked at the experimental conditions. It is hard to imagine that the nature of the electron acceptor modifies to such a point intramolecular electron transfer. Therefore it must be concluded that the solvent, pure MeCN and MeCN/H_2O, respectively, plays an important role, or, more concretely, that presence of water accelerates the kinetics of radical generation. Indeed, a control experiment, recording kinetic traces using MV^{2+} as an electron acceptor in a MeCN/H_2O (1:1) mixture confirms this hypothesis (see Figure 3.23 for **Ru-4Me**), as Ru(III) disappearance and radical formation become about 50 times faster in presence of 50% H_2O. A similar effect has been observed for all **Ru-xMe** complexes but for **Ru-4Me** the effect is most striking because in MeCN the slow phase is largest for this complex (Fig. 3.19). In presence of water the 440 nm transients are practically identical for the three complexes.

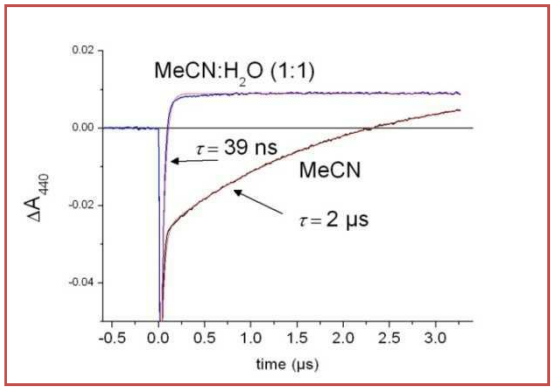

Figure 3.23: *Transient absorption traces at 440 nm for* ***Ru-4Me*** *in acetonitrile (red) and in acetonitrile water mixture (1:1) (violet); Ar-saturated solution. 20 mM methyl viologen (MV^{2+}) was present as external electron acceptor in both cases.*

When looking at the above Figure 3.23 it seems obvious that there must be a transition between slow (no water) and fast (50% water) kinetics for lower water concentrations. Experiments to investigate this will be presented later. At this point we just want to put forward two possible hypotheses to explain the effect of water. Water could, either due to its high dielectric constant and/or hydrogen-bonding interactions preferentially stabilize the oxidized state on the ligand. This would lead to an increased driving force and acceleration of the electron transfer reaction. Or water might act as a base to accept a proton released during oxidation of the ligand. As mentioned before deprotonation of the phenol group must occur upon oxidation due to the very low pK_a of oxidized phenol. Under this hypothesis, ETPT, as observed in our **Ru-Trp** study (see Chapter 4)[36], could then be ruled out because in this case the rate for ET is not expected to depend on a proton acceptor. But a concerted mechanism (CEP) or PTET could be consistent with the observations, although this is not straightforward either, as the hydrogen-bonded imidazole group could be expected to act as internal base for the phenolic proton released upon oxidation of the phenol group. On the other hand the ligand contains two potentially oxidizable species (imidazole, phenol) which makes things more complex.

Therefore in order to resolve this complexity in the electron/proton transfer we have decided to investigate the effect of water, base, acid, *etc.* on the reaction and compare our PS II mimics to simpler systems (**Ru-imi, Ru-cT-phOH**) as control.

Before going to describe these studies it is important to discuss a quantitative aspect related to the amplitudes of observed absorbance changes. The amount of flash-induced Ru(II)* excited state can easily be determined by the maximum bleaching around 450 nm and the known extinction coefficient of the chromophore. Under our experimental conditions ($\Delta ODca$ 0.1, $\varepsilon_{Ru}ca$ 14500 $M^{-1}cm^{-1}$) the concentration of Ru* formed by the laser flash is about 6 µM. However, even a fast quenching by MV (at high concentrations of the latter) leads to much lower concentration of Ru(III) due to the limited escape yield for the $MV^{+\bullet}$ radical (about 0.3).[37] In the presence of comparably fast internal electron transfer it is therefore not always facile to estimate which part of the absorption bleach in the 450 nm region corresponds to the Ru(II)* and the Ru(III) state. This problem can be solved by comparing the amplitude of positive absorption at 605 nm which is due to the $MV^{+\bullet}$ radical, the extinction coefficient of which is known (13700 $M^{-1}cm^{-1}$). The concentration of initially formed Ru(III) must be identical. A detailed analysis of this, given in the Appendix 1 (Section 1) and taking into

account corrections for small absorptions of MV at 440 nm and of Ru(III) at 605 nm, shows that if we compare 440 to 605 nm traces, for 100% Ru(III) we should have a bleaching at 440 nm with an amplitude which is 78% of the positive absorption at 605. This fits well with the experimentally observed ratio of amplitudes for **$[Ru(bpy)_3]^{2+}$** (Figure 3.19).

As seen in Figure 3.19, distinct differences in the Ru(III) decay monitored at 440 nm are observed for the three complexes. For **Ru-3Me** and **Ru-6Me** we observed two distinct phases. One is very fast (<100 ns), close to the kinetics of decay of the excited state, and one slower with a time constant of some µs. In the following we will call these two kinetic phases the "fast" and "slow" phase, respectively. Whereas for **Ru-3Me** and **Ru-6Me** the amplitudes of both phases are about equal, for **Ru-4Me** we have observed essentially only the slow phase.

To summarize these results in neat aprotic solvent:

- For **Ru-4Me** virtually all Ru(III) decays in one, slow phase
- For **Ru-3M**e and **Ru-6Me**, Ru(III) reduction is biphasic with a major fast phase and a second slower phase the rate of which is similar to the one observed in **Ru-4Me**.

In case of our complexes (**Ru-3Me** and **Ru-6Me**), the fast phase is always limited by the concentration of electron acceptor used. Therefore we cannot resolve the fast phase further. Apparent time constants for the slow phase are 9 µs, 5.6 µs and 4.9 µs for **Ru-3Me**, **Ru-4Me** and **Ru-6Me** respectively.

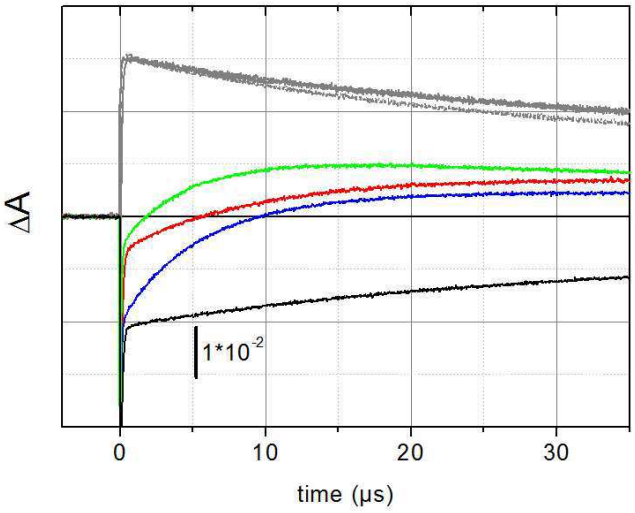

Figure 3.19 (reproduced): *Transient absorbance traces at 440 nm for* ***Ru-3-Me (red), Ru-4-Me (blue), Ru-6-Me (green)*** *and* ***$[Ru(bpy)_3]^{2+}$*** *(black) upon excitation with nanosecond laser flashes at 460 nm in MeCN, Ar-saturated solution. 20 mM methyl viologen (MV^{2+}) was present as external electron acceptor. Traces were normalized to equal concentrations of reduced MV^{2+} as measured by absorption at 605 nm (grey lines).*

We observed some variation in the slow rates from experiment to experiment which we attribute to slightly different experimental conditions[4]. In the following, we present additional experiments with the aim to rationalize the surprising (and interesting) findings of biphasic ET and the differences observed between the complexes.

The biphasic ET for **Ru-3Me** and **Ru-6Me** might be because of two reasons:

1) Heterogeneity. Two populations of complexes exist with different conformations or protonation states of the ligand and which are characterized by different kinetics ("fast" and "slow").
2) Energetic equilibrium between the oxidized state on Ru and on the ligand.

In the case of the first hypothesis, heterogeneity might arise from two populations of complexes which differ, for example, in conformation or protonation state. The second hypothesis merits some more explanation. Energetic equilibrium means that the difference in energy between two states is small, *i*.e. not exceeding some *kT* (*k* is the Boltzmann constant and *T* is temperature; *kT* is ca 25 meV at room temperature). In an electron transfer reaction between two species in energetic equilibrium (small driving force ΔG) the rate of the reverse reaction, k_{-1}, can then no longer be neglected and k_1 and k_{-1} are related by

$$k_1/k_{-1} = e^{-\Delta G/kT}$$

An equilibrium with partial oxidation of the electron donor and partial oxidation of the electron acceptor is established with an apparent rate $k_1^{app} \approx k_1 + k_{-1}$. However, taking into account such equilibrium is not sufficient to describe our biphasic absorption transients and we have to postulate a minimum reaction scheme (Scheme 3.4) with a second, consecutive reaction step with rate k_2 which depopulates the equilibrium state to yield the final product state, L_{ox}^2.

$$\mathrm{Ru(III)L} \underset{k_{-1}}{\overset{k_1}{\Leftrightarrow}} \mathrm{Ru(II)L_{ox}^1} \xrightarrow{k_2} \mathrm{Ru(II)L_{ox}^2}$$

Scheme 3.4*: Simplified reaction scheme of intramolecular reactions with reversible electron transfer. Reactions of complexes with electron acceptors have been omitted for clarity.*

[4]Especially dryness of solvent (see below).

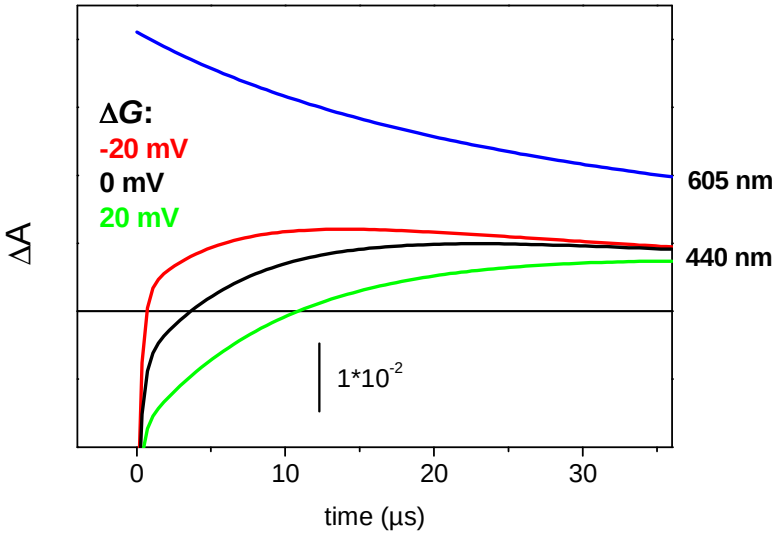

***Figure 3.24**: Effect of driving force on the kinetic traces at 440 nm. Decay of reduced electron acceptor is shown by the blue line. Amplitudes are determined by extinction coefficients deduced from spectral data like those in Figures 3.20 and 3.21.*

Figure 3.24 shows a mathematical simulation of absorption transients based on this reaction scheme (Scheme 3.4). It can easily be seen that for small ΔG the absorbance kinetics at 440 nm are indeed biphasic and that the ratio of amplitudes of fast and slow phase is **very sensitive** towards the driving force. The second hypothesis of energetic equilibrium between two states (oxidized chromophore and oxidized ligand) is therefore in principle able to explain the observed behavior and an interesting option, provided an interpretation for the slow phase can be obtained.

The slow phase (k_2) observed at 440 nm related to Ru(III) reduction and radical formation (ligand oxidation) is not restricted to this wavelength but appears at other wavelengths too. Some examples are shown in Figure 3.25. The spectra associated with the slow phase have been determined for the three complexes (for procedure see Appendix 1, Section 2) and are shown in Figure. 3.26.

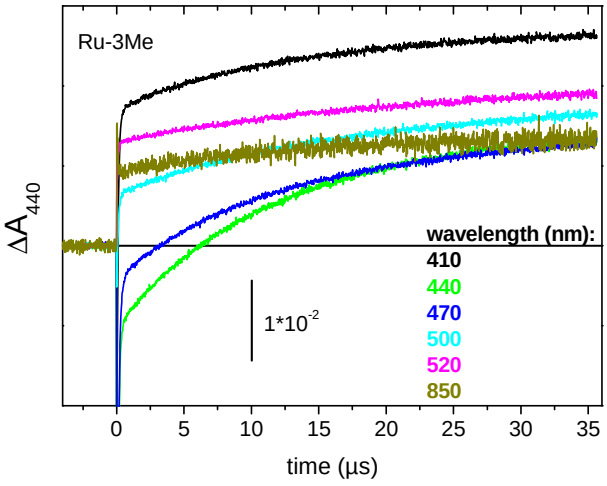

Figure 3.25: *Examples for wavelengths where the slow phase of absorption change is clearly visible. Sample* ***Ru-3Me****. For better visualization the decay due to back electron transfer from the external electron acceptor has been removed (see Appendix).*

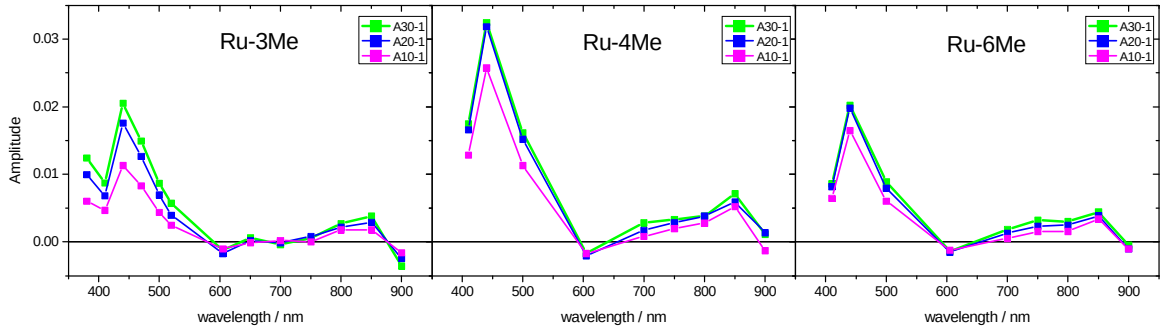

Figure 3.26: *Spectral absorption changes associated with the slow phase taken as the difference in absorption between t=1 µs and t=10, 20, 30 µs, respectively.*

These reconstructed "decay" associated spectra are complex but they can be fully rationalized. They clearly contain contributions from radical formation on the ligand (positive absorptions around 850 nm and in the 350-550 nm region), but also contributions from recovery Ru(III)→Ru(II) (positive absorption at 450, negative at 600 and 900 nm). However, the essential information is that the spectra don't show significant change with time. This is taken as evidence that one and the same transition between two states occurs in all complexes, *i.e.* Ru(III)L→Ru(II)L_{ox}^{2} and that an eventual intermediate (L_{ox}^{1}) is spectroscopically not significantly different from the final state L_{ox}^{2}. This is consistent with the hypothesis of reversible, biphasic ligand oxidation.

3.6 Effect of the methyl substitution

To answer the question whether the methyl substituent on the phenol ring can affect the electron transfer properties we performed similar experiments with **Ru-imi-phOH** using MV as an electron acceptor (Figure 3.27). The observed transient at 440 nm closely resembles the one of the **Ru-4Me** complex, with only a small fast phase of Ru(III) decay and a slow phase with an apparent time constant of 10 µs. This observation gives an interesting hint concerning the effect of the position of the methyl substitution. Substitution at the 4-position on the phenol ring has little effect, but substitutions at position 3 and 6 modify the properties of the ligand. As with the other complexes presence of water makes radical formation very fast (not shown).

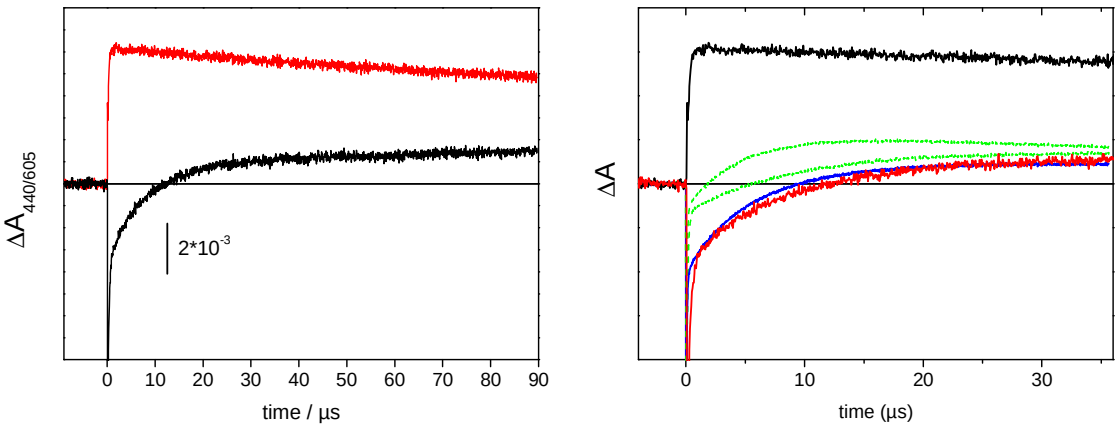

Figure 3.27: *left: Transient absorbance traces at 440 nm (red) and 605 nm (black) for* ***Ru-imi-phOH*** *upon excitation with nanosecond laser flashes at 460 nm in MeCN, Ar-saturated solution. 10 mM methyl viologen (MV^{2+}) was present as external electron acceptor. Right: comparison with the kinetic traces from the* ***Ru-xMe*** *complexes, reproduced from Figure 3.19,* ***Ru-4Me*** *in blue. Amplitudes normalized to identical $[MV^{\bullet+}]_0$.*

3.7 Role of hydrogen bond

The complexes investigated before had in common the presence of a hydrogen bond between the phenol group and an imidazole. To obtain information about the role of this biomimetic feature we have studied as control two other complexes which don't possess such a hydrogen bond, **Ru-cT-phOH** and **Ru-imi**. In Figure 3.28 are shown example traces obtained with **Ru-imi.** In pure MeCN (black traces) internal electron transfer is very slow characterized by a time constant of 43 µs. Addition of 5% H_2O (blue traces) leads to only weak acceleration (18 µs). But after addition of 10 mM buffer, pH 8 (green traces), internal electron transfer gets very fast (0.3 µs) showing the importance of a proton acceptor for oxidation of the imidazole moiety. Intriguingly, at 605 nm additional absorption is visible with the kinetics of radical

formation. This can be understood by inspection of the differential absorption spectra (Figure 3.28). Clearly these spectra are very different from those obtained before for the phenol complexes. In particular the spectra associated with ligand oxidation show well defined maxima of absorption at 382 and 578 nm and a characteristic negative band at 466 nm. The 578 nm band tails up beyond 600 nm and this ligand-based absorption contributes to the 605 nm absorption kinetics besides the major contribution from MV^{+}[5]. An absorption band in the NIR, around 850 nm, as in **Ru-xMe**, is missing. This information might tell us that in case of **Ru-xMe** the generated radical is localized primarily on the phenol and not on the imidazole.

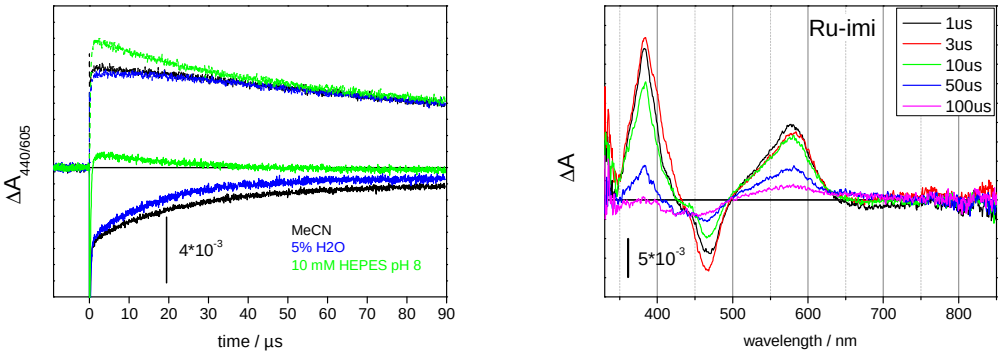

Figure 3.28:Left: *Transient absorbance traces at 440 nm (solid lines) and 605 nm (dashed lines) for* ***Ru-imi*** *upon excitation with nanosecond laser flashes at 460 nm. 20 mM methyl viologen (MV^{2+}) was present as external electron acceptor. Black: in neat MeCN, ; blue: +5% H_2O; green: +10 mM HEPES buffer, pH 8.* ***Right:*** *Transient absorption spectra for* ***Ru-imi*** *in MeCN, 10 mM HEPES pH 8 buffer. Contributions from MV have been subtracted.*

The complex **Ru-Et-imi** was produced as a variant of **Ru-imi** which has no proton on the imidazole ligand. In this case we would not expect that presence of a base (buffer) accelerates the internal ET. As shown in Figure 3.29, electron transfer kinetics was similar to **Ru-imi** (50 µs in MeCN) and not accelerated in presence of 10% H_2O (although the back reaction with MV was slightly faster). Unfortunately solubility problems after addition of buffer prevented to study the behavior at high pH. The relatively fast kinetics observed under such conditions are difficult to explain and might be due to some strange side effect of the buffer.

[5] This fact precludes normalization of kinetic traces at 605 nm.

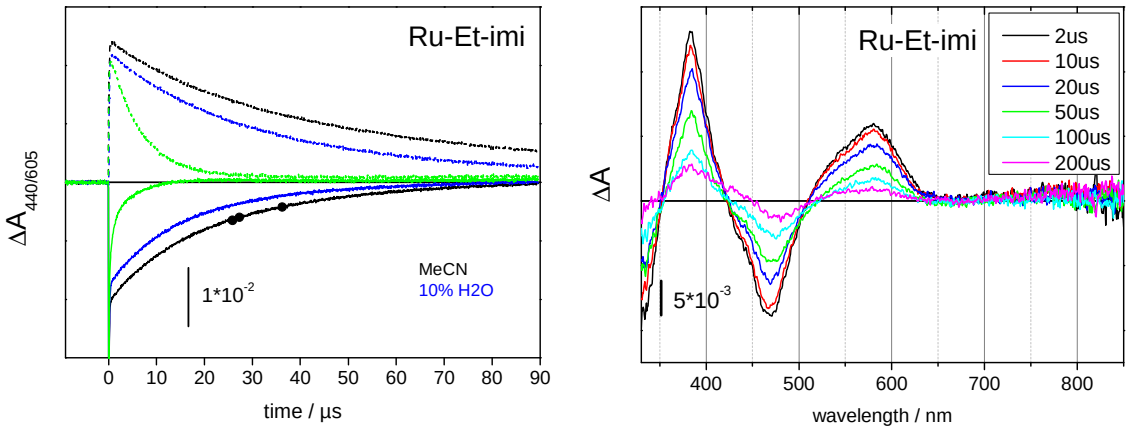

Figure 3.29:Left: *Transient absorbance traces at 440 nm (solid lines) and 605 nm (dashed lines) for* ***Ru-Et-imi*** *upon excitation with nanosecond laser flashes at 460 nm. 20 mM methyl viologen (MV^{2+}) was present as external electron acceptor. Black: in neat MeCN; blue: +10% H_2O.* ***Right:*** *Transient absorption spectra for* ***Ru-Et-imi*** *in MeCN, 10 mM phosphate pH 8 buffer. Contributions from MV have been subtracted.*

The Figure 3.30 shows transient kinetic traces obtained for **Ru-cT-phOH** in pure MeCN (black traces) and after addition of 10% H_2O in presence of 20 mM MV^{2+}. The observed internal electron transfer was slow with apparent time constant 34 µs in MeCN and addition of 10 % of water accelerates the rate of electron transfer to 6.7 µs. This is consistent with reports in the literature for the phenol case where water acts as a proton acceptor to fasten the rate of electron transfer.[15]

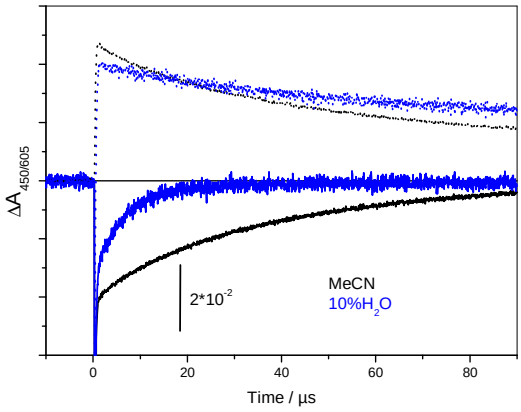

Figure 3.30: *Transient absorbance traces at 440 nm (solid lines) and 605 nm (dashed lines) for* ***Ru-cT-phOH*** *upon excitation with nanosecond laser flashes at 460 nm. 20 mM methyl viologen (MV^{2+}) was present as external electron acceptor. Black: in neat MeCN; green: +10% H_2O.*

3.8 Variation of water concentration

We had observed before (Figure 3.23) a striking difference in ligand oxidation kinetics between aprotic solvent and 50% water. In order to obtain a clearer picture about the role of

water we performed a study starting from pure MeCN and increasing successively the concentration of H_2O. The raw data are shown in Figure 3.31 and 3.32 for **Ru-6Me** and **Ru-4Me**, respectively. The data for **Ru-3Me** are very similar to **Ru-6Me** and are shown in the Appendix 1 Section 3. Again there appears a different behavior of **Ru-4Me** compared to the two other complexes. For **Ru-6Me** and **Ru-3Me** the relative amplitude of the fast phase progressively increases whereas the rate of the slow phase remains rather constant. Such a change can be easily rationalized in the framework of the energetic equilibrium model discussed above as an increase in driving force for the electron transfer reaction (see simulation Figure 3.24). For water concentrations higher than about 1 M radical formation is essentially monophasic and very fast.

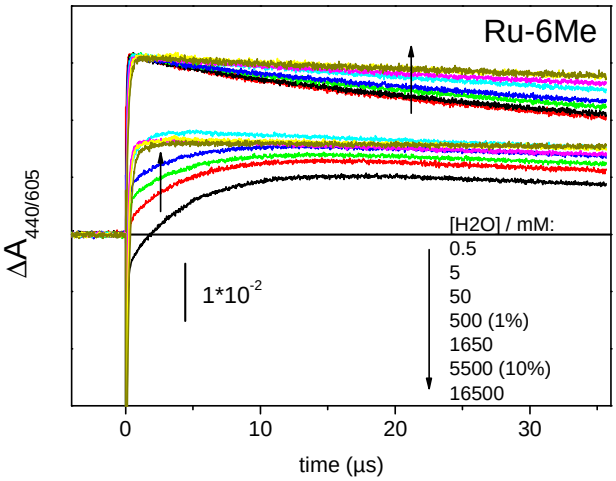

Figure 3.31: *Effect of increasing water concentration on absorption transients for* ***Ru-6Me****. 20 mM MV was used as electron acceptor. The black curve corresponds to neat MeCN. Arrows indicate changes with increasing water concentration.*

For **Ru-4Me** the results seem different. The kinetics are little sensitive towards low concentrations [up to 500 mM, (1%)] of H_2O, followed by a steep increase in the rate of the slow phase. An observation common to all complexes is a clear decrease in the rate of charge recombination (between $MV^{+\bullet}$and the oxidized ligand) as can be seen on the traces at 605 nm.

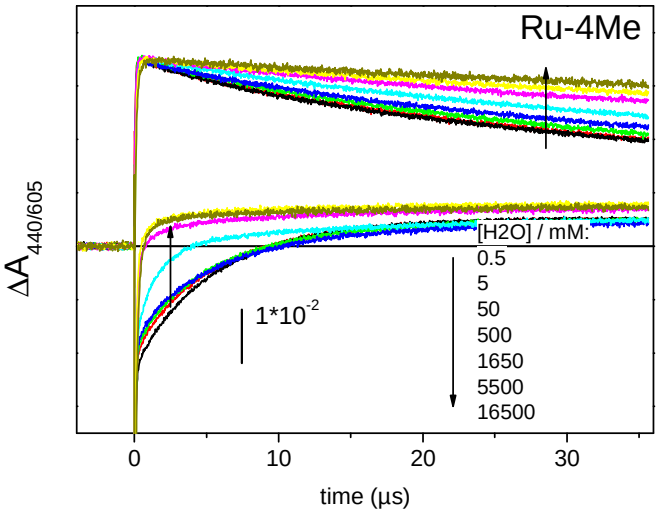

Figure 3.32: *Effect of increasing water concentration on absorption transients for* ***Ru-4Me****. 20 mM MV was used as electron acceptor. The black curve corresponds to neat MeCN. Arrows indicate changes with increasing water concentration.*

The change in the relative amplitudes of fast and slow phase observed for **Ru-3Me** and **Ru-6Me** (Figure 3.31), visually very impressive, has to be taken with same caution as we have observed at some occasions a decrease in the amplitude of the slow phase in older samples or after excessive flashing. The fact, that this is not observed with **Ru-4Me** measured the same day under the same conditions, gives us confidence that this feature is unlikely to be an artifact. Given the high sensitivity of this relative amplitude to the driving force of electron transfer reaction (see Figure 3.24) there is indeed only a relatively small change (less than 50 meV) in ΔG necessary to explain the observation. More information can be obtained by inspection of the fit parameters for absorption transients at 440 nm as a function of water concentration for the three **Ru-xMe** complexes (Figure 3.33). This data immediately show that the most significant change is observed for the time constant of the slow phase (Figure 3.33, blue traces) which decreases sharply around 100 mM of water concentration (slightly higher for **Ru-4Me**). At low concentrations of water there is a gradual decrease observed in the amplitude of the slow phase, Aslow, for **Ru-3Me** and **Ru-6Me**, whereas for **Ru-4Me** this amplitude stays high and rather constant up to 1 M. Another interesting feature is the increase of the amplitude of the absorption due to the radical at long times, which seems to mirror the decrease in Aslow for **Ru-3Me** and **Ru-6Me**. The decrease of this absorption at high concentration, above 1 M, might be due to diminished extinction coefficient but the increase at low concentrations of water probably indicates an increase in concentration of radical formed. A possible explanation is that even the state L_{ox}^2 is energetically not far below

Ru(III)/Ru(II) and that this equilibrium is gradually shifted in favor of the oxidized ligand with increasing concentration of water.

We conclude that there exist two regimes of water concentration with different effects. At low water concentrations the already described decrease in the amplitude of the slow phase is the main effect accompanied by an increase in radical absorption, but at higher concentration another mechanism is taking over. For **Ru-4Me** only the second regime seems to be operative and it sets in at higher water concentrations. As possible mechanisms responsible for these two regimes we might postulate action of H_2O as hydrogen-bonding partner to the imidazole and as a proton acceptor (external base), respectively. The results are consistent with an increased driving force induced by hydrogen bonding thereby strengthen the hypothesis of energetic equilibrium as the cause of the biphasic electron transfer kinetics.

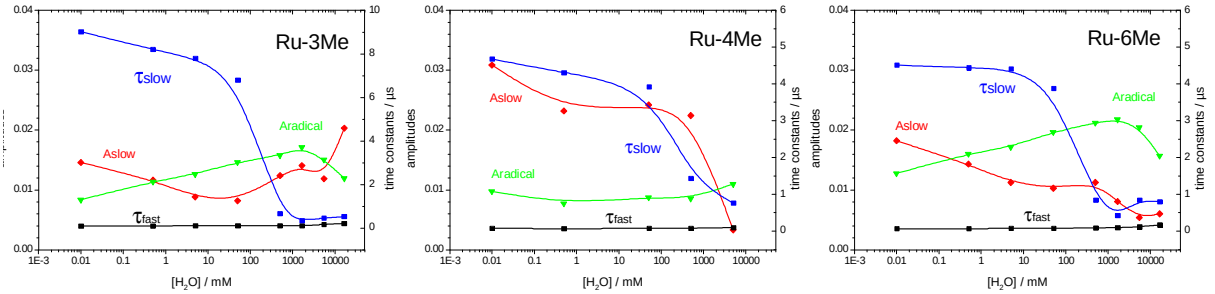

Figure 3.33: *Parameters obtained for best fit of absorption transients at 440 nm for* ***Ru-xMe*** *as a function of water concentration. Black, blue: time constants for fast and slow phase, respectively. Red: amplitude of slow phase. Green: amplitude of absorption at long times due to the radical on the ligand. To display the values for [H_2O]=0 mM these points were arbitrarily positioned at 0.01 mM. Note that at least in the case of* ***Ru-3Me*** *the time constants for the fast and slow phase become very similar making precise determination of Aslow difficult. This is probably the reason for the apparent increase of Aslow at high concentrations of water in* ***Ru-3Me****.*

To rationalize the effect of water on kinetics, its effect on electrochemistry was investigated. Changes in differential pulse voltammograms have been measured by adding sequential aliquots of water (Figure 3.34). The detailed Figures can be seen in Appendix 1 Section 4. Figure 3.34 shows combined effect of different concentration of water on **Ru-xMe**. In presence of 1% (5.5 M) water the DPV response was significantly modified. As seen **Ru-4Me** complex required twice higher water concentration than **Ru-3Me** and **Ru-6Me** to see a distinct separation between ligand and ruthenium redox potentials. But for all complexes, the point is to be noted that the separation between ligand and ruthenium has been narrowed from ~100 mV to 60 mV. This shows that water affects the potential of ligand oxidation but the narrowing is not in line with an increase in driving force for ET. However, the concentrations

used in these electrochemical studies are in the high concentration regime identified in the kinetic measurements and therefore might not catch the effect of water at low concentration. Furthermore, due to the proximity of the two oxidation potentials, the electrochemical measurements contain necessarily a double oxidation of the complexes (Ru(III) and L_{ox}), a situation which is not encountered in single flash experiments.

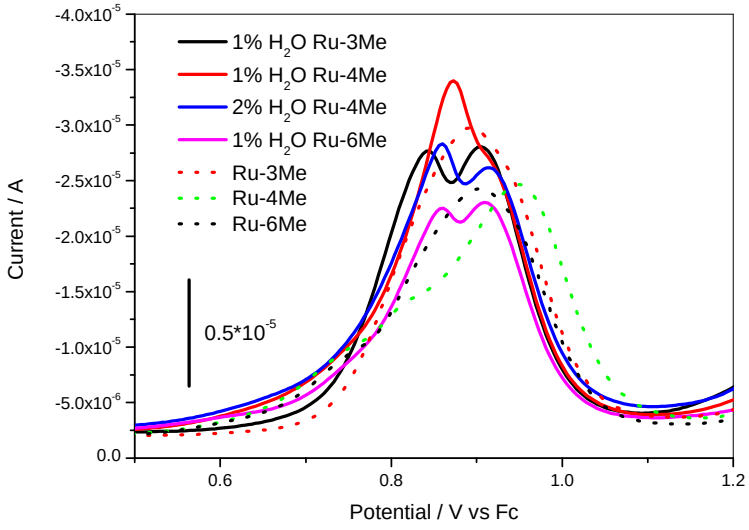

Figure 3.34: *Effect of water on differential pulse voltammograms of* ***Ru-xMe***

3.9 Kinetic isotope effect with D_2O

In a proton-coupled electron transfer reaction, the rate usually displays a kinetic isotope effect (KIE), *i.e.* it is slower when the involved proton is replaced by a deuteron (except in the case of rate-limiting ET, where k_H/k_D =1). We measured absorption transients with varying concentrations of H_2O or D_2O and analysed the kinetics of the slow phase for **Ru-4Me**.

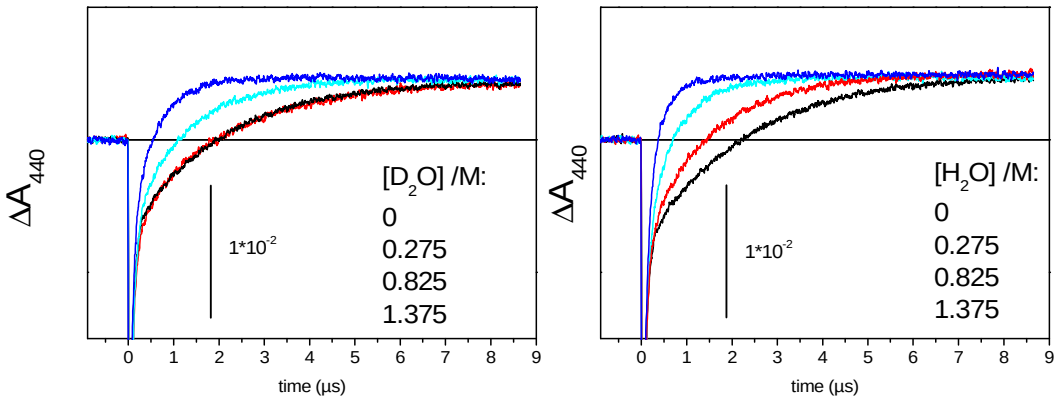

Figure 3.35: *Effect of D_2O (left) and H_2O (right) exchange on transient kinetic traces at 440 nm for* ***Ru-4Me****.*

We have obtained KIE≈2 indicating the involvement of protons in the rate limiting reaction (Figure 3.36).

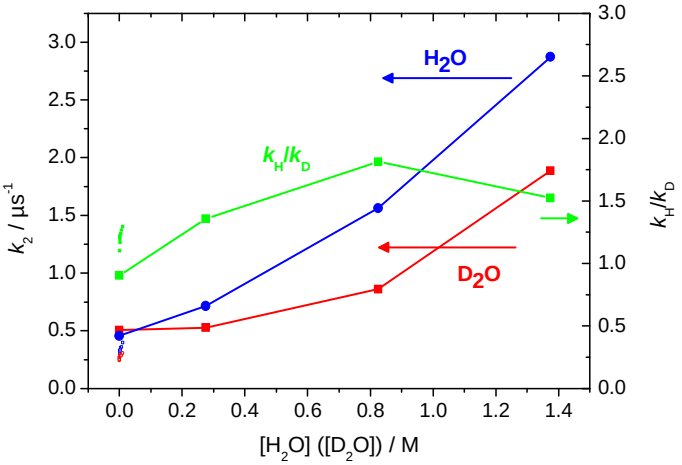

Figure 3.36: *Dependence of the rate of the slow phase on concentration of H_2O (blue) or D_2O (red) for* ***Ru-4Me****.*

3.10 Effect of proton acceptors

Pyridine titration

As explained in the previous part, water accelerates the rate of the slow phase of internal electron transfer. This acceleration due to water might be due to water acting as a base to abstract the proton of the imidazole group upon oxidation of the ligand. To investigate further on this hypothesis we performed experiments with pyridine as an external base. The pK_a of the pyridine is ~12.3 in acetonitrile[39] and therefore pyridine is a relatively strong base.

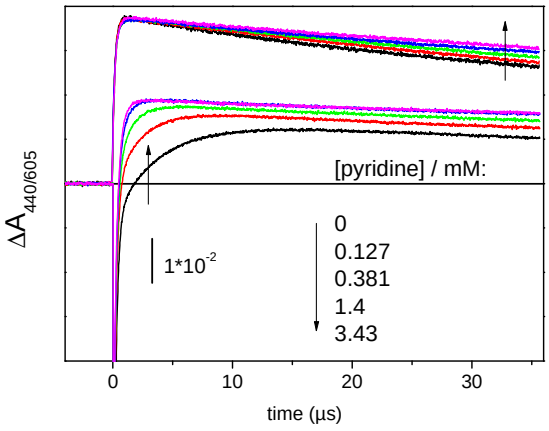

Figure 3.37: *Transient absorbance traces at 440 nm (lower traces) and 605 nm (upper traces) for* ***Ru-6-Me*** *upon excitation with nanosecond laser flashes at 460 nm in MeCN, Ar-saturated solution for increasing concentrations of pyridine. 20 mM methyl viologen (MV^{2+}) was present as external electron acceptor. Traces were normalized to equal concentrations of reduced MV^{2+} as measured by absorption at 605 nm.*

The effect of increasing concentration of pyridine on absorption transients is shown in Figure 3.37 for **Ru-6Me**. The data for **Ru-3Me** and **Ru-4Me** can be found in the Appendix 1, Section 5. It can be seen that for all complexes relatively low concentrations of pyridine (0.13 mM) lead to considerable acceleration of the slow phase. The variations of the fit parameters which describe the kinetics are shown in Figure 3.38. Indeed the decrease of τslow with increasing pyridine concentration is the most prominent effect, reminiscent of the situation with water, but occurring at concentrations three orders of magnitude lower. Other changes concern an increase in the amplitude of radical absorption (green traces in Figure 3.38) suggesting that presence of the base favors the extent of final radical. The changes in the amplitude of the slow phase observed at the higher concentrations seem also significant, but, as in the case of water titration, the precision of the parameters becomes low when the time constants of the two kinetic phases approach the same value. Therefore we refrain from drawing conclusions from this feature.

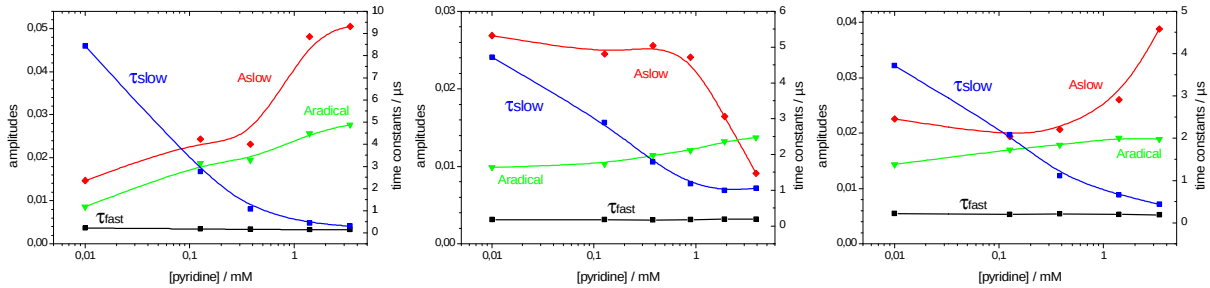

Figure 3.38: *Parameters obtained for best fit of absorption transients at 440 nm for* ***Ru-xMe*** *as a function of pyridine concentration. Black, blue: time constants for fast and slow phase, respectively. Red: amplitude of slow phase. Green: amplitude of absorption at long times due to the radical on the ligand. To display the values for [pyridine]=0 mM these points were arbitrarily positioned at 0.01 mM.*

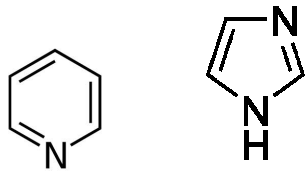

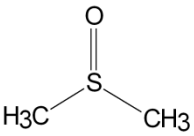

Figure 3.39: *Structures of pyridine, imidazole and DMSO*

In order to distinguish between effects of hydrogen bonding and proton acceptor action we performed some similar experiments with DMSO. DMSO is very polar and capable of accepting hydrogen bonds, but it is not a proton acceptor (pK_a = –1.5 in H_2O). The results are shown in the Appendix 1, Section 6. For **Ru-imi** DMSO has no effect up to 10% (1.5 M). For **Ru-4Me** acceleration of the slow phase is observed but for much higher concentrations compared to pyridine.

Pyridine as a strong base can eventually deprotonate the imidazole group (see below for determination of pK_a in H_2O). To check for this possibility we performed titration of the absolute absorption spectrum (Figure 3.40). Indeed characteristic spectral features attributable to deprotonation were detected and the concentration dependence indicated deprotonation in the ground state for concentrations higher than some hundred mM, similar for all three **Ru-xMe** complexes. The concentration of pyridine necessary to induce deprotonation is about 10^4 times higher than the concentration of the complexes used. This shows that the ground state pK_a of the imidazole in ACN must be about 4 units higher than the pK_a of pyridine (in MeCN), *ie*. it must be around 16.3, much higher than in water (pK_a ca. 8; see below). This might seem surprisingly high but compares favorably to values reported for benzimidazoles in MeCN.[39] The DMSO had no effect on the ground state UV-vis absorption spectra even at 10% concentration. We take this as indication that hydrogen bonding without proton transfer is spectroscopically silent although it accelerates formation of the radical on the ligand.

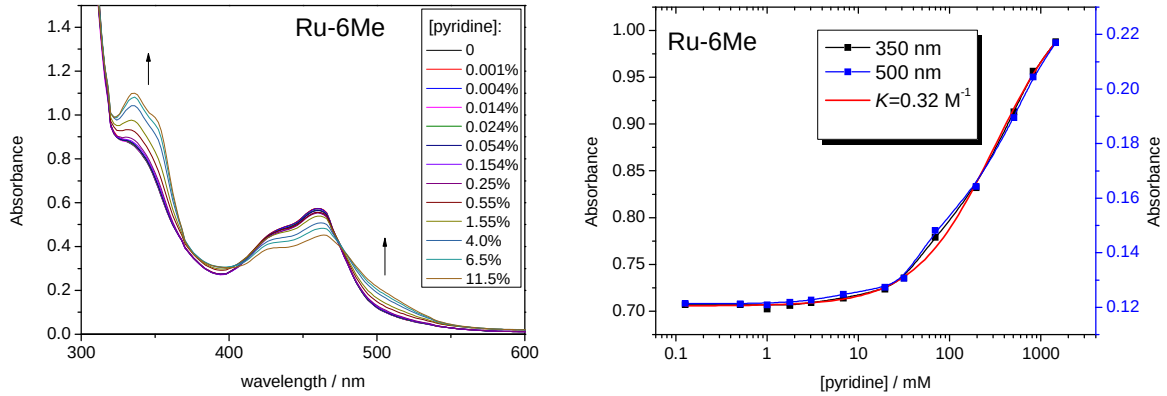

Figure 3.40: Left: *Titration of* ***Ru-6Me*** *in MeCN with increasing concentration of pyridine followed by changes in the UV/vis spectrum.* ***Right:*** *absorption increases at characteristic wavelengths.*

When we plot the rate of the slow phase, k_2, as a function of pyridine concentration (Figure 3.41), a saturation behavior can be observed. The data can be well fit with an equilibrium binding model similar to the one proposed by Pizano *et al.*[6] according to the equation,

$$k_2 = k_{ET} + k_{PCET}\frac{K_A[B]}{1+K_A[B]} \qquad (1)$$

where k_{ET} is the rate observed in absence of pyridine, k_{PCET} the maximum rate at saturating concentration of pyridine and K_A an association equilibrium constant describing effective binding of the complex to pyridine. The fit parameters are summarized in Table 3.2.

Table 3.2: *Parameters of fit curves according to Eq. 1 for data in Figure 3.41*

Complex	k_{ET} / s^{-1}	k_{PCET} / s^{-1}	K_A / M^{-1}
Ru-3Me	$3.1*10^4$	$4.6*10^6$	690
Ru-4Me	$1.7*10^5$	$0.95*10^6$	2230
Ru-6Me	$2.9*10^5$	$3.2*10^6$	510

We see that the rate k_{PCET} is two orders of magnitude higher than k_{ET}. This is taken to demonstrate the importance of proton coupled electron transfer in establishing the fully oxidized from of the ligand. For **Ru-4Me** the rates are smaller by a factor of 2-4 compared to the other two complexes but it shows a higher equilibrium constant.

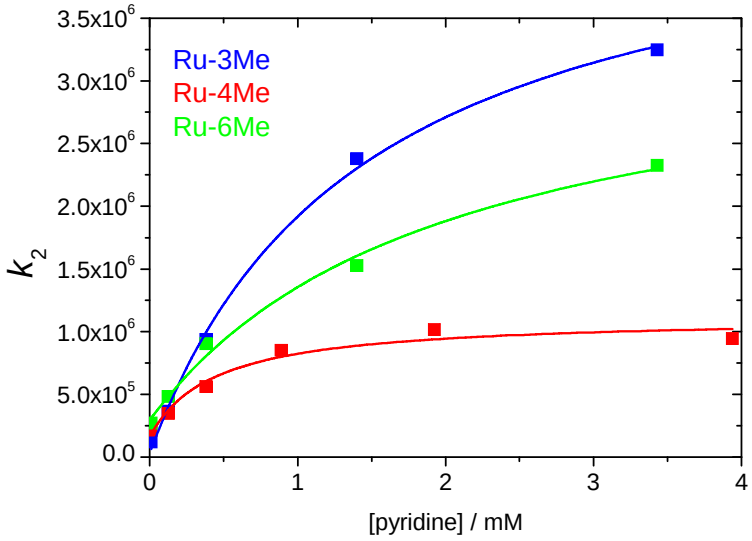

Figure 3.41: *Dependence of the apparent rate of the slow phase on pyridine concentration. Solid lines represent best fit with a equilibrium model equation 1. For parameters see Table 3.2.*

It is useful to summarize the results of these titration experiments concerning the changes in k_2. To do this we plot k_2 on a logarithmic scale for the concentrations (Figure 3.42). This visualization is quite instructive. The pattern of onset of acceleration of k_2 for the three complexes is similar for H_2O and pyridine, but the two are offset by a factor of 1000. Differences between the complexes observed for pyridine are reproduced for water, with **Ru-4Me** less sensitive than the others.

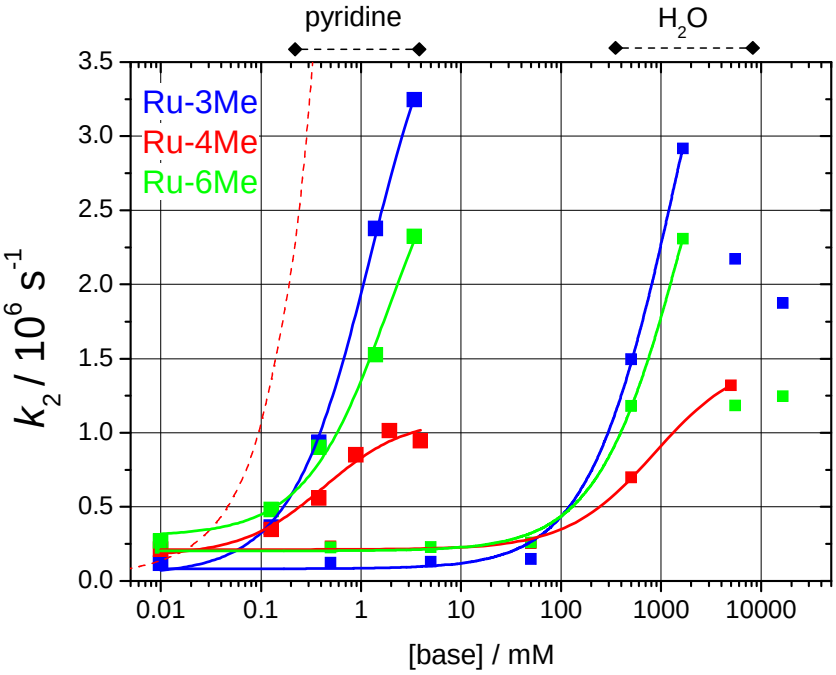

Figure 3.42: *Plot on a logarithmic scale of apparent rate of slow phase (k_2) as a function of concentration of pyridine (left) and water (right). Note that the points for neat MeCN is arbitrarily positioned at 0.01 mM. The dashed red line shows the diffusion limit ($k=10^{10}$ M^{-1} s^{-1}).*

The analysis of the dependence of the apparent rate for the slow phase based on an equilibrium binding model (Eq. 1) certainly gives good fits to the data points but it is not very satisfying, because it lets us with phenomenological parameters (K_A, k_{PCET}), the mechanistic meaning of which is not evident. We therefore propose an alternative model based on a rate limiting ET step following deprotonation of the imidazole according to the Scheme

$$\text{Ru(III)PhImiH} + \text{B} \underset{k_{-PT}}{\overset{k_{PT}}{\Leftrightarrow}} \text{Ru(III)PhImi}^- + \text{HB}^+ \xrightarrow{k_{ET}} \text{Ru(II) Ph}_{ox}\text{Imi} \qquad \text{Scheme 3.5}$$

In this model the left state, Ru(III)PhImiH, is in equilibrium with Ru(II)Ph_{ox}ImiH as discussed before (fast phase of Ru(III) reduction). Deprotonation of the imidazole group is necessary to allow complete oxidation of the ligand (mainly localized on phenol) for an equilibrium fraction of complexes characterized by the extent of slow phase of internal electron transfer from ligand to Ru(III). The protonation of the base is diffusion controlled thus depending on the concentration of base (k_{PT} = [base]*10^{10} $M^{-1}s^{-1}$) and deprotonation is given by modulated by the equilibrium between protonation of imidazole and protonation of the base (k_{-PT}=10^{10} $M^{-1}s^{-1}$ * $10^{pKbase-pKImi}$). Best fits with this model are shown as solid lines in Figure 3.42 and parameters are given in the Table below.

Table 3.3:*Parameters of fit curves according to Scheme 3.5 for data in Figure 3.41/3.42. For pK_a of pyridine (pKbase) in MeCN a value of 12.3 was used.*[39] *k_0 is the rate observed in neat MeCN.*

Complex	k_0 / s^{-1}	k_{ET} / s^{-1}	pK_A (Imi)
Ru-3Me	$4.2*10^4$	$4.3*10^6$	12.31
Ru-4Me	$1.7*10^5$	$0.93*10^6$	11.9
Ru-6Me	$3.0*10^5$	$3.1*10^6$	12.5

As expected this analysis reproduces the minimum and maximum rates for the electron transfer reaction determined above with the equilibrium model. The main results however are the values for the pK_a of the imidazole group which are found between 11.9 and 12.5 with **Ru-4Me** slightly more acidic than the other complexes. The fact that these values are lower by about 4 units than the ground state pK_a of the imidazole group (see pyridine titration of the ground state presented before) shows that deprotonation of imidazole occurs **after** phenol oxidation and that this preceding oxidation of the ligand causes a decrease in the imidazole pK_a.

A similar fit applied to the data for water titration (solid traces on right side of Figure 3.42) also gives good fits for the increase in the rate of k_2. For these fits we input the pK_a values for imidazole from Table 3.3 and obtained for the apparent pK_a of the base values between 9.0 and 9.3, indicating that water is a relatively weak base. It might be argued that the proton acceptor in the case of water is OH^- the concentration of which is $10^{-7}*[H_2O]$. However it can be doubted that this applies to small concentrations of water in MeCN making such consideration unreliable. In addition there are indications that a proton can be stabilized only in water clusters of a certain minimal size and that the structure of water in MeCN is significantly perturbed, making this case rather complex.[38] As a final point we want to mention that in the range of water concentration employed in the above study (up to 10%) the pK_a of the imidazole group is likely to change significantly and can no longer be treated as constant for precise simulation of the titration curve. The decrease of k_2 for the highest concentrations of water, a probably reliable feature visible in the data in Figure 3.42, might be a manifestation of such phenomena.

3.11 Acid/base properties of complexes

When electron transfer is coupled to proton transfer, the acid/base properties of the groups involved in the reaction are of great importance. Our **Ru-xMe** complexes have two functional groups, imidazole and phenol. In water the phenol has a pK_a of 10 while the pK_a for imidazole deprotonation is about 7. pK_a values in MeCN are difficult to determine, but we might presume that all pK_a values upshift by some units, as was deduced from the pyridine titrations presented before. The following pH titrations are therefore a tool to get information less on absolute values of pK_a than on relative values characterizing the different complexes.

Our complexes exhibit three ionization sites (Scheme 3.6). The effect of protonation and deprotonation events on these available sites can be followed by varying pH of the complex solution and measuring absorption or emission properties. As known from the literature deprotonation of the imidazole leads to reduced emission quantum yield whereas full protonation can be detected by shifts of the emission maximum.[33,34]

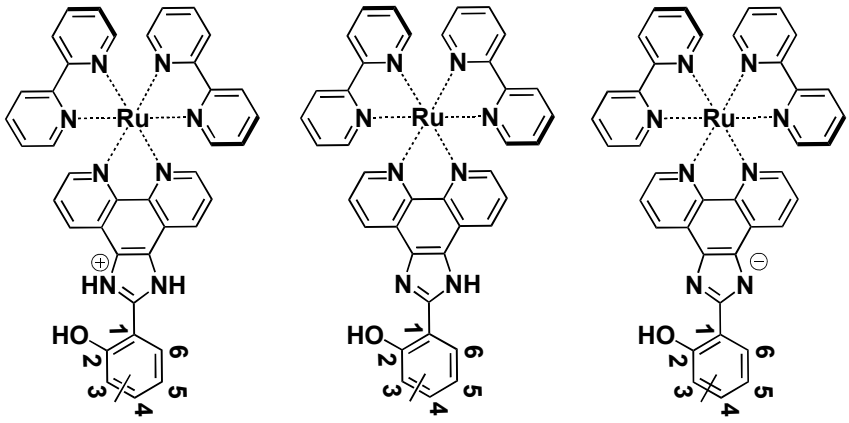

Scheme 3.6: *Possible protonation states of the complexes*

3.12 pH titration of absorption

We have performed UV Visible titration at different pH. These measurements are carried out by preparing a solution of the complex in acetonitrile and then 10% of an aqueous buffer solution of known pH was added. Each solution's absorption spectra were measured using a UV-Visible spectrophotometer.

Figure 3.43 shows titration of absorption spectra for **Ru-6Me** with increasing pH. As described in the literature we have observed increase in absorbance at 330 nm and 500 nm

which corresponds to the deprotonation of the imidazole.[33,34] A plot of absorbance *vs.* pH gives a pK_a value of 8.0. We expect to have similar pK_a value for **Ru-3Me** and **Ru-4Me**.

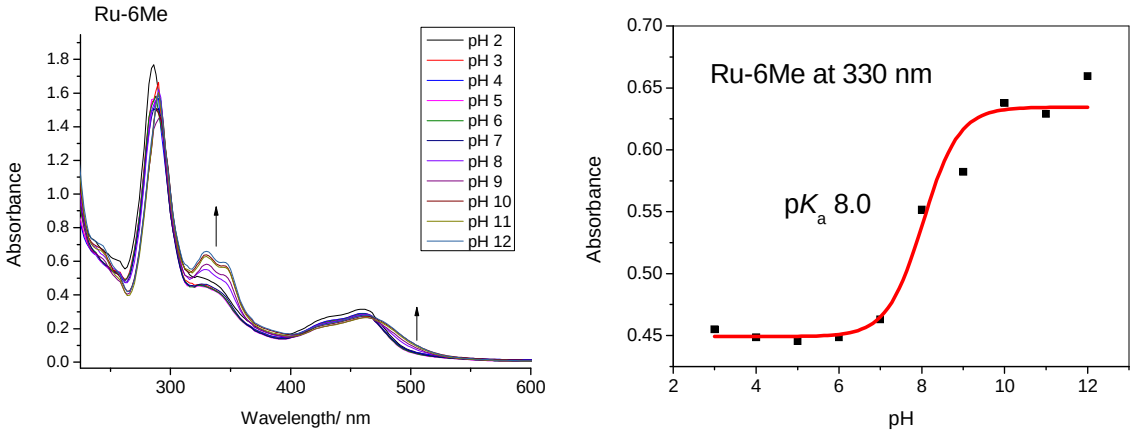

Figure 3.43: *Evolution of the absorption spectrum as a function of pH and fit of the absorbance at 330 nm.*

Similar to the ground state pK_a we have determined excited state pK_a* by measuring the relative yield of emission of an Ar purged solution at different pH in a fluorimeter. The sample concentration for each measurement was adjusted to an absorbance of 0.05 at 450 nm. The pH of the sample solution was varied by adding 10% buffer solution of known pH and the required pH was adjusted by adding either acid or base. The obtained emission spectra are shown in Figure 3.44. When the emission intensity is plotted *vs.* pH a pK_a 7.35 for **Ru-6Me** was determined. This is a pK_a for deprotonation of imidazole.[33,34] For the other complexes details can be found in Appendix 1, Section 8.

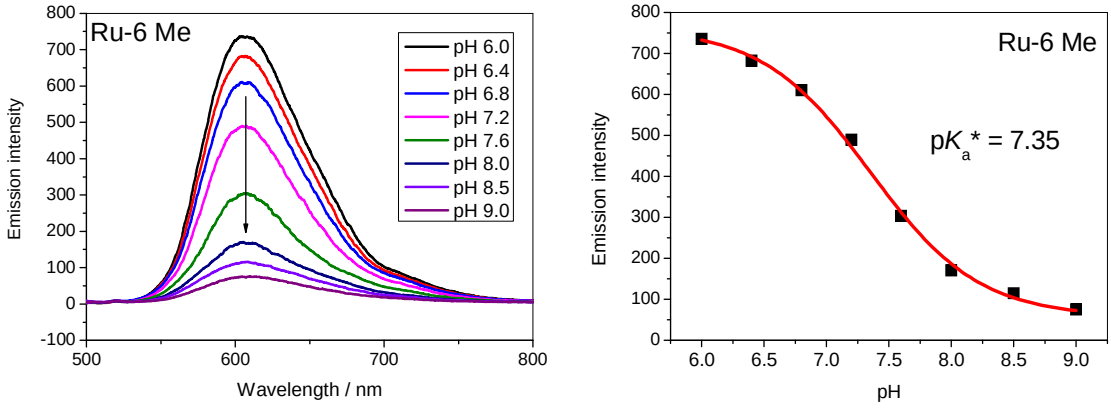

Figure 3.44: *Emission spectra at different pH and emission titration curve for* ***Ru-6Me****. The solid line is a fit giving pK_a* = 7.35*

Other experiments were performed to follow the variations of the wavelength of the emission maximum at very low pH and in these experiments revealed pK_a values of 0.17, 1.41 and 0.22

for **Ru-3Me, Ru-4Me** and **Ru-6Me,** respectively (Figure 3.45). The excited state pK_a values for protonation and deprotonation of the imidazole for **Ru-xMe** complexes are summarized in Table 3.4. It is very interesting to note that here again **Ru-4Me** behaves differently from the other two complexes, a feature which corroborates the differences found concerning kinetics of ligand oxidation. This gives a hint that the position of the methyl group might also influence on the acid/base properties of the ligand, with substitution on position 3 and 6 rendering it more acidic. When the complex is fully protonated by addition of strong acid ligand oxidation is severely inhibited if not blocked (data not shown). This corresponds to the situation on the left in Scheme 3.6 where the hydrogen bond between phenol and imidazole is no longer present.

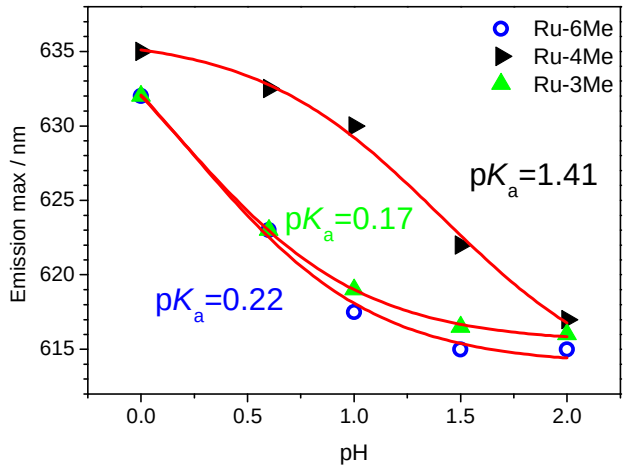

Figure 3.45: *Emission maximum wavelength as a function of pH for* ***Ru-xMe*** *complexes and fits giving pK_a*

Table 3.4: *Protonation and deprotonation pK_a^* values*

Complex	Protonation pK_a	Deprotonation pK_a
Ru-3Me	0.17	7.08
Ru-4Me	1.41	7.25
Ru-6Me	0.22	7.35

For comparison we have determined also the excited state pK_a values of **Ru-imi** and we have found values for pK_a* of 8.5 and 1.62 (Figure 3.46). The higher value of pK_a for

deprotonation is explained by an effect of hydrogen bonding interaction with the phenolic OH- group. The pK_a* for protonation is very close to the pK_a* value of **Ru-4Me**.

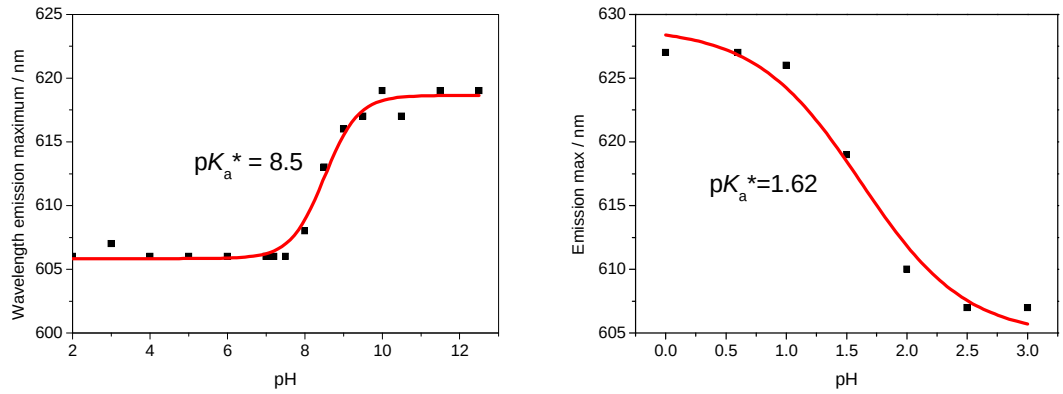

Figure 3.46: *pH titration plots for* ***Ru-imi;*** *deprotonation (left) and protonation state (right).*

3.13 Effect of temperature on the photophysical properties

With increasing temperature the rates of the k_2 phase accelerates (Figure 3.47) and the temperature dependence is well fitted with an Arrhenius equation. The activation energy obtained is 198 meV, typical for similar reactions but lower than the value of 320 meV for a Ru-Tyrosine complex.[22]

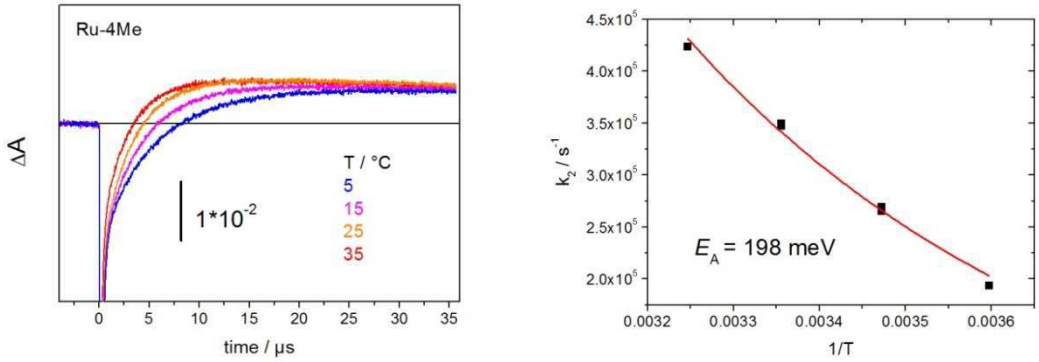

Figure 3.47:Left: *Effect of temperature on kinetic traces at 440 nm for Ru-4Me;* ***Right:*** *temperature dependence of the rate constant.*

3.14 Conclusions

We have successfully synthesized complexes with a chromophore electron relay system which are artificial mimics of photosystem II. According to electrochemistry these complexes were shown to exhibit higher ligand redox potentials compared to previously studied complexes. With redox potentials around 0.75 V *vs.* Fc these groups fulfill the thermodynamic requirement to function as electron relay in chromophore-catalyst assemblies for water oxidation. Therefore our first aim for synthesizing these complexes was fulfilled.

The higher redox potential implies a small driving force for electron transfer to the oxidized chromophore. Despite this fact, oxidation of the electron relay was found to be very fast, another prerequisite for efficient function of a final photocatalytic system.

Our three complexes **Ru-xMe** were shown to behave slightly differently when it comes to electron transfer properties which offer the possibility to investigate mechanistic details. The small driving force causes reversibility of the electron transfer reaction, which was detected by biphasic kinetics. A fast phase, dominant in **Ru-3Me** and **Ru-6Me**, but small in **Ru-4Me** was limited by the concentration of electron acceptor and could not be resolved further. Such fast electron transfer was only observed in complexes with a hydrogen bond demonstrating the important role of an internal base which assures fast deprotonation of the oxidized phenol. A slow phase, dominant in **Ru-4Me** but also present in the other two complexes was found to be very sensitive to external proton acceptors. According to our findings it is related with deprotonation of the imidazole 1-nitrogen, which is not involved in the hydrogen bond. The pK_a of this 1- nitrogen increases upon oxidation of the phenol and transfer of the proton in the H-bond and deprotonation stabilizes the oxidized state on the ligand by compensating for the positive charge. Imidazole with its two protonable sites therefore has a special role as a proton acceptor and donor.

The situation of small driving force observed for our complexes is very similar to the situation in PS II. In PS II, P680 is a shallow trap and already primary charge separation is reversible. Small energy differences also exist for the donor side reactions. However, due to reversibility kinetics become much more complicated as kinetics of subsequent steps has an influence on kinetics of previous steps. This makes analysis of kinetic data difficult as apparent kinetics of single molecular reaction steps become multiphasic and in general molecular rates cannot be observed directly. Comprehensive analysis then needs an adequate reaction scheme for the molecular processes together with an energetic scheme and additional information is usually

required to disentangle the underdetermined system. Comparison of energetic and dynamic features of the natural and artificial systems like those described here might therefore be particularly useful to advance our understanding of important principles of these energy conversion processes.

3.15 References

(1) Boussac, A.; Zimmermann, J.-L.; Rutherford, A. W.; Lavergne, J., Lavergne, J., Histidine oxidation in the oxygen-evolving photosystem-II enzyme. *Nature*, **1990**, 347, 303-306.

(2) Renger, G.; Renger, T., Photosystem II: the machinery of photosynthetic water splitting. *Photosynth. Res*, **2008**, *98*, 53-80.

(3) Saito, K.; Rutherford, A. W.; Ishikita, H., Mechanism of tyrosine D oxidation in Photosystem II., *Proc. Natl. Acad. Sci. U.S.A.*,**2013**, *110*, 7690-7695.

(4) Styring, S.; Sjöholm, J.; Mamedov, F., Two tyrosines that changed the world: Interfacing the oxidizing power of photochemistry to water splitting in photosystem II.*Biochim. Biophy. Acta, Bioenerg.*, **2012**, *1817*, 76-87.

(5) Sjödin, M.; Styring, S.; Åkermark, B.; Sun, L.; Hammarström, L., The mechanism for proton–coupled electron transfer from tyrosine in a model complex and comparisons with YZ oxidation in photosystem II. *Philos. Trans. R. Soc. London, Ser. B Biol. Sci.*,**2002**, *357*, 1471-1479.

(6) Pizano, A. A.; Yang, J. L.; Nocera, D. G., Photochemical tyrosine oxidation with a hydrogen-bonded proton acceptor by bidirectional proton-coupled electron transfer.*Chem. Sci.*,**2012**, *3*, 2457-2461.

(7) Meyer, T. J.; Huynh, M. H. V.; Thorp, H. H., The Possible Role of Proton-Coupled Electron Transfer (PCET) in Water Oxidation by Photosystem II.*Angew. Chem. Int. Ed.*, **2007**, *46*, 5284-5304.

(8) Blomberg, M. R.; Siegbahn, P. E.; Styring, S.; Babcock, G. T.; Åkermark, B.; Korall, P., A quantum chemical study of hydrogen abstraction from manganese-coordinated water by a tyrosyl radical: a model for water oxidation in Photosystem II. *J. Am. Chem. Soc.*,**1997**, *119*, 8285-8292.

(9) Siegbahn, P. E. M., Theoretical Studies of O−O Bond Formation in Photosystem II. *Inorg. Chem.*,**2008**, *47*, 1779-1786.

(10) Lin, X.; Hu, X.; Concepcion, J. J.; Chen, Z.; Liu, S.; Meyer, T. J.; Yang, W., Theoretical study of catalytic mechanism for single-site water oxidation process. *Proc. Natl. Acad. Sci. U.S.A.*,**2012**, *109*, 15669-15672.

(11) Brena, B.; Siegbahn, P. E.; Ågren, H., Modeling near-edge fine structure X-ray spectra of the manganese catalytic site for water oxidation in photosystem II. *J. Am. Chem. Soc.*,**2012**, *134*, 17157-17167.

(12) Glatzel, P.; Schroeder, H.; Pushkar, Y.; Boron III, T.; Mukherjee, S.; Christou, G.; Pecoraro, V. L.; Messinger, J.; Yachandra, V. K.; Bergmann, U., Electronic Structural Changes of Mn in the Oxygen-Evolving Complex of Photosystem II during the Catalytic Cycle.*Inorg. Chem.*,**2013**,*52*, 5642–5644.

(13) McEvoy, J. P.; Brudvig, G. W., Water-Splitting Chemistry of Photosystem II. *Chem. Rev.*,**2006**, *106*, 4455-4483.

(14) Moore, G. F.; Hambourger, M.; Gervaldo, M.; Poluektov, O. G.; Rajh, T.; Gust, D.; Moore, T. A.; Moore, A. L., A bioinspired construct that mimics the proton coupled electron transfer between $P680^{\bullet+}$ and the TyrZ-His190 pair of photosystem II. *J. Am. Chem. Soc.*,**2008**, *130*, 10466-10467.

(15) Irebo, T.; Zhang, M.-T.; Markle, T. F.; Scott, A. M.; Hammarström, L., Spanning Four Mechanistic Regions of Intramolecular Proton-Coupled Electron Transfer in a $Ru(bpy)_3^{2+}$–Tyrosine Complex.*J. Am. Chem. Soc.*, **2012**, *134*, 16247-16254.

(16) Moore, G. F.; Hambourger, M.; Kodis, G.; Michl, W.; Gust, D.; Moore, T. A.; Moore, A. L., Effects of Protonation State on a Tyrosine− Histidine Bioinspired Redox Mediator*J. Phy. Chem. B*,**2010**, *114*, 14450-14457.

(17) Costentin, C.; Louault, C.; Robert, M.; Savéant, J. M., The electrochemical approach to concerted proton—electron transfers in the oxidation of phenols in water. *Proc. Natl. Acad. Sci. U.S.A.*,**2009**, *106*, 18143-18148.

(18) Dixon, W. T.; Murphy, D., Determination of the acidity constants of some phenol radical cations by means of electron spin resonance.*J. Chem. Soc., Faraday Trans. 2***1976**, *72*, 1221-1230.

(19) Magnuson, A.; Berglund, H.; Korall, P.; Hammarström, L.; Åkermark, B.; Styring, S.; Sun, L., Mimicking electron transfer reactions in photosystem II: Synthesis and photochemical characterization of a ruthenium (II) tris (bipyridyl) complex with a covalently linked tyrosine. *J. Am. Chem. Soc.*,**1997**, *119*, 10720-10725.

(20) Zhang, M. T.; Irebo, T.; Johansson, O.; Hammarström, L., Proton-coupled electron transfer from tyrosine: a strong rate dependence on intramolecular proton transfer distance. *J. Am. Chem. Soc.*, **2011**, *133*, 13224-13227.

(21) Irebo, T.; Reece, S. Y.; Sjödin, M.; Nocera, D. G.; Hammarström, L., Proton-coupled electron transfer of tyrosine oxidation: Buffer dependence and parallel mechanisms. *J. Am. Chem. Soc.*, **2007**, *129*, 15462-15464.

(22) Sjödin, M.; Styring, S.; Åkermark, B.; Sun, L.; Hammarström, L., Proton-coupled electron transfer from tyrosine in a tyrosine-ruthenium-tris-bipyridine complex: Comparison with tyrosinez oxidation in photosystem II.*J. Am. Chem. Soc.*, **2000**, *122*, 3932-3936.

(23) Lachaud, F.; Quaranta, A.; Pellegrin, Y.; Dorlet, P.; Charlot, M. F.; Un, S.; Leibl, W.; Aukauloo, A., A Biomimetic Model of the Electron Transfer between P680 and the TyrZ–His190 Pair of PSII.*Ange. Chem. Int. Ed.*,**2005**, *44*, 1536-1540.

(24) Rappaport, F.; Lavergne, J., Coupling of electron and proton transfer in the photosynthetic water oxidase. *Biochim. Biophy. Acta, Bioenerg.*, **2001**, *1503*, 246-259.

(25) Dau, H.; Zaharieva, I.; Haumann, M., Recent developments in research on water oxidation by photosystem II. *Curr. Opin. Chem. Biol.*, **2012**, *16*, 3-10.

(26) Hiort, C.; Lincoln, P.; Norden, B., DNA binding of. DELTA.-and. LAMBDA.-[Ru (phen) 2DPPZ]$^{2+}$ *J. Am. Chem. Soc.*,**1993**, *115*, 3448-3454.

(27) Steck, E. A.; Day, A. R., Reactions of Phenanthraquinone with Aromatic Aldehydes and Ammonia in Alkaline Media.*J. Am. Chem. Soc.*,**1946**, *68*, 771-772.

(28) Cardinaels, T.; Ramaekers, J.; Nockemann, P.; Driesen, K.; Van Hecke, K.; Van Meervelt, L.; Lei, S.; De Feyter, S.; Guillon, D.; Donnio, B., Imidazo [4, 5-*f*]-1, 10-phenanthrolines: Versatile Ligands for the Design of Metallomesogens. *Chem. Materials*,**2008**, *20*, 1278-1291.

(29) Cardinaels, T.; Ramaekers, J.; Driesen, K.; Nockemann, P.; Van Hecke, K.; Van Meervelt, L.; Goderis, B.; Binnemans, K., Thermotropic ruthenium (II)-containing metallomesogens based on substituted 1, 10-phenanthroline ligands. *Inorg. Chem.*,**2009**, *48*, 2490-2499.

(30) Baron, A.; Herrero, C.; Quaranta, A.; Charlot, M. F.; Leibl, W.; Vauzeilles, B.; Aukauloo, A., Click chemistry on a ruthenium polypyridine complex.An efficient and versatile synthetic route for the synthesis of photoactive modular assemblies. *Inorg. Chem.***2012**, *51*, 5985-5987.

(31) Juris, A.; Balzani, V.; Barigelletti, F.; Campagna, S.; Belser, P. l.; Von Zelewsky, A., Ru (II) polypyridine complexes: photophysics, photochemistry, electrochemistry, and chemiluminescence.*Coord. Chem. Rev.*,**1988**, *84*, 85-277.

(32) Kalyanasundaram, K., Photophysics, photochemistry and solar energy conversion with tris (bipyridyl) ruthenium (II) and its analogues. *Coord. Chem. Rev.*,**1982**, *46*, 159-244.

(33) Quaranta, A.; Lachaud, F.; Herrero, C.; Guillot, R.; Charlot, M. F.; Leibl, W.; Aukauloo, A., Influence of the Protonic State of an Imidazole-Containing Ligand on the Electrochemical and Photophysical Properties of a Ruthenium(II)–Polypyridine-Type Complex. *Chem. Eur. J.*,**2007**, *13*, 8201-8211.

(34) Pellegrin, Y.; Forster, R. J.; Keyes, T. E., pH-Modulated photoinduced electron transfer in a {[ruthenium-adamantyl]·[β-cyclodextrin-methylviologen]} inclusion complex. *Inorg. Chim. Acta*,**2008**, *361*, 2683-2691.

(35) Pellegrin, Y.; Forster, R. J.; Keyes, T. E., pH Dependent photophysics and role of medium on photoinduced electron transfer between ruthenium polypyridyl complex and anthraquinone.*Inorg. Chim. Acta*,**2009**, *362*, 1715-1722.

(36) Sheth, S.; Baron, A.; Herrero, C.; Vauzeilles, B.; Aukauloo, A.; Leibl, W., Light-induced tryptophan radical generation in a click modular assembly of a sensitiser-tryptophan residue.*Photochem. Photobiol. Sci.*, **2013**, *12*, 1074-1078.

(37) Neshvad, G.; Hoffman, M. Z., Reductive quenching of the luminescent excited state of tris (2, 2'-bipyrazine) ruthenium (2+) ion in aqueous solution. *J. Phy. Chem.*,**1989**, *93*, 2445-2452.

(38) Huppert, D.; Kolodney, E., Picosecond proton transfer studies in water-alcohols solutions. *Chem. Phy.*,**1981**, *63*, 401-410.

(39) Kaljurand, I.; Rodima, T.; Leito, I.; Koppel, I. A.; Schwesinger, R., Self-consistent spectrophotometric basicity scale in acetonitrile covering the range between pyridine and DBU. *J. Org. Chem.*,**2000**, *65*, 6202-6208.

4.0 Light-induced Tryptophan oxidation

4.1 Introduction

In biological systems, electron transfer reactions are important and studied within the matrices.[1-3] Mostly in such biological systems the mechanism of the electron transport chain involves electrons and protons flow across the protein boundaries.[4] These charge transfer processes are difficult to study *in vivo*. Thus it would be quite convenient to study isolated biological complexes activated by various means like electrochemical[5], chemical, physical, and photochemical.[6] These kind of studies help us to elucidate complex mechanistic details behind charge transfer processes occurring in biological systems thus giving guidance to mimic biological processes.[1] In biological systems redox reactions of amino acids have been studied and still there is a growing interest in studying such reactions.

There are 20 amino acids present in natural systems and some of them play an important role in enzymatic reactions both in plants[7] and animals.[8,9] Out of these 20 amino acids redox active amino acids such as tyrosine[10] and tryptophan[11] (Figure 4.1) are most relevant for our study. Upon oxidation tyrosine and tryptophan undergo radical formation and these radicals are important mediators in enzymatic reactions.[12-14] Radical formation involves an electron transfer and this electron transfer from an amino acid is often coupled with deprotonation. This gives rise to the phenomenon of proton coupled electron transfer (PCET) , a topic which is intensely discussed.[15,16]

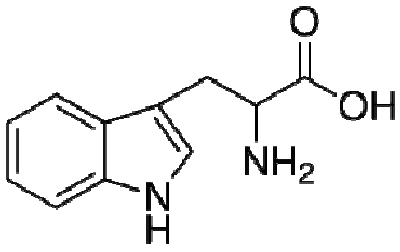

Figure 4.1: *Tryptophan*

Here we studied tryptophan radical generation by photoactivation. The Tryptophan radical gets generated by either electron transfer to the photogenerated oxidant or via H-atom transfer. Depending on that, tryptophan (Trp) radicals are either formed as protonated tryptophan ($TrpH^{\bullet+}$) or neutral tryptophan radical ($Trp^{\bullet}$) (Figure 4.2)[17]. For easy identification these radicals are depicted in Table 4.1.

These radicals are key intermediates in the ribonucleotide reductase[18], lignin peroxidase[19], cytochrome c peroxidase[20] and DNA photolyase.[21] Tryptophan is a secondary amine with pK_a of 17. The high value of pK_a indicates that the proton present in the tryptophan is not easily dissociable and this unique characteristic has important consequences in biological electron transfer. The pK_a of the protonated radical ($TrpH^{\bullet+}$) is 4.7[22] which means that it will deprotonate under physiological conditions.

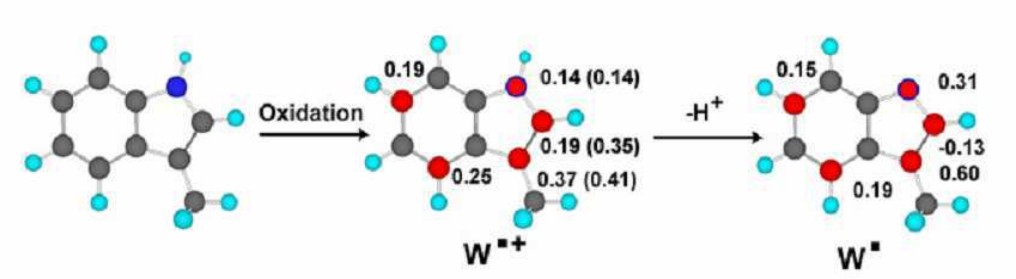

***Figure 4.2**: Schematic of a one-electron oxidation of tryptophan: Numbers correspond to spin density calculated by DFT methods. Color scheme: (●) proton (●) carbon (●) nitrogen (●) spin density.*[17]

Abbreviation	Name	Structure
$W^{\bullet+}$	tryptophan radical cation	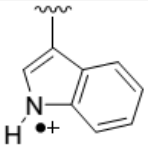
$W^{\bullet}$	tryptophan radical	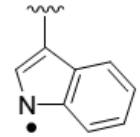

***Table 4.1:** Tryptophan radicals*

According to the literature these tryptophan radicals have typical transient absorption spectra shown in Figure 4.3 with maxima at around 510 and 570 nm for $Trp^{\bullet}$ and $TrpH^{\bullet+}$ radicals respectively.[23]

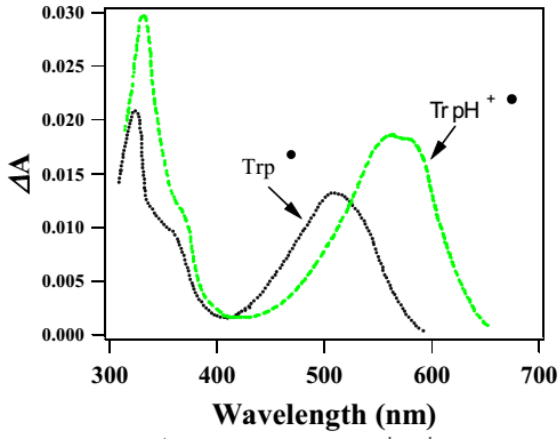

***Figure 4.3**: Absorption spectra of $TrpH^{\bullet+}$ and $Trp^{\bullet}$ radical*[23]

Detection of the formed tryptophan radical by various sophisticated techniques has been already reported in the literature. Techniques like electron paramagnetic resonance (EPR)[24] and flash photolysis[25] were applied.

Gray and his co-workers have reported X-band EPR spectrum of the tryptophan radical obtained in the *Pseudomonas aeruginosa* azurin protein environment (Figure 4.4).[24] The 285 GHz (Figure 4.4, lower left inset) yielded *g* values close to 2.003.

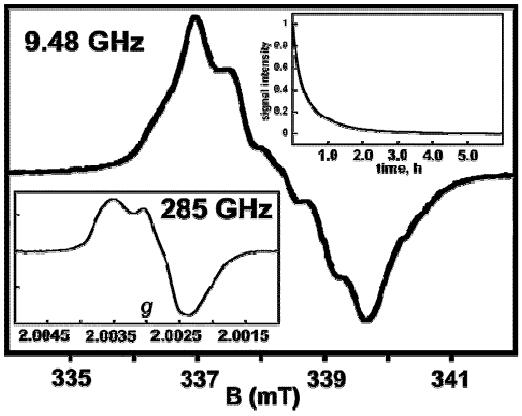

***Figure 4.4:** X-band EPR spectrum of **Pseudomonas aeruginosa azurin** under anaerobic conditions (77 K pH 7.2, ν = 9.4753 GHz). Lower left inset: 285 GHz EPR spectrum under nonsaturating conditions (50 K) Upper right inset: room-temperature decay of the EPR signal monitored at g = 2.011, ν = 9.7972 GHz)*[24]

4.2 Photo-activation of tryptophan

From the available published information the photoactivation of the tryptophan was carried out either via covalent linkage between chromophore and amino acid[26] or by bimolecular pathway by mixing chromophore and amino acid in the solution.[27,28] Based on these two

approaches we can easily classify in a broad sense the photoactivation of an amino acid by two ways:

1) Intermolecular (bimolecular) interaction of an amino acid with the photosensitizer in solution
2) Intra-molecular photoactivation by covalent linkage between photosensitizer and amino acid

These two methods have advantages and disadvantages over each other.

4.2.1 Intermolecular activation of tryptophan

Hammarström and his coworkers reported the intermolecular (bimolecular) oxidation of tryptophan with water as a primary proton acceptor.[27] Their study had shown that bimolecular tryptophan oxidation follows either a concerted electron-proton transfer mechanism or a stepwise electron transfer proton transfer mechanism. The kind of mechanism followed is depending on the pH and the oxidizing power of the Ru(III) used as photooxidant. They have used different tryptophan derivatives, **N-Ac-TrpH** and **O-Et-TrpH** (Figure 4.5) in order to avoid the complicated protonation behavior of the normal tryptophan. Figure 4.5 also shows the Ru-polypyridyl photosensitizers used in their study.

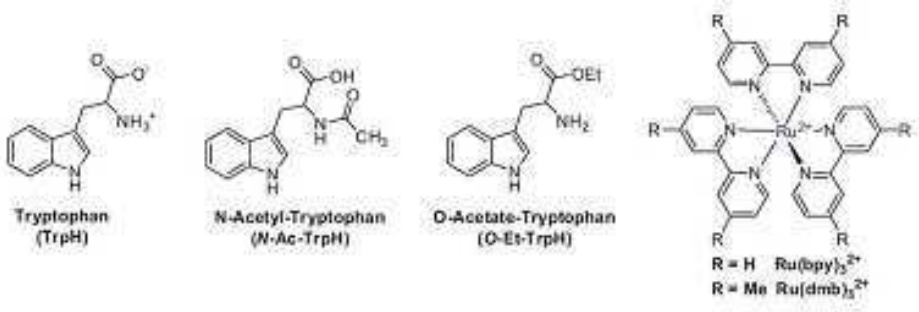

***Figure 4.5**: Structure of tryptophan derivatives and Ru(II) sensitizers used in Hammarström's study[27]*

The tryptophan oxidation studies were performed in the presence of 20 mM methyl viologen as an electron acceptor, 30 µM Ru(II)polypyridine complex and 1-5 mM of tryptophan derivative in 0.55 mM of phosphate buffer using Laser Flash Photolysis technique. The kinetic behavior as a function of pH is shown in Figure 4.6. From the obtained dependence on pH they were able to conclude that **O-Et-TrpH** and **$[Ru(dmb)_3]^{3+}$**were reacting via a concerted electron proton transfer (CEP) mechanism over the pH range 4.5 -11 with kinetic

isotope effect (KIE) of 2.3-2.6. For the rate of this CEP a slope of 0.3-0.5 was obtained when log *k* (reaction rate) *vs.* pH was plotted.

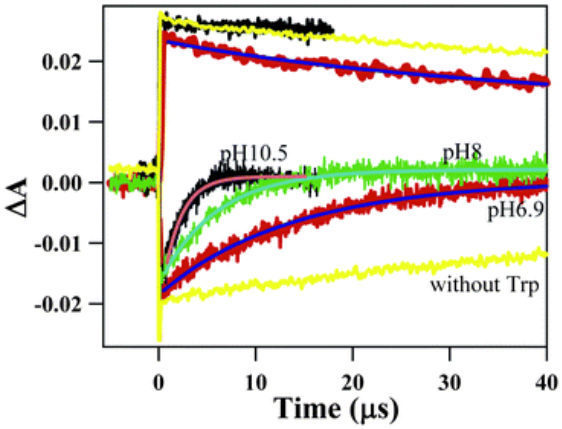

Figure 4.6: *Typical transient absorbance kinetic traces for the reaction between* ***O-Et-TrpH*** *and laser flash-quench generated* ***[Ru(dmb)$_3$]$^{3+}$*** *at different pH values, showing the rapid (<100 ns) generation of the MV$^{+\bullet}$ radical cation at 600 nm (upper traces) and bleach of the Ru(II) absorption at 450 nm (lower traces). The 450 nm absorption recovery monitors the subsequent bimolecularPCET from tryptophan to Ru(III) and shows pH-dependent kinetics.*[27]

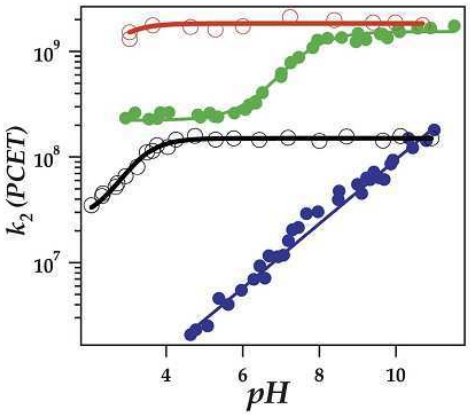

Figure 4.7: *pH dependence of the observed rate constants for intermolecular oxidation of tryptophan to the flash quench generated Ru(III) in 0.5 mM phosphate/borate buffer:* ***N-Ac-TrpH*** *and* ***[Ru(bpy)$_3$]$^{3+}$*** *(red open circles),* ***O-Et-TrpH*** *and* ***[Ru(bpy)$_3$]$^{3+}$*** *(green filled circles),* ***N-Ac-TrpH*** *and* ***[Ru(dmb)$_3$]$^{3+}$*** *(black open circles) and* ***O-Et-TrpH*** *and* ***Ru(dmb)$_3$]$^{3+}$*** *(blue filled circles respectively.*[27]

However, in the presence of **[Ru(bpy)$_3$]$^{2+}$**, a stronger oxidant, an electron-proton transfer (ETPT) mechanism was proposed to occur at pH < 6 with KIE = 1.0 whereas at pH > 6 the CEP mechanism dominates with KIE = 2.0. While in case of **N-Ac-TrpH** a pH independent kinetics was observed between pH 4-10 (Figure 4.7).

Another article concerning a similar bimolecular study of oxidation of tryptophan **(N-Ac-TrpH)** by the polypyridyl metal complex **[Os(bpy)$_3$]$^{3+}$** was published by Mayer and his co-workers.[28] Their article focuses on the oxidation of tryptophan following a concerted Electron-Proton transfer (EPT) mechanism using hydroxide as a base. (Scheme 4.1) They have used cyclic voltammetry and stopped flow spectrophotometry techniques for the study. First order rate dependence with respect to [OH$^-$] was observed for pH between 10-12. This gives an indication for CEP mechanism and no effect on kinetics was reported in the pH range 6-9.

$$Os(bpy)_3^{3+} + TrpNH \underset{k_{-1}}{\overset{k_1}{\rightleftharpoons}} Os(bpy)_3^{2+} + TrpNH^{+\bullet}$$

$$TrpNH^{+\bullet} \underset{k_{-2}}{\overset{k_2}{\rightleftharpoons}} TrpN^{\bullet} + H^{+}$$

$$TrpNH^{+\bullet} + TrpN^{\bullet} \xrightarrow{k_3} TrpNH + TrpN^{+}$$

$$TrpN^{+} \xrightarrow{H_2O/O_2} oxidation\ products$$

Scheme 4.1: *Mechanism showing [OH⁻] as a proton acceptor and subsequent generation of radical on the tryptophan.*[28]

4.2.2 Intramolecular activation of tryptophan

Recently Hammarström and his coworkers reported photo-activation of tyrosine and tryptophan by using covalent linkage with a chromophore.[26,29] Their findings have confirmed electron transfer and radical formation in such systems. The difference between tyrosine and tryptophan is the side chain which is a phenol or indole group, respectively (Figure 4.8). Thus both of these amino acids have one oxidizable species either phenol for tyrosine or indole for tryptophan. One electron oxidation generates radical species (either phenoxyl or tryptophanyl) and this oxidation is coupled with the movement of a proton, making these amino acids of great importance in bioenergetic systems. This kind of mechanism is called "proton coupled electron transfer" which describes electron and proton movement on thermodynamic grounds. From the pH dependence and varying again the strength of Ru(III) as an oxidant by varying substituents on the chromophore, Hammarström *et al.* have concluded on the PCET mechanism. In this PCET reaction there was competition between stepwise reaction in which electron transfer is followed by deprotonation of the radical, termed ETPT mechanism, and a concerted reaction, in which both (electron and proton) migrate in a single step better called CEP.

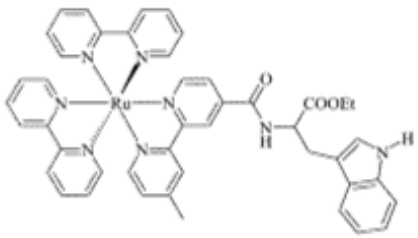

Figure 4.8: *Structures of covalently attached chromophore to tryptophan (Ru-Trp.)*[26,29]

The oxidation potential of an amino acid residue is measured as E^0 ($Trp^{\bullet}H^{+}$/ TrpH) = 1.21 V (vs. NHE).[30] An important thing which has to be considered besides redox potentials is that

the radical can exist in its protonated state. The Figure 4.2 and 4.3 shows that radical can exist as a protonated or neutral state. Upon oxidation the tryptophan first forms a protonated radical, $Trp^{\bullet}H^{+}$(p*K*a ~ 4.3-4.7),[25] which rapidly loses a proton to give $Trp^{\bullet}$ (τ = 1.1 µs). To favor a given pathway, proteins can stabilize either $Trp^{\bullet}$ or $Trp^{\bullet}H^{+}$. The determining factor for one over the other form of radical is the difference of redox potentials between these two species which is ~ 100 mV.[31] Thus it is absolutely necessary to distinguish and study these two states of radical. The technique laser flash photolysis will be helpful to distinguish one radical form from the other by recording transient absorption spectra and transitions between the two forms can be followed by observing kinetics of each one at corresponding wavelengths.

The intramolecular approach has some advantages over intermolecular electron transfer studies as it allows,

1) To fix the constitutive units at a given distance,
2) Exclude the energy needed for the encounter complex for electron transfer processes,
3) Minimize deleterious intermolecular pathways
4) Permit intramolecular electron transfer

Here we studied photoactivation of tryptophan covalently attached to the **$[Ru(bpy)_3]^{2+}$** chromophore via a click chemistry modular assembly, **Ru-Trp** (Figure 4.9).

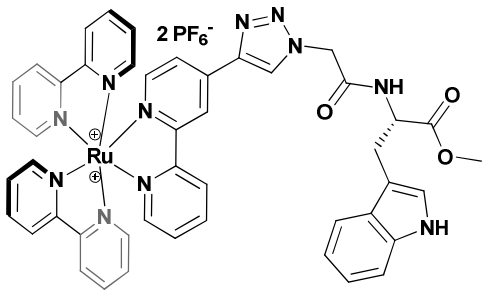

Figure 4.9: *Ru-Tryptophan (**Ru-Trp**)*

4.3 Synthesis

The idea behind the synthesis of the complex was two folds:

1) Validate click chemistry as a tool to link chromophore and redox active unit
2) Investigate the mechanism of electron transfer and proton transfer under suitable conditions

In click chemistry a triazole ring is formed during the reaction which acts as a coupling unit between chromophore and azido functionalized moiety.

4.3.1 Click chemistry - Introduction

The copper catalyzed azide cyclo addition, commonly called click chemistry, has been first described by Sharpless in 2001.[32] It is often used in a tailored approach to assemble quickly and to synthesize rapidly giant molecules by coupling small units together. Since then it has been used in wide disciplines of chemistry and biology.[33] The simplified scheme of click chemistry is exemplified by the following reaction Scheme 4.2.

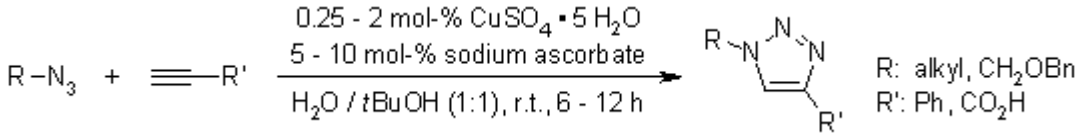

Scheme 4.2: *Typical conditions for the Copper-Catalyzed Azide-Alkyne Cycloaddition*[34]

4.3.2 Mechanism of the Copper-Catalyzed Azide-Alkyne Cycloaddition (CuAAC)

The copper-catalyzed azide-alkyne cycloaddition has many advantages over Huisgen 1,3-Dipolar Cycloaddition. Basically, Huisgen 1,3-Dipolar Cycloaddition requires elevated temperature to undergo reaction between alkyne and azide. High temperature used for such reaction produces two regioisomers when asymmetric alkynes are used. These kinds of drawbacks can be easily avoided by using copper-catalyzed azide-alkyne cycloaddition. The copper catalyst permits acceleration of the reaction rate by 10^7 to 10^8 compared to the uncatalyzed reaction. It works at low temperature, is insensitivity to aqueous environment, and operates in a broad pH range 4-12. The resulting product of the reaction can be isolated in pure form by simple filtration or extraction without use of routine purification techniques like chromatography.

The active Cu (I) catalyst can be generated from Cu (I) salts or Cu (II) salts using a reducing agent like sodium ascorbate. Oxidative homo coupling products can be prevented by addition of a slight excess of sodium ascorbate.

4.3.3 Ru-Tryptophan (Ru-Trp) Complex synthesis

The azide modified tryptophan derivative was synthesised following the method of Todd *et al*.[35] Nucleophilic substitution of 2-bromo acetic acid in presence of sodium azide (NaN_3) gave 2-azido acetic acid in high yield. The peptide linkage with tryptophan methyl ester yielded the azido tryptophan derivative quantitatively (Scheme 4.3).

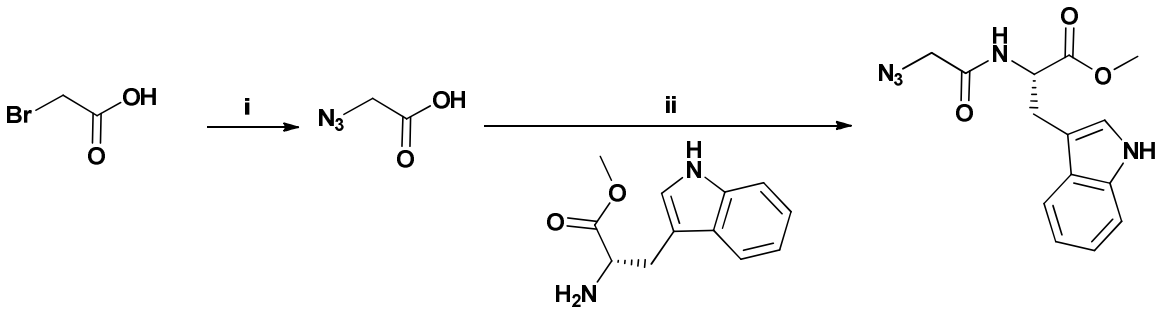

Scheme 4.3: *Reagents and Conditions: (i) NaN_3, H_2O (93%)[35,36] (ii) HBTU, DMAP, DIPEA, CH_3CN (99%)[35,36]. DMAP=4-(Dimethyl-amino)-pyridine; HBTU=O-Benzotriazole-N,N,N',N'-tetramethyl-uronium-hexafluoro-phosphate; DIPEA=N,N-Diisopropylethylamine*

The complex Ru-triazole-tryptophan **(Ru-Trp)** was obtained after performing a copper catalysed azide-alkyne cycloaddition reaction between the alkyne-derived complex, **Ru-CCH,** and the azido-derived tryptophan (Scheme 4.4).

This azido tryptophan was undergoing click reaction in presence of copper sulfate and sodium ascorbate as a reductant to form the ruthenium tryptophan complex.

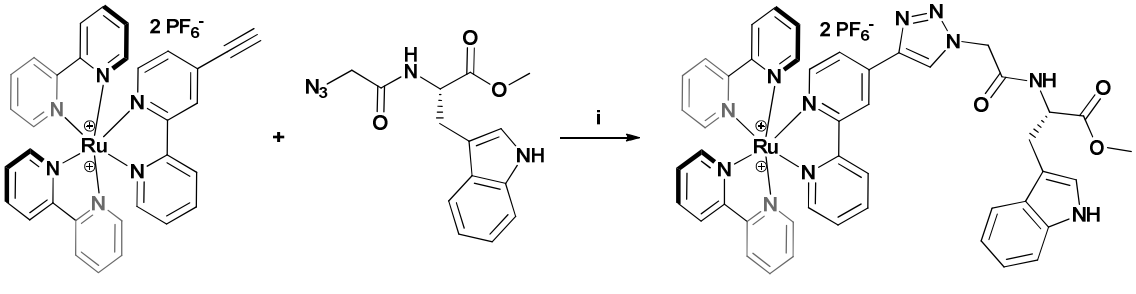

Ru-CCH **Ru-Trp**

Scheme 4.4: *Reagents and Conditions: (i) $CuSO_4.5H_2O$, sodium ascorbate, CH_2Cl_2/H_2O (90%)*

For synthetic details and its characterization refer to the experimental section.

4.4 Electrochemistry

The electrochemical properties of **Ru-Trp** in acetonitrile were studied by cyclic and differential pulse voltammetry using ferrocene as the reference. Besides the typical features of ruthenium trisbipyridyl complexes, *i.e.* a quasireversible Ru(III)/Ru(II) oxidation wave at 0.82 V (ΔEp = 110 mV) and three quasi reversible reduction waves for the bipyridine ligands (-2.25, -1.99, -1.78 V; (ΔEp = 90, 80, 60 mV), we observed an additional irreversible wave at 0.69 V (Figure 4.9) which is attributed to the oxidation of the tryptophan. For clear visualization of oxidation wave of cyclic voltammogram and differential pulse voltammogram refer Appendix 2 (Figure 4.A1 and Figure 4.A2).No redox activity of the triazole unit was detected in the potential window investigated in these experiments.

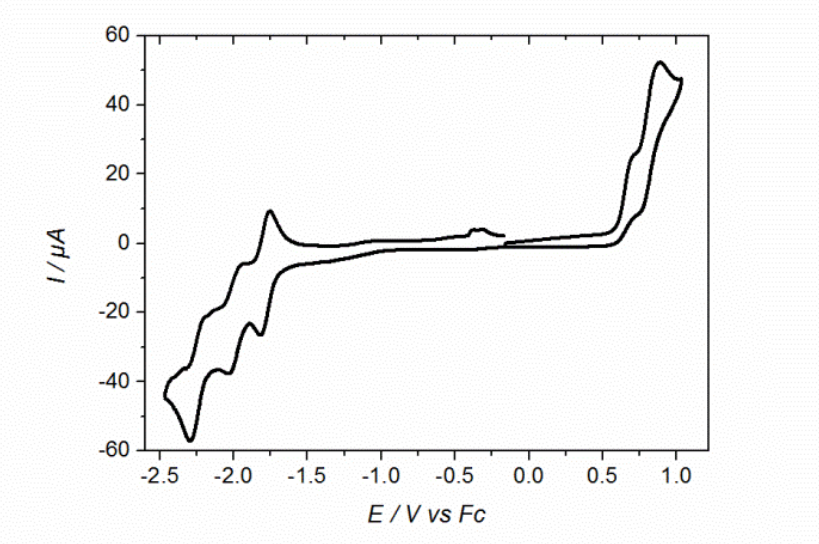

Figure 4.9: *Cyclic voltammogram of 1 mM* ***Ru-Trp*** *vs. ferrocene in argon-saturated acetonitrile with tetrabutyl ammonium hexafluoro phosphate as supporting electrolyte. Scan rate: 100 mV/s.*

The pH dependence on the oxidation potential of **Ru-Trp** was studied using differential pulse voltammetry in water while varying the pH of the solution by addition of diluted solutions of HCl and NaOH. The potential was independent of pH below pH 3 and displayed a slope of –30 mV/pH unit in the range pH 3-8, corresponding to a two-electron, one-proton process. These results are in agreement with those reported in similar systems.[26,29] A pK_a of about 2.7±0.5 (Figure 4.10) can be estimated for the oxidised tryptophan which is at least one unit lower than typical values for isolated tryptophan (pK_a~4.3-4.7).[22,37] No significant change of the Ru(III)/Ru(II) potential with pH was observed.

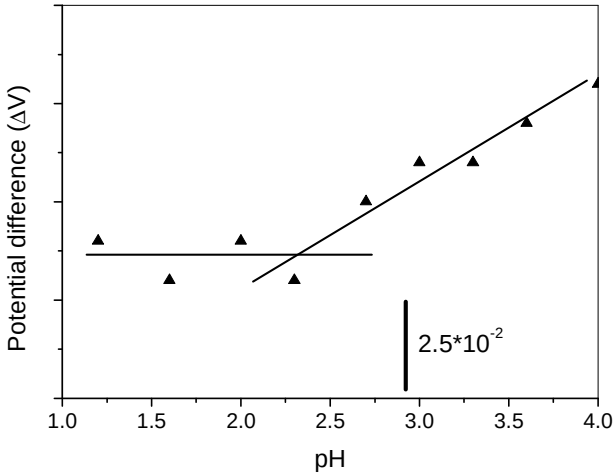

Figure 4.10: *Difference in potential between ruthenium and tryptophan as a function of pH; pK_a 2.7*± 0.5 *for tryptophan*

4.5 Photophysical studies

4.5.1 Absorption and emission properties

Ru-Trp shows ground state absorption properties very similar to those of the **Ru-CCH** and **$[Ru(bpy)_3]^{2+}$**parent compounds. Its absorption spectrum is dominated by strong π-π* (bpy) transitions at 290 nm, and a Metal to Ligand Charge Transfer (MLCT) absorption with maximum at 458 nm (Figure 4.11) both comparable to **$[Ru(bpy)_3]^{2+}$** as described in Chapter 1 Introduction.

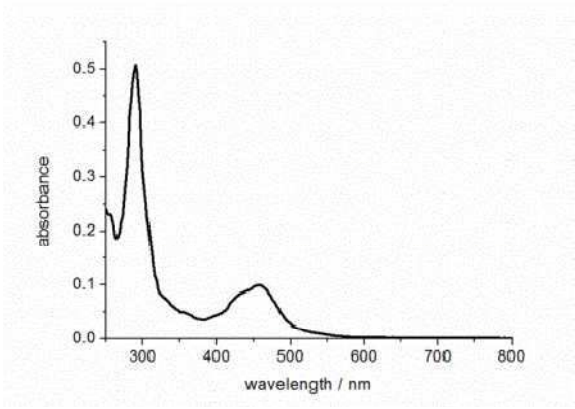

Figure 4.11: *Absorption spectrum of* ***Ru-Trp*** *in acetonitrile*

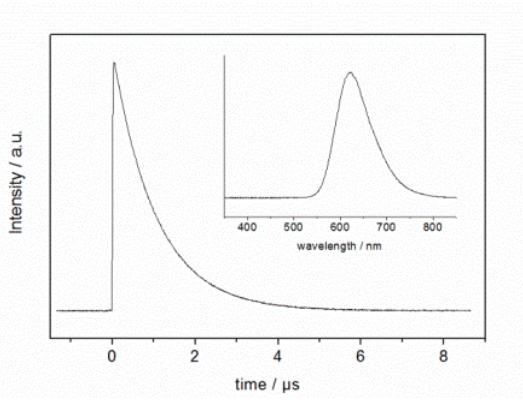

Figure 4.12: *Emission decay of* ***Ru-Trp*** *at 620 nm (inset: emission spectrum) in acetonitrile*

The **Ru-Trp** emission properties are characterized by an emission maximum at 620 nm and emission kinetics shows monoexponential decay with a lifetime of 1040 ns (Figure 4.12).This value is in agreement with the emission quantum yield of 0.074 which was determined from

steady state emission using **[Ru(bpy)$_3$]$^{2+}$** as reference.[38] These data show that the photophysical properties of the chromophore are unaltered in the Ru-triazole-tryptophan assembly, which is in agreement with previous results obtained on other triazole-connected chromophore-ligand assemblies.[39,40] The fact that the emission is not quenched shows the absence of either excited state energy transfer, or electron transfer between the ruthenium chromophore and the ligand.

4.5.2 Electron transfer studies

Flash photolysis experiments were performed in order to investigate the light-induced oxidation of the tryptophan residue. Excitation of **Ru-Trp** in a MeCN/H_2O (50:50) mixture with 460 nm laser flashes in presence of 10 mM methyl viologen acting as a reversible electron acceptor showed depletion of the Ru(II) signal as evidenced by a bleach in its 450 nm absorption band, and the concomitant formation of reduced methyl viologen ($MV^{+\bullet}$) observed as an increase in the absorption at 605 nm (Figure 4.13). The recovery of the 450 nm Ru(II) signal is very fast (350 ns) whereas the recovery of the oxidised methyl viologen occurs on a much longer time scale (≈ 300 µs, inset in Figure 4.13). These results clearly indicate that the Ru(II) ground state absorption is recovered by intramolecular electron transfer from the tryptophan ligand to the oxidised chromophore rather than by intermolecular charge recombination between Ru(III) and the reduced form of the electron acceptor. From a thermodynamic point of view, this process is in accord with the electrochemical data where the oxidation of Trp by the Ru(III) is expected to be exergonic by about 130 mV. Comparison of the emission lifetime in presence of the electron acceptor and the kinetics of recovery of Ru(II) reveals apparent rates which are identical within the error range. This indicates that, under the MV^{2+} concentrations used (10 mM), formation of the oxidised state of the chromophore by inter-molecular reduction of MV^{2+} is rate-limiting for the subsequent ligand oxidation, and that the intrinsic rate of internal electron transfer is significantly faster. Using higher MV^{2+} concentrations allows to accelerate the formation of the Ru(III) state to about 20 ns, as detected by the emission decay kinetics. Under these conditions the rate of internal electron transfer could be determined as 100 ns ($10^7 s^{-1}$) by kinetic analysis of the 450 nm kinetics. This value confirms the hypothesis of the triazole ring providing a link which allows for efficient electron transfer.[39,40]

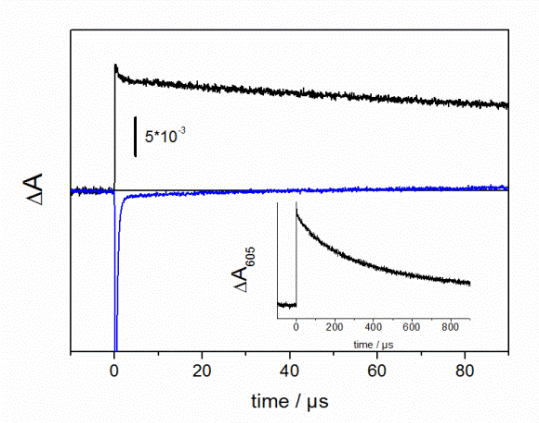

Figure 4.13: *Transient absorption traces for* ***Ru-Trp*** *in argon-saturated MeCN/H_2O (50:50) solutions at 605 nm (black) and 450 nm (blue) upon excitation with nanosecond laser flashes at 460 nm. 10 mM MV^{2+} was used as external electron acceptor. Inset: decay of 605 nm transient at longer time scale.*

These laser flash photolysis results suggest that light excitation of **Ru-Trp** in presence of an external electron acceptor leads to oxidation of the ligand, *i.e.* formation of a tryptophan radical.

4.6 Electron paramagnetic resonance (EPR)

We performed EPR experiments on a sample frozen during continuous illumination for 10 seconds in presence of 4-nitrobenzenediazonium tetrafluoroborate as sacrificial, irreversible electron acceptor. As depicted in Figure 4.14, we observed the formation of a narrow signal at *g*~2.00 (width 14 G) typical for an organic radical. This signal is attributed to the formation of the tryptophanyl radical which gives further confirmation to laser flash photolysis experiments. The broad signal at *g*~2.72 is attributed to Ru(III) species formed by additional oxidation of the ruthenium-tryptophanyl species.

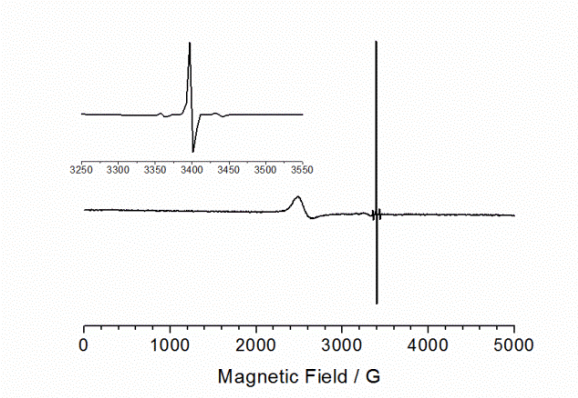

Figure 4.14: *X-band EPR spectrum (10 scans) of a mixture of 500 µM* ***Ru-Trp*** *with 25 mM 4-nitrobenzenediazonium tetrafluoroborate in acetonitrile after 10 second illumination with 450 nm light. Experimental conditions: microwave frequency 9.494 GHz, microwave power 0.100 mW, modulation amplitude 10 G, temperature 50 K, time constant 1.28 ms, scan width 5000 G, modulation frequency 100 kHz. Inset: zoom on the g~2.00 radical signal.*

4.7 Proton coupled electron transfer

The use of MV^{2+} as external electron acceptor has the advantage that its redox state can easily be followed due to the strong and characteristic absorption of its reduced form at 390 and 605 nm. However, the same property represents a drawback when monitoring changes in the visible range that might arise from the oxidation of the ligand. Therefore, hexammineruthenium(III) chloride, which shows negligible absorption changes in the visible region upon reduction was used as an alternative electron acceptor. Figure 4.15 shows the transient absorption spectra at 3 µs after the excitation flash of a mixture of complex **Ru-Trp** and 20 mM hexammineruthenium(III) chloride upon light excitation at 460 nm light in an acetonitrile/water mixture. Citric acid buffer was used to adjust the pH of the solution at values above and below the pK_a of the oxidised Trp. The two spectra are characteristic of the protonated (pH 2.4) and deprotonated (pH 5) forms of the tryptophan radical which show a broad absorption maximum at 530-600 nm for the former, and a sharper maximum at 500 nm for the latter.[23] At time = 3 µs after the excitation flash the two species are fully formed and decay in some hundred microseconds due to charge recombination with the reduced form of the electron acceptor.

At pH >pK_a($Trp^{\bullet}H^{+}$) oxidation of Trp is expected to be accompanied by deprotonation. Time-resolved spectra with a sample in water (neutral pH) show indeed transition from the protonated form of the Trp radical to the deprotonated form on a time scale of 1 µs (Figure 4.16).

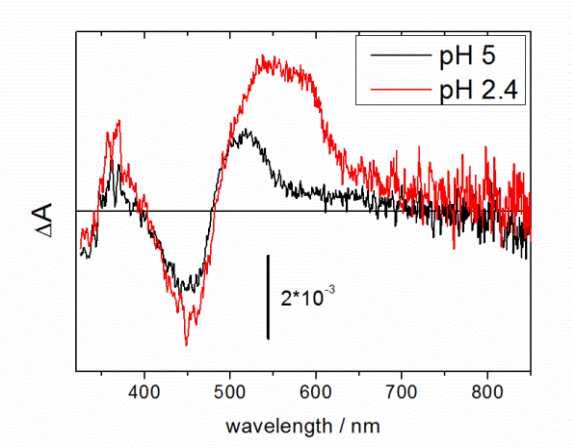

Figure 4.15: *Transient absorption spectra recorded 3 µs after the laser flash for* ***Ru-Trp*** *in MeCN/H_2O (50:50) with 20 mM $[Ru(NH_3)_6]^{3+}$ as electron acceptor and 5 mM citric acid as buffer.*

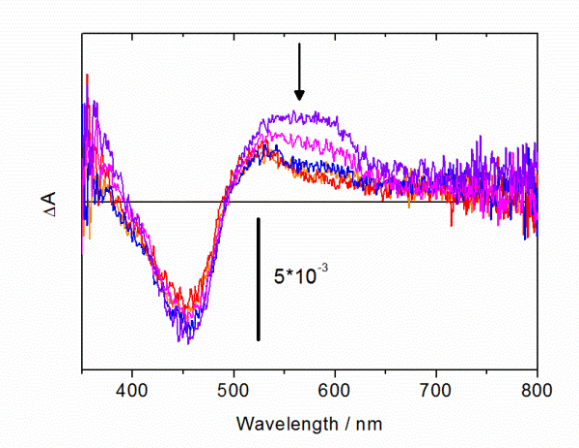

Figure 4.16: *Transient absorption spectra of* ***Ru-Trp*** *in water with 40 mM [Ru $(NH_3)_6]^{3+}$as electron acceptor measured at 200 (purple), 300, 500, 700, 1000 ns (red) after laser flash.*

From the spectra of the two forms (Figures 4.15 and 4.16) it appears that the deprotonation reaction could be followed in the 500 - 600 nm spectral region. Absorption transients at 570 nm and 510 nm are shown in Figure 4.17. At both wavelengths prompt rise in absorption is due to flash-induced formation of the Ru excited state which decays quickly in about 25 ns due to quenching by the electron acceptor. At 570 nm a slower decay phase is detected which is well described by single exponential with a time constant of 410 ns. This transient is attributed to fast (<100 ns) formation of the $Trp^{\bullet}H^{+}$ radical by internal electron transfer and its subsequent disappearance due to deprotonation to form $Trp^{\bullet}$ which has lower absorption at 570 nm. From the initial signal amplitude ($2.6*10^{-3}$) and using an extinction coefficient[23] for $Trp^{\bullet}H^{+}$ of 3000 M^{-1} cm^{-1}, an initial concentration of 0.9 µM could be estimated. This value compares well with the concentration of reduced electron acceptor (which equals the concentration of Ru(III)) formed under our experimental conditions (compare Figure 4.13) and shows that oxidation of the Trp is quantitative. At 510 nm an exponential rise in absorption is apparent, described by a rate of $(645\ ns)^{-1}$. Similar increases in absorption are observed at shorter wavelengths down to 495 nm and we assign this absorption rise to formation of $Trp^{\bullet}$, the deprotonated form of the Trp radical, which has a slightly higher extinction coefficient than the protonated form in this region. The similar kinetics observed at 570 nm and 510 nm show that under these conditions oxidation of the tryptophan residue is followed by deprotonation with a rate of $2*10^{6}\ s^{-1}$.

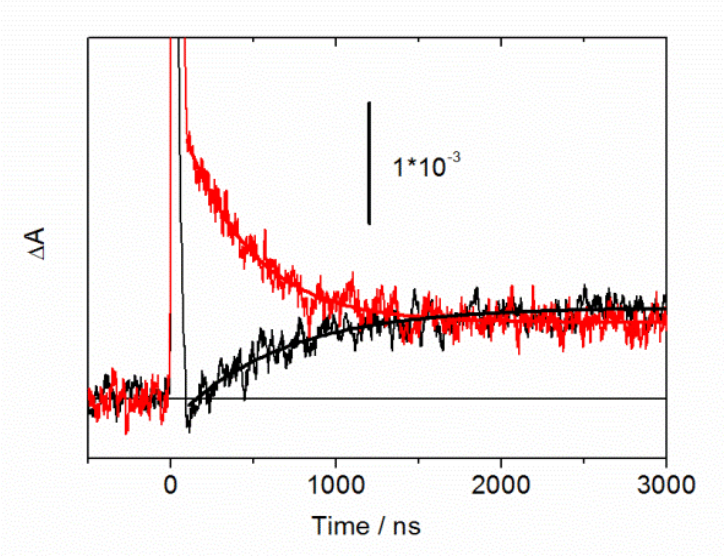

Figure 4.17: *Kinetic traces at 510 nm (black) and 570 nm (red) with 100 mM $[Ru(NH_3)_6]^{3+}$ as electron acceptor in MeCN/H_2O (50:50). The smooth lines represent best fits with monoexponential functions for t >100 ns.*

4.8 Effect of water on deprotonation

The deprotonation of the tryptophan residue at neutral pH is thermodynamically driven by the low pK_a of its oxidized form. However, from a kinetic point of view proton dissociation is controlled by preformation of a favorable configuration between the acid and a suitable base acting as the proton acceptor[41]. With water as the proton acceptor successful propagation of the dissociating proton requires a percolating network of hydrogen-bonded molecules. Addition of organic solvents has been reported to break this structure and lead to a decrease in the rate of deprotonation reactions.[42] This effect is also observed in our complex as demonstrated by the results shown in Figure 4.18 where the concentration of water is varied. Methyl viologen was used in these experiments because of the insufficient solubility of hexamine ruthenium(III) chloride in acetonitrile. The deprotonation of the $Trp^{\bullet}H^{+}$ radical can be followed by the distinct decay of absorption on top of the larger absorption due to the $MV^{+\bullet}$ radical, which decays on the hundreds microsecond time scale. With decreasing concentration of water, the rate of deprotonation is drastically slowed down. For 10 vol% the corresponding time constant is 5 µs and for 3% it is 74 µs. For concentrations below 3% deprotonation can no longer be observed as its rate approaches the rate of charge recombination between $MV^{+\bullet}$ and $Trp^{\bullet}H^{+}$.

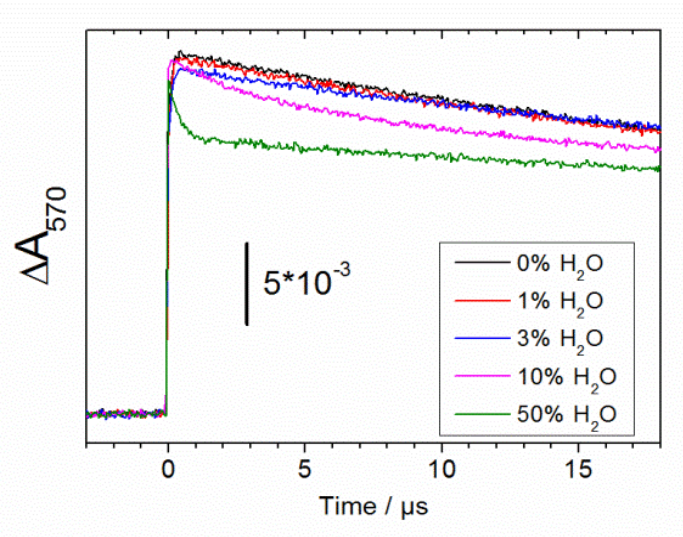

Figure 4.18: *Kinetic traces at 570 nm in MeCN with varying concentration of H_2O. 20 mM MV^{2+} was present as electron acceptor.*

4.9 Conclusions

In summary (Figure 4.19), we have used Click chemistry as an efficient tool to perform the modular assembly of a chromophore and an amino acid. Such easily prepared model systems

allow for time-resolved studies of one-electron oxidation reactions by creating a strongly oxidising state on the chromophore by excitation with a laser flash in presence of external electron acceptors.

Kinetic transient absorption studies in aqueous solution upon excitation with a nanosecond laser flash revealed fast intramolecular electron transfer leading to the formation of a protonated tryptophanyl ($Trp^{\bullet}H^{+}$) species detected by its characteristic absorption at 570 nm. At pH>pK_a ($Trp^{\bullet}H^{+}$), the absorption at 570 nm disappears in less than one microsecond with a concomitant increase in absorption at 510 nm, typical of the deprotonated form of Trp radicals. This observation demonstrates that electron transfer from Trp to Ru(III) is followed by deprotonation to yield the neutral $Trp^{\bullet}$ radical species. The kinetics of the deprotonation reaction is strongly dependent on the water concentration.

From a thermodynamic point of view, the system studied in this work is characterised by a moderate driving force for internal electron transfer from the ligand to Ru(III) resulting in formation of a weak acid. The value of ΔG = -130 meV deduced from the difference of the redox potentials of chromophore and ligand (below its pK_a) has to be considered as the maximum possible value for the electron transfer step. Corrections for electrostatic interactions would bring this value close to, or even below, 100 meV. Despite this low driving force, the rate of internal electron transfer is fast, (>10^7 s^{-1}). This fast rate is taken to indicate good electronic coupling between chromophore and the tryptophan via the triazole spacer, but the relative close proximity between the tryptophan and the sensitizer together with some flexibility of the amide link might also allow through-space electron transfer to occur. Estimation of the electron transfer rate in the framework of Marcus theory shows furthermore that the reorganization energy of the reaction must be relatively small. The latter fact is in agreement with a stepwise mechanism where electron transfer is independent of deprotonation of the Trp radical.

Figure 4.19: *Graphical summary showing click reaction and intramolecular electron transfer followed by deprotonation event (ETPT)*

The covalently linked chromophore-amino acid system described in this work can be looked at as a first step in an effort to bind a chromophore to a peptidic motif. Preparation of azide-functionalized proteins by different methods has been described. [43-45] Combining the high reaction yields, mild reaction conditions of click chemistry, and the stability of the triazole link, this approach seems like an optimal alternative for site-specific and selective post modification of proteins. Importantly, our results show that coupling of the ruthenium complex does not lead to significant modifications of the redox and acid-base properties of the addressed amino acid. This synthetic strategy can be used to address electron transfer studies in more sophisticated polypeptide and protein systems where visible light activation by a covalently linked chromophore can lead to photoactivation of complex units in both oxidation and reduction reactions.

4.12 References

(1) Kuznetsov, A. M.; Ulstrup, J., *Electron transfer in chemistry and biology: an introduction to the theory*; Wiley Chichester, **1999**.

(2) Müller, A.; Ratajczak, H.; Junge, W.; Diemann, E., *Electron and proton transfer in chemistry and biology*; Elsevier Science Publishers, **1992**.

(3) Marcus, R. A.; Sutin, N., Electron transfers in chemistry and biology. *Biochim. Biophy. Acta, Bioenerg.*,**1985**, *811*, 265-322.

(4) Reece, S. Y.; Nocera, D. G., Proton-coupled electron transfer in biology: Results from synergistic studies in natural and model systems. *Annu. Rev. Biochem.*,**2009**, *78*, 673-699.

(5) Dryhurst, G., *Electrochemistry of biological molecules*; Elsevier, **1977**.

(6) Hopfield, J., A critical test of the mechanism and range of biological electron transfer processes. *Biophy. J.*,**1977**, *18*, 311-321.

(7) Fischer, W.-N.; André, B.; Rentsch, D.; Krolkiewicz, S.; Tegeder, M.; Breitkreuz, K.; Frommer, W. B., Amino acid transport in plants.*Trends Plant. Sci.*,**1998**, *3*, 188-195.

(8) Meister, A., *Biochemistry of the amino acids*; Elsevier, **1965**.

(9) Christensen, H. N., Role of amino acid transport and countertransport in nutrition and metabolism. *Physiol. Rev.*,**1990**, *70*, 43.

(10) Barry, B. A.; Babcock, G. T., Tyrosine radicals are involved in the photosynthetic oxygen-evolving system. *Proc. Natl. Acad. Sci.,U.S.A.*,**1987**, *84*, 7099-7103.

(11) Reece, S. Y.; Stubbe, J.; Nocera, D. G., pH dependence of charge transfer between tryptophan and tyrosine in dipeptides. *Biochim. Biophy. Acta, Bioenerg.,* **2005**, *1706*, 232-238.

(12) Stubbe, J. A., Protein radical involvement in biological catalysis? *Annu. Rev. Biochem.*,**1989**, *58*, 257-285.

(13) Hawkins, C. L.; Davies, M. J., Generation and propagation of radical reactions on proteins. *Biochim. Biophy. Acta, Bioenerg.,* **2001**, *1504*, 196-219.

(14) Butler, J.; Land, E. J.; Prütz, W. A.; Swallow, A. J., Charge transfer between tryptophan and tyrosine in proteins.*Biochim. Biophy. Acta, Protein Structure Mol. Enzym.,* **1982**, *705*, 150-162.

(15) Cukier, R. I.; Nocera, D. G., Proton-coupled electron transfer. *Annu. Rev. Phy. Chem.*,**1998**, *49*, 337-369.

(16) Weinberg, D. R.; Gagliardi, C. J.; Hull, J. F.; Murphy, C. F.; Kent, C. A.; Westlake, B. C.; Paul, A.; Ess, D. H.; McCafferty, D. G.; Meyer, T. J., Proton-coupled electron transfer. *Chem. Rev.*,**2012**, *112*, 4016-4093.

(17) Miller, J. E., Radical formation and electron transfer in biological molecules; PhD thesis,**2012**.

(18) Eklund, H.; Uhlin, U.; Färnegårdh, M.; Logan, D. T.; Nordlund, P., Structure and function of the radical enzyme ribonucleotide reductase.*Prog. Biophy. Mol. Biol.***2001**, *77*, 177-268.

(19) Blodig, W.; Smith, A. T.; Winterhalter, K.; Piontek, K., Evidence from spin-trapping for a transient radical on tryptophan residue 171 of lignin peroxidase. *Archives Biochem. Biophy.*,**1999**, *370*, 86-92.

(20) Choudhury, K.; Sundaramoorthy, M.; Hickman, A.; Yonetani, T.; Woehl, E.; Dunn, M. F.; Poulos, T. L., Role of the proximal ligand in peroxidase catalysis. Crystallographic, kinetic, and spectral studies of cytochrome c peroxidase proximal ligand mutants.*J. Biol. Chem.*,**1994**, *269*, 20239-20249.

(21) Aubert, C.; Vos, M. H.; Mathis, P.; Eker, A. P.; Brettel, K., Intraprotein radical transfer during photoactivation of DNA photolyase. *Nature*,**2000**, *405*, 586.

(22) Harriman, A., Further comments on the redox potentials of tryptophan and tyrosine. *J. Phy. Chem.*,**1987**, *91*, 6102-6104.

(23) Solar, S.; Getoff, N.; Surdhar, P. S.; Armstrong, D. A.; Singh, A., Oxidation of tryptophan and N-methylindole by $N_3^{\bullet}$, $Br_2^{\bullet-}$, and $(SCN)_2^{\bullet-}$radicals in light-and heavy-water solutions: a pulse radiolysis study. *J. Phy. Chem.*,**1991**, *95*, 3639-3643.

(24) Miller, J. E.; Grădinaru, C.; Crane, B. R.; Di Bilio, A. J.; Wehbi, W. A.; Un, S.; Winkler, J. R.; Gray, H. B., Spectroscopy and reactivity of a photogenerated tryptophan radical in a structurally defined protein environment. *J. Am. Chem. Soc.*,**2003**, *125*, 14220-14221.

(25) Bryant, F. D.; Santus, R.; Grossweiner, L., Laser flash photolysis of aqueous tryptophan.*J. Phy. Chem.*, **1975**, *79*, 2711-2716.

(26) Zhang, M. T.; Hammarström, L., Proton-coupled electron transfer from tryptophan: A concerted mechanism with water as proton acceptor.*J. Am. Chem. Soc.*,**2011**, *133*, 8806-8809.

(27) Zhang, M.-T.; Nilsson, J.; Hammarström, L., Bimolecular proton-coupled electron transfer from tryptophan with water as the proton acceptor. *Energy Environ. Sci.*,**2012**, *5*, 7732-7736.

(28) Gagliardi, C. J.; Binstead, R. A.; Thorp, H. H.; Meyer, T. J., Concerted Electron–Proton Transfer (EPT) in the Oxidation of Tryptophan with Hydroxide as a Base. *J. Am. Chem. Soc.*, **2011**, *133*, 19594-19597.

(29) Sjödin, M.; Styring, S.; Wolpher, H.; Xu, Y.; Sun, L.; Hammarström, L., Switching the redox mechanism: models for proton-coupled electron transfer from tyrosine and tryptophan.*J. Am. Chem. Soc.*, **2005**, *127*, 3855-3863.

(30) Stewart, D. J.; Napolitano, M. J.; Bakhmutova-Albert, E. V.; Margerum, D. W., Kinetics and mechanisms of chlorine dioxide oxidation of tryptophan.*Inorg. Chem.*,**2008**, *47*, 1639-1647.

(31) DeFelippis, M. R.; Murthy, C.; Broitman, F.; Weinraub, D.; Faraggi, M.; Klapper, M. H., Electrochemical properties of tyrosine phenoxy and tryptophan indolyl radicals in peptides and amino acid analogs. *J. Phy. Chem.*,**1991**, *95*, 3416-3419.

(32) Kolb, H. C.; Finn, M.; Sharpless, K. B. , Click chemistry: diverse chemical function from a few good reactions. *Angew. Chem. Int. Ed.*,**2001**, *40*, 2004-2021.

(33) Moses, J. E.; Moorhouse, A. D., The growing applications of click chemistry. *Chem. Soc. Rev.*,**2007**, *36*, 1249-1262.

(34) Himo, F.; Lovell, T.; Hilgraf, R.; Rostovtsev, V. V.; Noodleman, L.; Sharpless, K. B.; Fokin, V. V., Copper (I)-catalyzed synthesis of azoles. DFT study predicts unprecedented reactivity and intermediates. *J. Am. Chem. Soc.*, **2005**, *127*, 210-216.

(35) Yu, M.; Price, J. R.; Jensen, P.; Lovitt, C. J.; Shelper, T.; Duffy, S.; Windus, L. C.; Avery, V. M.; Rutledge, P. J.; Todd, M. H., Copper, Nickel, and Zinc Cyclam-Amino

Acid and Cyclam-Peptide Complexes May Be Synthesized with "Click" Chemistry and Are Noncytotoxic. *Inorg. Chem.,***2011**, *50*, 12823-12835.

(36) Choi, I.; Kim, Y.-K.; Min, D.-H.; Lee, S.; Yeo, W.-S., On-Demand Electrochemical Activation of the Click Reaction on Self-Assembled Monolayers on Gold Presenting Masked Acetylene Groups. *J. Am. Chem. Soc.,* **2011**, *133*, 16718-16721.

(37) Posener, M. L.; Adams, G. E.; Wardman, P.; Cundall, R. B., Mechanism of tryptophan oxidation by some inorganic radical-anions: A pulse radiolysis study.*J. Chem. Soc., Faraday Trans. 1***1976**, *72*, 2231-2239.

(38) Juris, A.; Balzani, V.; Barigelletti, F.; Campagna, S.; Belser, P.; Von Zelewsky, A., Ru (II) polypyridine complexes: photophysics, photochemistry, electrochemistry, and chemiluminescence.*Coord. Chem. Rev.,***1988**, *84*, 85-277.

(39) Baron, A.; Herrero, C.; Quaranta, A.; Charlot, M.-F.; Leibl, W.; Vauzeilles, B.; Aukauloo, A., Click Chemistry on a Ruthenium Polypyridine Complex. An Efficient and Versatile Synthetic Route for the Synthesis of Photoactive Modular Assemblies.*Inorg. Chem.,***2012**, *51*, 5985-5987.

(40) Baron, A.; Herrero, C.; Quaranta, A.; Charlot, M.-F.; Leibl, W.; Vauzeilles, B.; Aukauloo, A., Efficient electron transfer through a triazole link in ruthenium(II) polypyridine type complexes. *Chem. Comm.,***2011**, *47*, 11011-11013.

(41) Gutman, M.; Nachliel, E., The dynamic aspects of proton transfer processes. *Biochim. Biophy. Acta, Bioenerg.,* **1990**, *1015*, 391-414.

(42) Huppert, D.; Kolodney, E., Picosecond proton transfer studies in water-alcohols solutions. *Chem. Phy.,***1981**, *63*, 401-410.

(43) van Dongen, S. F. M.; Teeuwen, R. L. M.; Nallani, M.; van Berkel, S. S.; Cornelissen, J. J. L. M.; Nolte, R. J. M.; van Hest, J. C. M., Single-step azide introduction in proteins via an aqueous diazo transfer.*Bioconjugate Chem.,***2008**, *20*, 20-23.

(44) Kiick, K. L.; Saxon, E.; Tirrell, D. A.; Bertozzi, C. R., Incorporation of azides into recombinant proteins for chemoselective modification by the Staudinger ligation.*Proc. Natl. Acad. Sci.,U.S.A.,* **2002**, *99*, 19-24.

(45) Best, M. D., Click chemistry and bioorthogonal reactions: unprecedented selectivity in the labeling of biological molecules. *Biochemistry,***2009**, *48*, 6571-6584.

5.0 Water oxidation catalysts

5.1 Introduction

Water oxidation using molecular photocatalysts is a key step in solar energy conversion for production of hydrogen.[1-3] The keen interest in this field has lead to the development of molecular catalysts based on transition metals like ruthenium, iridium, cobalt.[4-6] These transition metal complexes are able to split water with varying turnover numbers (TON). Most efficient catalysts with significant TON are still very few to the date. One point to be noted is that in most studies a sacrificial oxidant is used, mainly ceric ion [Ce(IV)], to check the activity of the catalyst. This avoids problems due to potential decomposition of a photosensitizer which could be the limiting factor in photocatalytic experiments.

In 1982 Meyer's group reported **cis,cis-$[(bpy)_2(H_2O)Ru^{III}ORu^{III}(OH_2)(bpy)_2]^{4+}$** as water oxidation catalyst commonly known as "blue dimer"[7,8]. The blue dimer contains twoRu(III)-OH_2 groups. These two ruthenium ions are bridged by a dianionic oxide ligand and each ruthenium is linked to two bipyridyl ligands[9] (Figure 5.1). In presence of Ce(IV), the blue dimer can oxidize water to yield TON = 19.[10] Blue dimer was one of the first reported molecular catalysts for water oxidation.

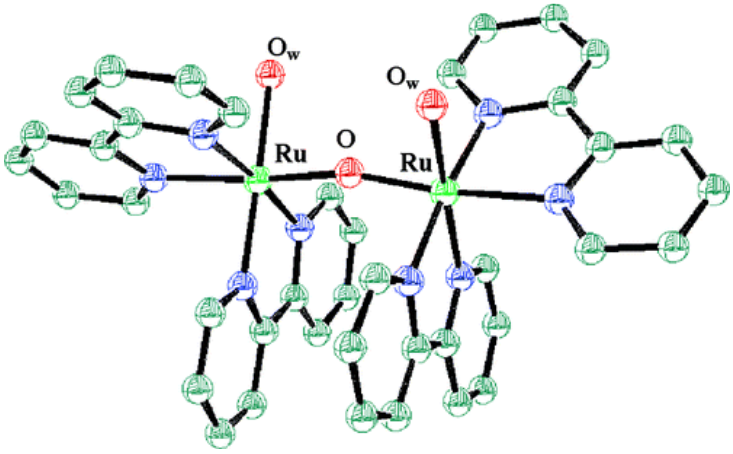

Figure 5.1: *Structure of the blue dimer,* ***cis,cis-$[(bpy)_2(H_2O)Ru^{III}ORu^{III}(OH_2)(bpy)_2]^{4+}$*** *(**Green** = carbon atoms, **Blue** = nitrogen atoms, **Red** = water molecules)*[9]

In a study by Grätzel and his co-workers as an improvement of Meyer's blue dimer a bis(aquo), bis(5,5'-dicarboxylated-2,2'-dipyridyl) ruthenium complex as a catalyst was reported [11](Figure 5.2). Upon oxidation this catalyst forms an oxo-bridged binuclear cluster

similar to Meyer's blue dimer. This catalyst was reported to give a TON of 75 using Co(III) as a sacrificial electron acceptor.

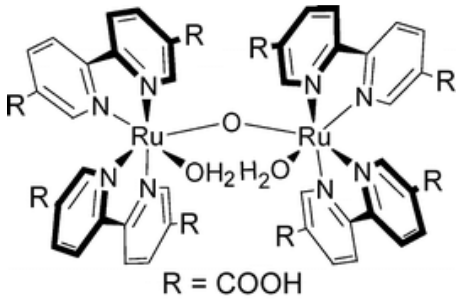

Figure 5.2: *Grätzel Ru-Ru catalyst*[11]

In 2005, Thummel and Zong published a detailed characterization of another diruthenium polypyridyl complex[12](Figure 5.3A). This complex at optimum conditions was reported to give a maximum TON of 3200. Tuning of properties can be possible by changing substituents on the linked pyridine ligand. However there is great complexity involved in the synthesis of the ligand.

Sun *et al*. also reported a diruthenium complex (Figure 5.3B) to generate TON of 1700 in presence of Ce(IV) as an oxidant.

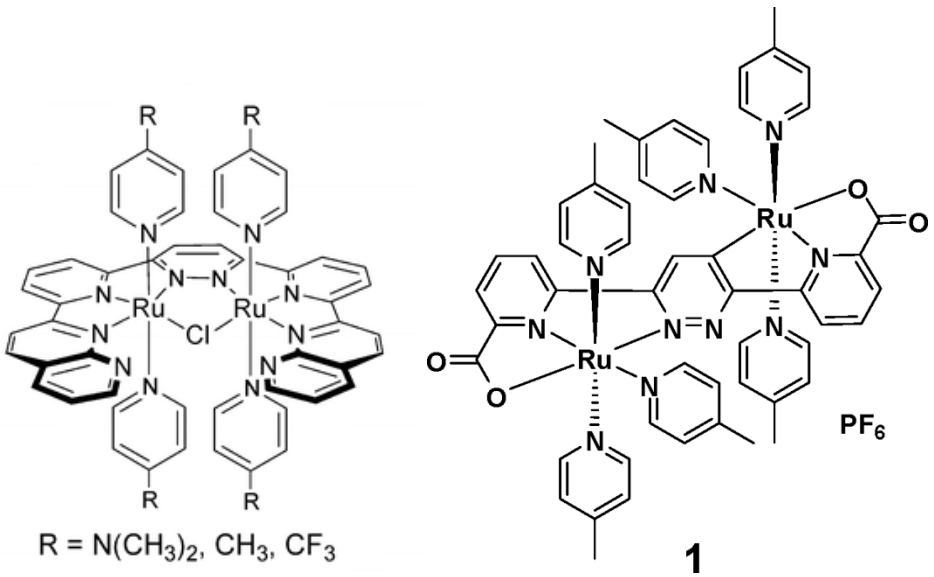

(A) (B)

Figure 5.3: *Catalytic complex of (A) Thummel*[12] *(B) Sun et al*[13]

Mononuclear complexes also have been shown to oxidize water. A family of **[Ru(tpy)(bpy)(OH_2)]** based complexes have been synthesized and characterized (Figure 5.4).[6] But in fact the reported TONs are few hundreds of magnitude.

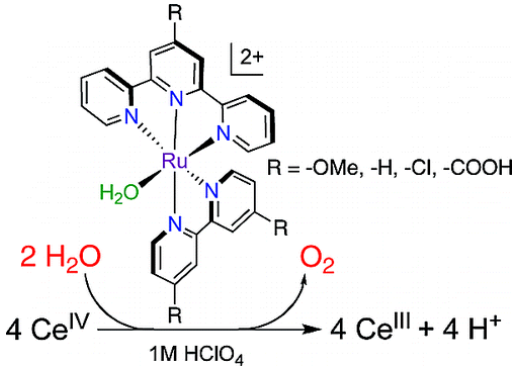

***Figure 5.4**: Mononuclear Ru complexes*[6]

Bernhard *et al*. have reported a series of organometallic complexes of iridium for homogeneous oxidation of water.[5] These complexes have general formula **cis-[Ir^{III} $(L)_2(H2O)_2]^+$** and have been synthesized with different ligands (Figure 5.5A). With this library of complexes TON up to 2760 were obtained. Only drawback of Ir catalysts is that it takes seven days to reach completion in order to show high TONs (Figure 5.5B), whereas ruthenium complexes undergo completion in less than one hour. This means that the turnover frequency must be very low.

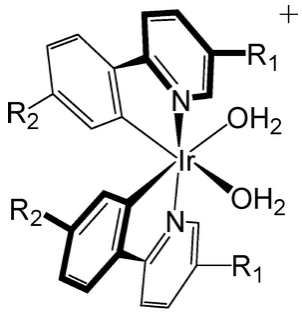

1 $R_1 = H$, $R_2 = H$
2 $R_1 = CH_3$, $R_2 = H$
3 $R_1 = CH_3$, $R_2 = Ph$
4 $R_1 = CH_3$, $R_2 = F$
5 $R_1 = CH_3$, $R_2 = Cl$

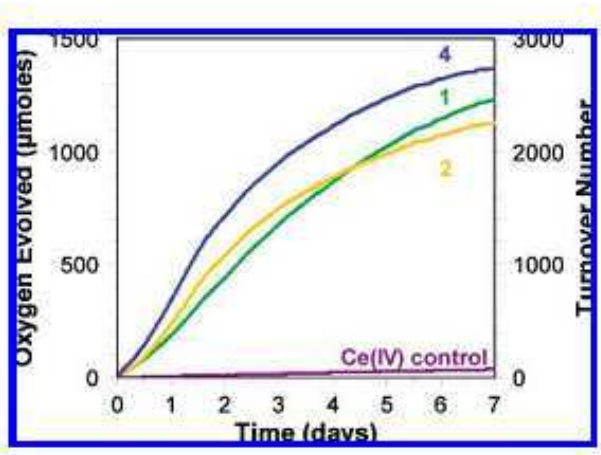

***Figure 5.5:** (A) Ir complexes*[5] *(B) Week-long oxygen evolution is shown from 10 mL aqueous solutions containing 0.5 µmol of 1, 2 and 4 and excessive 15 000 µmol of ceric ammonium nitrate along with a catalyst-free control. The axis on the left measures micromoles of oxygen produced, whereas the axis on the right gives the conversion to turnover numbers.*[5]

In short, there is no existing synthetic catalyst for homogeneous water oxidation which is simple, robust, and reasonably fast.

Elucidation of the mechanism of these catalysts to drive the water splitting reaction is still a great concern. This is due to the considerable complexities involved in the mechanistic prediction of removal of four electrons and four protons from two water molecules to generate the oxygen-oxygen double bond.

5.2: Our strategy

The thesis work deals with photocatalysts based on artificial mimics of photosystem II (for details see Chapter 1, Introduction). Therefore the final aim of our synthetic approach consists of realizing a molecular photocatalyst with three basic elements, *i.e.* a chromophore, an electron relay function and a covalently bound catalyst (Figure 5.6). As usual, we choose a **$[Ru(bpy)_3]^{2+}$** based chromophore, an imidazole-phenol group as electron relay and a Mn salen or **$Ru(tpy)(bpy)OH_2$** complex as catalyst.

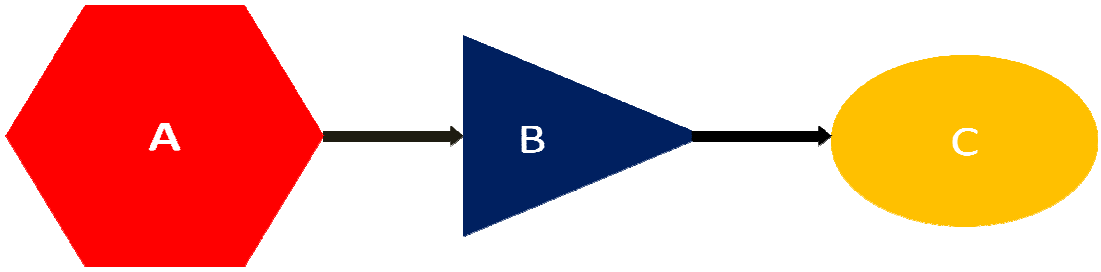

Figure 5.6: *our synthetic strategy showing A: Chromophore, B: Electron relay and C: Catalyst unit*

The Mn salen based Jacobsen's catalyst (Figure 5.7) is a well-known catalyst for oxidation of alkenes to form epoxides.[14,15] Scheme 5.1 illustrates epoxidation of olefin by the Jacobsen's catalyst. The catalytically active species is a Mn=O formed by a 2 electron/2proton activation of a metal-bound water molecule. This oxidation catalysis is therefore simpler than the $4H^+/4e^-$ oxidation of water. To start with light activation of a functional oxidation catalyst we decided to covalently bind the Jacobsen catalyst to a chromophore via an electron relay.

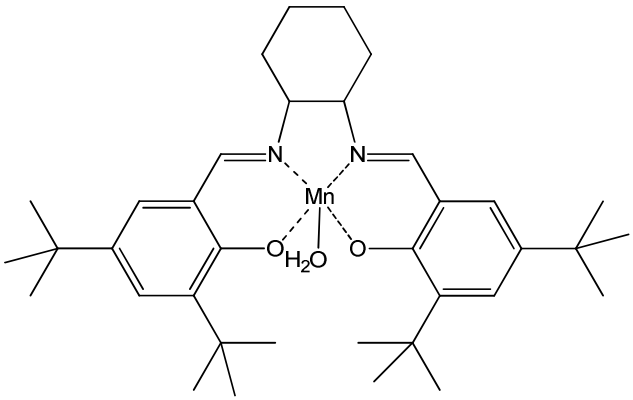

***Figure 5.7**: Salen based Jacobsen's catalyst*

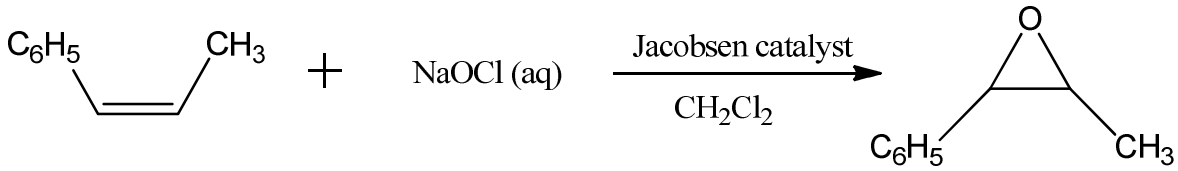

***Scheme 5.1:** Epoxidation of olefin using Jacobsen's catalyst*[15]

The traditional synthetic method is quite long (involves numerous steps) and tedious as purification is almost necessary at each and every step. To avoid this we decided to use again click chemistry to synthesize our oxidation photocatalyst. The click chemistry approach has already proven its ability with respect to efficient intramolecular electron transfer via the triazole linkage as for example shown in the case of **Ru-Tryptophan**[16] (refer Chapter 4). The targeted photocatalyst is shown in Figure 5.8 A.

Another catalyst that we decided to employ is **Ru(tpy)(bpy)OH_2**. As mentioned earlier in this chapter, the **Ru(tpy)(bpy)OH_2**complex is proven to be a useful catalyst for water oxidation(Figure 5.4).[6] Also our lab has recently reported on the mechanism of its photoactivation.[17] The targeted complex with this catalyst coupled to a photoactive unit *via* an electron relay is shown in Figure 5.8B.

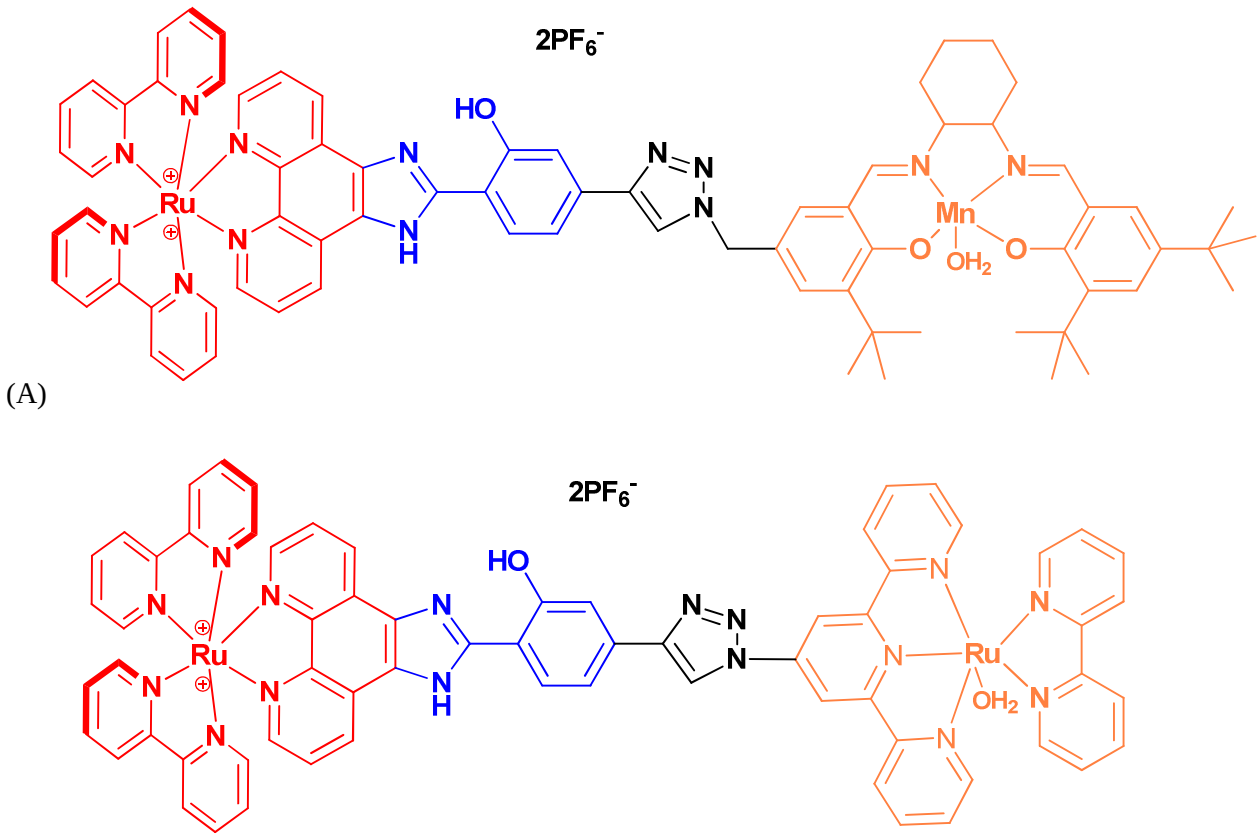

Figure 5.8: *Targeted modular complexes showing chromophore (red), electron relay (blue) and catalyst (orange) units.*

5.3 Synthesis

Synthesis of the catalytic complex has been carried out by using click chemistry, in a similar approach as described in detail in the Chapter 4. As described, in order to perform click chemistry we need to have precursors with proper functionalization of each unit *i.e.* with azide and alkyne.

This synthesis includes three steps:

5.3.1 Functionalization of ligand with alkyne

5.3.2 Complexation of ligand with ruthenium

5.3.3 Functionalization of the catalytic unit with azide

5.3.4 Click chemistry reaction between alkyne and azide unit of chromophore-electron relay and catalyst respectively.

5.3.1: Functionalization of ligand with active alkyne group

In order to functionalize the ligand with alkyne group we have started with 4-bromo salicyaldehyde. After palladium catalyzed reaction with trimethylsilyl acetylene followed by deprotection of alkyne group by K_2CO_3 we have obtained the 4-ethynyl salicyaldehyde. This alkyne derivative of salicyaldehye undergoes Steak and Day reaction[18] to form the ligand with active alkyne group (Scheme 5.2).

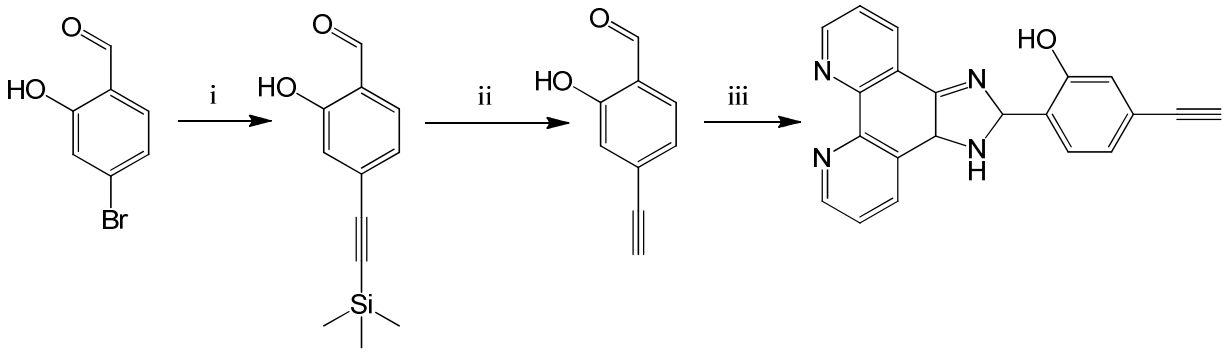

Scheme 5.2:*Functionalization of imidazole phenol ligand with active alkyne group (i)[$PdCl_2(PPh_3)_2$],PPh_3,CuI, ($(C_2H_5)_3N$,trimethylsilyl acetylene,dry THF, under Argon atmosphere, RT (ii)CH_3OH, K_2CO_3,RT (iii)1,10-phenanthroline-5,6- dione,CH_3COOH, NH_4COOCH_3, 80°C*

5.3.2 Complexation of ligand with $[Ru(bpy)_2Cl_2]$ to obtain Ru-imi-phOH-CCH

Starting with **$Ru(bpy)_2Cl_2$**we used $AgNO_3$ to replace chlorides with nitrites ($-NO_3$) in methanol. Then the formed white precipitate of AgCl was filtered off and the reaction continued with ligand obtained in the step 5.3.1 to get the product which was further precipitated as PF_6 using ammonium hexafluorophosphate salt in methanol (Scheme 5.3).

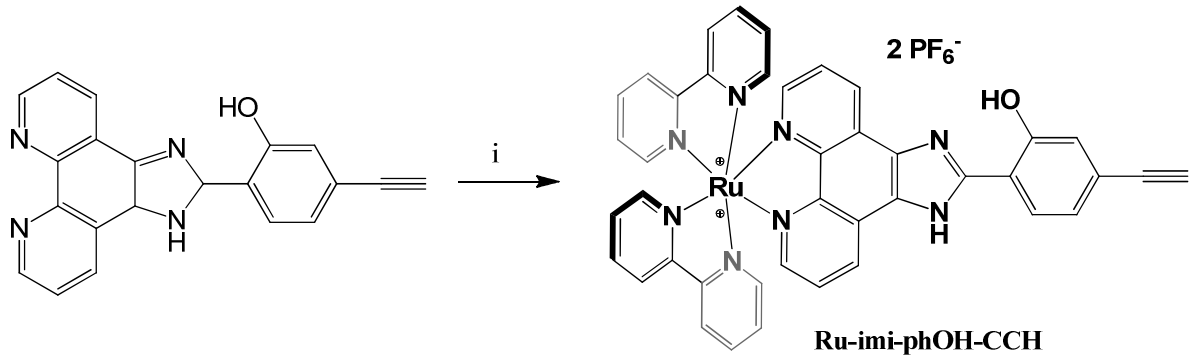

Scheme 5.3*: Complexation of ligand is to obtain* ***Ru-imi-phOH-CCH****. Reagent and condition: (i) [$Ru(bpy)_2Cl_2$],$AgNO_3$,CH_3OH.*

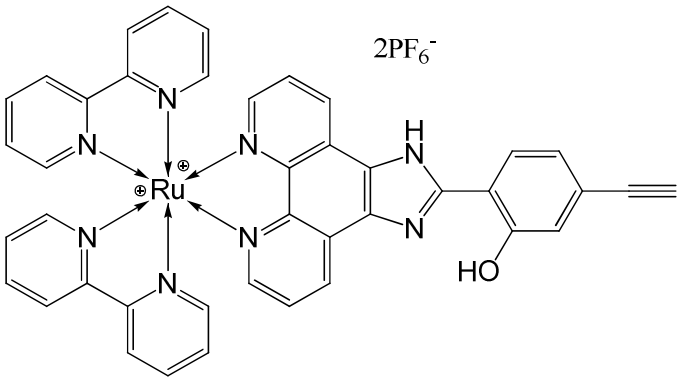

Figure 5.9: *Important intermediate* ***Ru-imi-phOH-CCH***

This complex is important as it is one of the intermediates for the click reaction. In fact, the active alkyne can undergo click reaction with a variety of azide functionalized compounds to create entirely new library of photoactive catalytic complexes. This library of complexes will help us to understand mechanisms of electron transfer from a chromophore with electron relay to catalysts. Characterization of this intermediate is described in a later part of this chapter.

For our two targeted complexes (Figure 5.8) we used this intermediate to synthesize them. Therefore the above mentioned first two steps are the same for our both target complexes.

5.3.3: Functionalization of the catalytic unit with azide

(i) <u>For the complex with salen-Mn, Figure 5.8A</u>

The photocatalytic complex (Figure 5.8A) is based on a Mn salen catalytic unit. In order to couple the Mn salen catalytic unit to the complex we need to functionalize it with azide to obtain the dissymmetric salen cavity shown in Figure 5.10.

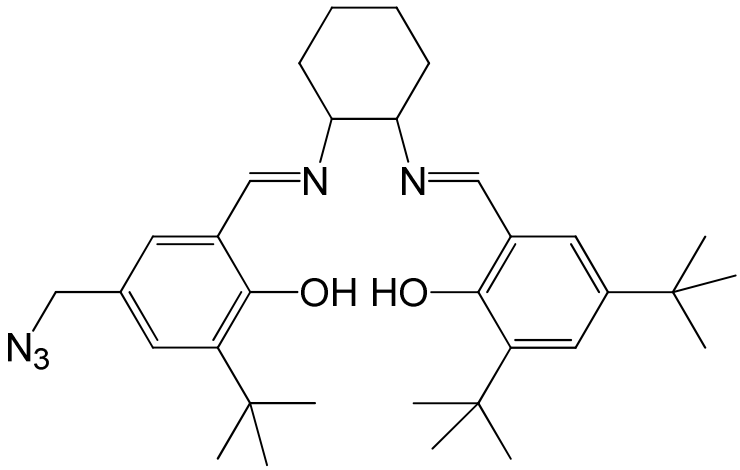

Figure 5.10: *Targeted dissymmetric salen*

The synthesis of targeted dissymmetric salen follows two steps as described below,

Step 1: To obtain *mono*-imine ammonium salt[19]

We started with cyclohexane diamine to obtain selectively the mono ammonium chloride salt under drastic acidic condition. Further reaction was with aldehyde to form the mono-imine ammonium salt (Scheme 5.4).

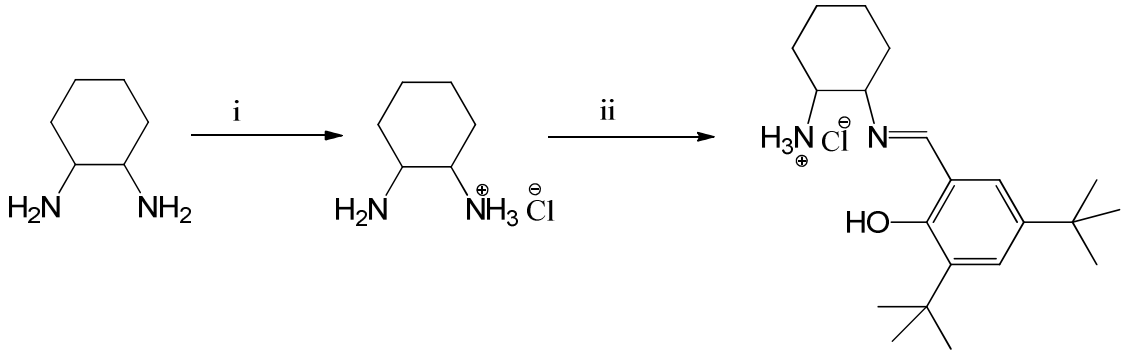

Scheme 5.4: *Synthesis of mono-imine ammonium salt (i) HCl, diethyl ether, RT, (ii) 3, 5-di(tert-butyl) salicyaldehyde, C_2H_5OH, RT*

Step 2: To obtain desired dissymmetric salen[19]

The *mono*-imine ammonium salt obtained in step 1 reacted with azido salicyaldehyde in ethanol for three days at room temperature. This step was supposed to give the desired dissymmetric salen but resulted into symmetric one (Scheme 5.5).

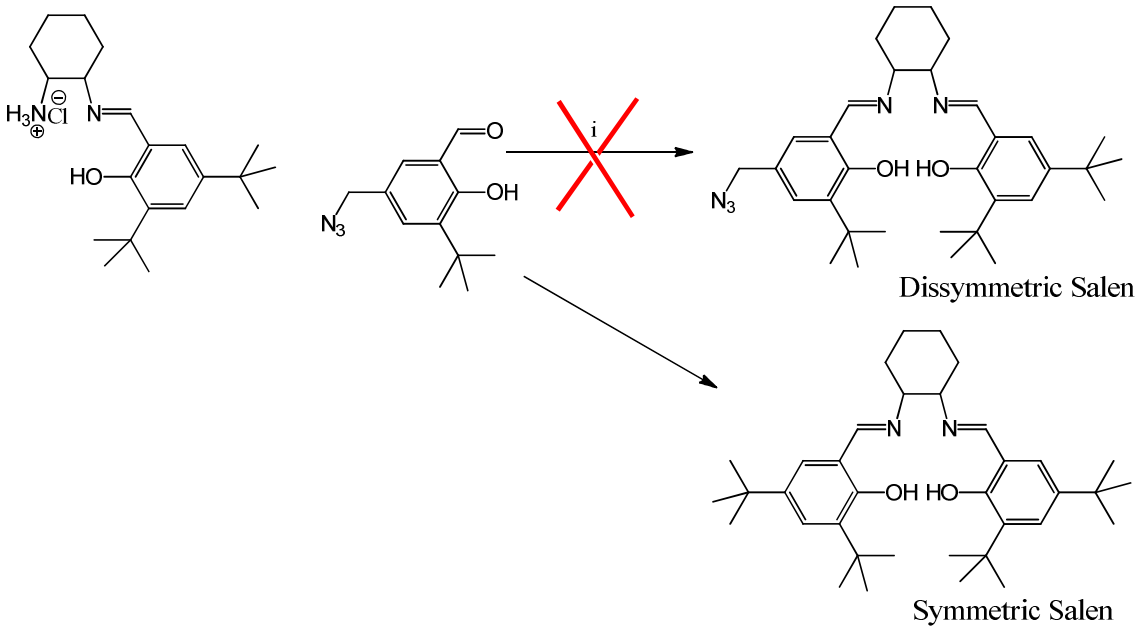

Scheme 5.5: *Dissymmetric salen synthesis: (i) $(C_2H_5)_3N$, C_2H_5OH, 4A° molecular sieves, RT, 3 days.*

The problem encountered in the step 2 reaction was that whenever we have tried the above reaction it always resulted into symmetric salen with a *tert*-butyl group rather than dissymmetric salen with an azide group (necessary for our synthesis) though the reaction was performed according to well known literature procedures.[19,20]

(ii) <u>For the complex with Ru(tpy)(bpy)(OH_2), Figure 5.8B</u>

We have obtained the 4-azido terpyridine (Figure 5.11) from our laboratory which was frequently used to synthesize various complexes.

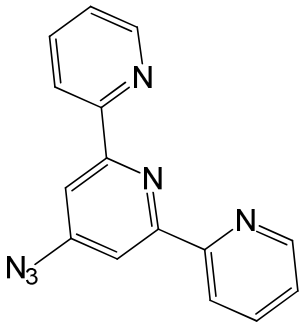

Figure 5.11: *4-azido terpyridine*

5.3.4: Click chemistry reaction between alkyne and azide unit of chromophore-electron relay and catalyst:

(i) <u>For the complex with salen-Mn, Figure 5.8A</u>

This reaction was not performed due to unavailability of desired asymmetric salen unit (Figure 5.10).

(ii) <u>For the complex with Ru(tpy)(bpy)(OH_2), Figure 5.8B</u>

This complex was supposed to be obtained by click reaction of**Ru-imi-phOH-CCH** with 4-azido terpyridine in presence of CuI as a catalyst (Scheme 5.6).

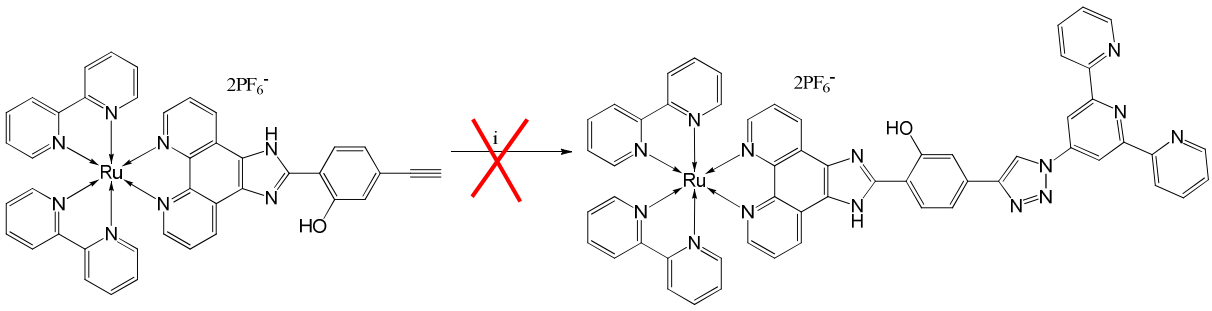

Scheme 5.6: *Click reaction (i) 4-azido terpyridine, CuI, C_2H_5OH*

But the expected complex was not obtained at the end of the reaction. In the reaction step it is necessary to remove the Cu(I) trapped in the cavity of the terpyridine. Therefore we have used solution of aqueous HEDTA as a complexing agent and stirred with the HEDTA for about two hours. This might be too drastic conditions for the removal of Cu. This condition might affect the phenol and lead to breakdown of the complex as observed.

In summary, despite many trials we were not successful to synthesize our targeted photocatalytic complexes.

5.4 Characterization of Ru-imi-phOH-CCH

Nevertheless, we have carried out experiments with the **Ru-imi-phOH-CCH** complex (Figure 5.9) to characterize it and to check whether in this complex the electron transfer properties are preserved and are as in the other complexes *i.e*. **Ru-3Me**, **Ru-4Me** and **Ru-6Me**.

The absorption spectrum is shown in Figure 5.12 and it has all the typical features of **$[Ru(bpy)_3]^{2+}$** type complexes as mentioned in the previous chapters.

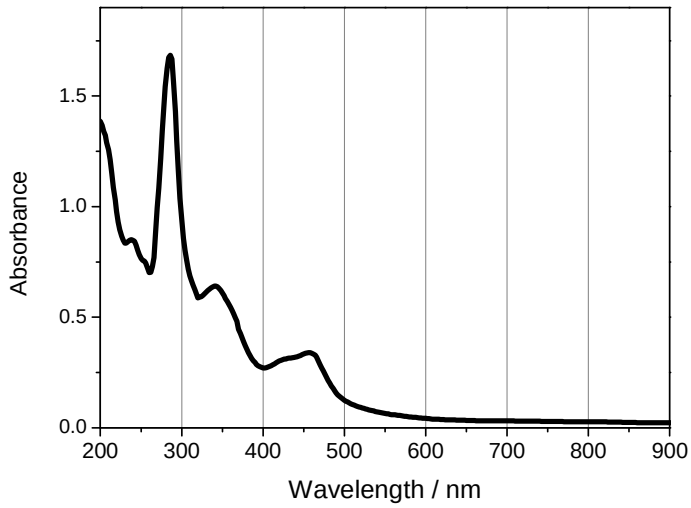

Figure 5.12: *Absorption spectrum of* ***Ru-imi-phOH-CCH*** *in acetonitrile showing all features of the typical* ***$[Ru(bpy)_3]^{2+}$*** *type complexes*

Emission properties of the **Ru-imi-phOH-CCH** were verified with laser flash photolysis and show the emission maxima at 605 nm (Figure 5.13A). The emission lifetime was 1.27 µs (Figure 5.13 B). These features compare well with those observed in the **Ru-xMe** complexes (see Chapter 3).

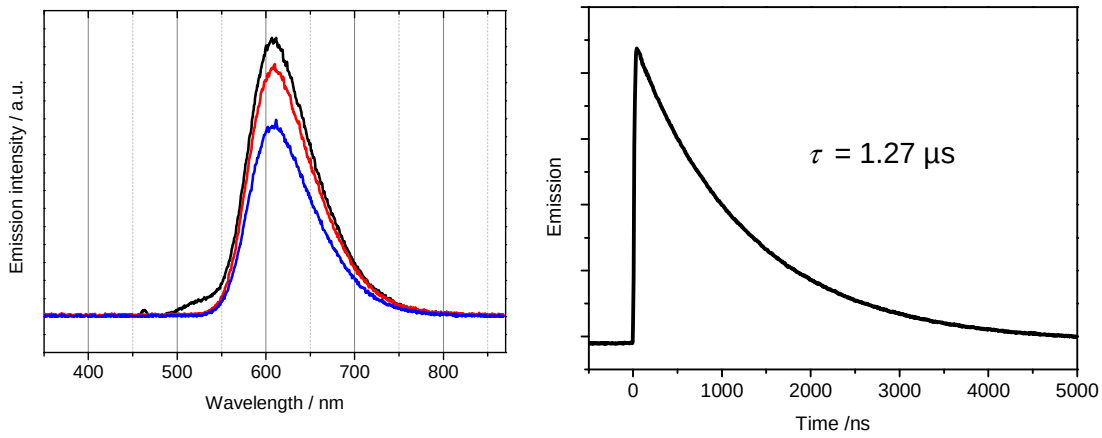

Figure 5.13:*A) Emission spectra for* ***Ru-imi-phOH-CCH*** *in acetonitrile recorded after10, 100,500 ns showing maxima at 605 nm B) Emission kinetics of* ***Ru-imi-phOH-CCH*** *at 605 nm*

In experiments with laser flash photolysis in presence of MV as electron acceptor the complex showed fast recovery at 440 nm like the **Ru-xMe** complexes and positive absorption at long times due to the radical formed on the ligand (black trace in Figure 5.14). The apparent rate of electron transfer was (11 μs^{-1}) and was accelerated in presence of 5% H_2O (blue trace in Figure 5.14).

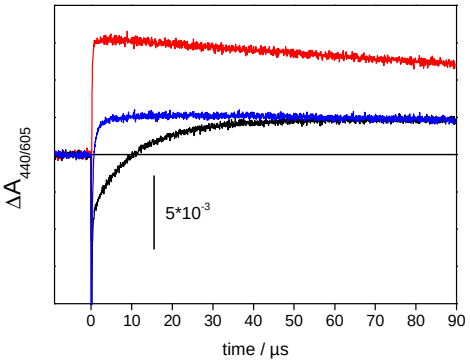

Figure 5.14: *Transient absorption traces at 440 nm (black) and 605 nm (red) for* ***Ru-imi-phOH-CCH*** *in acetonitrile; Ar-saturated solution. 10 mM methyl viologen (MV^{2+}) was present as electron acceptor. Blue: 440 nm in presence of 5% H_2O.*

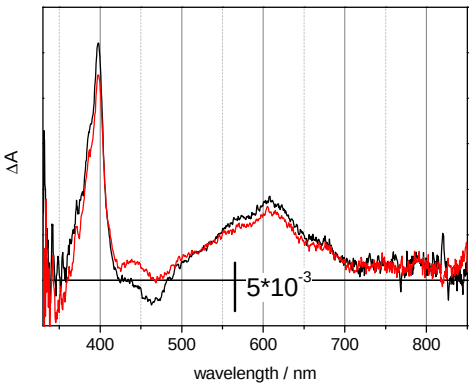

Figure 5.15: *Transient absorption spectra for* ***Ru-imi-phOH-CCH*** *recorded after 10 (black) and 50 (red) µs in presence of 10 mM MV; Ar-saturated solution.*

Transient absorption spectrum for **Ru-imi-phOH-CCH** in presence of MV shows the evolution of radical on the ligand (Figure 5.15). The radical on the ligand has absorption in the 440 nm region typical for our **Ru-xMe** complexes.

All this characteristics together show that the properties of the **Ru-imi-ph-CCH** are relatively unchanged compared to **Ru-xMe** complexes and that it resembles closely **Ru-imi-phOH** and **Ru-4Me**, *i.e.*the complex where the methyl substitution has the least effect.

5.5 Bimolecular activation of a Salen-Mn catalyst with Ru-3Me

By taking into account the failure of the synthesis of the complete target photocatalysts we have performed experiments with Mn salen in a bimolecular way using our Ru-imidazole-phenol (**Ru-3Me**) complex. We have already confirmed that the oxidized state of the chromophore is sufficiently oxidizing to create a phenoxyl radical on the ligand. The aim of the following experiments was to show that the oxidized state of the ligand can activate the catalyst and lead to Mn(V)=O formation. The schematic representation of the electron transfer sequence is show in Scheme 5.7.

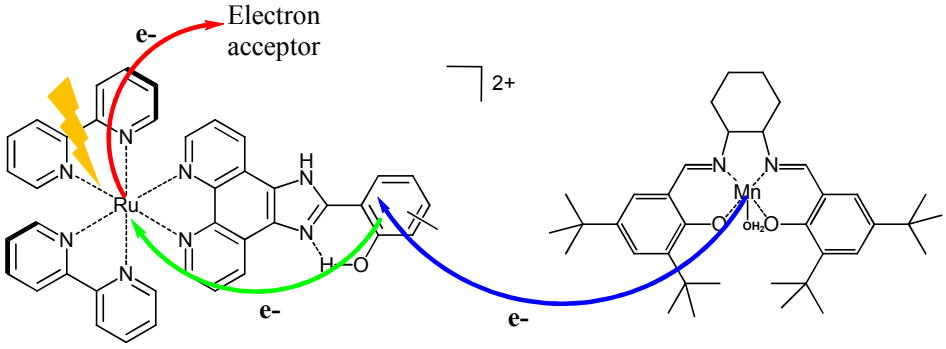

Scheme 5.7: *Driving activation of a Mn salen catalyst: light induced formation of Mn(IV)*

We have carried out laser flash induced experiments exciting **Ru-3Me** at 460 nm in presence of 200 µM Mn(III) salen catalyst and 5 mM of the irreversible electron acceptor, diazonium salt, which is an efficient quencher, soluble in MeCN. Special care was taken to not expose the sample to significant light during sample preparation and purging with Argon to avoid oxidation of complexes before excitation with the laser flash. We also refrained from signal averaging and the data below are single shot experiments. We know from the previous

experiments that in this complex the oxidized state of the ligand will be formed within some µs and that this radical does not show absorption bands above 550 nm.

The essential results of these experiments are shown in Figure 5.16 and 5.17. In the kinetic mode we have clearly observed a strong absorption increase at 680 nm, a wavelength typical for the Mn(IV) formation (Figure 5.16).[20,21] This is nicely confirmed by the transient absorption spectrum obtained at 100 µs after laser flash, shown in Figure 5.17, which shows a broad absorption centered at about 680 nm and attributed to formed Mn(IV). The kinetics of Mn(IV) formation, about 6 µs, is pseudo-first order because the catalyst is in large excess compared to the flash-induced phenoxyl radical (some µM). It seems diffusion limited with $k^{2nd} \approx 10^9$ $M^{-1}s^{-1}$.

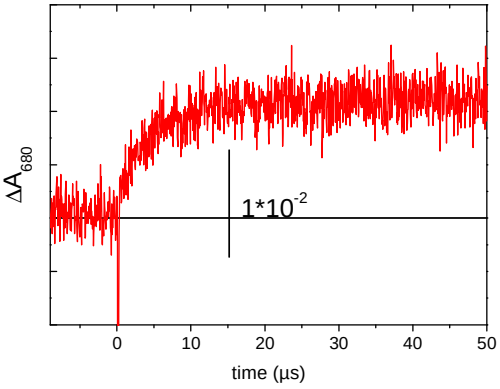

***Figure 5.16**: Laser flash induced formation of Mn (IV) shown by kinetic trace at 680 nm in presence of 5 mM diazonium salt as an acceptor in acetonitrile; Ar- saturated; single shot*

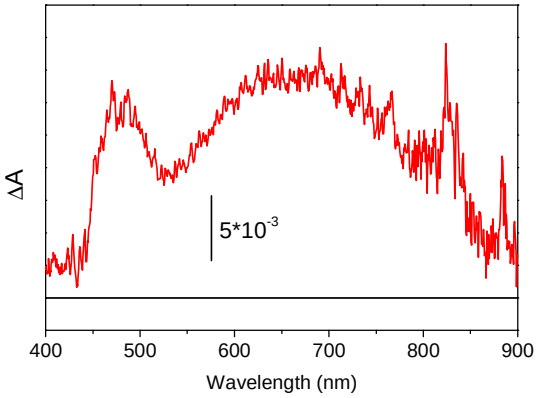

***Figure 5.17**: Transient absorption spectrum at 100 µs after laser flash of **Ru-3Me** in presence of 200 µM Salen-Mn catalyst, in presence of diazonium salt as an acceptor in acetonitrile; Ar-saturated;single shot*

To investigate whether the catalyst could be oxidized further we have performed experiments with continuous light illumination by using a light emitting diode (LED, emitting at ~450 nm), again using an irreversible electron acceptor. After illumination for a specific time we have recorded the absorption spectra (Figure 5.18). The figure shows increase of absorption at 680 nm after irradiating for 5 min. This gives confirmation for formation of Mn(IV) species. After 10 minutes of irradiation the absorption band decreased and disappeared after 15 min. This might be due to the formation of Mn(V)=O species although we lack more direct confirmation for this to be completely sure. A time scan with continuous illumination (Figure 5.19) gives transients consistent with the proposed formation of Mn(IV) species and gradual

decrease with further illumination. This kind of experiments could in principle be interesting to investigate effects of substrates for the catalyst and other experimental conditions (e.g. pH).

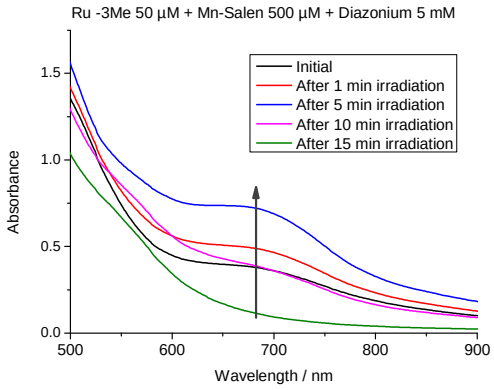

Figure 5.18: *Light-induced formation and disappearance of Mn(IV) shown by continuous illumination 450 nm.*

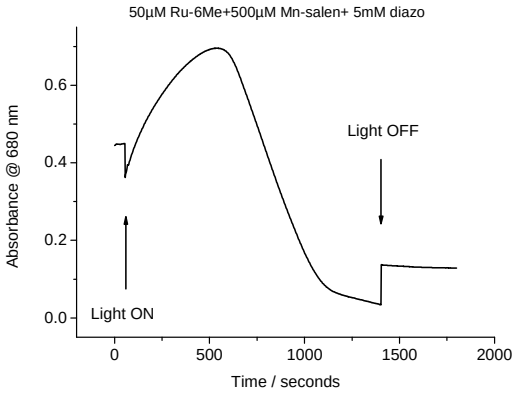

Figure 5.19*: Time scan recorded at 680 nm using UV-Visible spectrophotometer*

To summarize this study of bimolecular activation of a catalyst we propose that it follows the reaction sequence presented in Scheme 5.8. Further confirmation of Mn(V)=O formation should be obtainable by using EPR spectroscopy.

$$Ru(II)Lig + h\nu + EA \rightarrow Ru(III)\,Lig + EA^{-}$$

$$Ru(III)Lig \rightarrow Ru(II)\,Lig^{ox}$$

$$Ru(II)Lig^{ox} + Mn(III) \rightarrow Ru(II)Lig + Mn\,(IV)$$

Scheme 5.8*: Photoactivation of Mn(III) salen to generate Mn(IV); EA=Electron acceptor*

5.6 References

(1) Gust, D.; Moore, T. A.; Moore, A. L., Mimicking photosynthetic solar energy transduction. *Acc. Chem. Res.*, **2001**, *34*, 40-48.

(2) Lewis, N. S.; Nocera, D. G., Powering the planet: Chemical challenges in solar energy utilization.*Proc. Natl. Acad. Sci. U.S.A.*,**2006**, *103*, 15729-15735.

(3) Bard, A. J.; Fox, M. A., Artificial photosynthesis: solar splitting of water to hydrogen and oxygen. *Acc. Chem. Res.*, **1995**, *28*, 141-145.

(4) Sala, X.; Romero, I.; Rodríguez, M.; Escriche, L.; Llobet, A., Molecular catalysts that oxidize water to dioxygen.*Angew. Chem. Int. Ed.*,**2009**, *48*, 2842 -2852.

(5) McDaniel, N. D.; Coughlin, F. J.; Tinker, L. L.; Bernhard, S., Cyclometalated iridium (III) aquo complexes: efficient and tunable catalysts for the homogeneous oxidation of water.*J. Am. Chem. Soc.*,**2008**, *130*, 210-217.

(6) Wasylenko, D. J.; Ganesamoorthy, C.; Koivisto, B. D.; Henderson, M. A.; Berlinguette, C. P., Insight into Water Oxidation by Mononuclear Polypyridyl Ru Catalysts. *Inorg. Chem.*,**2010**, *49*, 2202-2209.

(7) Gersten, S. W.; Samuels, G. J.; Meyer, T. J., Catalytic oxidation of water by an oxo-bridged ruthenium dimer. *J. Am. Chem. Soc.*,**1982**, *104*, 4029-4030.

(8) Gilbert, J. A.; Eggleston, D. S.; Murphy Jr, W. R.; Geselowitz, D. A.; Gersten, S. W.; Hodgson, D. J.; Meyer, T. J., Structure and redox properties of the water-oxidation catalyst $[(bpy)_2(OH_2)\ RuORu\ (OH_2)(bpy)_2]^{4+}$. *J. Am. Chem. Soc.*,**1985**, *107*, 3855-3864.

(9) Liu, F.; Concepcion, J. J.; Jurss, J. W.; Cardolaccia, T.; Templeton, J. L.; Meyer, T. J., Mechanisms of water oxidation from the blue dimer to photosystem II. *Inorg. Chem.*,**2008**, *47*, 1727-1752.

(10) Concepcion, J. J.; Jurss, J. W.; Templeton, J. L.; Meyer, T. J., Mediator-assisted water oxidation by the ruthenium "blue dimer" cis, cis-$[(bpy)_2\ (H_2O)\ RuORu\ (OH_2)(bpy)_2]^{4+}$.*Proc. Natl. Acad. Sci. U.S.A.*,**2008**, *105*, 17632-17635.

(11) Rotzinger, F. P.; Munavalli, S.; Comte, P.; Hurst, J. K.; Graetzel, M.; Pern, F. J.; Frank, A. J.,A molecular water-oxidation catalyst derived from ruthenium diaqua bis (2, 2'-bipyridyl-5, 5'-dicarboxylic acid). *J. Am. Chem. Soc.*,**1987**, *109*, 6619-6626.

(12) Zong, R.; Thummel, R. P., A new family of Ru complexes for water oxidation. *J. Am. Chem. Soc.*,**2005**, *127*, 12802-12803.

(13) Xu, Y.; Åkermark, T. r.; Gyollai, V.; Zou, D.; Eriksson, L.; Duan, L.; Zhang, R.; Åkermark, B. r.; Sun, L., A new dinuclear ruthenium complex as an efficient water oxidation catalyst. *Inorg. Chem.*,**2009**, *48*, 2717-2719.

(14) Zhang, W.; Loebach, J. L.; Wilson, S. R.; Jacobsen, E. N., Enantioselective epoxidation of unfunctionalized olefins catalyzed by salen manganese complexes. *J. Am. Chem. Soc.*,**1990**, *112*, 2801-2803.

(15) Zhang, W.; Jacobsen, E. N., Asymmetric olefin epoxidation with sodium hypochlorite catalyzed by easily prepared chiral manganese (III) salen complexes.*J. Org. Chem.*,**1991**, *56*, 2296-2298.

(16) Sheth, S.; Baron, A.; Herrero, C.; Vauzeilles, B.; Aukauloo, A.; Leibl, W., Light-induced tryptophan radical generation in a click modular assembly of a sensitiser-tryptophan residue. *Photochem. Photobiol. Sci.***2013**, *12*, 1074-1078.

(17) Herrero, C.; Quaranta, A.; Leibl, W.; Fallahpour, R.-A.; Aukauloo, A., Identification of the Different Mechanisms of Activation of a $[RuII(tpy)(bpy)(OH_2)]^{2+}$ Catalyst by Modified Ruthenium Sensitizers in Supramolecular Complexes.*J. Phy. Chem. C*,**2013,** *117*, 9605–9612.

(18) Steck, E. A.; Day, A. R., Reactions of Phenanthraquinone with Aromatic Aldehydes and Ammonia in Alkaline Media. *J. Am. Chem. Soc.*,**1946**, *68*, 771-772.

(19) Campbell, E. J.; Nguyen, S. T., Unsymmetrical salen-type ligands: high yield synthesis of salen-type Schiff bases containing two different benzaldehyde moieties. *Tetrahedron Lett.*,**2001**, *42*, 1221-1225.

(20) Herrero, C.; Hughes, J. L.; Quaranta, A.; Cox, N.; Rutherford, A. W.; Leibl, W.; Aukauloo, A., Intramolecular light induced activation of a Salen–MnIII complex by a ruthenium photosensitizer. *Chem. Comm.*,**2010**, *46*, 7605-7607.

(21) Kurahashi, T.; Kikuchi, A.; Tosha, T.; Shiro, Y.; Kitagawa, T.; Fujii, H., Transient intermediates from Mn(salen) with sterically hindered mesityl groups: Interconversion between MnIV-phenolate and MnIII-phenoxyl radicals as an origin for unique reactivity.*Inorg. Chem.*,**2008**, *47*, 1674-1686.

6.0 Grafting of photosensitizer onto a TiO_2 surface and photoelectrochemical measurements

6.1 General concept

Hydrogen is considered as a green fuel and there are several options available for its generation.[1,2] But it would be more promising if we could generate hydrogen using most abundant element on the earth *i.e.* water. As explained in Chapter 1, Introduction, from the splitting of water hydrogen can be obtained according to the Eq. 6.1.

$$2H_2O \rightarrow 2H_2 + O_2 \qquad (6.1)$$

The energy required to drive this reaction is quite large, 474.4 kJ/mol. Actually in practice this energy could be supplied by using sunlight. But there is one problem since water does not absorb visible light. This problem could be overcome by employing a visible light harvesting device. Photolysis of water comprises two half reactions,

$$2H_2O \rightarrow O_2 + 4H^+ + 4e^- \qquad (6.2)$$

$$2H^+ + 2e^- \rightarrow H_2 \qquad (6.3)$$

which are best realized in two half cells of a photoelectrochemical cell as illustrated in Figure 6.1. Each electrode is made up of semiconducting material with attached photosensitizer (at least at the anode) and a catalyst for the respective half reaction. Two half cells are separated by a proton exchange membrane which allows diffusion of protons through the membrane and also prevents short-circuit reactions in the cell, for example oxidation of H_2 at the anode and reduction of O_2 at the cathode. Our project concerns the half reaction (Eq. 6.2) and we will discuss hereafter the development of a photoanode.

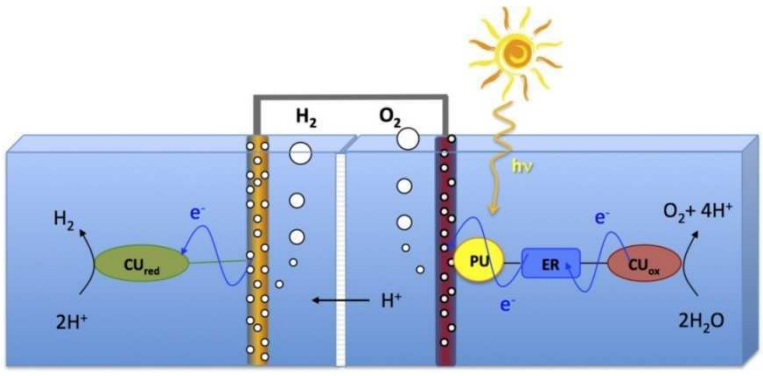

***Figure 6.1**: Photoelectrochemical cell*

For preparation of the photoanode the following elements are needed:

1) Glass plate coated with semiconducting material: here we used ITO (Indium tin oxide coated plates)
2) Nanostructured Titanium dioxide (TiO_2)
3) Chromophore which can absorb light in the visible region of the spectrum

TiO_2 is a semiconductor and it is ideal for such kind of photocatalytic studies due to its low cost, durability, stability, physical properties. TiO_2 absorbs light in the UV region and photocatalytic water splitting has been carried out using TiO_2 initially in the 70's.[3]This material has limited application only in the UV region because of its high band gap (3.2 eV). Therefore it can absorb only 4% of the available solar radiation. But our aim in the project is to use visible light not UV and therefore it is necessary to functionalize the TiO_2 with a photocatalytic assembly.

The unique property of TiO_2 allows us to make nanocrystalline thin films on the surfaces and much development has been done in this area by using colloidal suspensions.[4,5] Nanocrystalline thin films of TiO_2 can be visualized by Transmission electron microscopy (Figure 6.2). These nanocrystalline thin films possess extensively mesoporous morphological structure which leads to an increase in specific surface area by about a factor of 1000. When chromophores are grafted to this surface (dye sensitization) a significant part of the solar spectrum can be absorbed. Dye sensitization can be done by applying simple methods.

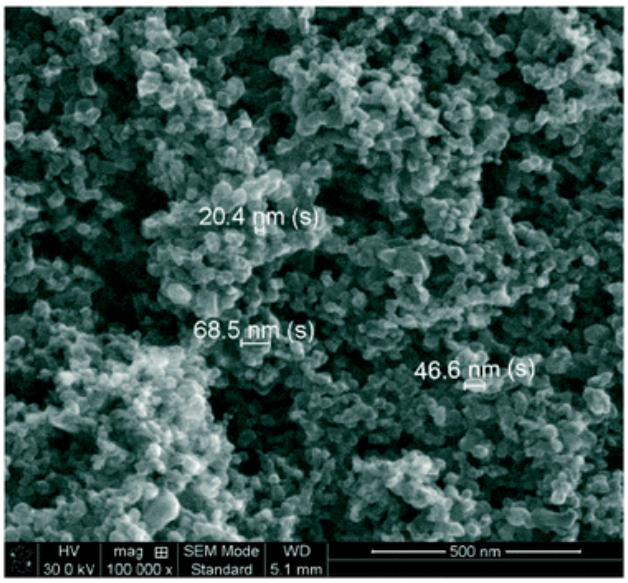

Figure 6.2: *SEM image of sintered nanoparticles TiO_2 layer*[33]

Several examples can be found in the literature which demonstrates grafting of a large variety of dye molecules on the surface of TiO_2 thin films.[6-10]

Light energy excites the photosensitized complex (S) to the excited state (S*). This excited state complex injects an electron into the conduction band of the semiconductor (TiO_2). The driving force for this charge injection process is the difference between oxidation potential of the excited sensitizer and conduction band of the TiO_2 (Figure 6.3).

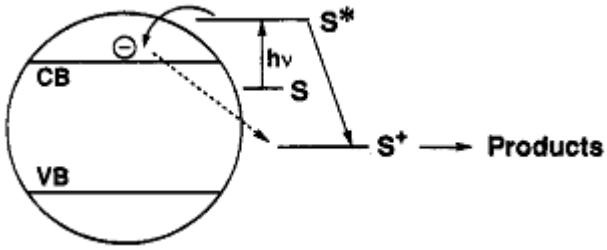

Figure 6.3: *Photosensitization of a semiconductor particle with a sensitizing dye; the conduction and valence bands of the semiconductor particle are indicated by CB and VB respectively. The electron donating energy levels (oxidation potential) of the ground and excited state of the sensitizer are indicated by S and S*.*[11]

This photosensitization of semiconducting surfaces was first used in the Dye Sensitized Solar Cell (DSSC) by O'Regan and Grätzel commonly called as Grätzel cell.[12] In a Grätzel cell (Figure 6.4) a photoanode is prepared by depositing fluoride doped tin oxide (SnO_2:F) on a glass plate (which gives 85% transmittance in visible region) and on this a 10 µm thick layer of TiO_2 nanoparticles was deposited by autoclaving at 450°C. After soaking this plate in the ruthenium polypyridine dye (Figure 6.5) solution they have obtained a homogeneous thin layer of the dye bound to the TiO_2 surface. Another electrode was prepared by depositing platinum on the conducting surface. Both these electrodes are joined together to make a complete cell putting iodide solution as an electrolyte (Figure 6.4). An overall energy conversion efficiency of 7.1-7.9 % was achieved in simulated solar light and 12% in diffused daylight.[12]

The overall efficiency is affected by one of the four components of the cell i) TiO_2 used either in the anatase or rutile form and its crystal size ii) Photosensitizer dye iii) Platinum coated electrode iv) Electrolyte. In this the important component concerning our study is the photosensitizer dye. Along with the visible light absorption characteristics it requires to have stable electronic coupling with TiO_2.[13-15] Physicochemical properties of the dye influence the covalent linkage between dye and TiO_2. This includes type of metal and ligand,[16,17] and anchoring groups of the dye.[18-20]

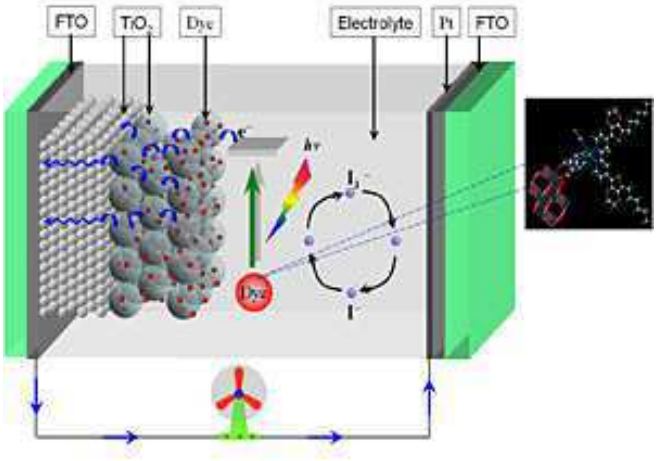

Figure 6.4: *Grätzel cell*[21]

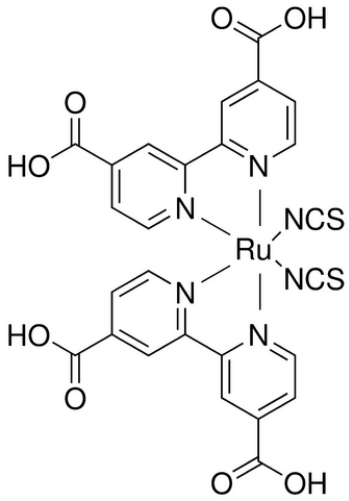

Figure 6.5: *Ruthenium polypyridine dye used in Grätzel cell.*[12]

Anchoring groups are used to graft the photosensitizer on the semiconductor surface. Several anchoring groups to graft on the TiO_2 surfaces are reported in the literature like phosphonate, carboxylate, acetylacenonate, silane, salicylate etc. Among these anchoring groups phosphonate and carboxylate and their acid analogs are most common.[6,22,23]

Although both carboxylate and phosphonate anchoring groups are frequently used, phosphonate groups have many advantages over carboxylate groups. In our lab we have also synthesized $\mathbf{[Ru(bpy)_3]^{2+}}$ based complexes with carboxylate groups and found that these complexes are less efficient compared to phosphonate groups for similar kind of study. Some advantages of phosphonate groups are,

1) Phosphonate groups have higher surface binding strength than carboxylate group. With$\mathbf{[Ru(bpy)_3]^{2+}}$complexes the surface binding constant of phosphonates is twice as high as carboxylate groups.[24]
2) Terpyridyl ligand with one phosphonate group has much stronger adsorption on TiO_2 surface as compared to four carboxylate groups.[10]
3) In water $\mathbf{[Ru(bpy)_3]^{2+}}$ with two carboxylate groups hardly adsorbed on the TiO_2 surface while complexes with two phosphonate groups adsorb well.[19]

Because of these advantages of phosphonate groups over carboxylate groups we have chosen phosphonate groups for our study.

Mayer *et al.* have reported photooxidation reactions on TiO_2 with a variety of chromophore catalyst molecular assemblies.[1,2,4,5,7] One of the best known examples in their study is the

Ruthenium complex with phosphonate anchoring groups shown in Figure 6.6.For this complex,**[Ru(Mebimpy)(4,4′-((HO)$_2$-OPCH$_2$)$_2$bpy)(OH$_2$)]$^{2+}$** where [Mebimpy = 2,6-bis(1-methylbenzimidazol-2-yl)-pyridine; bpy = 2,2′-bipyridine], they reported turnovers number of 3600 with turnover frequency of ~0.12 s^{-1} at 1.85 V *vs*. NHE at pH 1 (0.1 M HNO_3) after grafting it on an ITO electrode surface (Figure 6.6).[7]

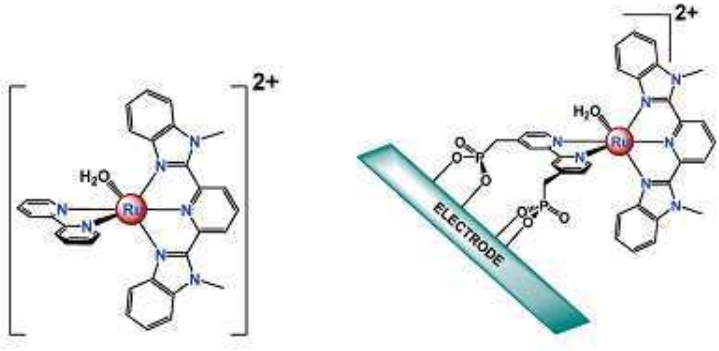

***Figure 6.6**: Structure of **[Ru(Mebimpy)(4,4′-((HO)$_2$-OPCH$_2$)$_2$bpy)(OH$_2$)]$^{2+}$** and schematic representation of its attachment to a metal oxide electrode.*[7]

6.2 Photosensitizer, [Ru(bpy)$_3$]$^{2+}$ with phosphonate groups

When photoanodes or photocathodes are to be made by grafting of modular photocatalytic systems, it is always the chromophore module which is directly attached to the surface. This is because it is the excited state of the chromophore which injects or extracts electrons from the semiconductor. The oxidized (reduced) form of the chromophore then drives oxidative (reductive) activation of the catalytic unit. At the end of this work a complete photocatalytic assembly (chromophore + electron relay + catalyst) was not available. Therefore we will report in the following the synthesis and characterization of a **[Ru(bpy)$_3$]$^{2+}$** chromophore functionalized with phosphonate anchoring groups *i.e.* **Ru-Phosphonate** (Figure 6.7) and present the corresponding experiments of sensitization of TiO_2 surfaces with this complex. The grafting on TiO_2 of a complete photocatalytic assembly should work in the same way.

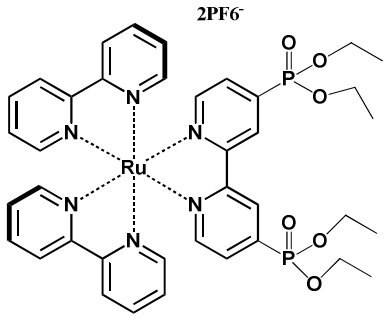

***Figure 6.7 : Ru-Phosphonate,** [Ru(II)(bpy)$_2$(4,4'-(PO$_3$Et$_2$)$_2$bpy)]*[18,19]

6.3 Synthesis of [Ru(II)(bpy)$_2$(4,4'-(PO$_3$Et$_2$)$_2$bpy)] complex (Ru-Phosphonate)

The synthesis involves several steps to obtain 4, 4'-diethyl phosphonato-2, 2'-bipyridine (Scheme 6.1) which was then used for complexation with **Ru(bpy)$_2$Cl$_2$** to get the desired **Ru-Phosphonate** complex by using known literature procedure (Figure 6.7)[18,19].

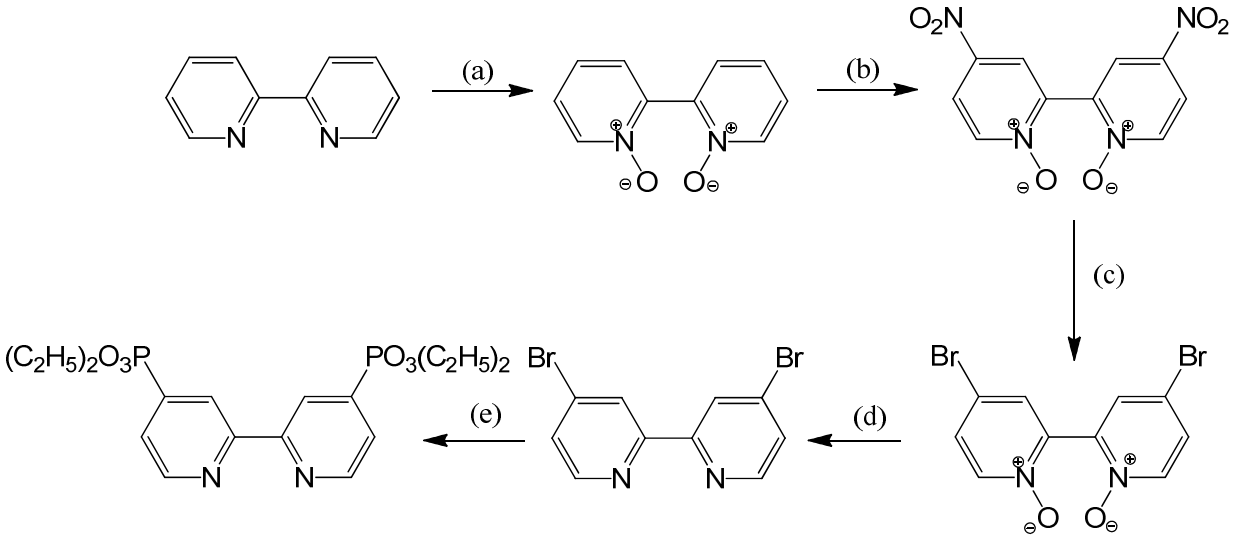

***Scheme 6.1** : Synthesis of 4, 4'-diethyl phosphonato-2,2'-bipyridine: (a) CH_3COOH, H_2O_2, 80°C[25] (b) H_2SO_4, HNO_3, 100°C[26] (c) CH_3COBr, CH_3COOH, 100°C[27,28] (d) PBr_3,MeCN, 95°C[27-29] (e) $(C_2H_5)_2PO_3H$,$Pd(PPh_3)_4$,PPh_3, $(C_2H_5)_3N$, Toluene, 110°C[30]*

6.4 Preparation of photoelectrochemical cell

6.4.1 Preparation of photoanode

ITO plates were purchased from Sigma Aldrich with surface resistivity of 30-60 Ω/sq and thickness of ITO coating of 300-600 Å (Figure 6.8). Its physical properties are summarized in Table 6.1.

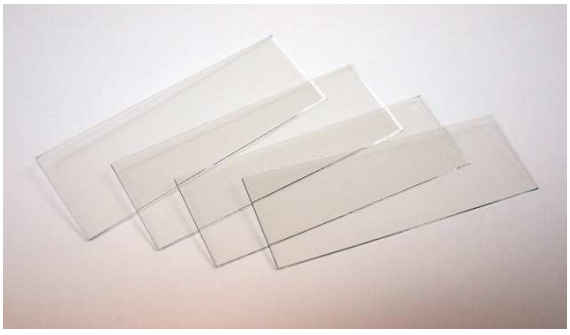

***Figure 6.8:** ITO plates used in our study*

Table 6.1: *Physical properties of ITO plate*

Surface resistivity	**30-60 Ω/sq**
L × W × thickness	**75 mm × 25 mm × 1.1 mm**
Transmittance	**>84%**

TiO_2 (Ti-Nanoxide T, Figure 6.9) was purchased from Solaronix. It is in the form of slurry (11% wt) of 15 -20 nm size anatase particles.

Figure 6.9*:TiO_2 paste (Ti-Nanoxide T) used in our study*

6.4.2 Procedure to deposit thin layer of TiO_2

First, the surface was cleaned using ethanol and kept in dust free environment. The conducting surface side was determined by electrical conductivity measurements using a multimeter. This side of the plate has an ITO layer deposited on it. We deposited a homogenous thin film of TiO_2paste, 10 μm thick, defined by Scotch tape by doctor blading technique. The layer was left to dry for approximately one hour in a dust free environment. After this theTiO_2 coated ITO plate was transferred into a furnace (Heraeus) where the temperature was maintained at 450°C for about 2 hours. The heating of the plate at such high temperature ensures binding of the TiO_2 to the ITO surface. Heating was then turned off and the furnace allowed cooling slowly to room temperature. The plate was removed from the furnace and was now ready to use for our study.

6.4.3 Grafting the photosensitizer complex on the electrode

For grafting we used 1mM solution of the complex to be grafted. Normally we dipped the plate in such solution for overnight.

6.5 Characterization of the Ru-Phosphonate complex

The photophysical properties of **Ru-Phosphonate** complex was studied in solution and on the surface of a TiO_2 electrode.

6.5.1 Absorption properties

Absorption spectra of **Ru-Phosphonate** in solution and on a TiO_2surface closely resemble spectra of **$[Ru(bpy)_3]^{2+}$** type complexes but the absorption maximum of the MLCT band is red shifted by 20 nm compared to **$[Ru(bpy)_3]^{2+}$** (Figure 6.10). The observed absorption maxima were 440 nm and 460 nm for complex in solution and on TiO_2 surface respectively. In the literature the reported value for similar complex with phosphonic acid groups is 467 nm in water[31] and 458 nm in methanol.[24]

The optical density of the chromophore film on the surface of TiO_2 indicates that there is quite good amount of complex grafted on the surface. The concentration of absorbed complex corresponds to a 20 µM solution in a 1 cm cuvette (since **$[Ru(bpy)_3]^{2+}$** ε = 14,600 M^{-1} cm^{-1}).[32]

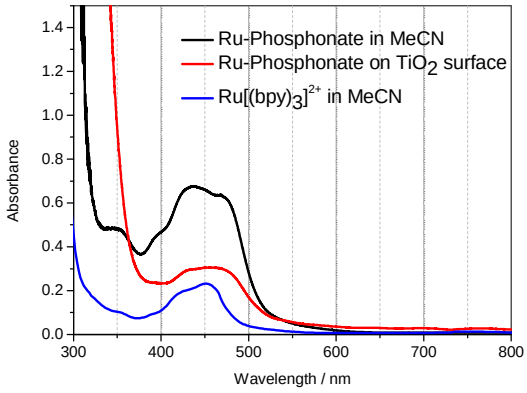

Figure 6.10: *Absorption spectra of* ***Ru-Phosphonate****in acetonitrile solution (black); on the TiO_2 surface (red) and for* ***$[Ru(bpy)_3]^{2+}$*** *in acetonitrile (blue).*

6.5.2 Emission properties

We have measured emission properties of **Ru-Phosphonate** using laser flash photolysis with a nanosecond excitation flash at 460 nm. The emission spectra in acetonitrile and on the TiO_2 surface are shown in Figure 6.11. The emission maximum is blue shifted by 20 nm on the TiO_2 surface as compared to the emission spectrum in solution. The observed emission maxima were 665 nm and 650 nm in solution and on TiO_2 surface, respectively. For **$[Ru(bpy)_3]^{2+}$** the emission maximum (in solution) is 607 nm thus functionalization with

phosphonate groups lead to a red shift of the emission maximum. Solvent also affects the emission properties of the **Ru-Phosphonate** as shown in Figure 6.12 and wavelength maxima are summarized in Table 6.2.

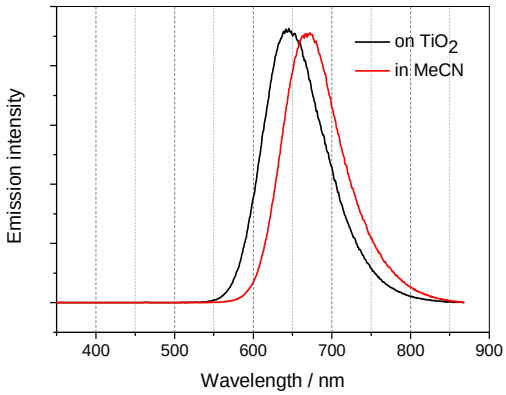

Figure 6.11: *Emission spectra of* ***Ru-Phosphonate*** *in acetonitrile at 100 ns after laser flash (red) and on the TiO_2 surface at 10 ns after laser flash (black).*

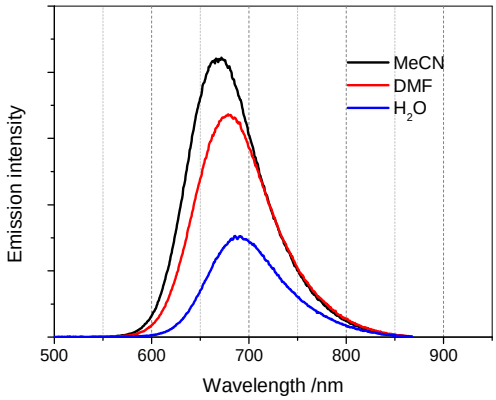

Figure 6.12: *Comparison showing Solvent effect on the emission spectra of* ***Ru-Phosphonate****; in acetonitrile (black), in DMF (red) and water (blue).*

Table 6.2: *Emission maxima and lifetime in different solvents obtained from LFP*

$[Ru(bpy)_3]^{2+}$	Solvent	λ_{max}	τ
	ACN	607 nm	870 ns
	H_2O	609 nm	600 ns
	DMF	615 nm	980 ns
Ru-Phosphonate	ACN	665 nm	690 ns
	H_2O	684 nm	185 ns
	DMF	675 nm	475 ns

Kinetic measurements of the emission decay at 670 nm for **Ru-Phosphonate** yielded a lifetime of 690 ns in acetonitrile solution (Figure 6.13), which is shorter than **$[Ru(bpy)_3]^{2+}$** (870 ns). In the case of **Ru-Phosphonate** complex grafted on the TiO_2 surface the emission lifetime was 13 ns with a minor phase of 150 ns when measured at 650 nm (Figure 6.14). The time constant of 13 ns corresponds to the time resolution of the detection system. This shows that the life time of the excited state is very short, consistent with fast electron injection into the conduction band of TiO_2. The small component of longer lived excited state probably

corresponds to a minor fraction of less well coupled chromophores. The Figure 6.13 also shows the effect of solvent on the emission kinetics and their lifetimes are summarized in the Table 6.2. This shows that change in solvent affect significantly lifetime of the emission.

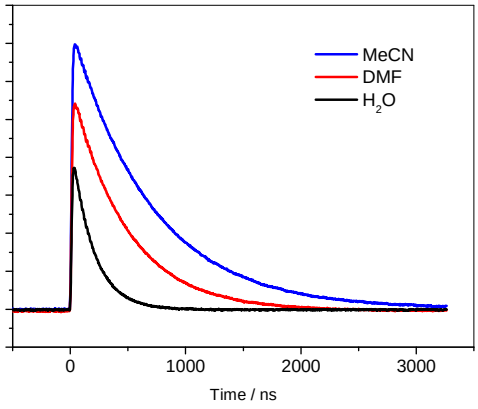

Figure 6.13: *Emission decay of* ***Ru-Phosphonate****x at 670 nm in acetonitrile (black), DMF (red) and water (blue).*

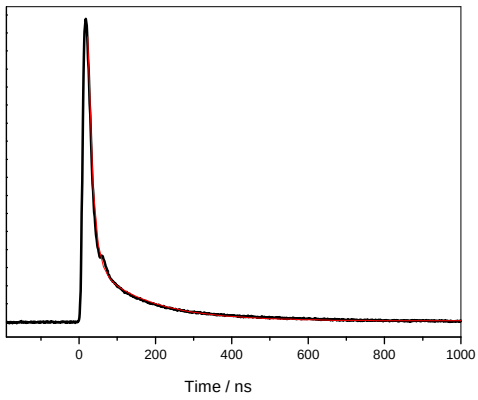

Figure 6.14: *Emission decay of* ***Ru-Phosphonate****at 650 nm on the TiO_2 surface. The red line represents a fit with two exponentials.*

6.5.3 Electrochemical properties

Electrochemical properties were studied by using cyclic voltammetry and differential pulse voltammetry. The comparison of cyclic voltammograms of **$[Ru(bpy)_3]^{2+}$** and **Ru-Phosphonate** is shown in Figure 6.15.

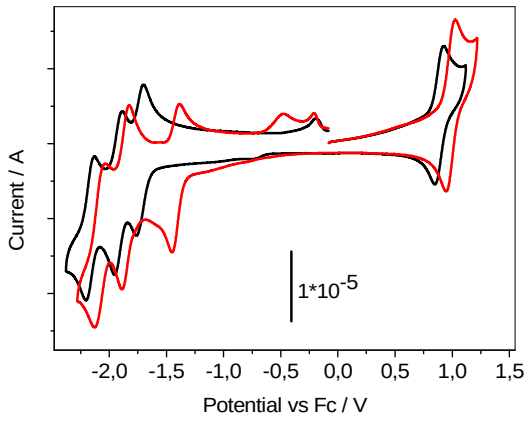

Figure 6.15: *Cyclic voltammograms of* ***$[Ru(bpy)_3]^{2+}$*** *and* ***Ru-Phosphonate*** *in acetonitrilevs. Ferrocene (Fc)shown in black and red respectivel; scan rate 100 mV/S*

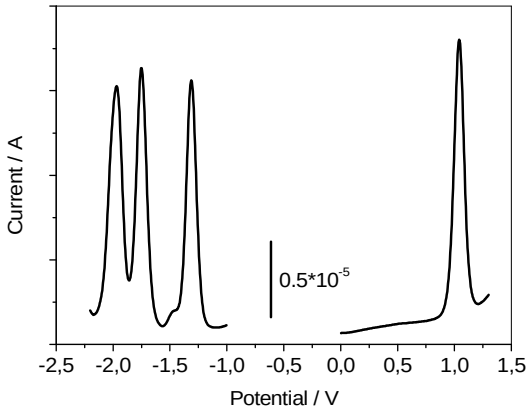

Figure 6.16: *Differential pulse voltammogram of* ***Ru-Phosphonate****in acetonitrilevs. Ferrocene (Fc).*

In the **Ru-Phosphonate** complex, Ruthenium is 110 mV more oxidizing than in **[Ru(bpy)$_3$]$^{2+}$**.The observed reduction waves are shifted towards less negative potential compared to **[Ru(bpy)$_3$]$^{2+}$**.The differential pulse voltammogram of Ru-Phosphonate *vs.* Ferrocene (Fc) is shown in Figure 6.16.

6.5.4 Photoelectrochemical measurements

The cell used for the photoelectrochemical measurements are shown in Figure 6.17. The ITO plate with the thin layered TiO_2 grafted with **Ru-Phosphonate** acts as a photoanode while a platinum plate was used as a cathode. Irradiation was done with visible light from a Xenon lamp from which UV irradiation was blocked by using a blue filter. An electrical shutter (not shown in the Figure) was used to switch illumination on and off. The photocurrent was measured by a current to voltage converter (Stanford Research Instruments) and recorded by an AD converter (Measurement Computing).

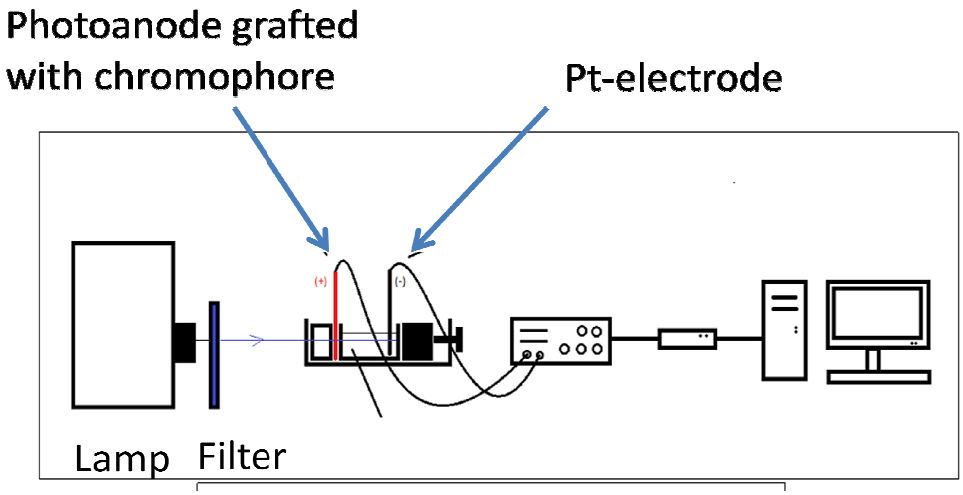

Figure *6.17:* *Experimental set up for the photoelectrochemical measurement*

For the measurement 200 mM tetrabutyl-ammoniumhexafluorophophate (TBAP) used as an electrolyte. This electrolyte, also used for electrochemical measurements, is not redox active and therefore, as expected no significant photovoltaic current response is observed. To simulate a photocatalytic situation we performed measurements in presence of small quantities of methanol and water. The rational for this was that the Ru(III) state formed after electron injection into TiO_2 is able to oxidize methanol and that the cathode will achieve a sufficiently negative potential to reduce protons to hydrogen. Under these conditions photocurrent measurement show rapid anodic current responses when irradiation was

switched on and off (Figure 6.18). Photocurrent densities were measured at different applied bias (from 100 mV to 400 mV) and a current density upto ~50 µA/cm^{2}was observed at 400 mV applied bias voltage (Figure 6.18).

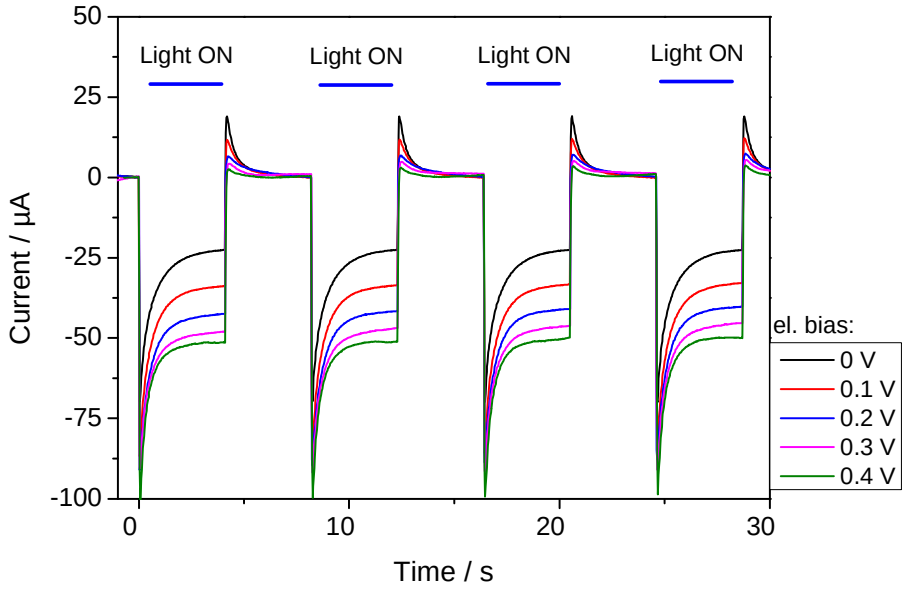

Figure 6.18:*Anodiccurrent response to on/off cycles of illumination with visible light at constant applied bias.*

These experiments show that with such a device it is in principle possible to measure catalytic activity as photocurrent. Variation of substrate, solvent conditions and applied external bias can be used to discriminate whether the cathodic or anodic reaction is limiting the overall current. In the absence of a complete photocatalyst to be grafted to the electrode we did not pursue such experiments further but work along this line with different potential photocatalysts is ongoing in the lab.

6.6 References

(1) Meyer, G. J., Molecular approaches to solar energy conversion with coordination compounds anchored to semiconductor surfaces. *Inorg. Chem.*,**2005**, *44*, 6852-6864.

(2) Trammell, S. A.; Moss, J. A.; Yang, J. C.; Nakhle, B. M.; Slate, C. A.; Odobel, F.; Sykora, M.; Erickson, B. W.; Meyer, T. J., Sensitization of TiO2 by phosphonate-derivatized proline assemblies. *Inorg. Chem.*,**1999**, *38*, 3665-3669.

(3) Stalder, C.; Augustynski, J., Photoassisted Oxidation of Water at Beryllium-Doped Polycrystalline TiO2 Electrodes. *J. Electrochem. Soc.*,**1979**, *126*, 2007-2011.

(4) Chen, Z.; Concepcion, J. J.; Hu, X.; Yang, W.; Hoertz, P. G.; Meyer, T. J., Concerted O atom–proton transfer in the O—O bond forming step in water oxidation.*Proc. Natl. Acad. Sci. U.S.A.*,**2010**, *107*, 7225-7229.

(5) Treadway, J. A.; Moss, J. A.; Meyer, T. J., Visible region photooxidation on TiO2 with a chromophore-catalyst molecular assembly. *Inorg. Chem.*,**1999**, *38*, 4386-4387.

(6) Li, L.; Duan, L.; Xu, Y.; Gorlov, M.; Hagfeldt, A.; Sun, L., A photoelectrochemical device for visible light driven water splitting by a molecular ruthenium catalyst assembled on dye-sensitized nanostructured TiO_2.*Chem. Comm.*,**2010**, *46*, 7307-7309.

(7) Chen, Z.; Concepcion, J. J.; Jurss, J. W.; Meyer, T. J., Single-site, catalytic water oxidation on oxide surfaces. *J. Am. Chem. Soc.*, **2009**, *131*, 15580-15581.

(8) Islam, A.; Sugihara, H.; Arakawa, H., *J.*, Molecular design of ruthenium (II) polypyridyl photosensitizers for efficient nanocrystalline TiO_2 solar cells. *Photochem. Photobiol. A: Chem.*,**2003**, *158*, 131-138.

(9) Hara, K.; Sugihara, H.; Tachibana, Y.; Islam, A.; Yanagida, M.; Sayama, K.; Arakawa, H.; Fujihashi, G.; Horiguchi, T.; Kinoshita, T., Dye-sensitized nanocrystalline TiO2 solar cells based on ruthenium (II) phenanthroline complex photosensitizers. *Langmuir*, **2001**, *17*, 5992-5999.

(10) Zakeeruddin, S.; Nazeeruddin, M. K.; Pechy, P.; Rotzinger, F.; Humphry-Baker, R.; Kalyanasundaram, K.; Grätzel, M.; Shklover, V.; Haibach, T., Molecular engineering of photosensitizers for nanocrystalline solar cells: synthesis and characterization of Ru dyes based on phosphonated terpyridines. *Inorg. Chem.*,**1997**, *36*, 5937-5946.

(11) Vinodgopal, K.; Hua, X.; Dahlgren, R. L.; Lappin, A.; Patterson, L.; Kamat, P. V., Photochemistry of Ru $(bpy)_2$ $(dcbpy)^{2+}$ on Al_2O_3 and TiO_2 surfaces. An insight into the mechanism of photosensitization.*J. Phy. Chem.*,**1995**, *99*, 10883-10889.

(12) O'Regan, B.; Grätzel, M., A low-cost, high-efficiency solar cell based on dye-sensitized. N*ature***1991**, *353*, 737-740.

(13) Hagfeldt, A.; Graetzel, M., Light-induced redox reactions in nanocrystalline systems. *Chem. Rev.*,**1995**, *95*, 49-68.

(14) Hagfeldt, A.; Grätzel, M., Molecular photovoltaics. *Acc. Chem. Res.*,**2000**, *33*, 269-277.

(15) Grätzel, M., Photoelectrochemical cells. *Nature,***2001**, *414*, 338-344.

(16) Nazeeruddin, M. K.; Kay, A.; Rodicio, I.; Humphry-Baker, R.; Müller, E.; Liska, P.; Vlachopoulos, N.; Grätzel, M., Conversion of light to electricity by cis-X2bis (2, 2'-bipyridyl-4, 4'-dicarboxylate) ruthenium (II) charge-transfer sensitizers (X= Cl-, Br-, I-, CN-, and SCN-) on nanocrystalline titanium dioxide electrodes. *J. Am. Chem. Soc.,***1993**, *115*, 6382-6390.

(17) Nazeeruddin, M. K.; De Angelis, F.; Fantacci, S.; Selloni, A.; Viscardi, G.; Liska, P.; Ito, S.; Takeru, B.; Grätzel, M., Combined experimental and DFT-TDDFT computational study of photoelectrochemical cell ruthenium sensitizers.*J. Am. Chem. Soc.,***2005**, *127*, 16835-16847.

(18) Park, H.; Bae, E.; Lee, J.-J.; Park, J.; Choi, W., Effect of the anchoring group in Ru-bipyridyl sensitizers on the photoelectrochemical behavior of dye-sensitized TiO2 electrodes: carboxylate versus phosphonate linkages. *J. Phy. Chem. B,* **2006**, *110*, 8740-8749.

(19) Bae, E.; Choi, W.; Park, J.; Shin, H. S.; Kim, S. B.; Lee, J. S., Effects of surface anchoring groups (carboxylate vs phosphonate) in ruthenium-complex-sensitized TiO2 on visible light reactivity in aqueous suspensions. *J. Phy. Chem. B,***2004**, *108*, 14093-14101.

(20) Nogueira, A. F.; Furtado, L. F. O.; Formiga, A. L.; Nakamura, M.; Araki, K.; Toma, H. E., Sensitization of TiO2 by supramolecules containing zinc porphyrins and ruthenium-polypyridyl complexes. *Inorg. Chem.,***2004**, *43*, 396-398.

(21) Shi, D.; Pootrakulchote, N.; Li, R.; Guo, J.; Wang, Y.; Zakeeruddin, S. M.; Grätzel, M.; Wang, P., New efficiency records for stable dye-sensitized solar cells with low-volatility and ionic liquid electrolytes. *J. Phy. Chem. C,* **2008**, *112*, 17046-17050.

(22) Hanson, K.; Brennaman, M. K.; Ito, A.; Luo, H.; Song, W.; Parker, K. A.; Ghosh, R.; Norris, M. R.; Glasson, C. R.; Concepcion, J. J., Structure–Property Relationships in Phosphonate-Derivatized, RuII Polypyridyl Dyes on Metal Oxide Surfaces in an Aqueous Environment.*J. Phy. Chem. C,***2012**, *116*, 14837-14847.

(23) Brennaman, M. K.; Patrocinio, A. O. T.; Song, W.; Jurss, J. W.; Concepcion, J. J.; Hoertz, P. G.; Traub, M. C.; Murakami Iha, N. Y.; Meyer, T. J., Interfacial Electron Transfer Dynamics Following Laser Flash Photolysis of [Ru (bpy) 2 ((4, 4′-PO3H2) 2bpy)] 2+ in TiO2 Nanoparticle Films in Aqueous Environments. *ChemSusChem,* **2011**, *4*, 216-227.

(24) Gillaizeau-Gauthier, I.; Odobel, F.; Alebbi, M.; Argazzi, R.; Costa, E.; Bignozzi, C. A.; Qu, P.; Meyer, G. J., Phosphonate-based bipyridine dyes for stable photovoltaic devices. *Inorg. Chem.,***2001**, *40*, 6073-6079.

(25) Simpson, P.; Vinciguerra, A.; Quagliano, J., The Donor Properties of 2, 2'-Bipyridine N, N'-Dioxide. *Inorg. Chem.*, **1963**, *2*, 282-286.

(26) Anderson, S.; Constable, E. C.; Seddon, K. R.; Turp, J. E.; Baggott, J. E.; Pilling, M. J., Preparation and characterisation of 2, 2′-bipyridine-4, 4′-disulphonic and-5-sulphonic acids and their ruthenium (II) complexes. Excited-state properties and excited-state electron-transfer reactions of ruthenium (II) complexes containing 2, 2′-bipyridine-4, 4′-disulphonic acid or 2, 2′-bipyridine-4, 4′ dicarboxylic acid.*J. Chem. Soc., Dalton Trans.*,**1985**, 2247-2261.

(27) Staats, H.; Eggers, F.; Haß, O.; Fahrenkrug, F.; Matthey, J.; Lüning, U.; Lützen, A., Towards Allosteric Receptors–Synthesis of Resorcinarene-Functionalized 2, 2′-Bipyridines and Their Metal Complexes. *Eur. J. Org. Chem.*,**2009**, *2009*, 4777-4792.

(28) Wenkert, D.; Woodward, R., Studies of 2, 2'-bipyridyl N, N'-dioxides. *J. Org. Chem.*,**1983**, *48*, 283-289.

(29) Maerker, G.; Case, F. H., The Synthesis of Some 4, 4'-Disubstituted 2, 2'-Bipyridines*J. Am. Chem. Soc.*,**1958**, *80*, 2745-2748.

(30) Penicaud, V.; Odobel, F.; Bujoli, B., Facile and efficient syntheses of 2, 2′-bipyridine-based bis (phosphonic) acids. *Tetrahedron Lett.*,**1998**, *39*, 3689-3692.

(31) Vlachopoulos, N.; Liska, P.; Augustynski, J.; Grätzel, M., Very efficient visible light energy harvesting and conversion by spectral sensitization of high surface area polycrystalline titanium dioxide films. *J. Am. Chem. Soc.*, **1988**, *110*, 1216-1220.

(32) Kalyanasundaram, K., Photophysics, photochemistry and solar energy conversion with tris (bipyridyl) ruthenium (II) and its analogues. *Coord. Chem. Rev.*,**1982**, *46*, 159-244.

(33) Van de Lagemaat, J., Park, N. G., & Frank, A. J., Influence of electrical potential distribution, charge transport, and recombination on the photopotential and photocurrent conversion efficiency of dye-sensitized nanocrystalline TiO_2 solar cells: a study by electrical impedance and optical modulation techniques. *J. Phy. Chem. B*, **2000,***104*, 2044-2052.

7.0 Conclusions and Perspectives

Artificial photosynthesis is often considered to have great potential to provide alternative, renewable fuels by harvesting, conversion and storage of solar energy. One promising approach is the development of modular molecular photocatalysts inspired by natural photosynthetic enzymes. The thesis deals with artificial mimics of the water oxidizing photosystem II composed of a chromophore and an electron relay as synthetic counterpart of the P680-TyrZ/His190 ensemble of photosystem II. Three ruthenium polypyridyl – imidazole - phenol complexes with varying position of a methyl group on the phenol ring (**Ru-xMe**) were synthesized and characterized by electrochemical and photophysical methods. As an improvement compared to earlier complexes the increased redox potential (~0.9 V *vs.* Ferrocene) of the phenol groups makes their function as an electron relay in a photocatalytic system for water oxidation thermodynamically possible. Time-resolved absorption studies revealed fast intramolecular electron transfer (<5-10 µs in aprotic solvent and <100 ns in water) despite the low driving force, and the importance of the hydrogen bond between the phenol and the imidazole group was put in evidence. Slight differences between the three **Ru-xMe** complexes and investigation of the effect of external bases allowed to derive a mechanistic picture in which the imidazole is involved in a "proton domino" reaction. Accepting the phenolic proton upon ligand oxidation (within the H-bond) renders its second nitrogen site more acidic and only deprotonation of this site pulls the overall equilibrium completely towards oxidation of the ligand.

A chromophore-tryptophan construct was synthesized using a click chemistry approach. Light-induced oxidation of Trp in this **Ru-tryptophan** complex was shown to follow a ETPT mechanism. Depending on the pH conditions tryptophan radicals, either $Trp^{\bullet}$ or $TrpH^{\bullet+}$were detected and spectral measurement at different time showed the transition between the two forms. Deprotonation of the radical was dependent on the concentration of water as proton acceptor.

Many efforts were made to covalently bind a catalytic unit to the previously characterized chromophore-electron relay module. The click chemistry approach was not successful to obtain the final photocatalytic assembly. Therefore bimolecular activation of a Mn salen catalyst was performed and formation of Mn(IV) species was observed. As a step towards utilization of these types of photocatalysts in a photoelectrochemical cell a $[Ru(bpy)_3]^{2+}$ chromophore with phosphonate anchoring groups (**Ru-Phosphonate**) was synthesized and

grafted on the surface of a TiO_2 mesoporous semiconductor surface anode to perform photocurrent measurements.

Perspectives

We have synthesized an artificial complex which likely represents the closest mimics of the electron transfer chain on the donor side of Photosystem 2. Energetic and kinetic properties of this system have been characterized and revealed similarities with observations made with the natural system. In order to obtain further information, in particular on the (de)localization of the radical on the imidazole-phenol ligand, other techniques could be used, like high field EPR, infrared spectroscopy and DFT calculations.

Infrared spectroscopy was available in the lab and we tried to employ this technique for characterization of our complexes. It should in principle allow to follow protonation and deprotonation events which are not spectroscopically distinguishable in visible spectroscopy. Unfortunately, the high sample concentrations necessary for these experiments lead to fast decay of the radicals by bimolecular back reactions. One possibility to overcome this problem could be to avoid soluble electron acceptors by using complexes grafted to TiO_2 but the fast internal electron transfer kinetics in our complexes will be very difficult to resolve. Preliminary results with IR spectroelectrochemistry were obtained (Figure 7.1) by recoding IR difference absorption spectra at different applied potentials (ox-red, red-ox). When contributions due to chromophore oxidation are subtracted these data indicate modifications in vibrational bands for phenol and imidazole. For a clear assignment however, model compounds should be compared or isotope effects looked after. In addition, it is not clear that electrochemical oxidation lead to the same oxidation states than photooxidation and it is not feasible to avoid simultaneous oxidation of the Ru chromophore, again a situation which does not exist in a flash experiment.

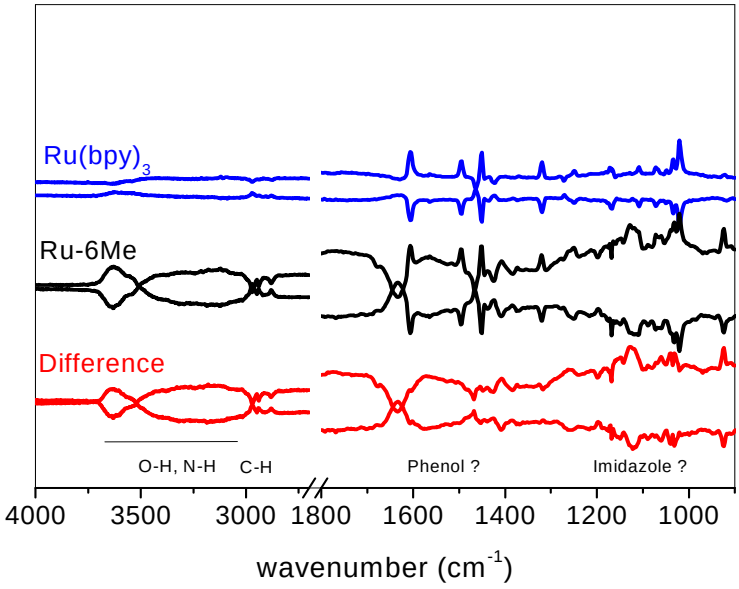

Figure 7.1: *Infrared spectroelectrochemistry of* ***Ru-6Me*** *(+0.8 V ←→ +1.2 V)*

In this work we encountered difficulties to obtain the final catalytic complex (chromophore + electron relay + catalyst). There might be some alternative ways out to synthesize similar complexes. In our laboratory we have already synthesized several ruthenium photosensitizer based complexes and Ru-Tryptophan is one of them. The complex **Ru-imi-phOH-CCH** was successfully obtained which can serve as an important reactant to make a new library of chromophore –electron relay –catalyst system. Due to limited thesis period we couldn't carry out synthesis by using other possibilities.

Instead of developing the catalytic unit on the **Ru-imi-phOHCCH** fragment, the complete, azide functionalized catalytic unit can be synthesized separately and click reaction performed between these two units i.e. chromophore-electron relay and a metal containing catalyst (Figure 7.2). This will certainly avoid the blockage of the cavity by trapping Cu inside it.

Another possibility would be to construct the electron relay catalytic unit by performing click chemistry reaction between alkyne functionalized phenanthroline-imidazole-phenol and azide functionalized catalytic unit (Figure 7.3).

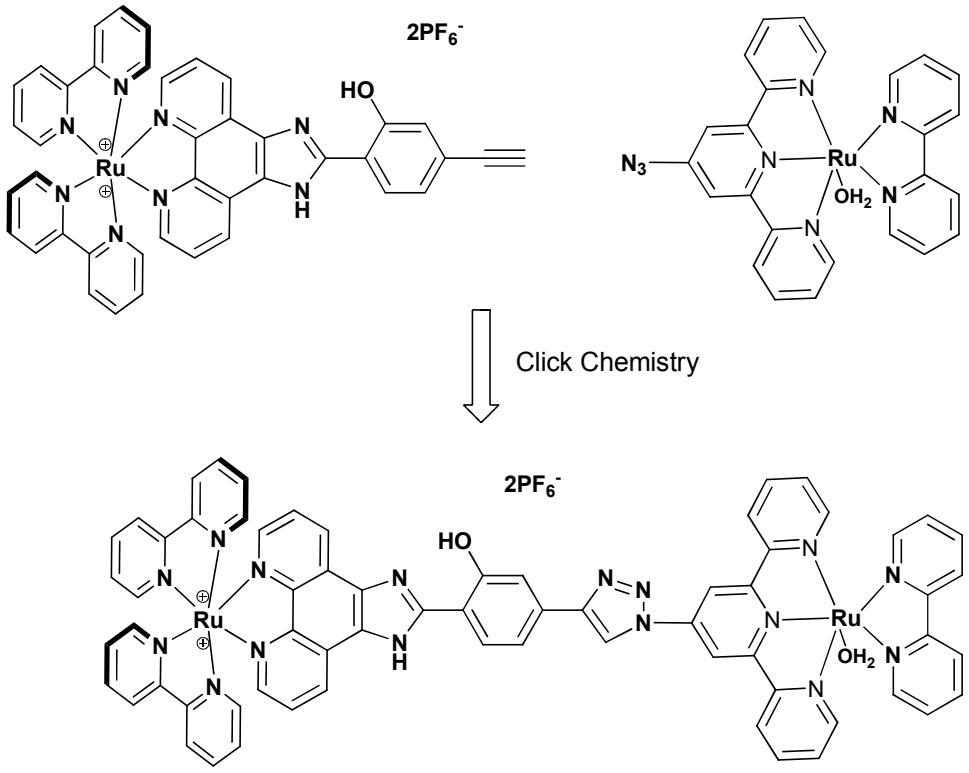

***Figure 7.2**: Click chemistry reaction between chromophore-electron relay and catalytic unit*

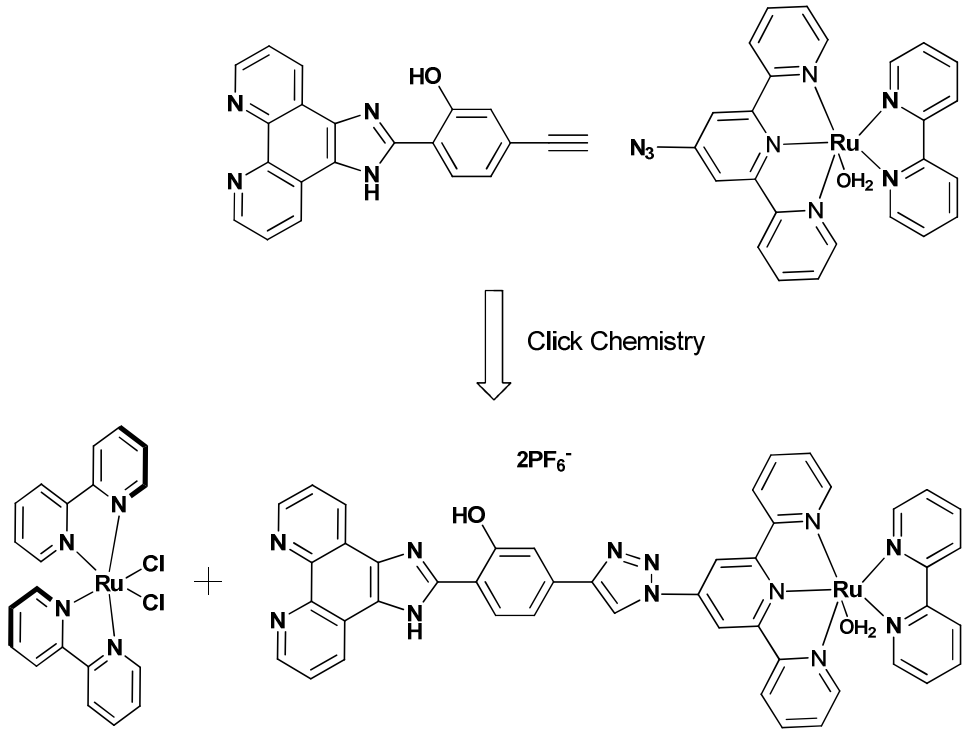

***Figure 7.3**: Another approach to synthesis chromophore electron relay catalyst via click chemistry reaction*

We have already successfully synthesized a chromophore with anchoring phosphonate groups (**Ru-Phosphonate**). We were also successful to graft this chromophore on the surface of a TiO_2 electrode to obtain a photoanodeand this photoanode was assembled in a photoelectrochemical cell and photocurrents were measured. The system seemed rather stable even after addition of water thus showing the usefulness of the phosphonate group over carboxylate groups. A complete photocatalytic complex can be grafted on the electrode the same way and photocurrent generation and photocatalytic substrate transformations can be measured.

A possible alternative for grafting a complete photocatalysts could be grafting a chromophore and a catalyst separately on the same electrode surface. Such an approach has recently been reported by Moore et al. Figure 7.4. By employing excess chromophore the light-limited rate of activation of the catalytic units can be increased in this way. The only drawback of this approach is that it is hard to control (and optimize) the interaction between the two components.

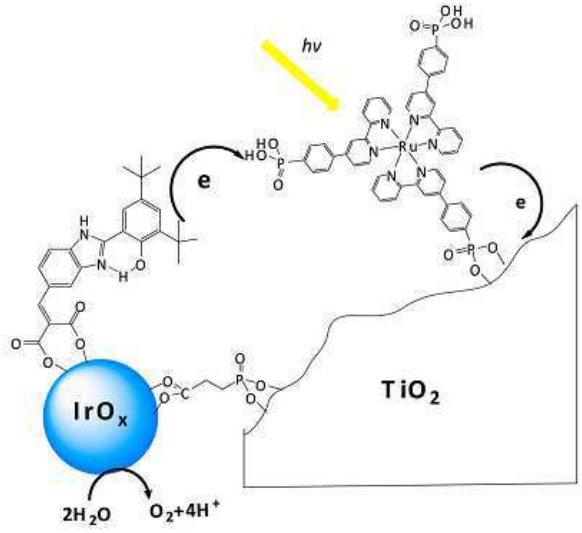

Figure 7.4: *Electron transfer reaction on the dye sensitized TiO_2 photoanode*[1]

For real future applications once efficient and stable photocatalyst have been developed the ruthenium metal has to be replaced by one of the more earth-abundant elements (Figure 7.5 shows annual production of metals in 2010) like Cobalt, Iron, Manganese. Nature also uses one of these abundant elements for the water oxidation catalyst.

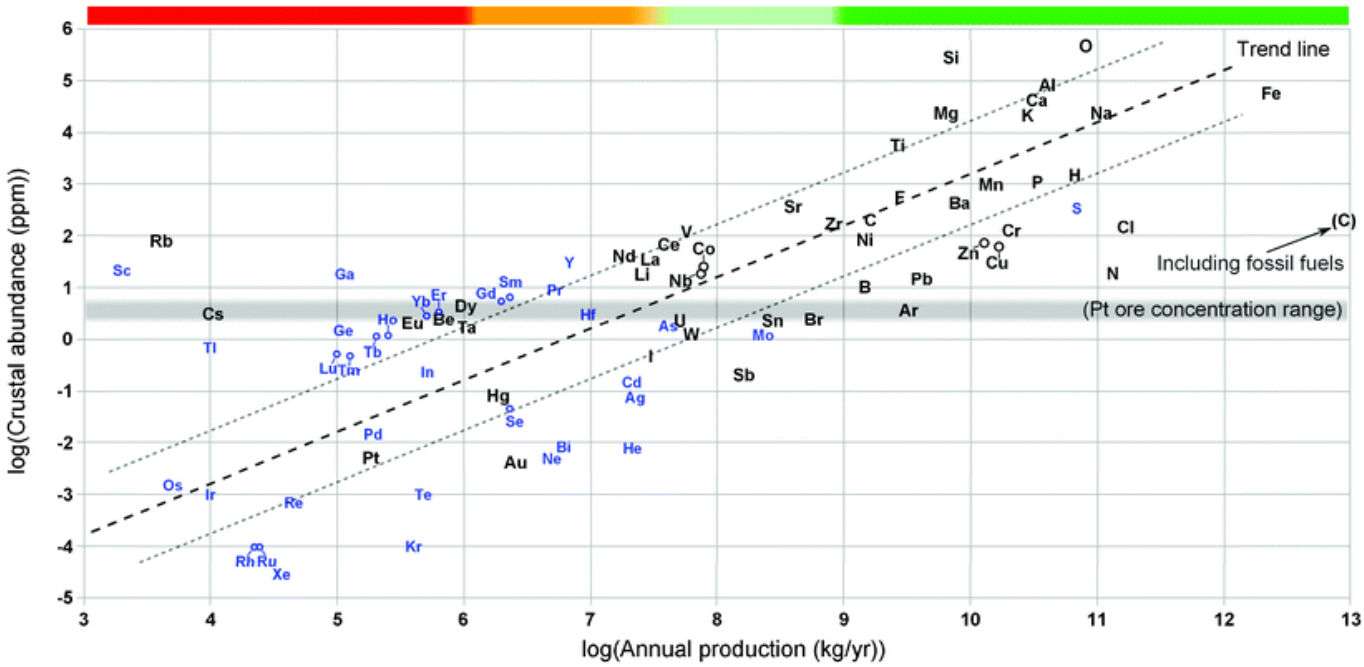

Figure 7.5: *Annual production of the elements in 2010.*[2]

References:

(1) Zhao, Y.; Swierk, J. R.; Megiatto, J. D.; Sherman, B.; Youngblood, W. J.; Qin, D.; Lentz, D. M.; Moore, A. L.; Moore, T. A.; Gust, D., Improving the efficiency of water splitting in dye-sensitized solar cells by using a biomimetic electron transfer mediator. *Proc. Natl. Acad. Sci. U.S.A.*,**2012**, *109*, 15612-15616.

(2) Vesborg, P. C.; Jaramillo, T. F., Addressing the terawatt challenge: scalability in the supply of chemical elements for renewable energy. *RSC Adv.*,**2012**, *2*, 7933 -7947.

EXPERIMENTAL PART

Chapter 3: Artificial mimics of TyrZ / His190 electron relay of photosystem II

1) 1, 10-Phenanthroline-5, 6-dione

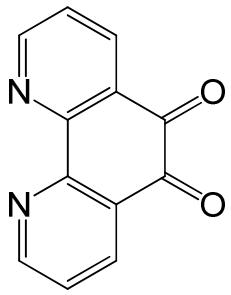

1, 10-Phenanthroline (5.00 g) was added in smaller portions to conc. H_2SO_4 (97%) while continuous stirring in a round bottom flask. To this obtained solution 2.5 g of NaBr and 15 mL of conc HNO_3 (52.5%) was added. The mixture was heated to 160°C for 3 h using reflux condenser. At end of the reaction heating was turned off and reflux condenser was removed to let all bromine vapors go out during gentle stirring. The reaction mixture was allowed to cool to room temperature and poured over 400 mL ice beaker and stirred to get a homogenous solution. This mixture was neutralized to pH 7 with 10 M sodium hydroxide solution. Obtained turbid solution was then filtered and solids were extracted with water. All combined aqueous solution was extracted with dichloromethane (5 X 80 mL). The organic phase was washed with 100 mL water and dried with anhydrous sodium sulfate. Then organic solvent was removed under reduced pressure to obtain crystalline crude product. This product was then recrystalized using 350 mL toluene to yield 2.73 g of the 1, 10-Phenanthroline-5, 6-dione (46.8% yield)

^{1}H NMR (400 MHz, $CDCl_3$) δ: 9.09 (dd, J = 4.6 and 1.9 Hz, 2H, H-aryl), 8.48 (dd, J = 7.8 and 1.8 Hz, 2H, H-aryl), 7.57 (dd, J = 7.9 and 4.6 Hz, 2H, H-aryl)

ESI-MS*m/z* = 233.0321 $[M + Na]^+$. Calcd.for $C_{12}H_6N_2O_2Na$ *m/z* = 233.0327

2) $Ru(bpy)_2Cl_2$

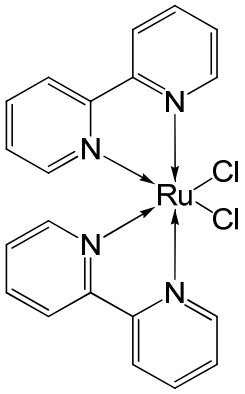

A mixture of $RuCl_3.H_2O$ (780 mg, 3.0 mmol, g, 1.0 eq), 2,2'-bipyridine (6.0 mmol, 937 mg, 2.0 eq) and LiCl (890 mg, 21 mmol, 7.0 eq) was dissolved in 10 mL dry DMF and refluxed for 16 h under an argon environment. Then reaction mixture was cooled to room temperture and 100 mL of acetone was added in a flask. This flask was kept at -20°C for complete precipitation. The next day obtained precipitate was filtered, washed with water and copious quantity of diethyl ether. Then drying under vacuum yielded 755 mg of pure product. Yield: 52%

^{1}H NMR (400 MHz**, DMSO) δ:** 9.97 (d, J= 5.9 Hz, 2H), 8.64 (d, J = 8.2 Hz, 2H), 8.48 (d, J = 8.3 Hz, 2H), 8.06 (t, 8.2 Hz, 2H), 7.77 (t, 6.5 Hz, 2H), 7.68 (t, 7.7 Hz, 2H), 7.51 (d, 5.7 Hz, 2H), 7.1 (t, J = 6.8 Hz, 2H)

ESI-MS*m/z* = 449.0091 $[M-Cl]^+$. Calcd.for $C_{20}H_{16}N_4$ Cl Ru *m/z* = 449.0107

3) 6'-methyl-2'-(1*H*-imidazo [4,5-*f*][1,10]phenanthroline-2-yl)phenol

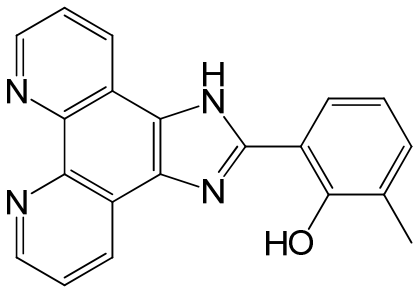

1, 10 Phenanthroline –5, 6-dione (210 mg, 1.0 mmol, 1.0 eq) and 3- methyl ,2-hydroxy benzaldehyde (137 mg, 1.0 mmol, 1.0 eq) was suspended in acetic acid. This reaction mixture

was heated to 80°C for 30 min; this resulted in homogeneous dark yellow solution. To this hot solution ammonium acetate (1.54 g, 20.0 mmol, 20.0 eq) was added resulting into reddish brown solution and reaction temperature was raised to 100°C. After 3 hours, thick solid solution was obtained. This solid solution was then filtered after cooling down to room temperature. The solid was washed repeatedly with water, diethyl ether and finally dried under vacuum to yield 281 mg product. Yield: 85%

^{1}H NMR (400 MHz, DMSO) δ: 9.01 (d, 3.4 Hz, 2H), 8.87 (d, J = 8.0 Hz, 2H), 8.01 (d, J = 7.5 Hz, 1H), 7.81 (dd, J = 7.5 Hz and 4.2 Hz, 2H), 7.24 (d, J = 7.2 Hz, 1H), 6.94 (t, J = 7.5 Hz, 1H)

ESI-MS*m/z* = 327.1240 $[M + H]^+$. Calcd.for $C_{20}H_{15}N_4O$ *m/z* = 327.1246

4) 5'-methyl-2'-(1*H*-imidazo [4,5-*f*][1,10]phenanthroline-2-yl)phenol

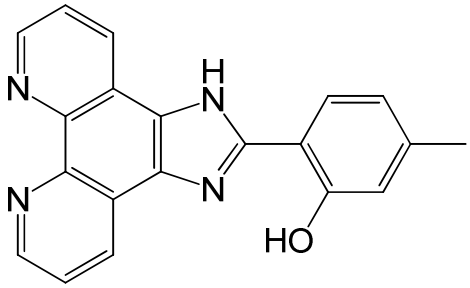

1, 10 Phenanthroline –5, 6-dione (210 mg, 1.0 mmol, 1.0 eq) and 4- methyl,2-hydroxy benzaldehyde (137 mg, 1.0 mmol, 1.0 eq) was suspended in acetic acid. This reaction mixture was heated to 80°C for 30 min, this resulted in homogeneous dark yellow solution. To this hot solution ammonium acetate (1.54 g, 20.0 mmol, 20.0 eq) was added resulting into reddish brown solution and reaction temperature was raised to 100°C. After 3 hours, thick solid solution was obtained. This solid solution was then filtered after cooling down to room temperature. The solid was washed repeatedly with water, diethyl ether and finally dried under vacuum to yield 256 mg product. Yield: 78%

^{1}H NMR (400 MHz, DMSO) δ: 9.05 (dd, J = 4.3 Hz and 1.6 Hz, 2H), 8.92 (dd, J = 8.2 Hz, 1.5 Hz, 2H), 8.08 (d, J= 8.3 Hz, 1H), 7.85 (dd, J = 8.0 Hz, 4.6 Hz, 2H), 6.91 (d, J = 6.1 Hz, 2H)

ESI-MS*m/z* = 327.1235 $[M + H]^+$. Calcd.for $C_{20}H_{15}N_4O$ *m/z* = 327.1246

5) 3'-methyl-2'-(1*H*-imidazo [4,5-*f*][1,10]phenanthroline-2-yl)phenol

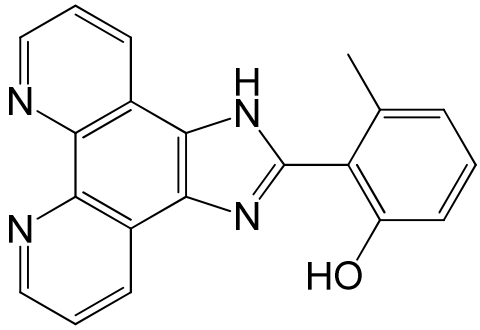

1, 10 Phenanthroline –5, 6-dione (210 mg, 1.0 mmol, 1.0 eq) and 6- methyl ,2-hydroxy benzaldehyde[1-3] (137 mg, 1.0 mmol, 1.0 eq) was suspended in acetic acid. This reaction mixture was heated to 80°C for 30 mins, this resulting in homogeneous dark yellow solution. To this hot solution ammonium acetate (1.54 g, 20.0 mmol, 20.0 eq) was added resulting into reddish brown solution and reaction temperature was raised to 100°C. After 3 hours, thick solid solution was obtained. This solid solution was then filtered after cooling down to room temperature. The solid was washed repeatedly with water, diethyl ether and finally dried under vacuum to yield 137 mg product. Yield: 45%

^{1}H NMR (400 MHz, DMSO) δ: 8.9 (d, J=8.1 Hz, 2H), 8.8 (d, J= 8.0 Hz, 2H), 8.0 (d, J = 7.5 Hz, 1H) 7.7 (dd, J=8.0 Hz, 2H), 7.2 (d, J=7.0 Hz, 1H), 6.9 (t, J = 8.0 Hz, 1H), 2.2 (s, 3H).
ESI-MS*m/z* = 327.12 $[M + H]^+$

6) Ru-3Me

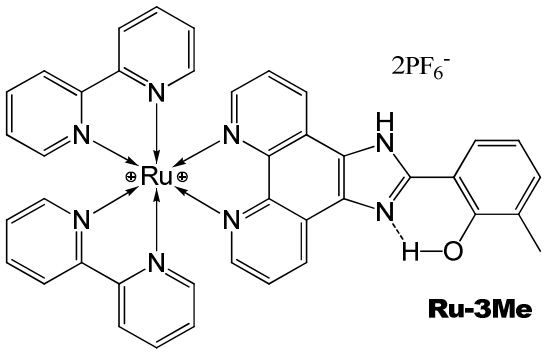

Ru-3Me

In a typical reaction $Ru(bpy)_2Cl_2$ (73 mg, 0.15 mmol, 1 eq) was treated with silver nitrate (51 mg, 0.30 mmol, 2.0 eq) in methanol for 3 hours at room temperature. The solution was filtered in order to remove silver salts and the filtrate was added to a round bottom flask

containing 6'-methyl-2'-(1H-imidazo [4,5-*f*][1,10]phenanthroline-2-yl)phenol (49 mg, 0.15 mmol, 1.0 eq). The solution was refluxed for 3 hours in dark under an argon atmosphere. At this time the reaction mixture was allowed to go to room temperature and the solvent was evaporated under reduced pressure. The obtained solid was dissolved in a minimum amount of MeOH and precipitated as a PF_6 salt by adding saturated aqueous solution of ammonium hexafluorophosphate. The flask was kept at -20 °C overnight to obtain complete precipitation and filtered. After repeated washings with water and copious quantity of diethyl ether, the obtained product was dried under vacuum (131 mg).Yield: 84%.

^{1}H NMR (400 MHz, CD_3CN) δ: 9.0 (d, J = 8.1 Hz, 2H), 8.54 (d, 8.1 Hz, 2H), 8.5 (d, J = 8.1 Hz, 2H), 8.11 (td, J = 7.9 Hz and 1.5 Hz, 2H), 8.04 (dd, J = 5.3 Hz and 1.1 Hz, 2H), 7.99 (td, J = 8.0 Hz and 1.5 Hz, 2H), 7.91 (d, J = 8.4 Hz, 1H), 7.86 (dd, J= 5.7 Hz, 0.8 Hz, 2H), 7.78 (dd, 8.2 Hz and 5.4 Hz, 2H), 7.6 (dd, 5.6 Hz and 0.9 Hz, 2H), 7.46 (td, J = 6.7 Hz and 1.8 Hz, 2H), 7.32 (d, J = 7.7 Hz, 1H), 7.22 (td, J = 6.7 Hz, 1.2 Hz, 2H), 7.0 (t, J = 7.6 Hz, 1H)

ESI-MS*m/z* = 370.07 $[M]^{2+}$, 739.34 $[M\text{-}H]^{+}$

7) Ru-4Me

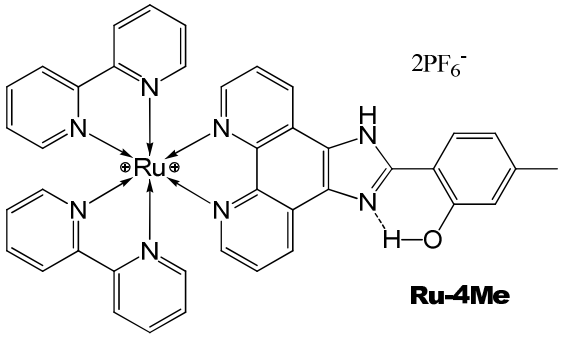

Ru-4Me

In a typical reaction $Ru(bpy)_2Cl_2$ (150 mg, 0.31 mmol, 1.0 eq)was treated with silver nitrate (106 mg, 0.62 mmol, 2.0 eq) in methanol for 3 hours at room temperature. The solution was filtered in order to remove silver salts and the filtrate was added to a round bottom flask containing 5'-methyl-2'-(1H-imidazo [4,5-*f*][1,10]phenanthroline-2-yl)phenol (101 mg, 0.31 mmol, 1.0 eq). The solution was refluxed for 3 hours in dark under an argon atmosphere. At this time the reaction mixture was allowed to go to room temperature and the solvent was evaporated under reduced pressure. The obtained solid was dissolved in a minimum amount of MeOH and precipitated as a PF_6 salt by adding saturated aqueous solution of ammonium hexafluorophosphate. The flask was kept at -20 °C overnight to obtain complete precipitation

and filtered. After repeated washings with water and copious quantity of diethyl ether, the obtained product was dried under vacuum (224 mg). Yield: 71 %.

^{1}H NMR (400 MHz, CD_3CN) δ: 8.89 (d, J = 7.5 Hz, 2H), 8.56 (d, J = 8.7 Hz, 2H), 8.52 (d, J = 8.2 Hz, 2H), 8.11 (td, J = 7.9 Hz and 1.4 Hz, 2H), 8.06-7.96 (m, 4H), 7.87 (dd, J = 5.7 Hz, 1.0 Hz, 2H), 7.8 (d, J = 9.1 Hz, 1H), 7.71 (dd, J = 7.4 Hz and 5.5 Hz, 2H), 7.67 (d, J = 5.9 Hz, 2H), 7.46 (td, J = 6.7 Hz and 1.3 Hz, 2H), 7.26 (td, J = 6.7 Hz, 1.5 Hz, 2H), 6.64 (s, 1H), 6.52 (d, J = 7.4 Hz, 1H), 1.96 (s, 3H)

ESI-MS m/z = 370.05 $[M]^{2+}$, 739.28 $[M-H]^+$

8) Ru-6Me

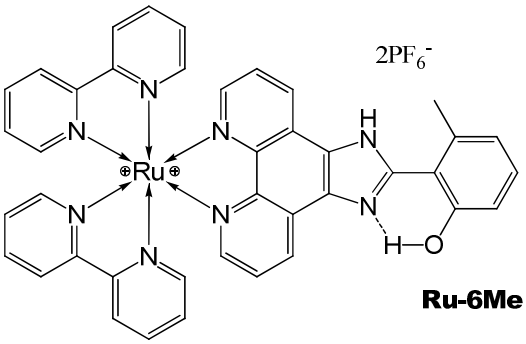

Ru-6Me

In a typical reaction $Ru(bpy)_2Cl_2$ (194 mg, 0.4 mmol, 1.0 eq)was treated with silver nitrate (136 mg, 0.8 mmol, 1.0 eq) in methanol for 3 hours at room temperature. The solution was filtered in order to remove silver salts and the filtrate was added to a round bottom flask containing 3'-methyl-2'-(1H-imidazo [4,5-*f*][1,10]phenanthroline-2-yl)phenol (131 mg, 0.4 mmol, 1.0 eq). The solution was refluxed for 3 hours in dark under an argon atmosphere. At this time the reaction mixture was allowed to go to room temperature and the solvent was evaporated under reduced pressure. The obtained solid was dissolved in a minimum amount of MeOH and precipitated as a PF_6 salt by adding saturated aqueous solution of ammonium hexafluorophosphate. The flask was kept at -20 °C overnight to obtain complete precipitation and filtered. After repeated washings with water and copious quantity of diethyl ether, the obtained product was dried under vacuum (249 mg).Yield: 61%.

^{1}H NMR (400 MHz, CD_3CN) δ: 9.03 (d, J = 8.1 Hz, 2H), 8.55 (d, J = 8.2 Hz, 2H), 8.51 (d, J = 8.2 Hz, 2H), 8.1 (td, J = 8.0 Hz and 1.4 Hz, 2H), 8.06-7.94 (m, 5H), 7.86 (d, J = 5.6 Hz, 2H), 7.74 (dd, J = 8.5 Hz and 5.2 Hz, 2H), 7.63 (d, J = 5.7 Hz, 2H), 7.46 (td, J = 6.6 Hz and 1.4 Hz, 2H), 7.29-7.18 (m, 3H), 6.83 (t, J = 7.5 Hz, 1H), 2.27 (s, 3H)

ESI-MS*m/z* = 885.1222 $[M - PF_6]^+$. Calcd. for $C_{40}H_{30}F_6N_8OPRu$ *m/z* = 885.1228; *m/z* = 739.1497 $[M-H]^+$ Calcd. for $C_{40}H_{29}N_8ORu$ *m/z* = 739.1508;*m/z* = 370.0800 $[M]^{2+}$ Calcd. for $C_{40}H_{30}N_8ORu$ *m/z* = 370.0788.

References

(1) Gray, M.; Parsons, P. J., Directed alkylation of phenols- a convenient synthesis of highly substituted aromatic rings. *Synlett***1991**, 729-730.

(2) Werbovetz, K. A.; George, T. G.; Richard, J.; Barszcz, T.; Capers, J., Flavylium Salts as Precursors of Biologically Active Chalcones. *Lett. Drug Design &Discovery*, **2008**, *5*, 69-73.

(3) Coulter, M. M.; Kou, K. G.; Galligan, B.; Dong, V. M., Regio-and Enantioselective Intermolecular Hydroacylation: Substrate-Directed Addition of Salicylaldehydes to Homoallylic Sulfides. *J. Am. Chem. Soc.*,**2010**, *132*, 16330-16333.

EXPERIMENTAL PART

Chapter 4: Light-induced Tryptophan oxidation

Synthesis of Ruthenium-Tryptophan (Ru-Trp)

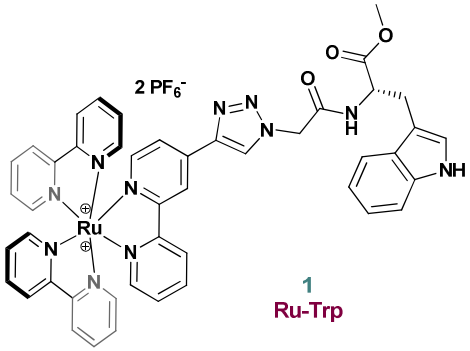

Chart 1 : *Structures of the complex Ru-Trp.*

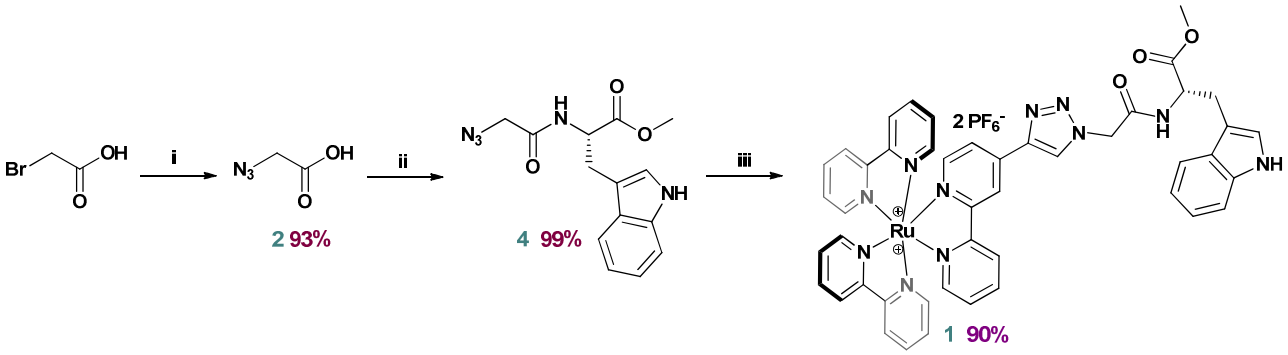

Scheme 1 : *Reagents and Conditions: (i) NaN_3, H_2O (93%);[1,2] (ii) (**3**) HBTU, DMAP, DIPEA, CH_3CN (99%);[2] (iii) (**5**),[3] $CuSO_4.5H_2O$ (15 mol%), sodium ascorbate (45 mol%), CH_2Cl_2/H_2O (1:1) (90%).*

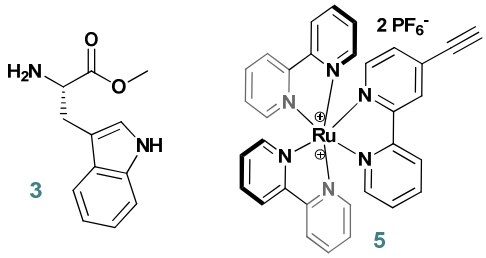

Chart 2 : *Structures of the compounds (3) and (**5**)[3]*

2-Azidoacetic acid (2)[1,2]

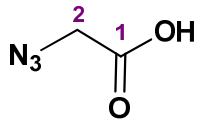

To sodium azide (3.74 g, 57.6 mmol) in H_2O (25 mL) was added bromoacetic acid (1.60 g, 11.5 mmol). The reaction mixture was stirred at room temperature overnight, acidified to pH 1 with 32% hydrochloric acid and extracted with EtOAc (3 × 75 mL). The combined organic extracts were washed with saturated aqueous NaCl solution then dried ($MgSO_4$), filtered and concentrated under reduced pressure to give 1.08g (10.6 mmol, 93%) of 2-azidoactic acid (**2**) as a colourless oil.

2-Azidoacetic acid (2): $C_2H_3N_3O_2$.

^{1}H NMR (400 MHz, $CDCl_3$) δ: 10.98 (br s, 1H, COO**H**); 3.96 (s, 2H, **H-2**).

^{13}C NMR (100 MHz, $CDCl_3$) δ: 174.7 (**C-1**); 50.2 (**C-2**).

MS (ESI$^-$): *m/z* 100.0 $[M-H]^-$.**HRMS (ESI$^-$)**: calculated for $C_2H_2N_3O_2$ 100.0152, found 100.0149.

(S)-Methyl 2-(2''-azidoacetamido)-3-(1*H*-indol-3''-yl)propanoate (4)[2]

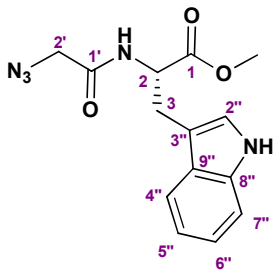

To a solution of 2-azidoacetic acid (**2**) (0.53 g, 2.10 mmol, 1.0 eq.) and L-tryptophan methyl ester hydrochloride (**4**) (0.21 g, 2.10 mmol, 1.0 eq.) in anhydrous CH_3CN (52.0 mL) were added HBTU (0.79 g, 2.10 mmol, 1.0 eq.), DMAP (51.0 mg, 0.42 mmol, 0.2 eq.) and *N*,*N*-diisopropylethylamine (1.1 mL, 0.81 g, 6.29 mmol, 3.0 eq.). The reaction mixture was stirred at room temperature under argon atmosphere for 12 hours and concentrated under reduced pressure. The residue was dissolved in EtOAc and washed with 10% citric acid (2 × 40 mL),

5% $NaHCO_3$ (2 × 40mL) and brine (1 × 40 mL). The organic phase was dried over $MgSO_4$, filtered and concentrated under reduced pressure. The residue was purified by flash column chromatography using silica gel (cyclohexane/EtOAc, 1:1) to give 0.62 g (2.07 mmol, 99%) of the desired amide (**4**) as colourless glue.

(S)-Methyl 2-(2''-azidoacetamido)-3-(1*H*-indol-3''-yl)propanoate (4): $C_{14}H_{15}N_5O_3$.

^{1}H NMR (400 MHz, $CDCl_3$) δ: 8.15 (br s, 1H, N**H$_{Ar}$**); 7.51 (ddd, 1H, $^3J_{4'',5''}$ 7.9, $^4J_{4'',6''}$ 1.1, $^5J_{4'',7''}$ 0.9 Hz, **H-4''**); 7.35 (ddd, 1H, $^3J_{7'',6''}$ 8.1, $^4J_{7'',5''}$ 1.1, $^5J_{7'',4''}$ 0.9 Hz, **H-7'')**; 7.19 (ddd, 1H, $^3J_{6'',7''}$ 8.1, $^3J_{6'',5''}$ 7.0, $^4J_{6'',4''}$ 1.1 Hz, **H-6''**); 7.12 (ddd, 1H, $^3J_{5'',4''}$ 7.9, $^3J_{5'',6''}$ 7.0, $^4J_{5'',7''}$ 1.1 Hz, **H-5''**); 6.98 (d, 1H, $^3J_{2'',NH}$ 2.4 Hz, **H-2''**); 6.75 (br d, 1H, $^3J_{NH,2}$ 8.0 Hz, CON**H**); 4.92 (dt, 1H, $^3J_{2,NH}$ 8.0, $^3J_{2,3}$ 5.5 Hz, **H-2**); 3.90 (s, 2H, 2 **H-2'**); 3.69 (s, 3H, OC**H$_3$**); 3.33 (d, 2H, $^3J_{3,2}$ 5.5 Hz, 2 **H-3**).

^{13}C NMR (100 MHz, $CDCl_3$) δ: 171.9 (**C-1**); 166.6 (**C-1'**); 136.3 (**C-8''**); 127.7 (**C-9''**); 122.9 (**C-2''**); 122.6 (**C-6''**); 120.0 (**C-5''**); 118.6 (**C-4''**); 111.5 (**C-7''**); 110.0 (**C-3''**); 53.1 (**C-2**); 52.7 (**C-2'**, O**C**H_3); 27.8 (**C-3**).

MS (ESI$^+$): *m/z* 324.1 $[M+Na]^+$.**HRMS (ESI$^+$)**: calculated for $C_{14}H_{15}N_5NaO_3$ 324.1067, found 324.1063.

(Bipyridine)$_2$-(bipyridine-triazol-tryptophan) ruthenium hexafluorophosphate (1):

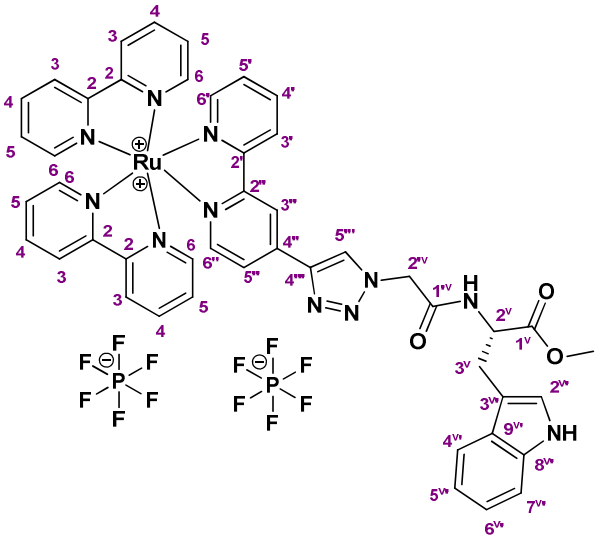

Ruthenium complex (**5**) (151.3 mg, 0.17 mmol, 1.0 eq.) was suspended in CH_2Cl_2 (8.6 mL) under an argon atmosphere. (S)-Methyl 2-(2''-azidoacetamido)-3-(1*H*-indol-3''-

yl)propanoate (**4**) (77.4 mg, 0.26 mmol, 1.5 eq.) were added, followed by successive addition of water (8.6 mL), sodium ascorbate (15.3 mg, 0.08 mmol, 0.45 eq.) and copper sulfate pentahydrate (6.4 mg, 0.03 mmol, 0.15 eq.). After 20 hours of stirring at room temperature, the reaction mixture was concentrated under vacuum. The crude solid was partially dissolved in a mixture of CH_2Cl_2/EtOAc then filtered through an alumina plug. The excess of azido derivative was removed by washing with CH_2Cl_2 and EtOAc. Then the desired ruthenium complex (**1**) was recovered by dissolving the crude solid and washing the alumina plug with CH_3CN and a solution of ammonium hexafluorophosphate in CH_3OH. The solvents were evaporated, The residue was dissolved in a minimum amount of CH_2Cl_2, then added drop wise at a large volume of pentane. The formed precipitate was filtered, washed several times with H_2O then Et_2O and dried under vacuum to yield 181.5 mg (0.15 mmol, 90%) of the desired hexafluorophosphate ruthenium complex (**1**) as an orange/red solid.

(Bipyridine)$_2$-(bipyridine-triazol-tryptophan) ruthenium hexafluorophosphate (1):
$C_{46}H_{39}F_{12}N_{11}O_3P2Ru$.

^{1}H NMR (400 MHz, CD_3CN) δ: 9.20 (br s, 1H, N**H**); 8.88 (d, 1H, ^4J 1.6 Hz, **H-3’’**); 8.65 (d, 1H, ^3J 8.0 Hz, **H-3’)**; 8.54-8.47 (m, 4H, 4 **H-3**); 8.42 (br s, 1H, **H-5’’’**); 8.11-8.02 (m, 5H, 4 **H-4**, **H-4’**); 7.82-7.71 (m, 5H, 4 **H-6**, **H-6’**); 7.79 (dd, 1H, ^3J 6.0, ^4J 1.6 Hz, **H-5’’**); 7.73 (d, 1H, ^3J 6.0 Hz,**H-6’’**); 7.50 (br d, 1H, ^3J 7.8 Hz, **H-4^{v}’**); 7.44-7.36 (m, 5H, 4 **H-5**, **H-5’**); 7.36 (br d, 1H, ^3J 8.0 Hz, **H-7^{v}’**); 7.12 (br d, 1H, ^3J 7.4 Hz, CON**H**); 7.12 (br d, 1H, ^3J 2.4 Hz, **H-2^{v}’**); 7.09 (br dd, 1H, ^3J 8.0, ^3J 6.8 Hz, **H-6^{v}’**); 7.04 (br dd, 1H, ^3J 7.8, ^3J 6.8 Hz, **H-5^{v}’**); 5.18 (d, 1H, ^2J 16.6 Hz, **H-2’^{v}a**); 5.13 (d, 1H, ^2J 16.6 Hz, **H-2’^{v}b**); 4.75 (ddd, 1H, ^3J 7.4, ^3J 6.7, ^3J 5.7 Hz, **H-2^{v})**; 3.66 (s, 3H, OC**H$_3$**); 3.29 (dd, 1H, ^2J 14.6, ^3J 5.7 Hz, **H-3^{v}a**); 3.22 (dd, 1H, ^2J 14.6, ^3J 6.7 Hz, **H-3^{v}a**).

^{13}C NMR (100 MHz, CD_3CN) δ: 173.0 (**C-1^{v}**); 166.3 (**C-1’^{v}**); 158.9 (**C-2’’**); 158.3 (4 **C-2**, **C-2’**); 153.3 (**C-6’’**); 153.1 (4 **C-6**); 153.0 (**C-6’**); 144.4 (**C-4’’’**); 141.2 (**C-4’’**); 139.2 (4 **C-4**, **C-4’**); 137.7 (**C-8^{v}’**); 129.1 (**C-5’**); 128.9 (4 **C-5**); 128.8 (**C-9^{v}’**); 126.9 (**C-5’’’**); 125.8 (**C-3’**); 125.6 (4 **C-3**); 125.3 (**C-2^{v}’**); 124.3 (**C-5’’**); 123.0 (**C-6^{v}’**); 121.4 (**C-3’’**); 120.5 (**C-5^{v}’**); 119.6 (**C-4^{v}’**); 112.8 (**C-7^{v}’**); 110.6 (**C-3^{v}’**); 54.9 (**C-2^{v}**); 53.5 (**C-2’^{v}**); 53.3 (O**C**H$_3$); 28.5 (**C-3^{v}**).

MS (ESI$^+$): *m/z* 1040.2 $[M+PF_6]^+$.**HRMS (ESI$^+$)**: calculated for $C_{46}H_{39}F_6N_{11}O_3PRu$ 1040.1929, found 1040.1904; calculated for $C_{46}H_{39}N_{11}O_3Ru$ 447.6141, found 447.6140.

References

1. Choi, I.; Kim, Y.-K.; Min, D.-H.; Lee, S.; Yeo, W.-S., On-Demand Electrochemical Activation of the Click Reaction on Self-Assembled Monolayers on Gold Presenting Masked Acetylene Groups. *J. Am. Chem. Soc.*, **2011,***133*, 16718-16721.
2. Yu, M.; Price, J. R.; Jensen, P.; Lovitt, C. J.; Shelper, T.; Duffy, S.; Windus, L. C.; Avery, V. M.; Rutledge, P. J.; Todd, M. H., Copper, Nickel, and Zinc Cyclam-Amino Acid and Cyclam-Peptide Complexes May Be Synthesized with "Click" Chemistry and Are Noncytotoxic. *Inorg. Chem.*, **2011,***50*, 12823-12835.
3. Baron, A.; Herrero, C.; Quaranta, A.; Charlot, M.-F.; Leibl, W.; Vauzeilles, B.; Aukauloo, A., Click Chemistry on a Ruthenium Polypyridine Complex. An Efficient and Versatile Synthetic Route for the Synthesis of Photoactive Modular Assemblies.*Inorg. Chem.*, **2012,***51*, 5985-5987.

Synthèse en français

1.0 Introduction

La demande mondiale en énergie ne cesse de croitre, en 2050 elle est estimée à 28 – 35 TW comparée à 16 TW en 2012. Cette augmentation est liée principalement à la population mondiale croissante qui est estimée à 10 - 11 milliards en 2050. Pour satisfaire cette demande nous dépendons surtout des combustibles fossiles (Figure 1). Les statistiques de l'an 2012 montrent que 87 % de l'énergie mondiale provient des combustibles fossiles dont les sources sont limitées. Leur surconsommation mènera à leur manque dans un proche avenir. De plus, leur combustion produit du dioxyde de carbone, du monoxyde de carbone et des particules en suspension, et cause ainsi des problèmes environnementaux.

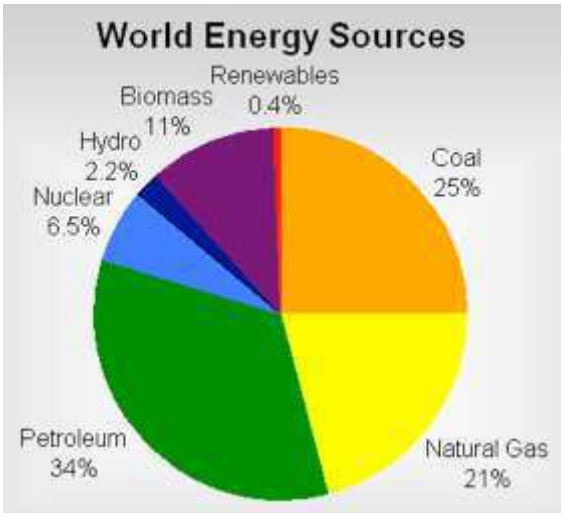

Figure 1: *Sources d'énergie mondiales.*

L'énergie, dite renouvelable, représente seulement 0.4%, d'après la figure 1, de toutes les productions actuelles d'énergie. Elle est de différents types tels que l'énergie éolienne, l'énergie géothermique ou l'énergie solaire. Parmi ces différentes sources d'énergie renouvelable, l'énergie solaire est la plus importante avec une capacité en énergie disponible dépassant nos besoins de consommation. Par exemple, la quantité d'énergie solaire arrivant chaque heure sur notre planète satisferait un an de consommation d'énergie par l'humanité. L'utilisation de l'énergie solaire nous aiderait donc, à surmonter les problèmes d'énergie à venir.

L'eau est l'élément le plus abondant (79 %) sur notre planète et la lumière du soleil y est librement disponible. L'utilisation de ces deux éléments pour produire de l'hydrogène,

considéré comme un carburant vert (puisque le produit de sa combustion est l'eau, Eq. 1), pourra répondre éventuellement à notre future crise d'énergie.

$$2H_2 + O_2 \rightarrow 2H_2O \qquad \text{(Eq. 1)}$$

$$2H_2O \rightarrow 4H^+ + 4e^- + O_2 \qquad \text{(Eq. 2)}$$

La décomposition de l'eau (Eq. 2) est une partie essentielle de la photosynthèse naturelle.

Donc, l'imitation du processus de la photosynthèse naturelle devrait nous permettre de décomposer l'eau. Pour cela, nous avons besoin de photo-catalyseurs robustes. Dans la nature, la réaction de décomposition de l'eau est effectuée par une enzyme appelée« photosystème II » (Figure2). Le photosystème II (PS II) consiste en environ 20 sous-unités de protéine dans le cyanobacterium *Thermosynechococcus (T.) elongatus*.

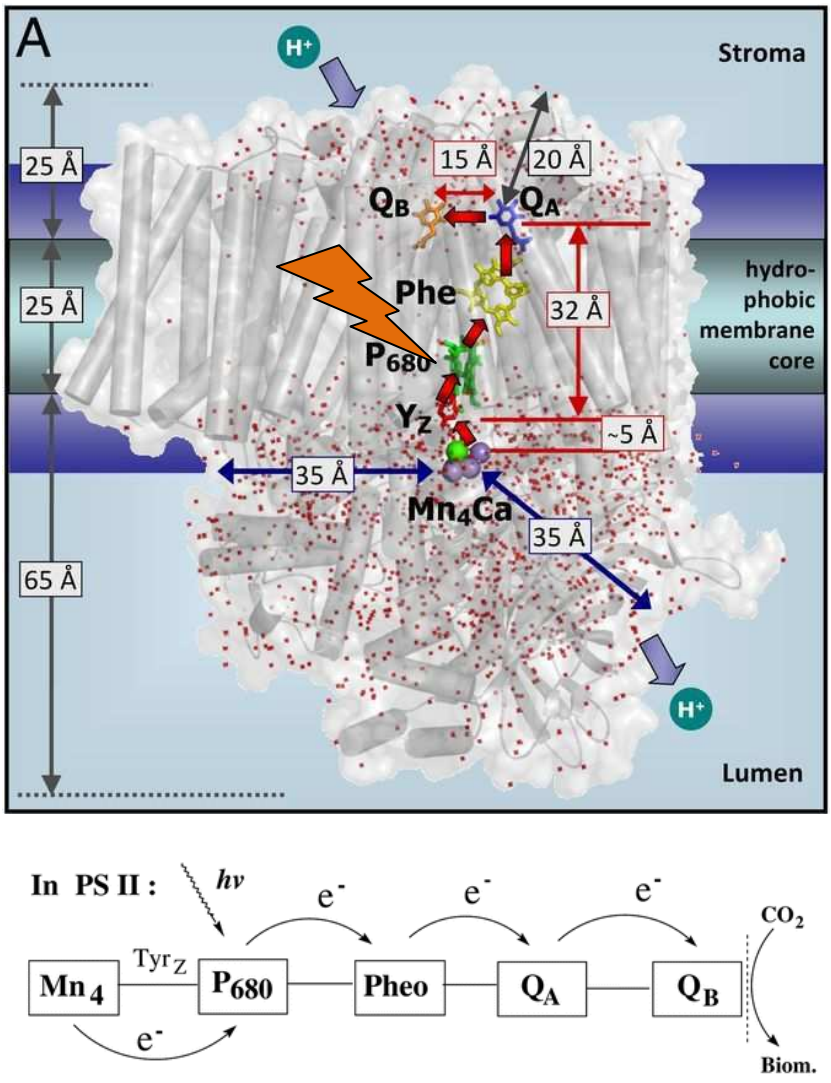

Figure 2: *Chaîne de transport d'électron dans le Photosystème II.*

Un important aspect du PS II est son utilisation de la lumière visible entre 400 nm et 700 nm pour déclencher la réaction d'oxydation de l'eau (Eq. 2). Le processus de transfert électronique est initié par l'excitation du donneur primaire d'électron (P680). A partir de son état singulet, P680 transfère un électron à laquinone (QA) conduisant à la formation des ions respectifs $P680^{+}$et QA^{-}. Le $P680^{+}$ est réduit par un résidu tyrosine (TyrZ) conduisant au radical $TyrZ^{\bullet}$ neutre. Ce dernier a été caractérisé par la résonance paramagnétique électronique haut champ. Le radical $TyrZ^{\bullet}$ photo-produit est par la suite réduit en tirant un électron du « oxygen evolving complex » (OEC).Ce travail de thèse concerne la synthèse et la caractérisation de molécules artificielles biomimétiques du photosystème II. Nous avons utilisé plusieurs techniques expérimentales pour caractériser nos complexes synthétisés telles que :

1) Électrochimie (EC)
2) Spectroscopie UV-VISIBLE (UV-VIS)
3) Spectroscopie de fluorescence
4) Photolyse par Lumière Flash (LFP)
5) Résonance Paramagnétique Électronique (EPR)
6) Spectroscopie infrarouge (IR)

Vu l'importance des cinétiques des réactions de transfert d'électron pour nos études, la photolyse par éclair laser est discutée dans la section suivante.

2.0 Photolyse par éclair laser (LFP)

La technique de photolyse par lumière flash joue un rôle important dans les études d'espèces passagères, produites par des impulsions laser, dans des systèmes chimiques et biologiques. Elle fût développée par George Porter et Norris en 1949.

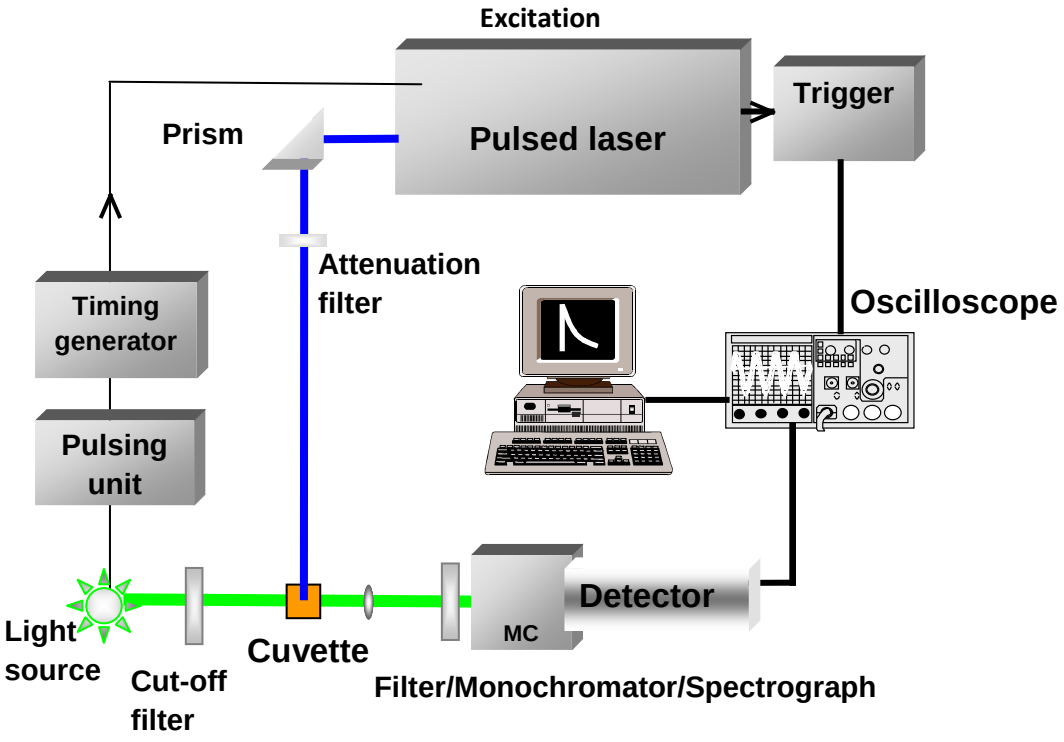

Figure 3: *Schéma détaillé de la photolyse par lumière flash. La source d'excitation est un laser nanoseconde (430 – 650 nm) la sonde est une lampe flash à Xénon couplée à un système de détection constitué d'un photomultiplicateur ou une camera CCD.*

Le système de la photolyse par lumière flash utilisé est un Edinburgh Instruments LP920 (Figure 3). Ce spectromètre nous permet de réaliser des mesures spectrales résolues en temps par l'étude du comportement de l'absorption transitoire des espèces induites. Ces mesures permettent la caractérisation des propriétés de l'état excité des complexes ainsi que du processus de transfert électronique. Notre montage instrumental incorpore un oscillateur paramétrique optique (Surelite OPO) assurant l'excitation des échantillons (durée d'impulsion~ 5 ns). Le laser de pompe est un laser Nd:YAG livrant des impulsions à 355 nm. L'énergie du faisceau laser est de 4 mJ / flash.

Pour les complexes basés sur le $\mathbf{[Ru(bpy)_3]^{2+}}$, la longueur d'onde d'excitation utilisée est 460 nm. Le LP920 est équipé d'une lampe pulsée de Xénon à arc d'une puissance de 450 W. La détection du signal est effectuée soit par un photomultiplicateur (PMT) de Hamamatsu pour les études spectrales soit par un dispositif à transfert de charge (caméra CCD de Andor). Le logiciel L900 fourni avec le LP920 est utilisé pour enregistrer les spectres et les traces cinétiques.

2.1 Préparation des échantillons

Des cuves en Quartz de 1 cm d'épaisseur sont utilisées pour toutes les mesures. Les cuves sont fermées avec un septum en caoutchouc permettant le dégazage des échantillons avec de l'Argon. Le dégazage avec ce gaz inerte permet d'éviter l'interférence de l'oxygène moléculaire puisque ce dernier est à la fois un bon quencher des états triplets et un bon accepteur d'électron. La plupart des expériences est effectué avec une concentration de 30 µM des complexes en acetonitrile.

3.0 Complexes biomimétiques du couple TyrZ / His 190 comme relais électroniques du photosystème II

Au sein de notre laboratoire, une série de complexes ruthenium avec un ligand d'imidazole-phénol en liaison hydrogène a été synthétisée et publiée précédemment (Figure 4). Ceci représente la première approche dans le but d'imiter cette fonction caractéristique du PS II naturel.

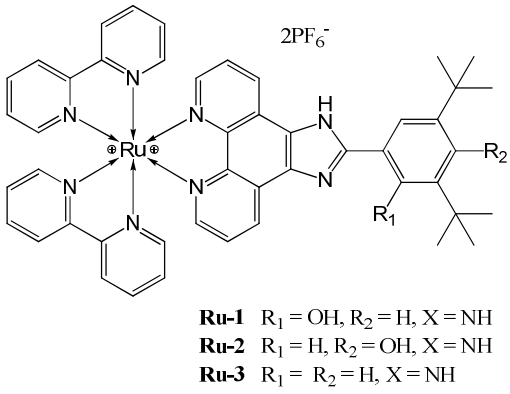

Figure 4: *Complexes étudiés auparavant,* ***Ru-tert-imi-phOH***

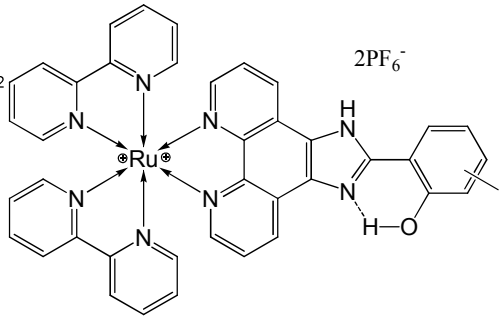

Figure 5: *Complexes* ***Ru-xMe***

Mais l'inconvénient principal de ces complexes se trouve dans le potentiel redox du ligand. En raison de la présence des groupes *tert*-butyle, considérés comme donneurs d'électron forts, sur le phénol, les potentiels d'oxydation des ligands étaient très bas (0,19 V*/vs*. ferrocène). Donc, afin de surmonter cet inconvénient nous avons synthétisé une série de complexes (**Ru-xMe**, Figure 5) en utilisant une méthodologie synthétique semblable à celle utilisée pour synthétiser les complexes précédents. Les complexes synthétisés diffèrent en ce qui concerne la position des groupements du méthyl sur le phénol : **Ru-3Me**, **Ru-4Me** et **Ru-6Me**. Le but est d'observer les différences éventuelles dans les propriétés électroniques.

Le remplacement des groupes *tert*-butyle (forts donneur d'électron) par des groupes de méthyl (faibles donneurs d'électron) devra avoir un impact important sur le potentiel redox du ligand **Ru-xMe** comparé à **Ru-tert-imi-phOH**. Ainsi, pour vérifier le potentiel redox des ligands de nos nouveaux complexes synthétisés, **Ru-xMe**, nous avons mesuré leurs propriétés électrochimiques par voltammétrie cyclique (CV) et par voltammétrie à impulsion différentielle (DPV). Les potentiels obtenus sont présentés dans la Table 1.

Table 1: *Résumé des potentiels redox par rapport à l'électrode de ferrocène (Fc) dans l'acetonitrile [a]les potentiels sont convertis de vs. ECS à vs. Fc (0,395 V vs ECS Fc^+/Fc). L'attribution du potentiel redox du ligand est préliminaire (0,8 – 1 V).*

	$E_{1/2}$ **Ru(III)/Ru(II)**	$E_{1/2}$ **Lig_{ox}/Lig (ligand)**	$E_{1/2}$ **(bi-pyridines)**		
Ru-3Me	0,89	0,75	-1,78	-1,98	-2,33
Ru-4Me	0,95	0,75; 0.82	-1,78	-1,98	-2,33
Ru-6Me	0,89	0,75	-1,77	-1,98	-2,33
Ru-tert-imi-phOH[a]	0,90	0,19	-	-2,00	-2,40

La comparaison des potentiels de **Ru-xMe** et de **Ru-tert-imi-phOH** (Table 1) montre que le potentiel d'oxydation du ligand augmente de 0,19 V à 0,75 V. Ceci est attribué au remplacement des groupes *tert*-butyle. Ainsi, notre premier but dans la synthèse des complexes de **Ru-xMe** ayant un potentiel redox accru a été atteint. D'un point de vue thermodynamique ces complexes pourraient être capables d'activer des systèmes catalytiques d'oxydation de l'eau.

Les spectres d'absorption de **Ru-3Me**, **Ru-4Me** et **Ru-6Me** sont semblables à ceux des complexes de $\mathbf{[Ru(bpy)_3]^{2+}}$. Ces spectres montrent une bande intense dans la région visible avec un maximum à 460 nm correspondant à la transition du métal, Ru (dπ) au ligand centré sur les orbitaux (π*). Cette transition est appelée transition du transfert de charge du métal au ligand (MLCT). Une autre bande intense dans la région de l'UV à 290 nm correspond à la transition intra-ligand **(π→π*)** des bipyridines. En plus de ces deux bandes, une bande supplémentaire est observée autour de 330 nm ainsi qu'un épaulement de la transition MLCT

allant jusqu'à 550 nm. Ces caractéristique sont déjà été observées dans le cas de **Ru-imi-tert-phOH** et sont attribuées aux transitions intra-ligand impliquant la phénantroline et le groupe imidazole.

3.1 Transfert d'électron

Selon les mesures électrochimiques, la différence des potentiels redox entre le ruthénium et le ligand est faible pour tous les complexes de **Ru-xMe** (ΔE ~80 à 100 mV). Ceci indique que la force motrice pour le transfert électronique interne doit être relativement petite (Table 1). Pour examiner si l'état oxydé du chromophore peut oxyder le ligand, des expériences de transfert électronique en présence de MV^{2+} comme accepteur d'électron externe ont été effectuées (MV= méthyl viologène).

La Figure6 montre les changements d'absorption transitoires induits par flash laser, en présence de 20 mM MV^{2+} comme accepteur d'électron externe, pour **Ru-3Me**, **Ru-4Me** et **Ru-6Me**, avec **$[Ru(bpy)_3]^{2+}$** comme référence. Les changements d'absorbance de la bande MLCT du chromophore Ru, induits par le flash laser, sont dus à la formation de l'état excité, suivi d'un quenching de ce dernier en raison de la réduction de l'accepteur d'électron externe (MV). Cette réduction mène à la formation de l'état oxydé Ru(III) du chromophore et éventuellement à la réduction du Ru (III) par transfert interne d'électron (ET) du ligand vers Ru(III). Le Schéma 1 décrit l'ordre de la réaction.

$$\mathrm{Ru(II)L + MV^{2+} \xrightarrow{h\nu} Ru(II)^{*}L + MV^{2+} \xrightarrow{k_q} Ru(III)L + MV^{\bullet+} \xrightarrow{k_{et}} Ru(II)L_{ox} + MV^{\bullet+} \xrightarrow{k_{rec}} Ru(II)L + MV^{2+}}$$

Schéma 1: *Schéma réactionnel simplifié*[6]

Résumés des résultats obtenus au sein d'un solvant pur et aprotique :

· Pour **Ru-4Me** : le déclin Ru(III) se produit en une seule phase lente;

· Pour **Ru-3Me** et **Ru-6Me** : la réduction de Ru (III) est biphasique, avec une phase rapide majeure et une deuxième phase plus lente dont la vitesse est similaire à celle observée pour le **Ru-4Me**.

Dans le cas de nos complexes (**Ru-3Me** et **Ru-6Me**), la cinétique de la phase rapide est toujours limitée par la concentration d'accepteur d'électron utilisé. Donc nous ne pouvons pas

[6] La réaction de recombinaison de charge entre MV^{+} et Ru(III) est négligée vue que : $k_{et} >> k_{rec} * [MV^{\bullet+}]_0$

aller plus loin dans l'analyse de cette phase. Les constantes de temps apparent pour la phase lente sont 9 µs ; 5,6 µs et 4,9 µs respectivement pour **Ru-3Me**, **Ru-4Me** et **Ru-6Me**.

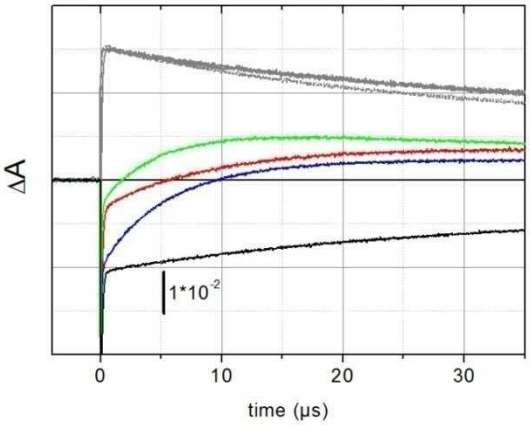

Figure 6: *Absorption transitoire à 440 nm pour* ***Ru-3-Me (rouge), Ru-4-Me (bleu), Ru-6-Me (vert)*** *et* ***[Ru(bpy)$_3$]$^{2+}$*** *(noir) suite à une excitation par un flash laser nanoseconde à 460 nm dans une solution de MeCN saturée avec de l'argon en présence de 20 mM de méthyl viologène (MV^{2+}) comme accepteur d'électron externe. Les traces ont été normalisées pour égaliser les concentrations de $MV^{\bullet+}$comme le montre les absorbances représentées par les lignes grises.*

Nous avons aussi enregistré les spectres d'absorption résolues dans le temps en présence de Ru-hexamine dans une solution aqueuse. Dans ces conditions la formation du radical est beaucoup plus rapide. L'attribution de cet effet à la présence d'eau a été confirmée par une titration avec de l'eau (Figure 7).La haute constante diélectrique de l'eau et/ou des interactions par liaisons hydrogène, stabilisant préférentiellement l'état oxydé sur le ligand pourraient expliquer ces résultats. Une autre explication serait que l'eau pourrait agir comme une base pour accepter un proton issu de l'oxydation du ligand.

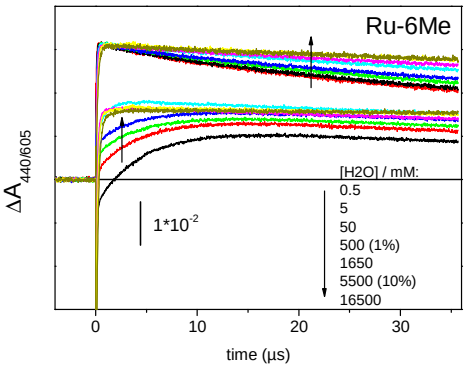

Figure 7: *Effet de la concentration d'eau sur l'absorption transitoire pour* ***Ru-6Me*** *en présence de 20 mM MV comme accepteur d'électron. La courbe noire correspond au MeCN pur. Les flèches représentent un guide visuel des changements ayant lieu en fonction de la concentration d'eau.*

La Figure 8 montre l'effet de la concentration croissante de pyridine sur les absorptions transitoires du **Ru-6Me**. Nous constatons que pour tous les complexes, les concentrations relativement faibles de pyridine (0,13 mM) mènent à une considérable accélération de la phase lente.

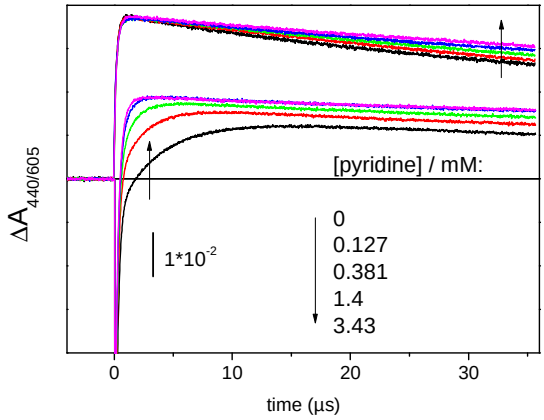

Figure 8: *Absorptions transitoires à 440 nm (lignes de bas) et à 605 nm (lignes de haut) du* ***Ru-6-Me****, dans MeCN saturé avec l'argon, en fonction de la concentration de pyridine. Les solutions contenaient 20 mM méthylviologène (MV^{2+}) comme accepteur externe d'électron. Les traces ont été normalisées pour égaliser les concentrations de $MV^{\bullet+}$comme le montrent les absorbances à 605 nm.*

4.0 Photo-oxidation de tryptophane

Nous avons étudié la génération du radical tryptophane par photoactivation. Ce radical est produit soit par transfert d'électron à l'oxydant photoproduit, soit par transfert d'atome H. Selon le cas, les radicaux du tryptophane (Trp) sont soit sous leur forme protonnée ($TrpH^{\bullet+}$) soit sous leur forme neutre ($Trp^{\bullet}$). Pour mieux les identifier, ces radicaux sont présentés dans la Table 2.

Ces radicaux sont des intermédiaires clés dans le mécanisme réactionnel de la ribonucléotide réductase, la lignine peroxidase, lacytochrome c peroxidase et la photolyase. Le Tryptophane est une amine secondaire dont le pK_a est de 17. La haute valeur de pK_a indique que le proton présent dans le tryptophane n'est pas facilement dissociable. Cette unique caractéristique a des conséquences importantes dans le transfert électronique en milieu biologique. Le pK_a du radical protoné ($TrpH^{\bullet+}$) est égal 4,7 ce qui signifie qu'il perdra son proton dans des conditions physiologiques.

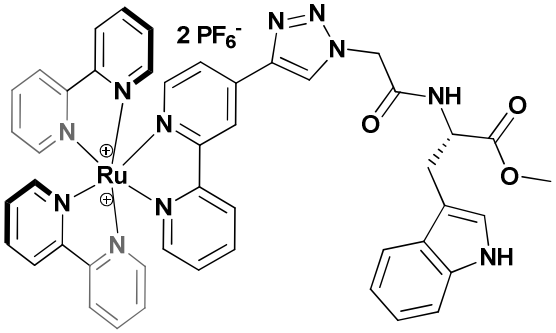

Figure 9: *Ru-Tryptophane (**Ru-Trp**)*

Table 2: *Radicaux du Tryptophane*

Abbreviation	Name	Structure
$W^{\bullet+}$	tryptophan radical cation	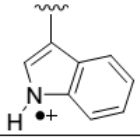
$W^{\bullet}$	tryptophan radical	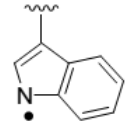

Nous avons étudié la photooxidation du tryptophane dans un assemblage modulaire, **Ru-Trp** (Figure9) avec le Trp attaché au chromophore $[Ru(bpy)_3]^{2+}$par des liaisons covalentes via une chimie « click ».

Les expériences de photolyse par lumière flash ont été effectuées pour examiner l'oxydation du résidu tryptophane induite par la lumière. L'excitation de **Ru-Trp** dans un mélange $MeCN/H_2O$ (50:50) par un flash laser à 460 nm en présence de 10 mM de méthyl viologène agissant comme accepteur d'électron réversible a montré l'épuisement du signal Ru(II) par photoblanchissement de sa bande d'absorption à 450 nm et la formation simultanée de $MV^{\bullet+}$ observée comme une augmentation de l'absorption à 605 nm (Figure 10). La récupération à 450 nm du signal de Ru (II) est très rapide (350 ns) tandis que la récupération du méthyl viologène oxydé est beaucoup plus lente (~ 300 µs, l'encart dans la Figure 10)

Ces résultats indiquent clairement que Ru(II) à son état fondamental est plutôt régénéré par transfert électronique intramoléculaire à partir du ligand tryptophane vers le chromophore oxydé que par la recombinaison de charge intermoléculaire entre Ru(III) et la forme réduite

de l'accepteur d'électron. D'un point de vue thermodynamique, ce processus est en accord avec les données électrochimiques où on attend à ce que l'oxydation de Trp par Ru(III) soit exergonique (-130 mV). La comparaison de la durée de vie de l'état excité (émission) en présence et la cinétique de rétablissement de Ru(II) révèle des constantes de vitesse apparentes identiques. Ceci indique qu'en présence de 10 mM de MV^{2+}, la formation de l'état oxydé du chromophore par réduction intermoléculaire du MV^{2+} est l'étape limitante pour l'oxydation du ligand et que la constante de vitesse intrinsèque de transfert interne d'électron est plus rapide.

Les cinétiques de déclin d'émission montrent que l'utilisation de concentrations plus importantes en MV^{2+} permet d'accélérer la formation du Ru(III) à environ 20 ns. Dans ces conditions la constante de vitesse du transfert interne d'électron pourrait être déterminée par analyse de la cinétique à 450 nm. Cette constante est égale à 10^7 s^{-1} (temps égal à 100 ns). Cette valeur confirme l'hypothèse de l'anneau de triazole assurant un lien permettant un transfert efficace d'électron.

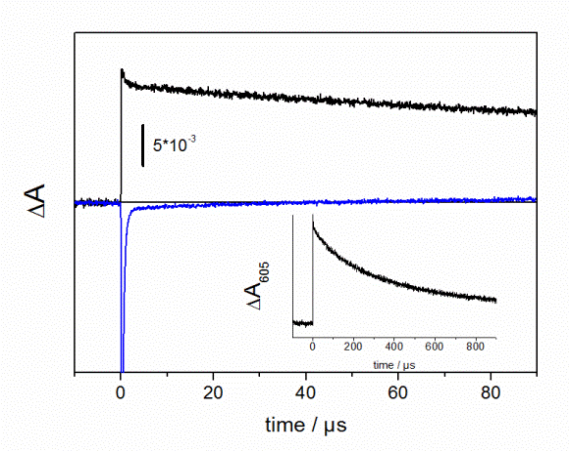

Figure 10: *Absorption transitoire à 605 (noir) et 450 nm (bleu) du* ***Ru-Trp*** *dans une solution de MeCN/H_2O (50:50) saturée à l'argon et en présence de 10 mM MV2+ comme accepteur externe d'électron, suite à une excitation par une lumière flash nanoseconde à 460 nm. Figure en insert: cinétique à 605 nm enregistrée sur un temps plus long.*

Ces résultats de photolyse par lumière laser flash suggèrent que la photo-excitation de **Ru-Trp** en présence d'un accepteur externe d'électron mène à l'oxydation du ligand, c'est-à-dire à la formation d'un radical tryptophane. On prévoit que à pH >pK_a($Trp^{\bullet}H^+$) l'oxydation de Trp soit accompagnée d'une déprotonation. Les spectres d'absorption transitoire d'un échantillon dans l'eau (pH neutre) montrent la transition de la forme protonée du radical Trp à la forme déprotonée en environ 1 µs (Figure11).

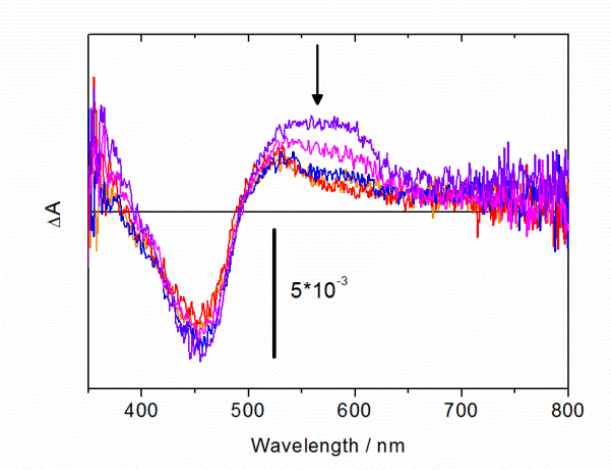

Figure 11: *Spectres d'absorption transitoire du* ***Ru-Trp*** *dans l'eau en présence de 40 mM de [Ru $(NH_3)_6]^{3+}$comme accepteur d'électron, enregistrées à 200 (violet), 300 (magenta), 500 (bleu), 700 (orange) et 1000 ns (rouge) suite à une excitation par un flash laser.*

A partir des spectres des deux formes (protonée et déprotonée), il apparaît que la réaction de déprotonation pourrait être observé dans la région spectrale entre 500 et 600 nm. La Figure 12 montre les absorptions transitoires à 510 et 570 nm. Aux deux longueurs d'ondes, l'augmentation rapide de l'absorption est due à la formation, induite par flash, de l'état excité du Ru qui décline rapidement en 25 ns environ à cause du quenching par l'accepteur d'électron. À 570 nm une cinétique plus lente est observée ayant un temps de demi-vie de 410 ns. La montée rapide en absorption est attribuée à la formation rapide (<100 ns) du radical $TrpH^{\bullet+}$ par transfert interne d'électron alors que le déclin est dû à la déprotonation de ce dernier pour former $Trp^{\bullet}$ dont l'absorbance à 570 nm est plus petite.

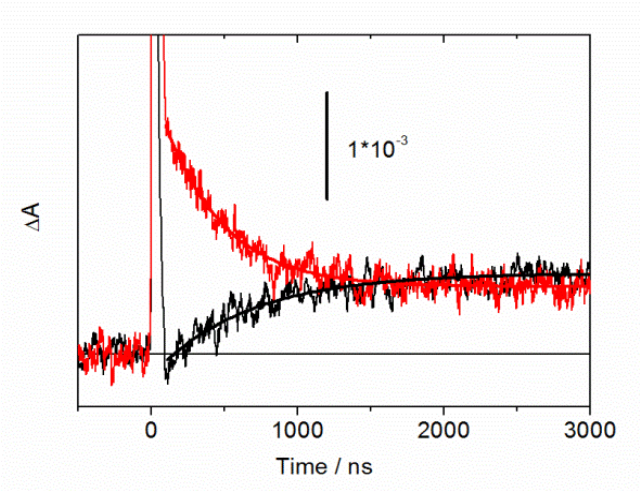

Figure 12: *Cinétiques à 510 (noir) et à 570 nm (rouge) enregistrées dans une solution de MeCN/H_2O (50:50) en présence de 100 mM de [Ru $(NH_3)_6]^{3+}$comme accepteur d'électron.*

La déprotonation du résidu tryptophane à pH neutre est thermodynamiquement initiée par un faible pK_a de sa forme oxydée. Cependant, d'un point de vue cinétique, la déprotonation est contrôlé par la préformation d'une configuration favorable entre l'acide et une base appropriée agissant comme accepteur de proton. Avec l'eau comme accepteur de proton, la propagation réussie de la dissociation de proton exige une percolation des molécules liées par de liaisons hydrogène. L'addition de solvants organiques a été reportée pour casser cette structure menant à une diminution dans la vitesse des réactions de déprotonation.

Cet effet est aussi observé dans notre complexe comme le montre les résultats dans la Figure13 où la concentration d'eau est variée. Pour des concentrations au-dessous de 3%, la déprotonation ne peut plus être observée car sa vitesse s'approche de celle de la recombinaison de charge entre $MV^{\bullet+}$ et $TrpH^{\bullet+}$.

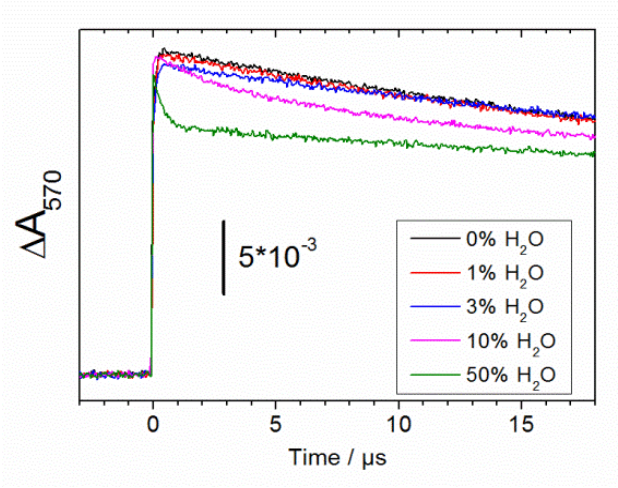

Figure 13: *Cinétiques enregistrées à 570 nm au sein d'une solution de MeCN contenant 20 mM de MV^{2+} comme accepteur d'électron et en présence de quantité variée en eau.*

En résumé (Figure14), la chimie « Click »est un outil efficace pour réaliser l'assemblage modulaire d'un chromophore et d'un acide aminé. De tels modèles, préparés facilement, permettent des études résolues en temps des réactions d'oxydation à un électron en créant un état fortement oxydant sur le chromophore par excitation par un flash laser en présence d'accepteurs externes d'électron.

Figure 14: *Résumé graphique montrant la réaction "Click" et le transfert d'électron intramoléculaire suivi d'un évènement de déprotonation (ETPT)*

5.0 Photocatalyseurs

La thèse traite le cas des photocatalyseurs basés sur des complexes artificiels bioinspirés du photosystème II. Donc le but final de notre approche synthétique consiste à réaliser un photocatalyseur moléculaire avec trois éléments de base, c'est-à-dire un chromophore, un relais d'électron et un catalyseur attaché par une liaison covalente (Figure 15). Comme d'habitude, nous choisissons un chromophore à base de $\mathbf{[Ru(bpy)_3]^{2+}}$, un groupe imidazole-phénol comme relais d'électron et comme catalyseur un complexe de type salen-Mn, ou un complexe $\mathbf{[Ru(tpy)(bpy)OH_2}$

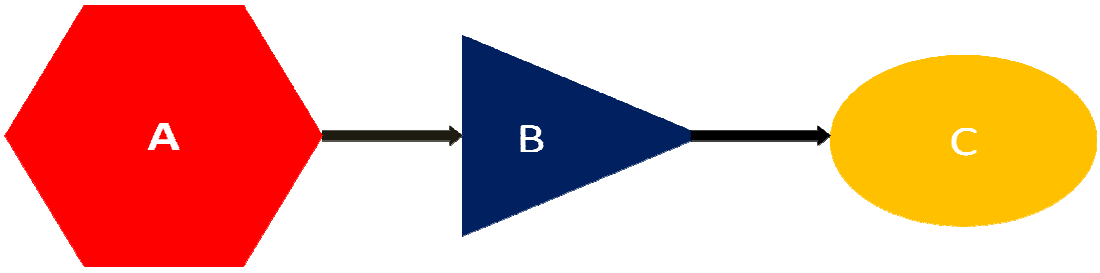

Figure 15: *Notre stratégie de synthèse avec: A : chromophore, B : relais d'électron et C : unité catalytique.*

En prenant en compte l'échec de la synthèse des photocatalyseurs cibles, nous avons effectué des expériences bimoléculaires en utilisant un catalyseur salen-Mn et notre complexe Ru-imidazole-phénol (**Ru-3Me**). Nous avons déjà confirmé que l'état oxydé du chromophore est suffisamment oxydant pour créer un radical phenoxyl sur le ligand. Le but de ces expériences était de montrer que l'état oxydé du ligand peut activer le catalyseur et le mèner à la formation de Mn(V)=O. Le Schéma 2 montre la séquence de transfert d'électron.

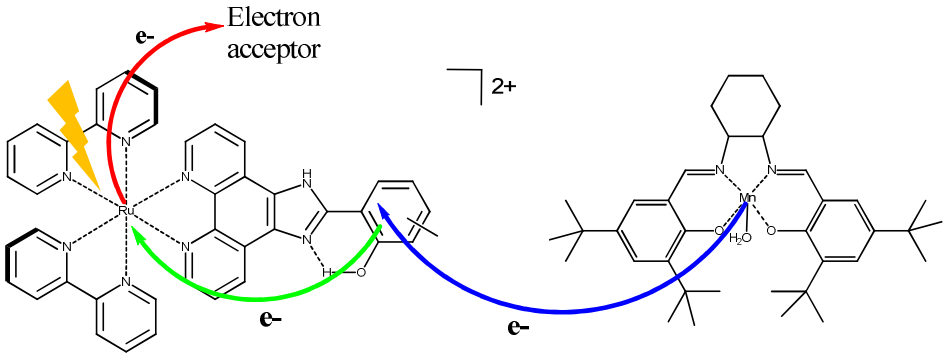

Schéma 2: *Activation du catalyseur salen- Mn : formation de Mn(IV) induite par la lumière*

Pour récapituler cette étude d'activation bi-moléculaire d'un catalyseur, nous proposons qu'elle suive l'ordre de la séquence réactionnelle présentée sur le Schéma 3. Le flash laser et des mesures absorbantes stables d'état ont confirmé la formation d'un Mn (IV) espèce caractérisée achète une large bande absorbante autour de 680 nm. Une confirmation de formation de Mn(V)=O devrait être obtenue en utilisant la spectroscopie RPE.

$$Ru(II)Lig + h\nu + EA \rightarrow Ru(III)Lig + EA^{-}$$

$$Ru(III)Lig \rightarrow Ru(II)Lig^{ox}$$

$$Ru(II)Lig^{ox} + Mn(III) \rightarrow Ru(II)Lig + Mn\ (IV)$$

Schéma 3*: Photoactivation du salen-Mn(III) pour former l'état oxydé Mn(IV); EA = accepteur d'électron*

6.0 Greffage d'un catalyseur sur une surface

Une autre partie de notre travail concerne l'étude de greffage d'un photocatalyseur sur la surface d'une électrode pour former la partie photoanode d'une cellule photoélectrochimique (Figure 16). Chaque électrode est faite d'un matériel semi-conducteur sur lequel est attaché, au moins pour l'anode, un photosensibilisateur et un catalyseur. Deux demi-cellules sont séparées par une membrane d'échange protonique qui permet la diffusion des protons à travers la membrane et empêche les réactions parasites dans la cellule comme, par exemple, l'oxydation de H_2 sur l'anode et la réduction d'O_2 sur la cathode.

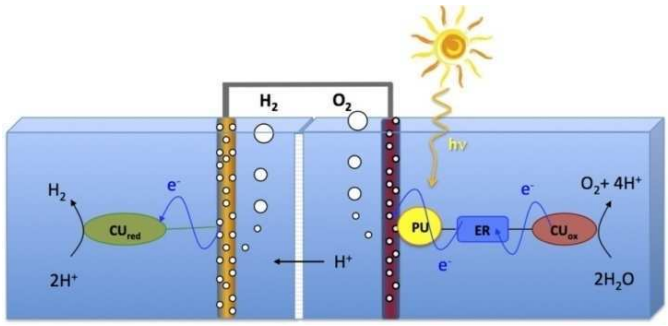

***Figure 16**: Cellule photoélectrochimique*

Quand les photoanodes ou les photocathodes sont faites par greffage de systèmes photocatalytiques modulaires, le chromophore est toujours le module directement attaché à la surface. En effet, c'est l'état excité du chromophore qui injecte ou extrait des électrons du semi-conducteur. La forme oxydée (réduite) du chromophore induit alors l'activation oxydative (réductive) de l'unité catalytique. À la fin de ce travail un assemblage photocatalytique complet (chromophore + relais d'électron + catalyseur) n'était pas disponible.

Par la suite, nous reporterons la synthèse et la caractérisation d'un chromophore $[Ru(bpy)_3]^{2+}$ fonctionnalisé par des groupes phosphonate, qui servent de groupes d'ancrage, **Ru-Phosphonate** (Figure17). Nous présenterons également les expériences de sensibilisation de la surface de TiO_2 avec ce complexe. Le greffage d'un ensemble photocatalytique complet sur le TiO_2 devrait fonctionner de la même façon.

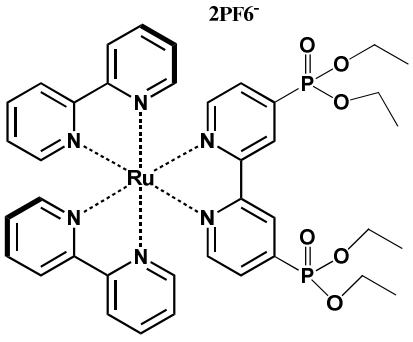

***Figure 17 : Ru-Phosphonate,** [Ru(II)(bpy)$_2$(4,4'-(PO$_3$Et$_2$)$_2$bpy)]*

Nous avons effectué des mesures photoélectrochimiques en utilisant une cellule photoélectrochimique. Une plaque de verre couvert d'ITO avec une couche mince de TiO_2et avec **Ru-Phosphonate** greffé agit comme une photoanode, tandis qu'une plaque de platine est utilisée comme une cathode. L'irradiation a été faite avec la lumière visible d'une lampe de Xénon dont l'irradiation UV a été bloquée en utilisant un filtre bleu. Pour simuler une

situation photocatalytique nous avons effectué des mesures en présence de petites quantités de méthanol et d'eau.

L'état Ru(III), formé après l'injection d'électron sur le TiO_2, est capable d'oxyder le méthanol et la cathode à un potentiel suffisamment négatif pour réduire les protons en hydrogène. Sous ses conditions, les mesures du photocourant montrent des réponses anodiques rapides quand l'irradiation a été mise en marche ou en arrêt (Figure 18). Un photocourant d'intensité de ~50 $\mu A/cm^2$ à été obtenu avec un bias de 400 mV comme le montre la Figure 18.

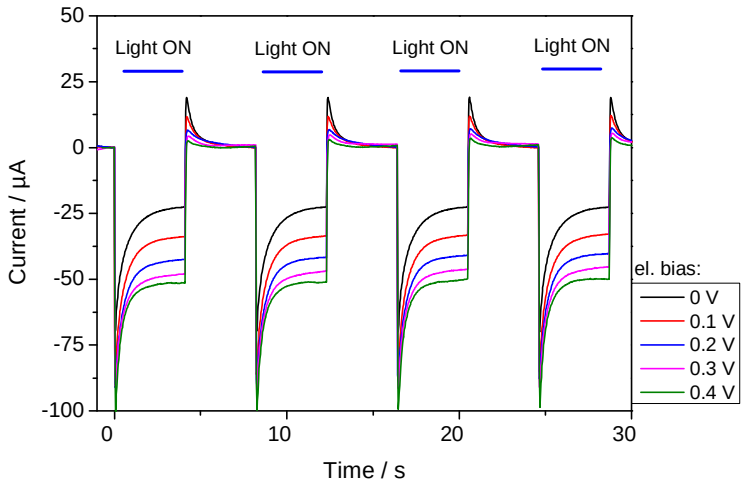

Figure 18: *Courant anodique en réponse à la mise en marche/arrêt de l'illumination par une lumière visible.*

Parallèlement au greffage du **Ru-Phosphonate**, un catalyseur peut lui aussi être greffé sur la surface de l'électrode. Une telle approche a récemment été reportée par Moore et al. (Figure19). En utilisant un chromophore en excès, la vitesse d'activation des unités catalytiques peut être augmentée. Le seul inconvénient de cette approche est l'interaction des deux composants qui est difficile à contrôler et à optimiser.

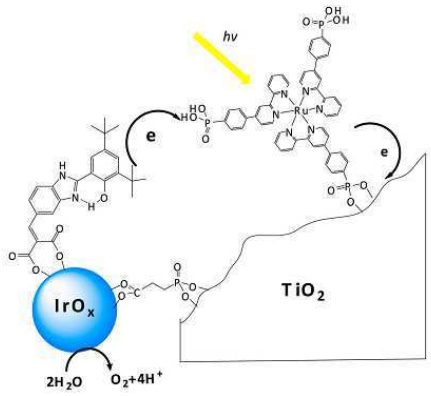

Figure 19: *Réaction de transfert d'électron sur l'anode de TiO_2*

APPENDIX 1

Chapter 3.0 Artificial mimics of TyrZ / His190 electron relay of photosystem II

Section 1: Extinction coefficients for $[Ru(bpy)_3]^{2+}$ and MV at 440/450 nm and 605 nm

An important advantage of using MV as oxidative quencher of the excited state of a chromophore is that the strong absorption of its reduced state allows to follow the time course of the back reaction i.e. return of the electron to the photooxidized complex. As long as the electron resides on the reversible external electron acceptor there must be a positive charge (oxidized state) on the complex under study. In many laser flash photolysis studies the occurrence of internal electron transfer from a ligand to a $Ru(bpy)_3$-type chromophore is inferred from observation of different kinetics of absorption decay at 605 nm (MV^{red}) and other wavelengths, in particular around 450 nm, where $Ru(bpy)_3$-type chromophores display pronounced bleaching when not in the ground state. This is rather straightforward as long as the decay of the Ru MLCT bleaching is monophasic or not too fast so that recovery due to electron transfer can be kinetically separated from the excited state quenching reaction. If this is not the case a method is needed to quantify what part of MLCT bleaching decay is due to excited state decay and which part is due to Ru(III) decay. This can be done by considering extinction coefficients for Ru and MV at the two wavelengths, based, of course, on the fact that concentrations $[Ru(III)]_{t0}$.= $[MVred]_{t0}$directly after decay of the excited state (the kinetics of which is identical to the kinetics of reduction of the acceptor when the latter is exclusively formed from this excited state).

For the MV radical the following extinction coefficients are taken from literature or from absorption spectra: ε_{605} = 13700 $M^{-1}cm^{-1}$, ε_{440} = 1370 $M^{-1}cm^{-1}$, slightly less (1100 $M^{-1}cm^{-1}$) for 450 nm (see spectrum).

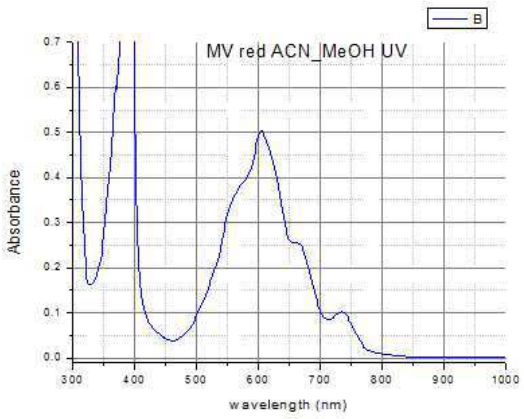

Figure 3.A1*: UV/vis spectrum of reduced MV, prepared by UV irradiation of a MeCN solution in presence of MeOH.*

For $[Ru(bpy)_3]^{2+}$, typical literature values[1] are $\varepsilon_{450}^{Ru(II)}$ = 14600 $M^{-1}cm^{-1}$ which we assume to be valid for similar complexes without major modifications of the Ru coordination sphere. Values for the extinction coefficient of the Ru(III) state are more difficult to find. From published spectra[1], reproduced below, we can roughly estimate $\varepsilon_{450}^{Ru(III)}$/ $\varepsilon_{450}^{Ru(II)}$= 0.19/0.83 at

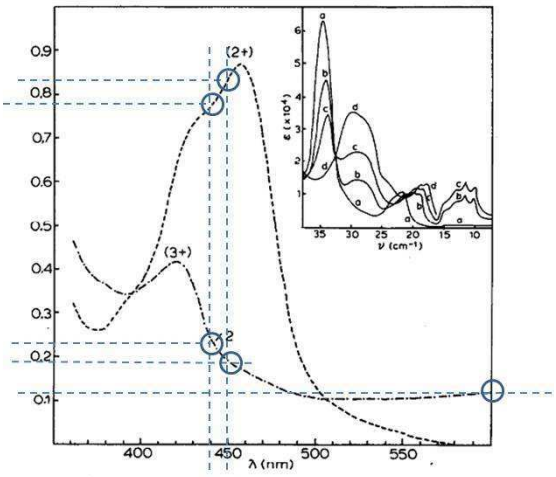

Fig. 3. Absorption spectrum of $Ru(bpy)_3^{3+}$ in 1 N H_2SO_4, prepared from by oxidation with PbO_2. Shown in the insert are the absorption spectra forms of $[Ru(bpy)_3]^z$ complexes with $z = +2$ (spectrum a); $z = +1$ (spectrum c); $z = -1$ (spectrum d).

Figure 3.A2: *Absorption spectra of* ***$[Ru(bpy)_3]^{3+}$***

450 nm and $\varepsilon_{605}^{Ru(III)}$/ $\varepsilon_{605}^{Ru(II)}$ = 0.11/0.83 at 605 nm. This yields $\varepsilon_{450}^{Ru(III)}$=3340 $M^{-1}cm^{-1}$or a differential$\varepsilon_{450}^{Ru(III)}$-$\varepsilon_{450}^{Ru(II)}$= -11260$M^{-1}cm^{-1}$ at 450 nm and $\varepsilon_{450}^{Ru(III)}$=2000 $M^{-1}cm^{-1}$ at 600 nm. Together this would mean that amplitudes of absorption at 605 and 450 nm should have a ratio of (13700+2000) / (1100-11260)=0.65. This value seems too low and we therefore reexamined the case by own measurements using $[Ru(bpy)_3]^{2+}$.

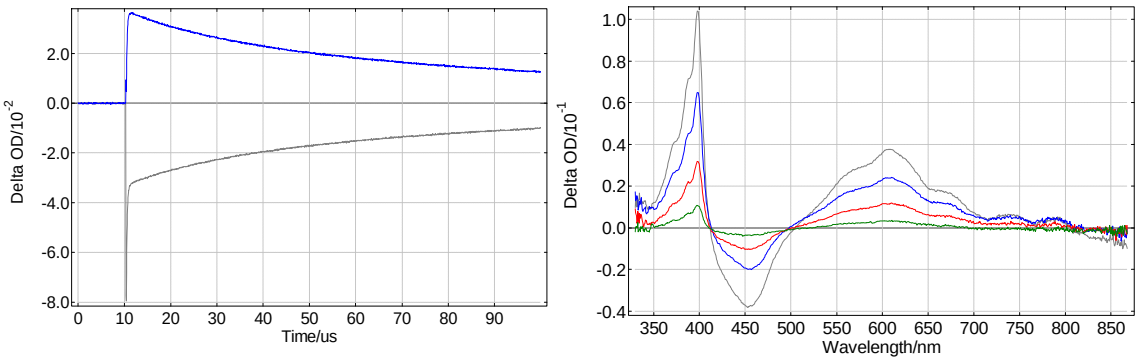

Figure 3.A 3:*Absorption kinetics of $[Ru(bpy)_3]^{2+}$ at 450 and 605 nm and spectra at different times (3-300 µs).*

From these data a ratio of A_{450}/A_{605} of -0.9 is deduced. This ration is independent of precise individual extinction coefficients and contains all contributions from both species at both wavelenghts. It can be used to recalculate more precise values for extinction coefficients.

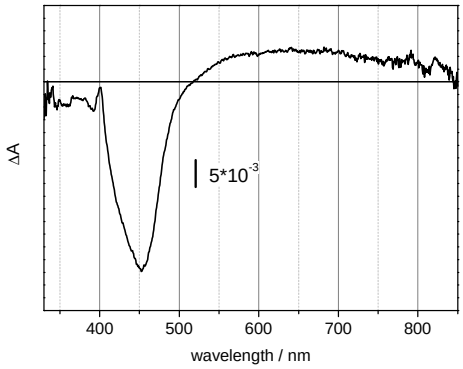

Figure 3.A 4:*Absorption spectrum at 3 µs, MV contribution subtracted.*

First, an absorption spectrum of Ru(III)/Ru(II) was calculated by subtracting the MV spectrum (see Figure 3.A4). From this plot an absorption at 605 nm is due to Ru(III) of 15% of the bleaching at 450 nm can be deduced. From this and with the known values for ε_{605}^{MV} and $\varepsilon_{450}^{Ru(II)}$ we can calculate $\varepsilon_{450}^{Ru(III)}$ as 1000 $M^{-1}cm^{-1}$ or for the differential extinction coefficient $\varepsilon_{450}^{Ru(III)} - \varepsilon_{450}^{Ru(II)}$. = -13600 $M^{-1}cm^{-1}$.

In our analysis of transient absorption traces instead of 450 nm we often use 440 nm as detection wavelength as it catches better absorption of the formed radical. For this wavelength the ratio $A_{440}/A_{605}$is reduced to -0.78.

Remarks:

Formation of Ru(III) and MVred have the same kinetics (which is identical to the emission decay kinetics). Therefore the absorption due to MVred at 440 or 450 nm will not be visible

as a separate kinetics. The same is true for the absorption rise at 605 which contains contribution due to Ru(III) absorption but the latter has the same kinetics as the MVred absorption rise. However, contributions of Ru(III) decay (due to internal electron transfer) to the absorption transients at 605 nm can be more problematic. MVred has a long life time and its concentration will not change much on the time scale of fast internal ET. However, Ru(III) disappears upon internal ET and this will modify the kinetics at 605 nm. Also radicals formed by internal ET might have large ε around 450 nm (like eg. imidazole). Then their absorption has to be taken into account, too.

Section 2: Determination of spectral changes associated with the slow phase

We wanted to determine the spectrum associated with this phase taking advantage of the high precision of these transient absorption measurements. One problem is that the decay of the charge separated state due to bimolecular back reaction with the reduced electron acceptor interferes, preventing easy analysis. We therefore applied a numerical correction of the transients to eliminate this decay. This approach is based on the fact that the measured absorption *A*'(t) can be described by a multiplication of the absorption transients in the absence of back reaction,*A*(t) with a second order reaction according to

$$A'(t) = A(t) * (1/(1+ k_{rec} * t))$$

If the parameter k_{rec} is known *A*(t) can be calculated from *A*'(t) by multiplication with a function of the form $f(t)=1+k_{rec} * t$.

k_{rec} was determined by nonlinear fit of the transient (for t>15us) at 605 nm, a wavelength where absorption is almost exclusively due to MV.

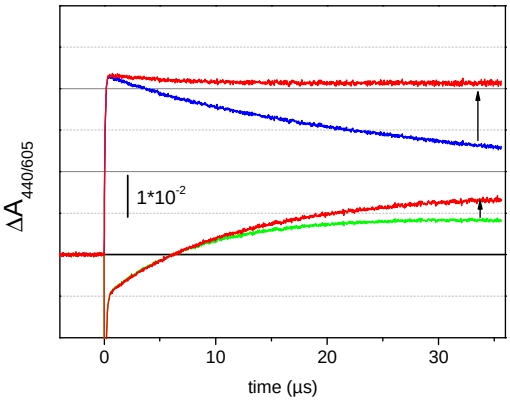

Figure 3.A5: *Visualization of the procedure of deconvolution of decay due to back reaction. Blue, green: experimental transients at 605 and 440 nm, respectively and red: after application of the deconvolution procedure. (Remark: the small decay still visible at 605 nm after correction is due to Ru(III) decay).*

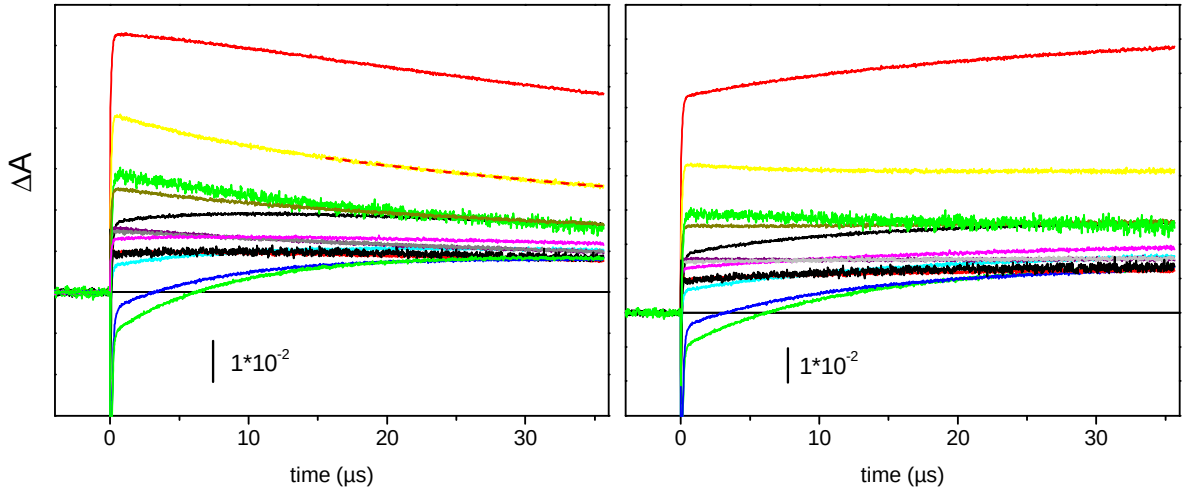

Figure 3.A6*: Original data (left) and after deconvolution (right). The dashed line in the left plot represents the best fit of the decay by a second order function.*

From this data it is easy to construct time resolved spectra (largely dominated by $MV^{+\bullet}$ absorption):

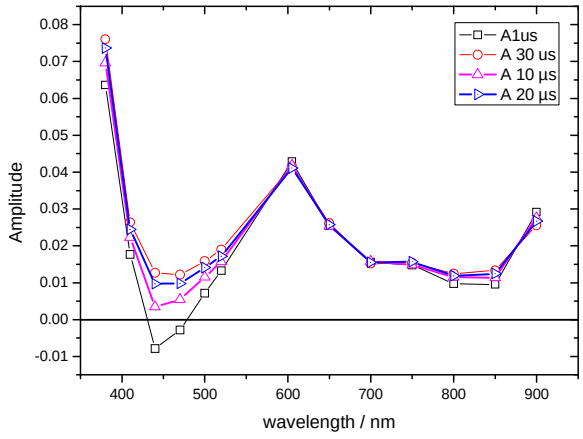

Figure 3.A7*: Amplitudes of absorption transients at 1, 10, 20, 30 µs.*

Subtraction of the amplitude at 1 µs then yields the data shown in Figure 3.26. As the $MV^{+\bullet}$ radical is fully formed at 1 µs and decays on a much slower time scale than the slow phase, MV contributions to the spectra is efficiently suppressed.

Section 3: Effect of water on photophysics

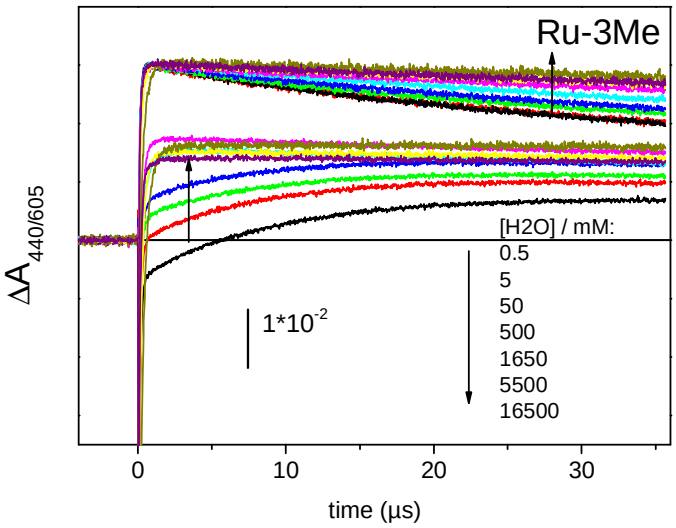

Figure 3.A8: *Effect of increasing water concentration on absorption transients for* ***Ru-3Me****. 20 mM MV was used as electron acceptor. The black curve corresponds to neat MeCN.*

Section 4: Effect of water on electrochemistry

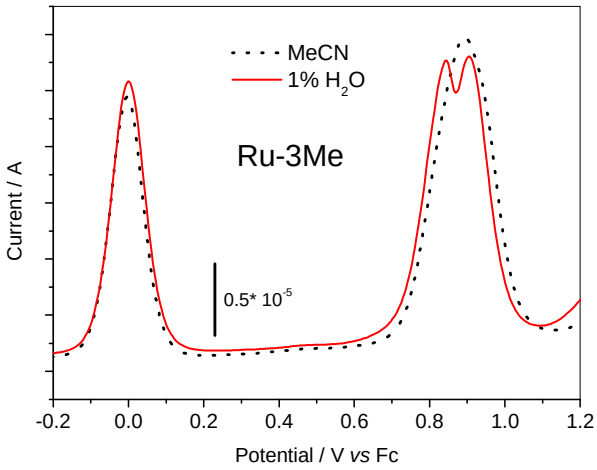

Figure 3.A9: *Differential pulse voltammogram showing effect of water on* ***Ru-3Me***

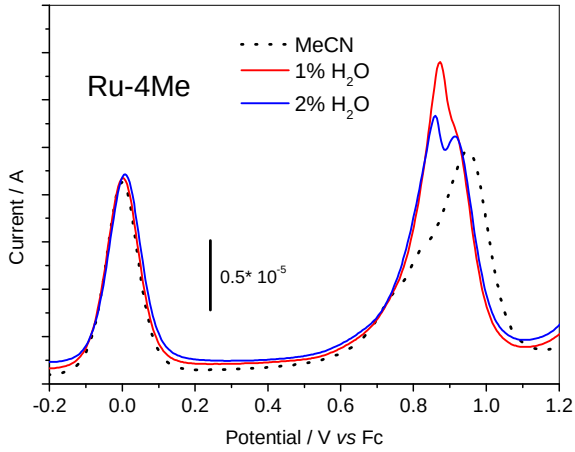

Figure 3.A10: *Differential pulse voltammogram showing effect of water on* ***Ru-4Me***

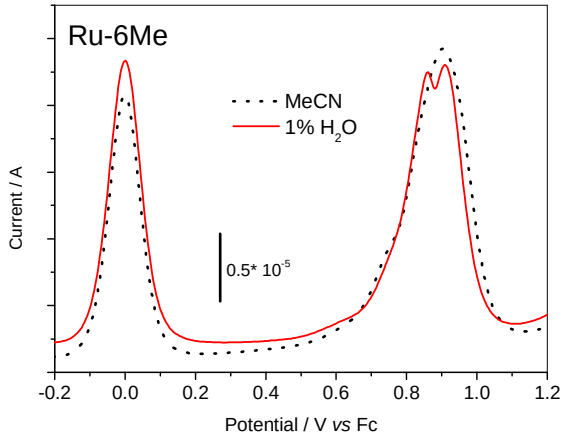

Figure 3.A11: *Differential pulse voltammogram showing effect of water on* ***Ru-6Me***

Section 5: Pyridine as base

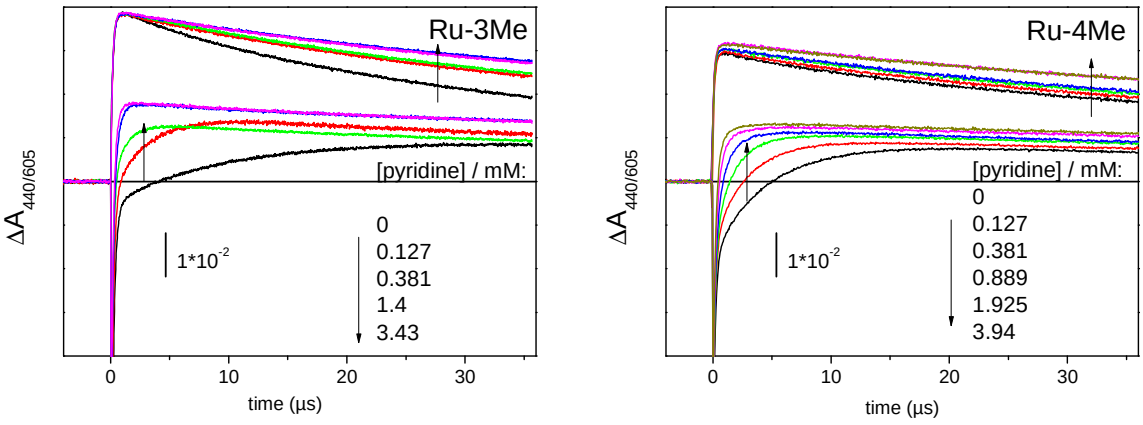

Figure 3.A12: *Transient absorbance traces at 440 nm (lower traces) and 605 nm (upper traces) for* ***Ru-3Me and Ru-4Me*** *upon excitation with nanosecond laser flashes at 460 nm in MeCN, Ar-saturated solution for increasing concentrations of pyridine. 20 mM methyl viologen (MV^{2+}) was present as external electron acceptor.*

Section 6: Imidazole as base

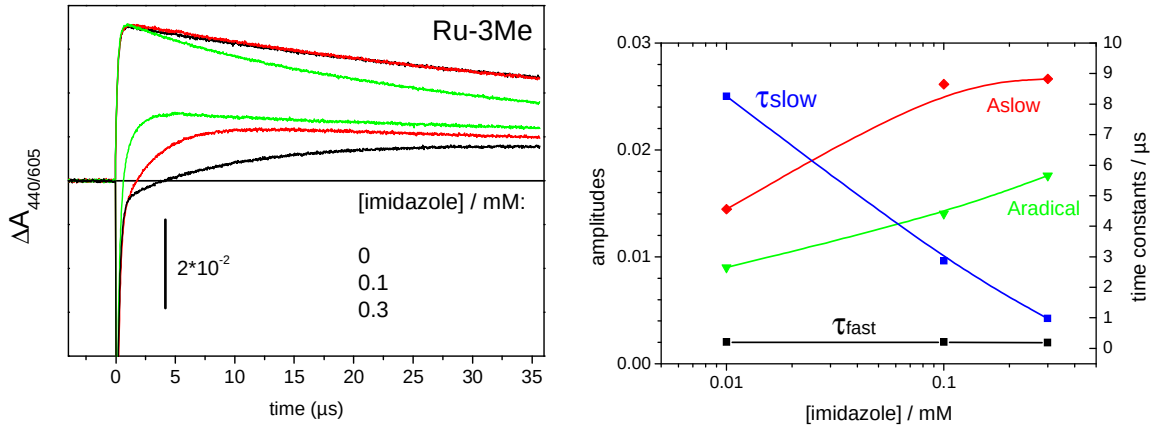

Figure 3.A13: Right: *Transient absorbance traces at 440 nm (lower traces) and 605 nm (upper traces) for* ***Ru-3Me****upon excitation with nanosecond laser flashes at 460 nm in MeCN, Ar-saturated solution for increasing concentrations of imidazole. 20 mM methyl viologen (MV^{2+}) was present as external electron acceptor.* ***Left:*** *Parameters obtained for best fit of absorption transients at 440 nm a function of imidazole concentration. Black, blue: time constants for fast and slow phase, respectively. Red: amplitude of slow phase. Green: amplitude of absorption at long times due to the radical on the ligand. To display the values for [imidazole] =0 mM these points were arbitrarily positioned at 0.01 mM.*

Section 7: DMSO as hydrogen bond acceptor

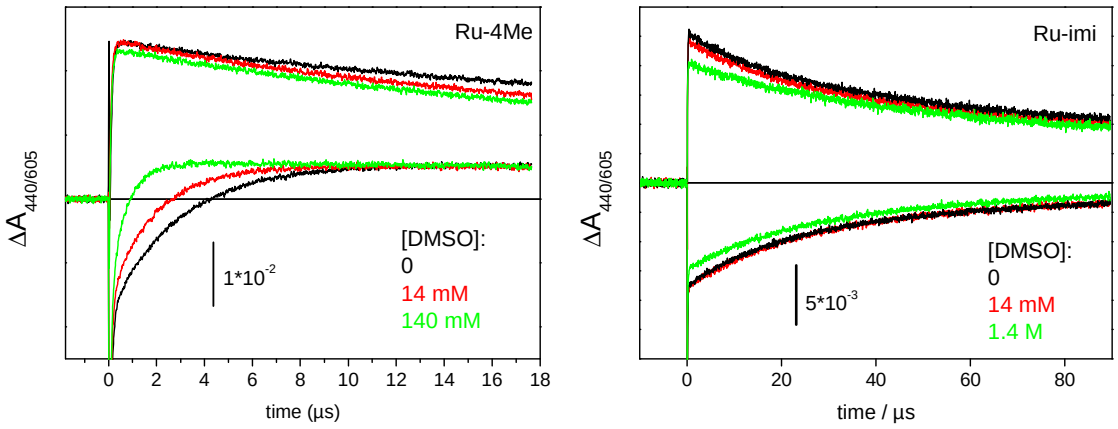

Figure 3.A14: *Transient absorbance traces at 440 nm (lower traces) and 605 nm (upper traces) for* ***Ru-4Me*** *(left) and* ***Ru-imi*** *(right) upon excitation with nanosecond laser flashes at 460 nm in MeCN, Ar-saturated solution for increasing concentrations of DMSO. 20 mM methyl viologen (MV^{2+}) was present as external electron acceptor. The decrease in amplitudes at DMSO=1.4 M (=10%) is due to dilution.*

Section 8: pH absorption titration

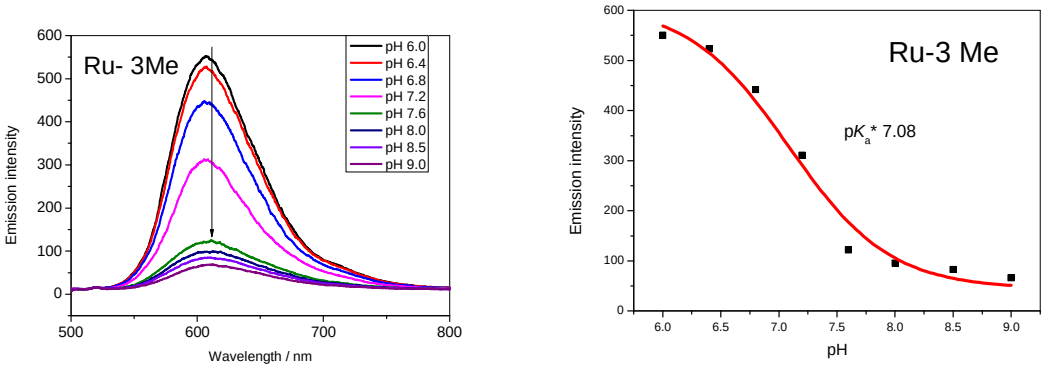

Figure 3.A15: *Emission spectra at different pH and emission titration curve for* ***Ru-3Me****. The solid line is a fit giving* $pK_a^* = 7.08$

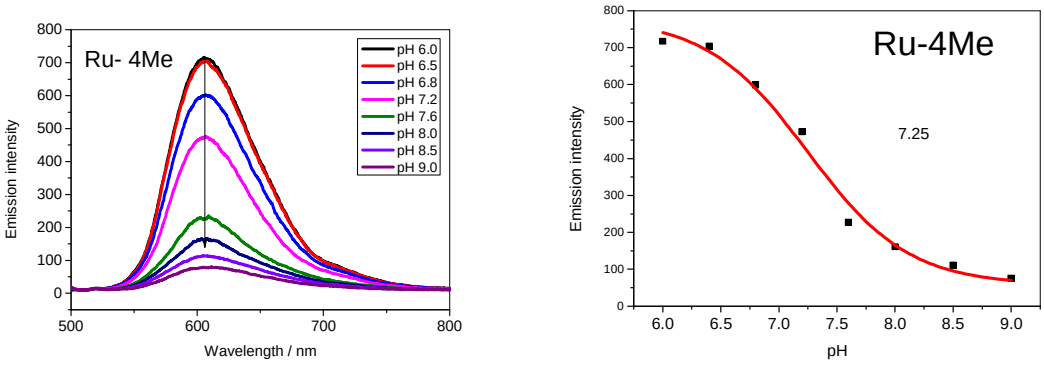

Figure 3.A16: *Emission spectra at different pH and emission titration curve for* ***Ru-6Me****. The solid line is a fit giving* $pK_a^* = 7.25$

References

(1) Kalyanasundaram, K., Photophysics, photochemistry and solar energy conversion with tris (bipyridyl) ruthenium (II) and its analogues.*Coord. Chem. Rev.*,**1982**, *46*, 159-244.

APPENDIX 2

Chapter 4.0Light-induced Tryptophan oxidation

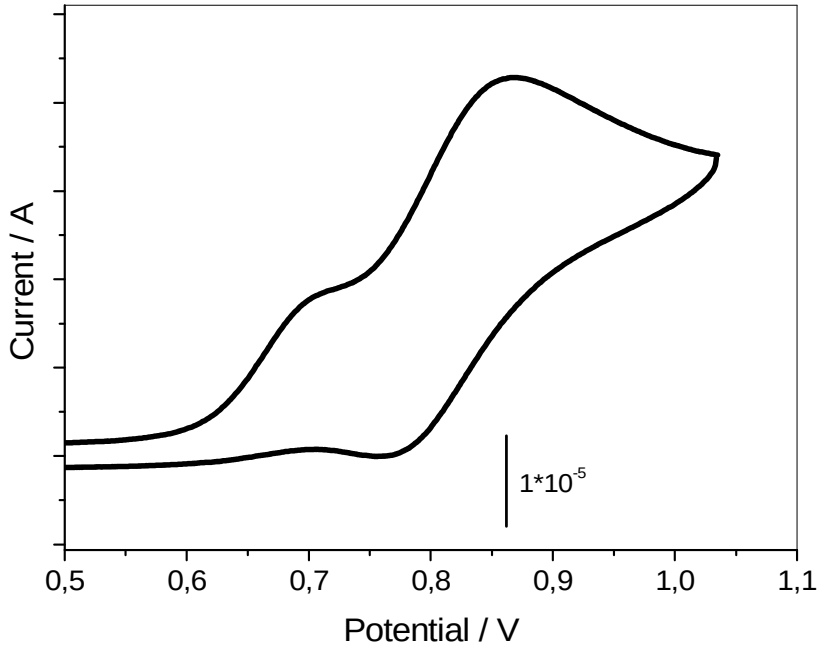

Figure 4.A1: *Cyclic voltammogram of 1 mM* ***Ru-Trp*** *vs. ferrocene in argon-saturated acetonitrile with tetrabutyl ammonium hexafluoro phosphate as supporting electrolyte. Scan rate: 100 mV/s.*

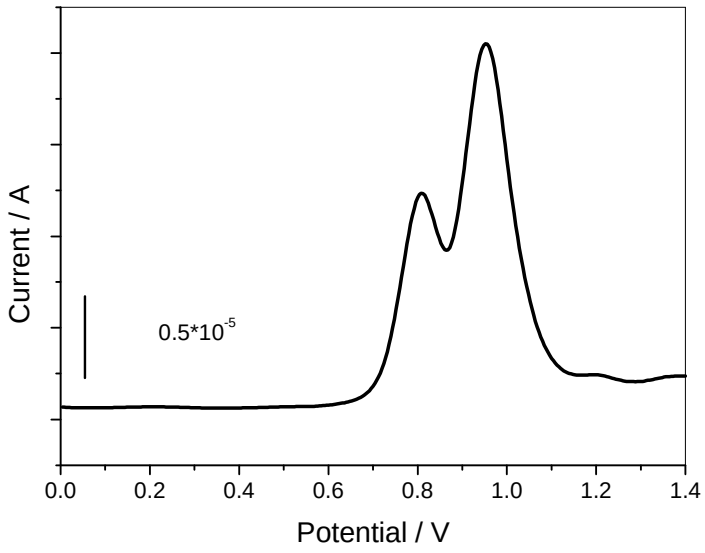

Figure 4.A2: *Differential pulse voltammogram of 1 mM* ***Ru-Trp*** *vs. ferrocene in argon-saturated acetonitrile with tetrabutyl ammonium hexafluoro phosphate as supporting electrolyte.*

Abstract

Artificial photosynthesis is often considered to have great potential to provide alternative, renewable fuels by harvesting, conversion and storage of solar energy. One promising approach is the development of modular molecular photocatalysts inspired by natural photosynthetic enzymes. The first part of this thesis deals with artificial mimics of the water oxidizing photosystem II composed of a chromophore and an electron relay as synthetic counterpart of the P680-TyrZ/His190 ensemble of photosystem II. Three ruthenium polypyridyl – imidazole - phenol complexes with varying position of a methyl group on the phenol ring (**Ru-xMe**) were synthesized and characterized by electrochemical and photophysical methods. As an improvement compared to earlier complexes the increased redox potential (~0.9 V *vs.* Ferrocene) of the phenol groups makes their function as an electron relay in a photocatalytic system for water oxidation thermodynamically possible. Time-resolved absorption studies revealed fast intramolecular electron transfer (<5-10 µs in aprotic solvent and <100 ns in water) despite the low driving force and the importance of the hydrogen bond between the phenol and the imidazole group was put in evidence. Slight differences between the three **Ru-xMe** complexesandinvestigation of the effect of external bases allowed to derive a mechanistic picture in which the imidazole is involved in a "proton domino" reaction. Accepting the phenolic proton upon ligand oxidation (within the H-bond) renders its second nitrogen site more acidic and only deprotonation of this site pulls the overall equilibrium completely towards oxidation of the ligand. Another part of this thesis comprises a chromophore-tryptophan construct synthesized using a click chemistry approach. Light-induced oxidation of Trp in this **Ru-tryptophan** complex was shown to follow ETPT mechanism. Depending on the pH conditions tryptophan radicals, either $Trp^{\bullet}$ or $TrpH^{\bullet+}$ were detected and spectral measurement at different time showed the transition between the two forms. Deprotonation of the radical was dependent on the concentration of water as proton acceptor.Later part of the thesis deals with efforts to covalently bind a catalytic unit to the previously characterized chromophore-electron relay module. The click chemistry approach was not successful to obtain the final photocatalytic assembly. Therefore bimolecular activation of a Mn salen catalyst was performed and formation of Mn(IV) species was observed. As a step towards utilization of these types of photocatalysts in a photoelectrochemical cell a $\mathbf{[Ru(bpy)_3]^{2+}}$ chromophore with phosphonate anchoring groups (**Ru-Phosphonate**) was synthesized and grafted on the surface of a TiO_2 mesoporous semiconductor surface anode to perform photocurrent measurements.

Résumé

La photosynthèse artificielle est considérée comme étant un atout capable de fournir des carburants alternatifs et renouvelables par conversion et stockage de l'énergie solaire. Une approche prometteuse consiste en un développement de photo-catalyseurs moléculaires inspirés par des enzymes photosynthétiques naturelles. La première partie de cette thèse concerne les modèles artificiels du photosystème II (qui catalyse l'oxydation d'eau), composé d'un chromophore et d'un relais d'électrons comme équivalent synthétique correspondant à l'ensemble P680-TyrZ/His190 du photosystème II. Trois complexes ruthénium polypyridyl - imidazole - phénol avec un groupe méthylique à différentes positions sur l'anneau phénolique (**Ru-xMe**) ont été synthétisés et caractérisés par des méthodes électrochimiques et photophysiques. L'augmentation, comparée aux complexes précédents, du potentiel redox des groupes phénols (0.20 V→0.90 V par rapport à l'électrode de ferrocène) rend leur fonction de relais d'électron dans un système photocatalytique pour l'oxydation d'eau thermodynamiquement possible. Des études d'absorption transitoire ont révélé que le transfert d'électron intramoléculaire est rapide (5-10 µs dans solvant aprotique et < 100 ns dans l'eau) malgré la faible force motrice, mettant en evidence l'importance de la liaison hydrogène entre le phénol et le groupe imidazole. Les légères différences entre les trois complexes **Ru-xMe** ainsi que l'étude de l'effet de bases externes nous ont permis d'établir un mécanisme dans laquelle l'imidazole est impliqué dans une réaction de transfert de proton en cascade. L'acceptation du proton phénolique durant l'oxydation du ligand rend son deuxième site azote plus acide et seulement la déprotonation de ce dernier bascule l'équilibre réactionnel complétement vers l'oxydation du ligand.La deuxième partie de cette thèse consiste en la synthèse d'un complexe chromophore-tryptophane en utilisant une approche de chimie dite « click ». On a montré que l'oxydation, induite par la lumière, du Trp au sein du complexe **Ru-tryptophane** suit un mécanisme ETPT. Selon le pH, les radicaux du tryptophane ($Trp^{\bullet}$ ou $TrpH^{\bullet+}$) ont été détectés et les mesures spectrales à différents temps ont montrés la transition entre les deux formes radicalaires. La déprotonation du radical dépend de la concentration d'eau assurant la fonction d'accepteur de proton.La dernière partie de la thèse concerne nos efforts à lier, par une liaison covalente, une unité catalytique au module de chromophore- relais électronique caractérisé précédemment. L'approche de chimie « click » n'était pas efficace pour l'obtention de l'assemblage photocatalytique final. Donc, l'activation biomoléculaire d'un catalyseur Mn salen a été effectuée et la formation de l'espèce Mn(IV) a été observée. Etant une étape vers l'utilisation de ces types de photocatalyseurs dans une cellule photoélectrochimique, un chromophore $\mathbf{[Ru(bpy)_3]^{2+}}$ avec des groupes d'ancrage phosphonate a été synthétisé (**Ru-phosphonate**) et greffé sur la surface méso-poreuses d'un semi-conducteur de TiO_2 pour effectuer des mesures du photocourant.